LBL-7766
UC-34C
CONF-780766

4th High Energy Heavy Ion Summer Study

July 24-28, 1978

LAWRENCE BERKELEY LABORATORY
UNIVERSITY OF CALIFORNIA/BERKELEY

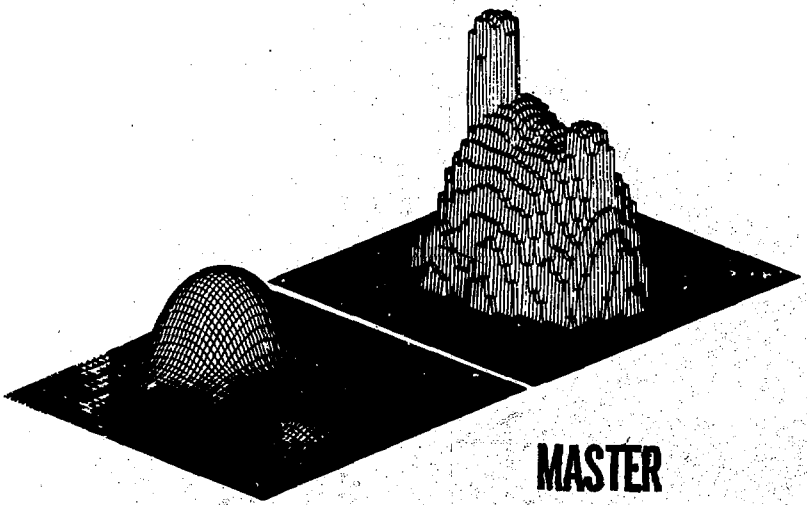

LBL-7766

Prepared for the U.S. Department of Energy Under Contract W-7405-ENG-48

4th High Energy Heavy Ion Summer Study

July 24-28, 1978

LAWRENCE BERKELEY LABORATORY

Editors
Catherine Webb
Jane Kingston
Jeannette Mahoney

FOURTH SUMMER STUDY ON

HIGH ENERGY NUCLEAR COLLISIONS

CONTENTS

FOREWORD

This conference was a pleasure to organize because of the excitement, enthusiasm, and very lively discussion throughout the conference. The interest in this field is truly international as is evident from the 100 participants from outside LBL, including 45 from 14 countries outside the United States. The participants, the speakers, and the chairpeople are all thanked for a lively meeting.

The organizing committee, which shared the burden of planning this meeting, consisted of Norman Glendenning, Miklos Gyulassy, David Hendrie, and Lee Schroeder. Many thanks go to Eileen Eiland and Maureen Jeung, who were essential to the smooth running of the conference. In addition, we are indebted to Jeannette Mahoney, Cathy Webb, and Jane Kingston for preparing these Proceedings. The cartoons that appear at the end of the volume were done by Steve Chessin. It should be noted that only the texts of the invited talks, which were presented during the morning sessions, were included in these Proceedings.

Arthur M. Poskanzer
Chairman of the
Organizing Committee

PROGRAM

Fourth Summer Study on
High Energy Nuclear Collisions
Lawrence Berkeley Laboratory
24-28 July 1978

MONDAY 9:00 a.m. Henriette Faraggi, Chairperson

Hans H. Gutbrod (LBL and GSI) (60 minutes)
MEASUREMENTS AT LOW AND INTERMEDIATE
RAPIDITY

Shoji Nagamiya (LBL) (60 minutes)
MEASUREMENTS OF PIONS AND HIGH ENERGY
PROTONS AT LARGE ANGLES

2:00 p.m. Lee S. Schroeder, Chairperson

EXPERIMENTS

W. Schimmerling (LBL)
PRELIMINARY RESULTS ON NEUTRON PRODUCTION

A. Ogloblin (Kurchatov Institute)
HIGH ENERGY HEAVY ION RESEARCH AT
KURCHATOV INSTITUTE, MOSCOW

J.J. Lu (U.C. Riverside)
MULTIPION PRODUCTION MECHANISMS

K. Wolf (LBL)
LOW ENERGY PION SPECTRA SELECTED ON ASSOCIATED
CHARGED PARTICLE MULTIPLICITIES

K. Van Bibber (LBL)
POSSIBLE NEW PHENOMENON IN
PERIPHERAL COLLISIONS AT 100 MeV/n

P. Haustein (BNL)
TARGET FRAGMENTATION OF Cu BY
RELATIVISTIC HEAVY IONS AND PROTONS

N. Porile (Purdue University)
FINAL RESULTS ON THE INTERACTION OF
Ag WITH 2.1 GeV/n ^{12}C

P.L. Jain (SUNY - Buffalo)
INTERACTIONS OF 500 MeV/n ^{40}Ar WITH EMULSION

5:00 p.m. Reception, LBL Cafeteria

TUESDAY 9:00 a.m. Jakob Bondorf, Chairperson

Jörg Hüfner (University of Heidelberg) (60 minutes)
APPROACH TO EQUILIBRIUM BASED ON MICROSCOPIC MODELS OF NUCLEAR COLLISIONS

James Carroll (UCLA and LBL) (20 minutes)
LIGHT FRAGMENT PRODUCTION AND ASSOCIATED MULTIPLICITIES FROM COLLISIONS OF 1.85 GeV/NUCLEON ^{40}Ar

Pierre Radvanyi (Saturne, Saclay and IPN, Orsay) (30 minutes)
SCIENTIFIC PROGRAM FOR SATURNE II

Alex Ogloblin (Kurchatov Institute) (10 minutes)
PROPOSAL FOR DUBNA-KURCHATOV HIGH ENERGY HEAVY ION ACCELERATOR

K. Sugimoto (INS, Tokyo) (10 minutes)
THE PRESENT STATUS OF THE NUMATRON PROJECT

2:00 p.m. Norman K. Glendenning, Chairperson

THEORY

L. Wilets (University of Washington)
CLASSICAL EQUATIONS OF MOTION

R. Hatch (Cal. Tech.)
SINGLE COLLISION HARD SCATTERING

G. Wolschin (University of Heidelberg)
COMPARISON STUDY OF 20 AND 2100 MeV/NUCLEON FRAGMENTATION

K. Smith (Duke University)
TIME EVOLUTION IN CASCADE

J. Bondorf (Niels Bohr Institute)
GROUND STATE ISOSPIN CORRELATION EFFECTS ON SPECTATOR RESIDUES

R. Landau (LBL)
SCALING AND NON-SCALING OF π^- PRODUCTION

WEDNESDAY 9:00 a.m. T.D. Lee, Chairperson

Mannque Rho (CEN, Saclay) (60 minutes)
CRITICAL REVIEW OF CRITICAL PHENOMENA
IN NUCLEAR COLLISIONS

Arthur Kerman (MIT) (60 minutes)
QUARK MATTER

2:00 p.m. Miklos Gyulassy, Chairperson

Sun-Yiu Fung (U.C. Riverside)
FIRST DATA ON TWO π^- CORRELATIONS!

Sin Ah Chin (University of Illinois)
TRANSITION TO HOT QUARK MATTER

Joe Kapusta (LBL)
HIGH T QUANTUM CHROMODYNAMICS

Norman K. Glendenning (LBL)
ROLE OF ASYMPTOTIC HADRON SPECTRUM
IN NUCLEAR COLLISIONS

James P. Vary (Iowa State University)
HEAVY PARTICLE PRODUCTION

Naohiko Masuda (Yamagata University)
HYDRODYNAMIC MODEL FOR E > 100 GeV/A

THURSDAY 9:00 a.m. Larry Wilets, Chairperson

Wit Busza (MIT) (60 minutes)
HADRON- NUCLEUS COLLISIONS ABOVE 10 GeV

Ingvar Otterlund (University of Lund) (60 minutes)
CENTRAL HEAVY ION REACTIONS AT
1-1000 GeV/NUCLEON

2:30 p.m. Buses leave for Wine Tour

FRIDAY 9:00 a.m. Cheuk-Yin Wong, Chairperson

C. Konrad Gelbke (Michigan State University) (60 minutes)
INTERMEDIATE ENERGY HEAVY IONS -- FROM
THE LOW ENERGY PERSPECTIVE

Steven E. Koonin (Cal Tech) (60 minutes)
WHAT LIES BEYOND INCLUSIVE MEASUREMENTS?

MEASUREMENTS AT LOW AND INTERMEDIATE RAPIDITY

Hans H. Gutbrod

Ladies and Gentlemen. In 1492 Christopher Columbus sailed westward to look for a shorter way to India in order to get the pepper back home more quickly. Unfortunately, he didn't reach his goal but found America. In 1971, Marc Lefort switched on his accelerator ALICE looking for super-heavies. He didn't find them, but luckily he found deep-inelastic scattering. And when we switched on the Bevalac here at Berkeley, we expected quite shocking effects and the very early experiments seemed to indicate them. But after two years of study we found nothing but hot gas. Last year it seemed that the expanded fireball model, the firestreak model (Fig. 1.1), was absolutely capable of describing nearly everything we produced as data. I don't have to introduce you to that model. It looked like thermalization occurred in these short time scales, and even chemical equilibrium was reached in the reaction zone, both of which would be quite spectacular discoveries.

When we saw the fireball fits two years ago, however, we felt it was too early to be convinced of our own model. So we decided to start a program to really look into details and measure much more than just single-particle inclusive spectra. Also we wanted to measure the spectra better than we did at that time in order to really look into the details of the individual models and test the validity of the models. As you know, the earlier data were described within a factor of 2 to 4 by nearly everybody. We decided to measure single-particle inclusive data with better equipment. We also wanted to measure associated charged-particle multiplicities of each event to be able to get more understanding of the event from which we measured just one single particle. These new data show exciting results that will have an impact on the various theories.

First, I will plague you a little bit with experimental details, which I think are necessary to give you a feeling for the improvements we tried to make. I will describe our detector which looks for particles at the low and intermediate rapidity. It is a silicon-germanium telescope that we built here. Then I will describe the ionization chamber for very slow, but heavy fragments that are coupled to the low rapidity region. After that I will show you the overall layout of the experiment. Next I will discuss the data by introducing to you the associated charged-particle multiplicity in the way we have measured it. I will discuss the projectile and target dependence of the multiplicity and the influence of the trigger particle that we measured in the telescope. Then I will show some ϕ- and θ-correlations of the telescope versus these fast particles. Finally I will show new data, both single-particle inclusive and super-inclusive measurements. (Super-inclusive means that we have measured the associated charged-particle multiplicity where we can study selections of low multiplicity and high multiplicity events.) Finally, I'll try to draw conclusions as to where we stand.

All the work I will discuss today was done in the LBL/GSI/Marburg

collaboration. I am also very grateful for the strong help I got in the preparation of my talk, specifically by Andres Sandoval and Bill Meyers who worked many nights to get the data available. The people in the group are: Chuck King, George King, Bill Meyer, Van Sen Nguyen, Arthur Poskanzer, Andres Sandoval, Reinhart Stock, Kevin Wolfe, and myself. They are all members of the experimental group doing the 284 H experiment which measures low and intermediate rapidity particles, π^+'s, protons, deuterons, and tritons. Jean Gosset, Jean Claude Jourdain, Chris Lukner, and Gary Westfall were earlier collaborators who left the group. The 377 H experiment was done by the little sub-group of Bill Meyer, Chris Lukner, Andres Sandoval, and myself and measures the heavy, very slow fragments.

Now to jump right into experimental discussions. We designed a new telescope consisting of two silicon detectors, two large-area germanium counters and one Li-drifted silicon detector (see Fig. 1.2). The idea was to use this telescope to measure protons from a very low energy, say 5 MeV, up to a total energy of 200 MeV. This telescope represents, I would say, the ultimate in what can be used to measure protons using a spectrometer without any magnetic design, since making it larger means coming to more than an interaction length. In that case, we'd have to apply tremendous corrections for scattering and for reaction loss.

In this slide (Fig. 1.3) I draw the specifications again. We can measure π^+ (from 17 to 100 MeV), up to tritons (from 7 MeV to 300 MeV). The π^+ identification is of special interest. When a π^+ entering the telescope comes to a rest (Fig. 1.4) it then decays into a μ^+ and a neutrino with a very short lifetime of 26 nsec. This yields an energy deposit of 4.2 MeV if the μ^+ is stopped in the detector. After a long time, about 2.2 μsec, the μ^+ decays into a positron plus a neutrino and an anti-neutrino. So by measuring the positions from the decay of the μ^+ in delayed coincidence with the first π^+ signal, we can identify π^+ from all the garbage that is in this area in the ΔE-E plane due to the π and due to protons that had undergone collisions in the detector. So we get a signal (see dashed curve) that corresponds to the energy deposited by the π^+ plus the little energy from the μ^+ of 4.2 MeV, which we can subtract later. Next we measure the delayed coincidence and then the pulse height of the positron. That allows us to clearly identify π^+ particles and the quality of identification shown in Fig. 1.5 yields a clear separation of π^+, protons, deuterons and tritons. You can see the quality of the delayed coincidence measurement in Fig. 1.6. We have here the time-to-amplitude convertor signal plotted over the time up to 8 microseconds; the slope indicates exactly the decay time of the μ^+ decay, which is 2.2 microseconds.

Next I show you the ionization chamber that measures the slow particles (Fig. 1.7). Those of you who have done low energy nuclear physics at the HILAC, for instance, will recognize the very large area ionization chamber using a Frisch grid. The solid angle of this device is about 20 mrad. The particles go through 14 cm of gas and get stopped in solid state counters. For extreme low noise we built the preamplifiers inside the system.

In the next slide (Fig. 1.8) you see the layout of the whole experiment. The germanium telescope described previously sits (as indicated) on a rotating arm. Associated with particles measured in this telescope, we measure the multiplicities of charged particles that go out through the scattering chamber into the scintillator paddles. The scattering chamber thickness is about 3 mm, so we absorb all low energy particles and the scintillators detect only particles that have an energy of 25 MeV or higher. Eighty scintillators are arranged around the scattering chamber in four angular domains. The first one is ring A from 9-20°, ring B is from 20 to 45, and ring C is from 45 to 80°. Four detectors are located at back angles. We generate a trigger signal in the telescope and scan all 80 scintillation detectors within 20 to 30 nsec to see whether a particle has reached them or not. That is how we measure the associated multiplicity and its pattern in ϕ and in θ.

The next slide (Fig. 1.9) shows such a pattern. We have on top a very low multiplicity event. This is the 80 counter array as seen by a particle that just left the target and is flying downstream. In the center we have ring A, then comes ring B, and finally ring C. In the upper part of Fig. 1.9 you see a low multiplicity event. Everything is focused on the left side, the telescope sits there. Right in the center we have a large multiplicity of central events (the dark-shaded areas are counters that have fired) whereas here on the lower part we have also reasonably high multiplicity but a totally asymmetric distribution. Nothing is in this domain, this hemisphere, everything is on the side where the telescope is.

The next slide (Fig. 1.10) shows the same setup, but here the ionization chamber is looking for low rapidity particles, or very slow fragments, from beryllium to fission-like events. Opposite to it we installed five solid-state counters to measure any correlated event that might occur with a total energy of up to 100 or 150 MeV. So we are looking only for slow particle-slow particle correlations. With this setup, of course, we have again the measurement of the total associated multiplicity which is, in 377 H, a slow particle-fast particle correlation.

In order to overcome problems with beam normalization we have installed a calibration device (a beam sampler scintillator developed by Arthur Zingher et al.) that enables us to measure the beam particle at low intensities. We built one of these and installed it behind our beam ionization chamber to calibrate and normalize the very high flux where you can't count the particles any longer. This device is good for 10^8 particles whereas the beam ionization chamber can go up to 10^9 and more. Now in order to double check its calibration at high intensities, we have in addition a monitor sitting at 90° out-of-plane to watch the reaction products coming from the targets. So we make sure that the monitor-to-beam ionization-chamber ratio stays constant and we are not fooled by saturation processes in the ionization chamber. We think that we have the beam normalization and the beam counting well in hand. The next slide (Fig. 1.11) shows this sampler——it is just a piece of lucite with 1 mm scintillator rods attached so that the beam sees only about 3% active area. This allows us to count beams roughly 30 times higher than would be possible with a full scintillator. The next slide (Fig. 1.12) shows the whole setup. The beam comes from the right into the chamber, and we look

downstream to the scattering chamber.

With this system we measured the following data. We did a survey using various projectiles and targets at different energies (see Fig. 1.13). We decided to use the heaviest target possible to come close to nuclear matter studies using uranium as a target with all projectiles and at all energies. Furthermore, we wanted to check the target dependence and chose neon on targets of aluminum, silver, gold and uranium. With argon, the heaviest available particle at the Bevalac with aufficient intensity for counter experiments, we investigated the symmetric system argon on calcium at both energies and then the asymmetric system argon on uranium, also at both energies.

Let me now come to the concept of associated charged-particle multiplicity. We are measuring the particle (or better, the trigger particle) in the telescope, identifying it according to mass, charge, energy, and detection angle. Simultaneously we measure coincident fast particles but don't identify them. We know only that they are above a certain energy. In order to show you roughly what the detectors that measured those coincidence particles are sensitive to, I have plotted p transverse versus rapidity (Fig. 1.14). We see that ring A doesn't extend to far transverse momenta, that ring B really covers the intermediate rapidity region, and that ring C and the detector D at back angles cover mainly the target rapidity region. So keeping that in mind, I want to show you now how the associated multiplicity behaves (see Fig. 1.15). In this transparency the mean multiplicities in each individual ring are calculated with the assumption that the distribution is isotropic in ϕ, ignoring any asymmetry observed, and that we can correct for the missing solid angle since we don't have all 360° covered with the scintillators. Using these assumptions, we calculate mean multiplicity for ring A, ring B, and ring C. We see that if we change the target mass for 400-MeV/nucleon neon (Fig. 1.15, bottom), we don't see any change in ring A. This means that our ring A is dominantly fired in the average reaction by decaying fragments from neon. However, we see that the mean multiplicity in ring C rises, as does the mean multiplicity in ring B. As we go up to higher energies, at 2.1 GeV (Fig. 1.15, top), we see a slight change in the mean multiplicity for ring A and we see a dramatic change as a function of target for the larger angles. This means that if we look just in ring A we wouldn't get a picture of what is going on, and that for all experiments you have to cover as much solid angle as possible in order to be sensitive to the total reaction.

Let me show you now the total multiplicity plotted versus the average number of proton participants as calculated in the fireball geometry (see Fig. 1.16). The number of proton participants allows us to avoid comparison first with the projectile and then with the target. It takes into account the geometry of both the target and the projectile. That's why one likes, for comparison, the geometry part of the fireball model. The total multiplicity, the sum of the means integrated over angle, is rising at 250 MeV/nucleon reasonably well according to the proton participants involved. But if you go to larger energies you see that the data deviate from this picture until they have a slope which is three times steeper than the predictions of the participant model. So what does that mean? Do we really get a change in the number of participants? I would say, yes. Always recall that we measure the associated

multiplicity. That means that in addition to these charged particles in the multiplicity counter, we have the telescope sitting at 90° detecting a high momentum particle, for example a 100- or 200-MeV proton. Because of this we select very violent reactions suppressing low multiplicity events. The rise with energy shows us that in this kind of selection we get more and more particles from the spectator brought out to large angles. I will come to that point in a minute. To summarize these findings (Fig. 1.17) and state them perhaps a little more clearly: the strong increase in multiplicity as a function of projectile energy is an indication that we cannot keep the picture of the participants being swept out of the target nucleus to decay behind the target. Their number would stay constant if they decayed outside. They have to decay more or less inside the nucleus and share their energy with the surrounding spectator matter.

Let us now look at the more-or-less raw data. We want to see the influence of the trigger particle and how the charged-particle multiplicity changes depending upon the kind of particle we detect in the telescope. I show you now the m-fold coincidences (Fig. 1.18). These are the raw data not the calculated mean multiplicities. This is exactly the number of paddles which fire when I measure, in this case, a proton in the telescope. Fig. 1.19 shows the distribution of paddles which fire when I measure a slow helium in the telescope (the helium has a low total energy from 15 to 40 MeV). Again keeping in mind that we still believe that high multiplicity means central collision (low multiplicity means peripheral collision), we would say that ^{4}He is a particle that is usually produced less in peripheral reactions. Next I compare this with another trigger particle (Fig. 1.20). This is the oxygen detected at a very low energy. The oxygen is at about 20 to 100 MeV, whereas before we had 15 to 200 MeV, which is a much higher velocity of particles. The oxygen is, in that respect, only 1 to 5 or 6 MeV/nucleon. We see that at 400 MeV/nucleon neon on gold, the oxygen has a higher multiplicity than the multiplicity associated with protons or with alphas. Let's see whether we have something even higher than that if we go to heavier elements which are between Z = 13 and 26 (Fig. 1.21). We see that they can't match the high multiplicity observed in oxygen, but that they shift toward lower multiplicity and again try to fill up the region that before was much more filled up with protons and alphas. Let us go to even heavier Z's (Fig. 1.22). Here we see that in neon on gold for particles with Z larger than 26 the low multiplicity is filling up dramatically. In this region we don't have, with this ionization chamber, any method of separating the elements. We would have to do time-of-flight, but in order to discover what this component is, we use uranium as a target. In uranium we know from low multiplicities that a fission cross section of up to 1 barn has been observed by the Seaborg group. For neon on uranium at the same energy (Fig. 1.23), there is only the low multiplicity component left for fragments with Z > 26, and we can now clearly identify them as fission products because we measured the partner in the E1, E2 coincidence setup. Since in gold we have a higher fission barrier, peripheral reactions have to be quite violent in order to open the fission channel. In uranium we can just tickle the nucleus and obtain fission. Therefore we interpret this small contribution at low multiplicities (Fig. 1.22) as being due to fission from gold. The high multiplicity part reminds us that there are even heavy particles coming from more central

collisions at these energies. If we plot the mean multiplicity as a function of Z of the trigger particle, we get the following picture (see Fig. 1.24). In the case of neon on uranium, if we measure a proton with high momentum at 90° we get about the same charged particle multiplicity as if we were detecting something with a Z of 14. However, the maximum associated multiplicity is observed if we measure particles like oxygen or neon coming slowly out of the target nucleus. In the case of silver, we have a flat response curve. We do not expect fission, at least not in very far peripheral collisions. So, we obtain heavy products with large multiplicity.

Let us now see whether we get some more information by looking into the angular distribution of these fast particles. I will draw that to make clear what I mean (see Fig. 1.25). We still have our telescope as a trigger for the charged-particle multiplicity. Using the angular binning of rings A, B, C, D, we can obtain the average angular distribution of the coincident charges observed in the rings. We plot the mean multiplicity in ring A divided by the solid angle, the mean multiplicity in B divided by the solid angle C, and so on, and get an angular distribution, as well as perhaps some insight into the mechanics of the reaction. We have plotted here (Fig. 1.26) the angle domain of ring A, and that of rings B, C, and D, so it is a four-point angular distribution. Nevertheless it is enough to show that for the fission products we have a very strongly forward-peaked curve. This means that the spray of particles associated with fission is focused more or less into ring A which, as we discussed before, is the signature of a peripheral reaction. Ring A tells us mainly how the neon, or whatever we shot in, explodes, and we get the full picture from the target in the fission products. But if we go to oxygen fragments we see that it is much less forward peaked, and it has also the highest yield in multiplicity. The dashed line is for a proton trigger that is lower than the oxygen curve. Remember that the integration gives us the total multiplicity, which we have found to be highest for oxygen. Now all that I've told you so far is true only for the cases measured. And we have measured this kind of behavior at 400-MeV/nucleon neon on uranium and gold. If we go to argon on calcium, where in the central collision everything is blown to pieces, I don't expect to observe oxygen with the highest associated multiplicities. Or if we go to 2.1-GeV/nucleon neon on uranium, where we have also observed tremendously high multiplicities, I again doubt that this finding would be verified. But at 400 MeV or 250 MeV, that might be the story.

So let us now have a look into the very interesting ϕ-distribution (see Fig. 1.27). We want to study the correlation between a particle detected at $\theta = 90°$ and $\phi = 0$ and the fast charged particles detected in rings A and B. Ring C has some structure in the response of the scintillation due to unavoidable mechanical shadows. We claim to get the cleanest picture in rings A and B, and I will show you now some of those data. On the upper graph in Fig. 1.28 the ϕ-correlation is shown for a proton measured at $\theta = 90°$, $\phi = 0$ with fast particles in the reaction of 1.05-GeV protons on uranium. We see here a very strong correlation peaked at 180° on the opposite side of the telescope. The same is true in ring B where we also get a strong enhancement at the opposite side of the telescope. The correlation function tells you whether to measure a more symmetric event and whether it is asymmetric

towards this side or the other side. A positive R means that you get more particles at this angle ϕ. At 180° it means everything is focused away from the telescope. If we look at the reaction α on uranium at 1.05 GeV/nucleon and again for a proton at 90°, this effect is washed out. We don't see strong correlations anymore. I remind you that a proton at 90° with finite energy cannot come from a collision of a nucleon onto a proton in the target at rest. In order to see a proton out at 90°, therefore, there has to be quasi-free scattering, and that's what we think we see here, namely, the strong two-body correlation of proton-proton collisions, but with the proton being quasi-free in the nucleus. In α + U we don't find it, so we want to see whether two-body correlations show up in other reactions.

Let me show you now 400-MeV/nucleon neon on uranium (Fig. 1.29). They are also correlation functions. The trigger particle is again a proton between 35 and 200 MeV. I will change the trigger angle at the request of Steve Koonin. I'm looking now only in ring A, and if the telescope is at 50°, 90°, or 130°, we see that we have mainly flat correlation functions; at most, perhaps, a 10-20% effect, much less than we observed with the proton on uranium case. Nevertheless, we observe a slight tilt favoring the opposite side of the telescope. And now if we shoot neon on aluminum where one could think there was negligible absorption from spectator matter, we can observe the first stage of collisions much more clearly. We still don't see a dramatic difference from neon on uranium.

We have just looked into the correlation of fast particles with intermediate rapidity particles. Now I will show you another ϕ-correlation, but this time we are looking for heavy, slow fragments. Here we have a correlation between very slow particles and the fast shower particles (Fig. 1.30). We measure a particle at 90°, in the lower case an oxygen that originates from a very central collision (we know that now from the multiplicity distribution). We see that the response is very flat within the error bars, something we expect from a central collision. But going to heavier Z's, we get an indication that there's an enhancement at 180° in rings A and B that is more pronounced as we go to the very heavy products, as here from neon on gold where we don't have fission, or fission only as approximately a 10% admixture. We see here a strong 180° asymmetry. If we look at the angular correlation for fission particles as in Ne on U, which I don't have with me, where we are sure that we have fission, we observe a very flat response. Next, I will illustrate what that looks like when we observe a heavy particle at 90°, associated on the average with a lot of fast fragments on the other side (Fig. 1.31). At first I talked about the firestreak model in which we assume fast thermalization and chemical equilibrium. I would say this is clear evidence that we have to consider strong perpendicular momentum transfer in the reactions and cannot hold on to the clean-cut assumption. But how should we explain this side-kick? Is it a shadow effect? Is it evidence for coherent scattering resulting in a large momentum transfer but little internal excitation so that the large spectator fragment doesn't get exploded but only pushed out? I would suggest leaving this up to the appropriate theorists. I should also mention that in intersecting storage-ring experiments in Geneva a nonzero correlation has been measured. Also, it has been observed that whenever a large $p_{\perp}$ particle is seen, its momentum is not balanced by only one other fast particle but

by many. Now that may be a simple entropy argument, but I won't go into that.

Let us now look at an alternative view of how we could explain the observed correlation between slow and fast particles. You all know by now Ray Nix's calculations with the hydrodynamical code. If we look now into the picture (Fig. 1.32) at an impact paramter of .5 b_{max} and follow the reaction down in sequence of time, we see that the spectator matter really gets a kick and that the projectile gets deflected toward large angles. In this model we get predictions of in-plane quasi—two-body scattering, or whatever you want to call it, but definitely in-plane correlations. Now if one takes Ray Nix's pictures seriously and goes into detail in measuring the distance, the time, the speed, then one finds this bulk moving out with the speed of about .04 c. Now I wondered whether this speed shows up somewhere in our reactions or whether there was no relation. If you translate .04 c into energies assuming some masses, you find that it is .75 times the mass, and then you can get the energy in MeV. If we have mass-50 particles, we have 35 or 40 MeV, so those particles (Fig. 1.30) might be candidates. If we consider heavier particles, we come up to 50 to 80 MeV, which is covered by the uncorrected spectrum for the heavy fragments (Fig. 1.33).

Now that we have some side-kicks explained by the hydrodynamical model, we might try it out on different effects. Let's go to the oxygen particles or to those fragments that we know result from very central collisions. Here (Fig. 1.34) we measure them in the reaction ^{20}Ne on Au at two angles. Then we can use the old explanation of a moving system with a certain temperature emitting the neon in its rest frame. We can define the velocity by comparing the two angles, and it is .02 c. We are ignoring any perpendicular momentum of the moving system. The particle would come out to 90° just because of Coulomb barrier effects or because of the Coulomb repulsion, assuming the existence of another big fragment. But on the other hand, we know from the high charged-particle multiplicity that this system got shattered tremendously. It is a central collision. It had a lot of kinetic energy in the participants, which are observed in the TAC counter array, so there goes a lot of energy and a lot of momentum. In order to allow for a second big fragment, we have to accelerate the whole spectator to .02 c, and any heat has to be shared with the two partners. The oxygen has to come off directly or be an evaporation residue of a heavier product. That picture is well established, but it is not even successful in describing all the old proton data, much less the angular distribution of those particles from 20 to 160°. One has to make a lot of assumptions when using it, so I thought perhaps there might be another explanation. If we have a look now at 1.05-GeV/nucleon helium on gold and watch the spectra of the so-called evaporation particles (Fig. 1.35), we see that their peak shifts according to Z. Now if you assume that a particle is emitted from a front which moves with a constant velocity, you get the same picture because the energy of particles with the same velocity but different masses is just proportional to the mass. So by observing in-place correlations, side-kicks, and this mass-dependence, it is possible to observe compression effects in these reactions.

Let me now cover quickly the fission products. Here we saw already that they have very low multiplicity, and when we measure the ϕ-correlation, we

see no enhancement at 180°. By measuring energy spectra at forward and backward angles, we can deduce the parallel momentum transfer onto the fissioning system (Fig. 1.36). We find that it is clearly in the vicinity of peripheral reactions, as seen in the studies by the Heckman/Greiner group, but we have about two to three times higher longitudinal momentum transfer than they do (Fig. 1.37). They observed 30 MeV/c up to 200 MeV/c. This means that by looking for fission you can also study something about peripheral reactions.

Since we have now studied enough low rapidity particles, let me have a look at intermediate rapidity and give some single-particle cross sections. Here is (Fig. 1.38) the π^+ distribution that will be discussed in detail by Kevin Wolfe in the afternoon session. I will just give propaganda for it and show that we have data, and a lot more of it. I'll show only the 400-MeV/nucleon neon on uranium data, the curves drawn through are the firestreak calculations. You see that at back angles they reasonably reproduce the data, but at forward angles and at low energies the trend is a little bit off. Next I'll show you the non-selected single-particle cross section for protons from 250-MeV/nucleon neon on uranium (Fig. 1.39). These are now the new data which supercedes all preceding data. (Our group apologizes for the trouble we caused, we must also learn some new tools and tricks to deal with the relativistic heavy ions.) For this data we have summed up the charges and they are available for the groups who want to try their luck at describing them with their models. We see that the lines for firestreak calculations do not fit at all. This is a firestreak which predicts the proton spectra, taking into account the particle production. It also doesn't describe the data at 400 MeV/nucleon (Fig. 1.40). At back angles the agreement seems reasonable, but the behavior at forward angles is not described at all. Let me now use our 80 scintillator array and do some selections. I will show you angular distributions of single-particle inclusive spectra selected on high versus low multiplicity. We stay at 400-MeV/nucleon neon on uranium. Drawn quickly, as there was no time to do better, these lines are not theoretical curves but data (see Fig. 1.41). If we select low multiplicity events, events with only very few particles reaching the TAC counters, we observe that this leads to a spreadening out of the spectra (Fig. 1.42). We have a component that reaches forward more. If we now switch on the high multiplicity selection (by high I mean red and a hot reaction) (Fig. 1.43) we see that everything is compressed. The spectra are compressed and the cross section is going more and more sideways, enhancing the contribution at large angles. Specifically, I want to draw your attention to the reversal of the cross section at 30° and 20°. This is $d^2\sigma/dEd\Omega$, nothing is weighted with a sin θ factor. One wonders if this effect is again describable in the firestreak. Let's compare firestreak calculation, taking only very small impact parameters (Fig. 1.44). Chuck King did that for us. He integrated from $b = \emptyset$ to $1b_{max}$, taking only a small fraction of the total cross section. Indeed, you see the compression of the spectra we observed, but it doesn't match at all when we try to match at 150°. We could line up data and calculations at 90°, but then we get even worse agreement up front. If we compare the firestreak, taking a different cut, i.e., if we take a little bit more cross section than we see here (Fig. 1.45), the general behavior of opening the spectra is there but there is definitely

no reversal of 20° and 30°.

I can show now the same effect in gold. Taking now the low multiplicity selection in neon on gold (Fig. 1.46) and the high multiplicity selection (Fig. 1.47), we have to make a choice as to where to adjust them. You see that the spectra at 90° are drastically different. In a temperature picture you would say that the central collision is much, much hotter. In a non-thermal picture you would say we get large momentum transfer. Again, the change of sequence is a slight one, but it's really there between 20° and 30°.

I can find that again in neon on silver (Fig. 1.48, 49, 50). Now we will go further down in mass to see whether this inversion effect has something to do with uranium. At aluminum it seems (see Figs. 1.51, 52) that the spectrum is a little bit reduced but the sequence of 20° being higher than 30° is still there. (I have only the non-selected versus the high multiplicity adjusted at 90°.) So perhaps aluminum doesn't have enough spectator matter to do this kind of inversion.

Let us now look at slow protons from 1.05-GeV/nucleon argon on calcium. This is the low multiplicity selection (Fig. 1.53) and this is the high multiplicity selection (Fig. 1.54). We interpret that the slow particles result from an evaporating spectator, or definitely from some part of the spectator. If we switch on a high multiplicity selection, this whole part at low energy disappears (Figs. 1.53, 54) and we get the behavior that is more or less that of participants. Now in argon on calcium we have a symmetric system and little or no spectator left. We compare that with the firestreak calculation (Fig. 1.55) and the firestreak reproduces this diving at low energies, but you can see the different spreading out of the spectra. It has a much, much too high forward component. If we normalize data and calculations at 150°, 90° would be right, but 30° would be an order of magnitude higher in the calculation. Finally we plot neon on uranium in a $p_{\perp}$ versus rapidity plot. We get the following picture (Fig. 1.56). We have rapidity here versus $p_{\perp}$ for protons, high multiplicity selection; the beam rapidity is way out here and you can see that there is a ridge going out, a preferential push to the side.

So in high multiplicity selections we see that the particle flux into the forward angular region is strongly reduced so that the 20° and 30° cross sections are actually inversed. We don't see this effect at neon on aluminum, so it has to be something to do with the amount of spectator matter available. We see a strong depletion of the low energy protons in argon on calcium in high multiplicity events, so we conclude that the spectator is totally disintegrated at this energy.

I think I should summarize shortly. The associated multiplicity increases strongly with projectile energy, i.e., we really have more and more energy dissipated into the spectator. Next, the in-plane correlation of heavy, slow target fragments with fast charged particles in the multiplicity array shows us that there is a kind of quasi-two-body scattering or perhaps a pressure forcing the particles into a transverse motion. Further, we show that the

high multiplicity selection increases the contribution of large p events. For heavy targets we observe sidewise peaking in high multiplicity events.

So, to finish, we have to use models that don't exclude transverse momentum transfer. Yesterday Arthur gave me some calculations from Ray Nix that were compared with our data of integrated charges (which, as I said, are available to you) and here are the new data with absolute cross section and no multiplicity selection (Fig. 1.57). It's really a total charge cross section compared with the two-fluid dynamics, and the agreement is quite nice. Remember this model doesn't exclude compression effects. If we take a totally different model, the cascades by Fraenkel and Yariv (see Fig. 1.58), again we have surprisingly good agreement for non-multiplicity selected. Therefore we challenge them to do some selections (of small impact parameters only) now that we have small impact parameter data, and we'd like very much to know what their model predictions look like.

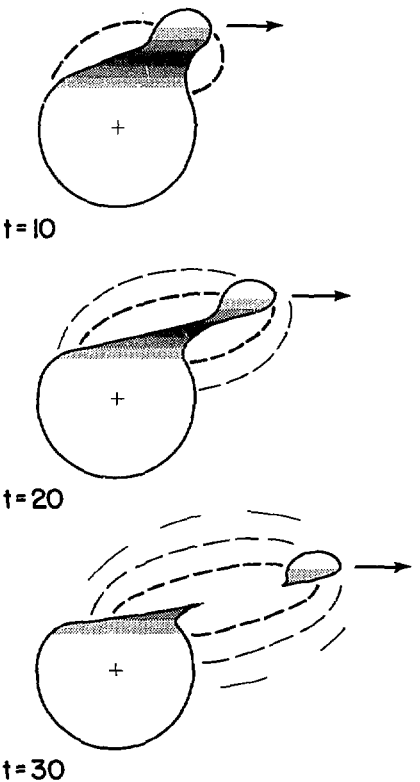

Fig. 1.1

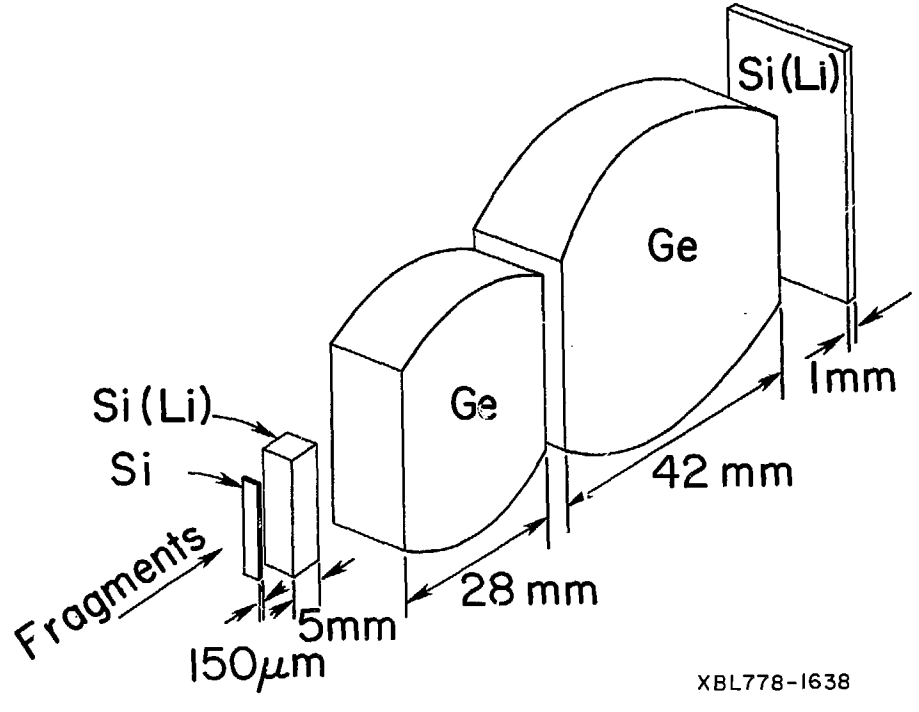
Si(Li)
Ge
Ge
1mm
Si(Li)
Si
42 mm
Fragments
28 mm
5mm
150μm
XBL778-1638

Fig. 1.2

New	Si-Si-Ge-Ge-Si-Telescope			
150μ	5mm	28mm	42mm	1mm
π^+		$17 \leq E_n \leq 100$ MeV		
p		$5 \leq E_p \leq 200$ MeV		
d		$6 \leq E_d \leq 250$ MeV		
t		$7 \leq E_t \leq 300$ MeV		

Energy resolution for protons ca. 100-500 keV

Fig. 1.3

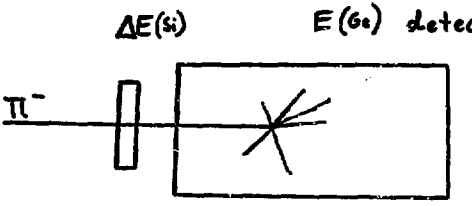

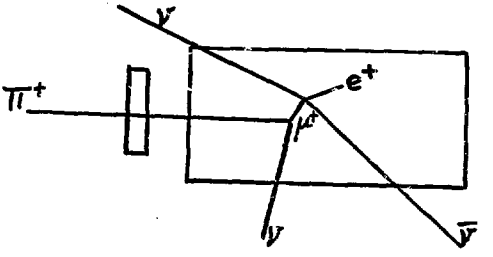

$\pi^+ \xrightarrow{26\,nsec} \mu^+ + \nu$

$\mu^+ \xrightarrow{2.2\,\mu sec} e^+ + \nu + \bar{\nu}$ $\quad E_{\mu^+} = 4.2$ MeV

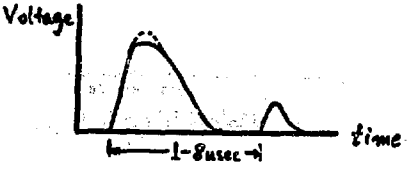

Fig. 1.4

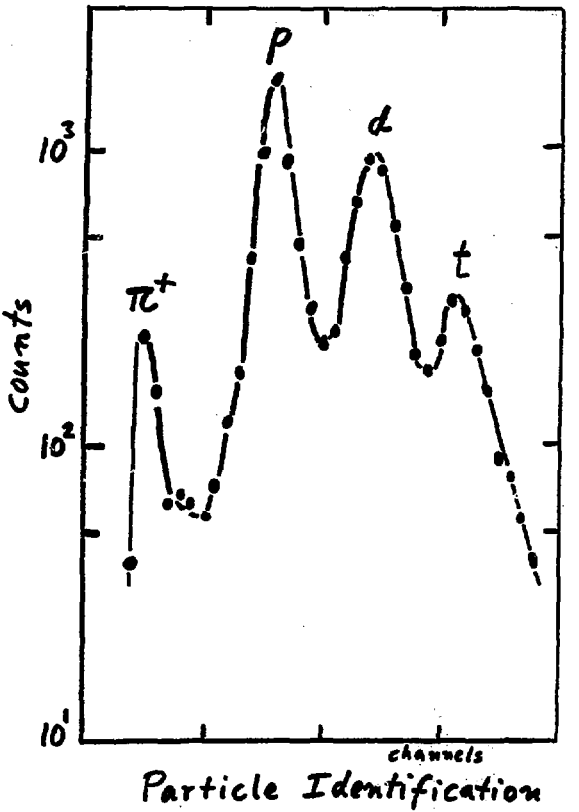

Fig. 1.5

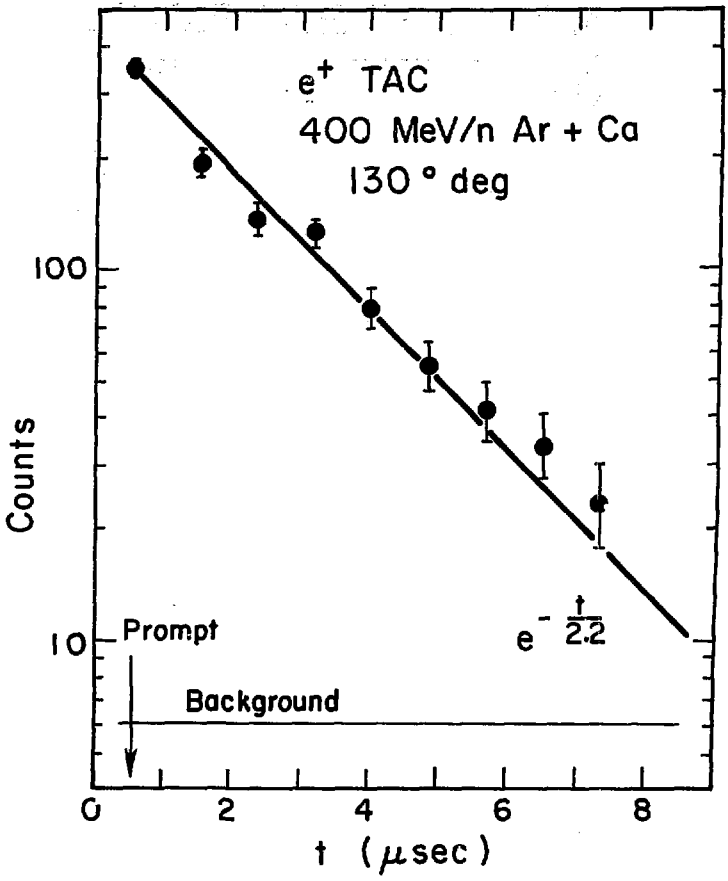
e+ TAC
400 MeV/n Ar + Ca
130 ° deg
100
10
Counts
Prompt
Background
e^- t/2.2
0
2
4
6
8
t (μsec)
XBL778-1637

Fig. 1.6

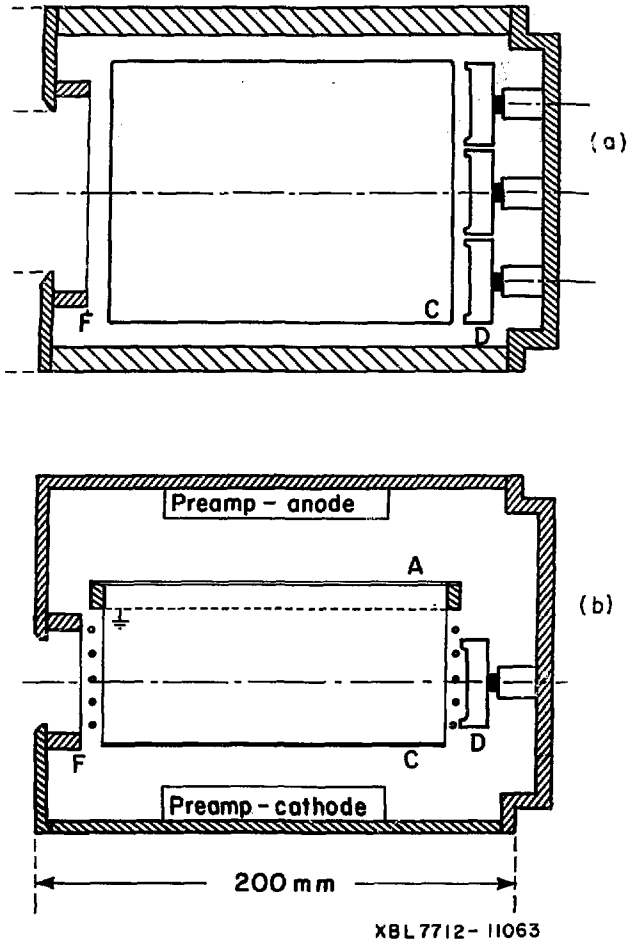
(a)
F
C
D
Preamp – anode
A
(b)
F
C
D
Preamp – cathode
200 mm
XBL7712-11063

Fig. 1.7

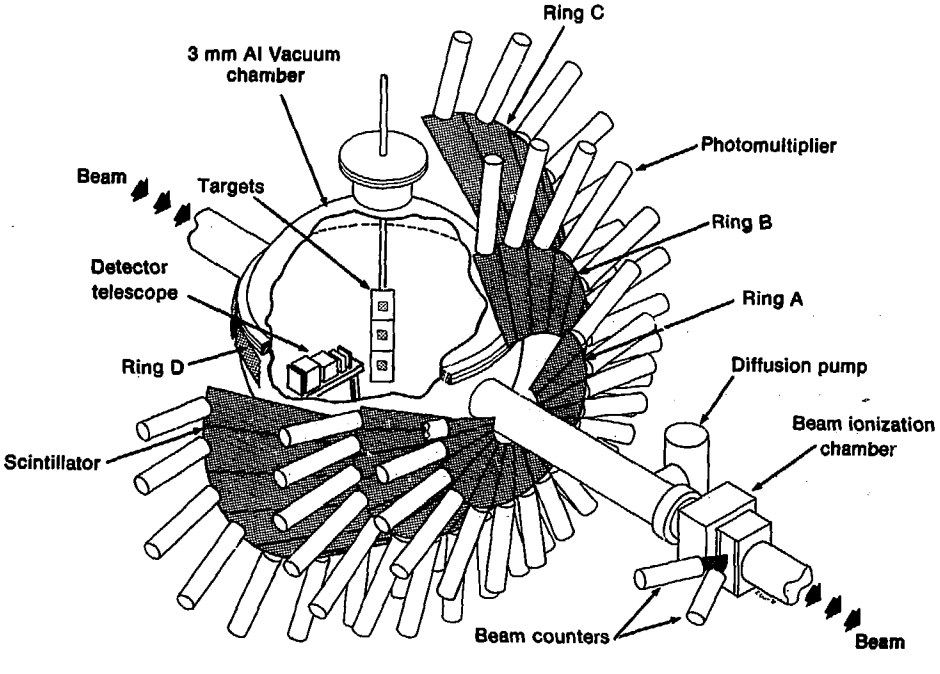
Ring C
3 mm Al Vacuum chamber
Photomultiplier
Beam
Targets
Ring B
Detector telescope
Ring A
Ring D
Diffusion pump
Beam ionization chamber
Scintillator
Beam counters
Beam
XBL 782-7229C

Fig. 1.8

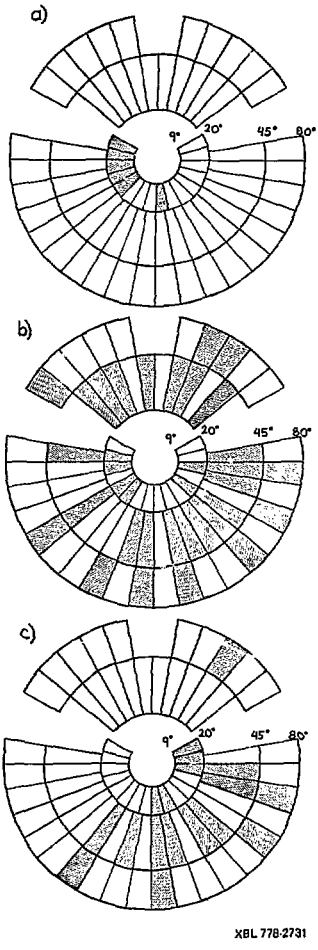

Fig. 1.9

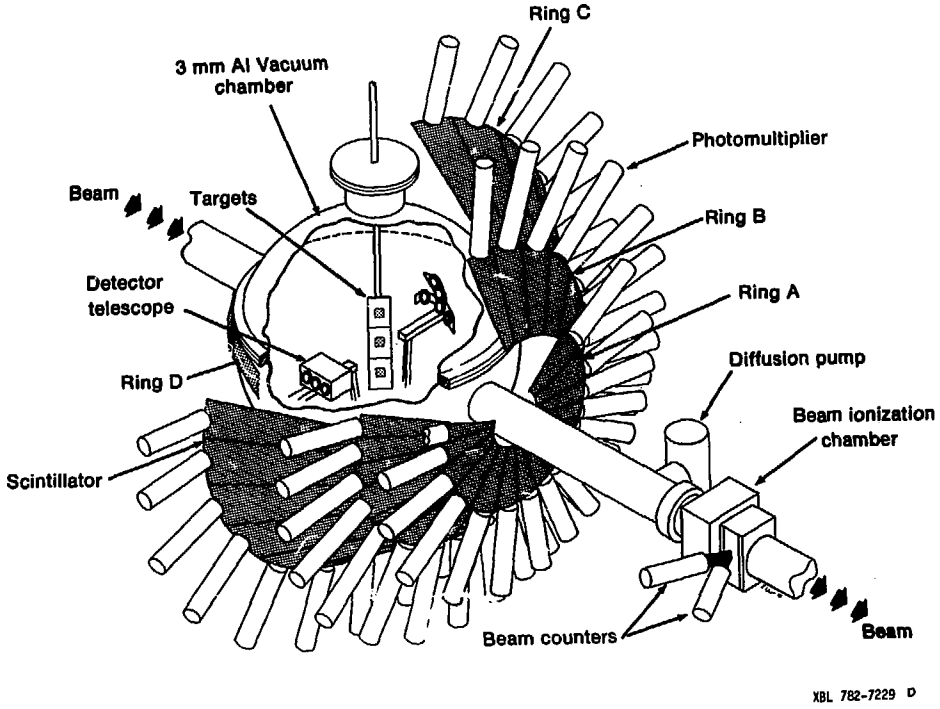
Ring C
3 mm Al Vacuum chamber
Photomultiplier
Beam
Targets
Ring B
Detector telescope
Ring A
Ring D
Diffusion pump
Beam ionization chamber
Scintillator
Beam counters
Beam
XBL 782-7229 D

Fig. 1.10

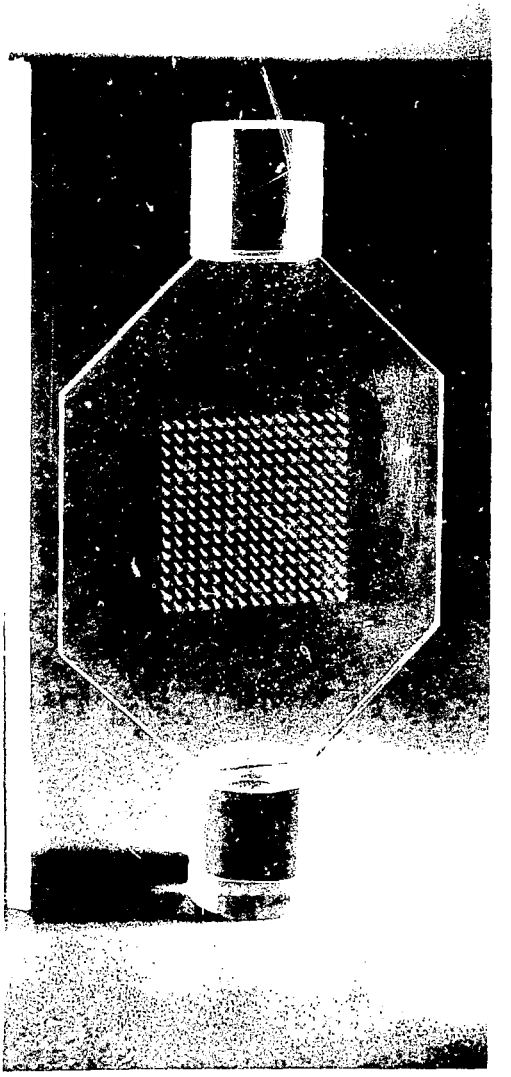

Fig. 1.11

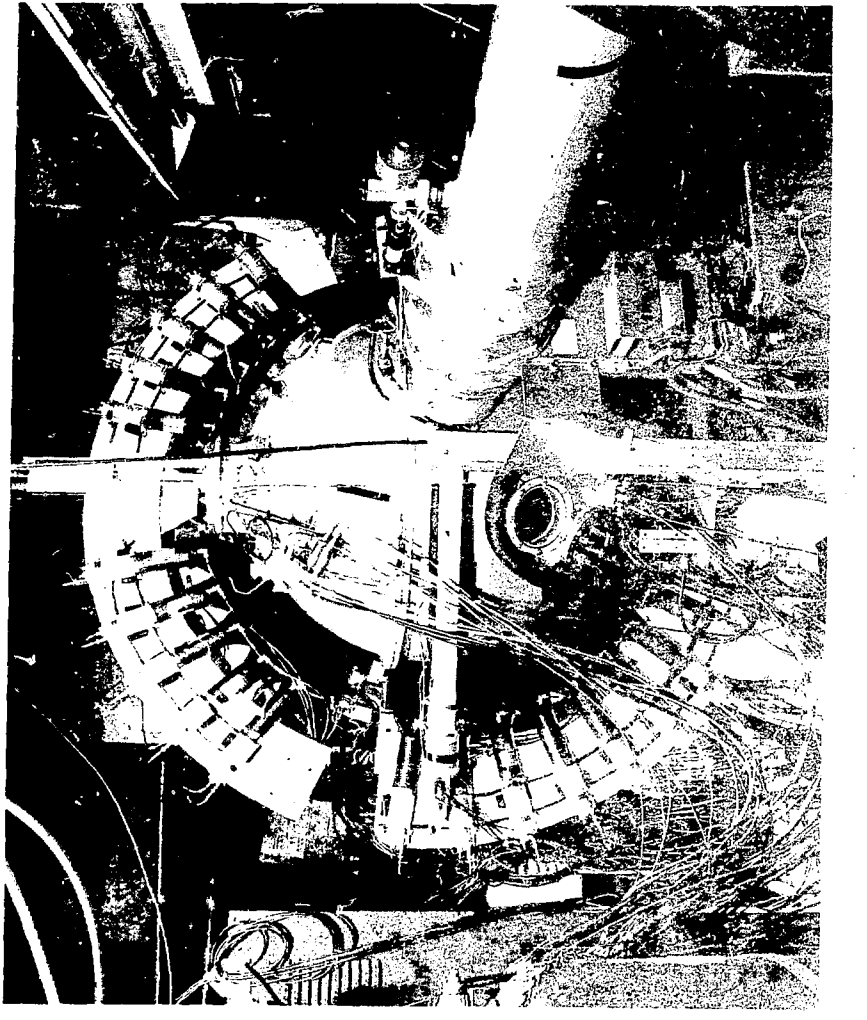

Summary of Data from Exp. 284H

Proj.	Energy (GeV/n)	Targets Al	Ca	Ag	Au	U
p	1.05	-	-	-	-	x
^{4}He	0.40	x	-	-	-	x
	1.05	-	-	-	-	x
^{20}Ne	0.25	-	-	-	-	x
	0.40	x	-	x	x	x
	1.05	-	-	-	-	x
	2.10	-	-	-	-	x
^{40}Ar	0.40	-	x	-	-	x
	1.05	-	x	-	-	x

Summary of Data from Exp. 377H

^{4}He	0.40			x	x	x
	1.05				x	x
	2.10				x	x
^{20}Ne	0.40				x	x

Fig. 1.13

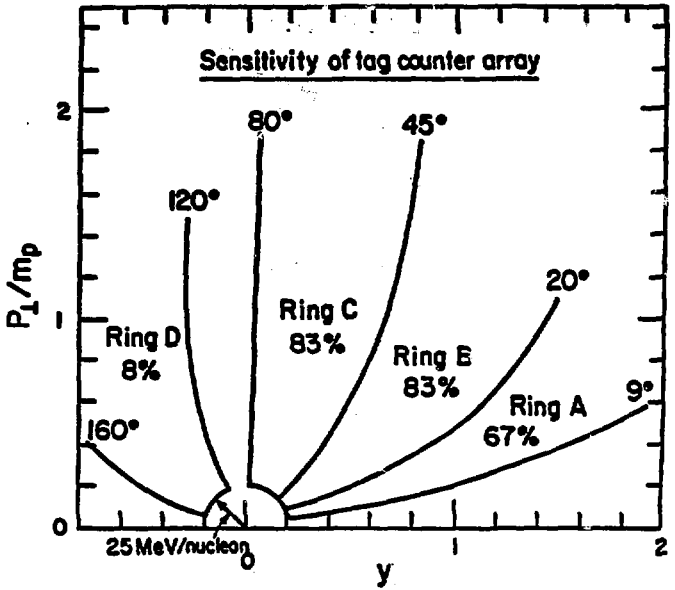

$$y = \frac{1}{2}\ln\left(\frac{E+p_\parallel}{E-p_\parallel}\right) = \frac{1}{2}\ln\left(\frac{1+\beta_\parallel}{1-\beta_\parallel}\right) = \tanh^{-1}\beta_\parallel \to \beta_\parallel$$

Fig. 1.14

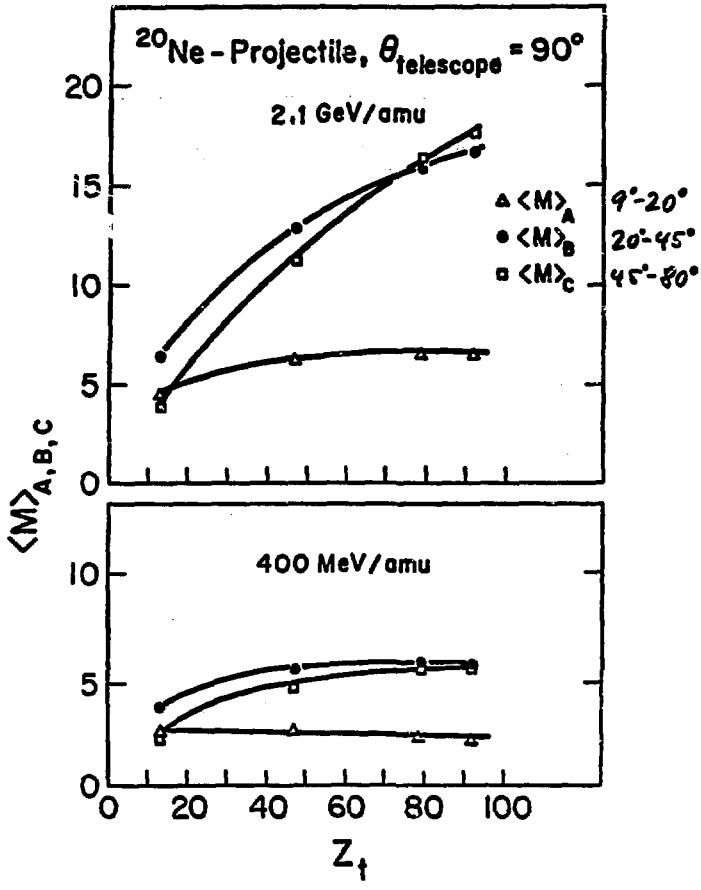
^{20}Ne - Projectile, $\theta_{telescope}$ = 90°
2.1 GeV/amu
400 MeV/amu
△ ⟨M⟩$_A$ 9°-20°
● ⟨M⟩$_B$ 20°-45°
□ ⟨M⟩$_C$ 45°-80°
⟨M⟩$_{A,B,C}$
Z_t
0
5
10
15
20
40
60
80
100

Fig. 1.15

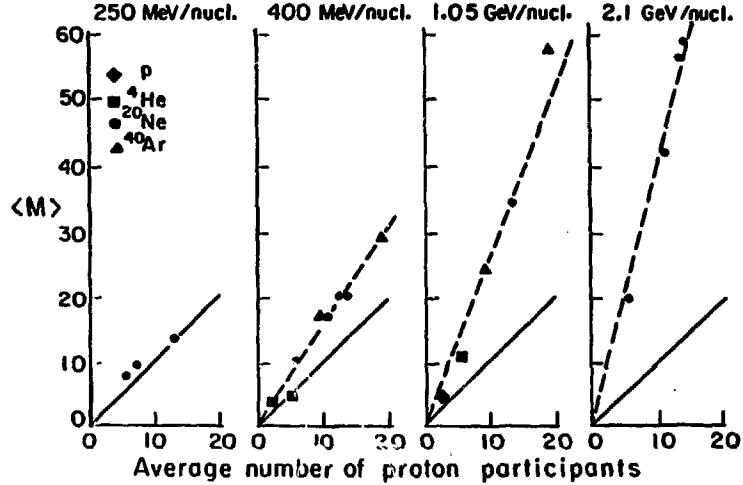

$$= \frac{\pi r_o^2 \left(Z_T A_P^{2/3} + Z_P A_T^{2/3} \right)}{\pi r_o^2 \left(A_P^{1/3} + A_T^{1/3} \right)^2}$$

Fig. 1.16

The strong increase in multiplicity as a function of projectile energy indicates:

a) There is no clean cut or hole with the participants exploding outside of the spectator environment

b) The energy and momentum transfer from the participant-region increases with increasing projectile energy thus creating more fast charged particles at intermediate rapidity.

Fig. 1.17

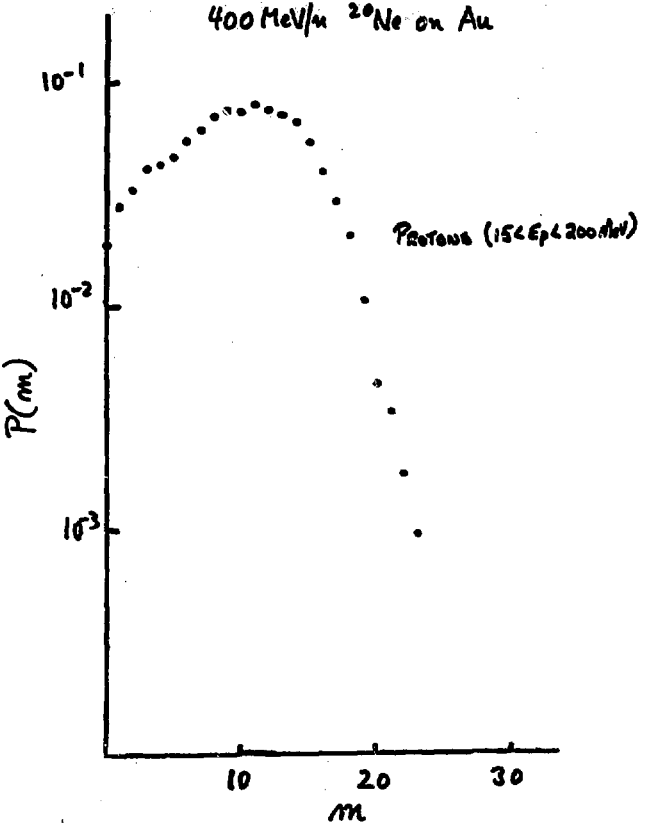
400 MeV/u ^{20}Ne on Au
10^{-1}
10^{-2}
10^{-3}
P(m)
$P_{Protons}$ (15 < E_p < 200 MeV)
10
20
30
m

Fig. 1.18

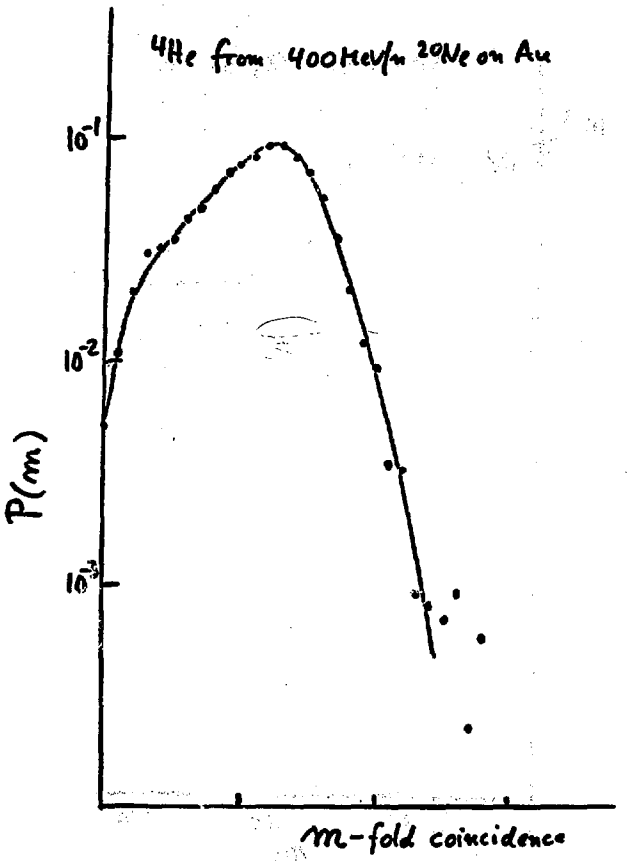

Fig. 1.19

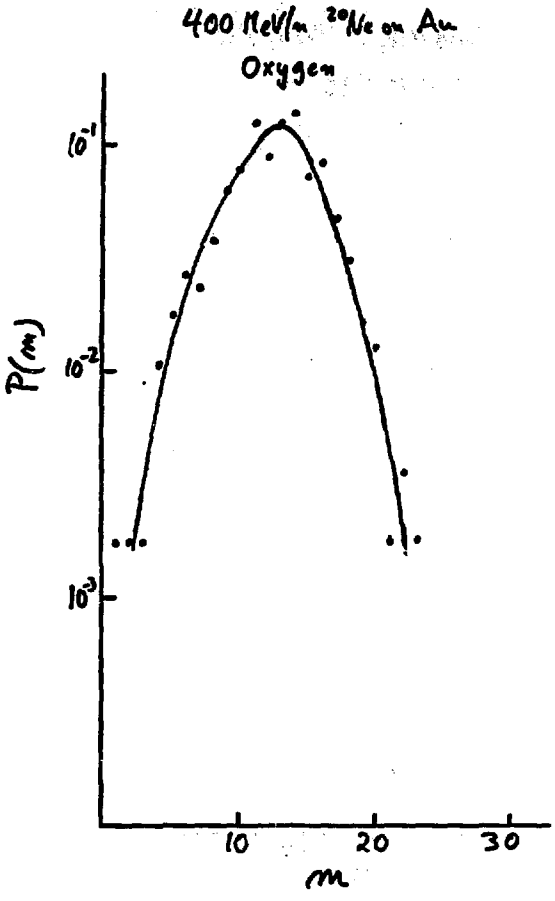

Fig. 1.20

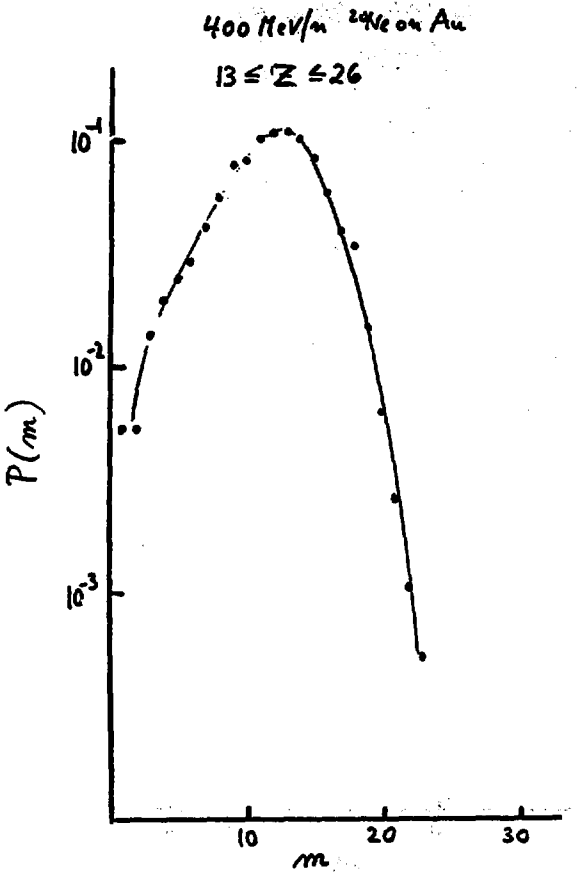

Fig. 1.21

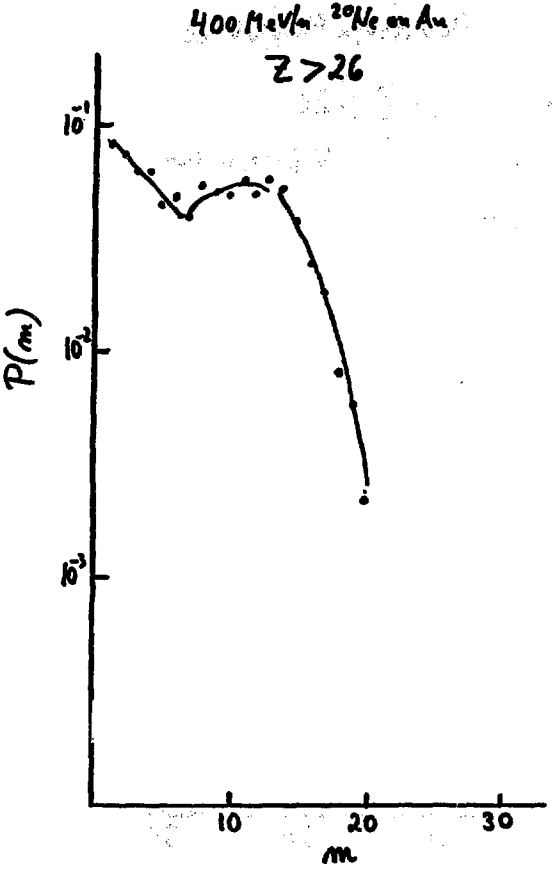

Fig. 1.22

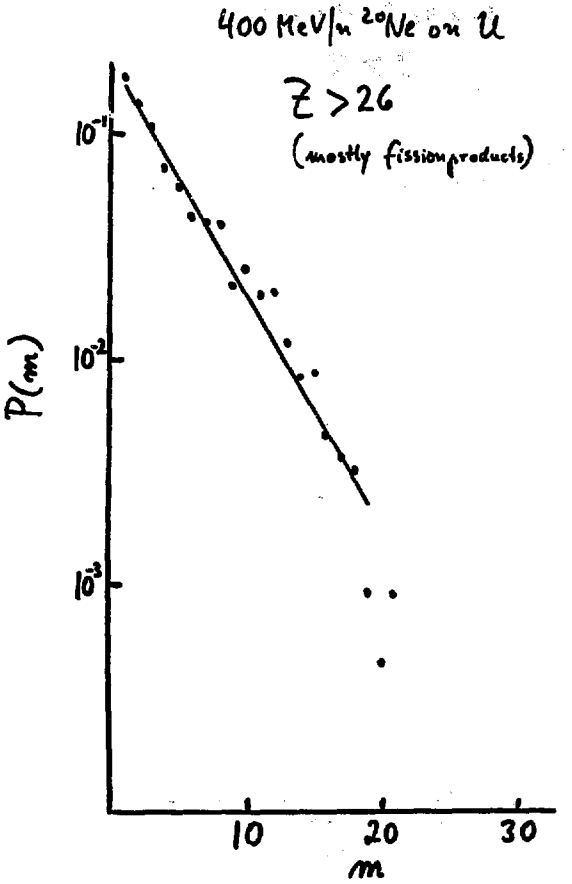
400 MeV/n ^{20}Ne on U
Z > 26
(mostly fission products)
10^{-1}
10^{-2}
10^{-3}
P(m)
10
20
30
m

Fig. 1.23

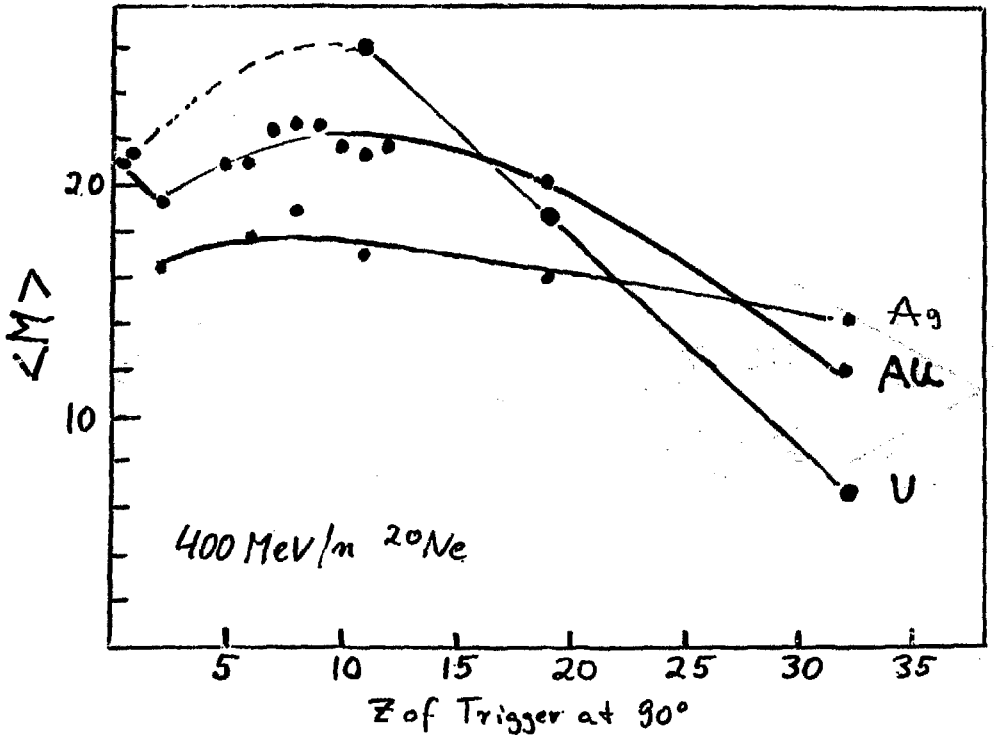

Fig. 1.24

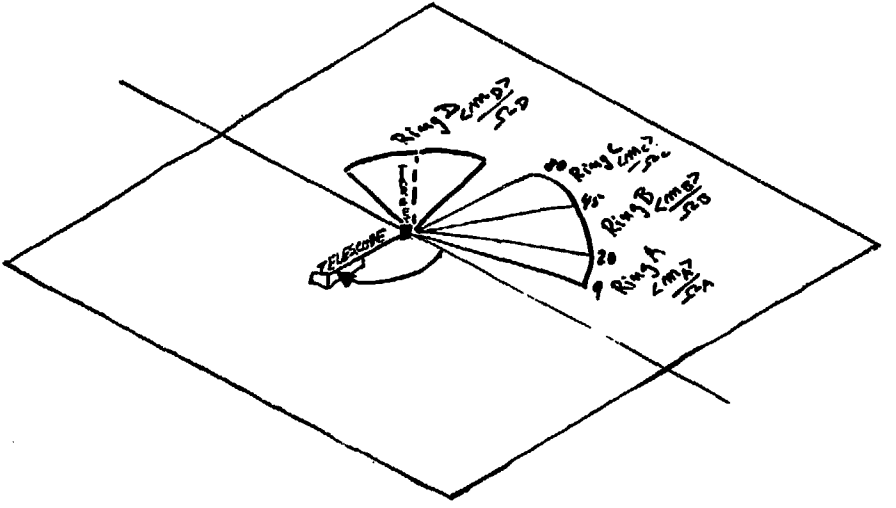
Ring D (cm-2)/sr
Ring C (cm-2)/sr
Ring B (cm-2)/sr
Ring A (cm-2)/sr
TELESCOPE
30
20
9

Fig. 1.25

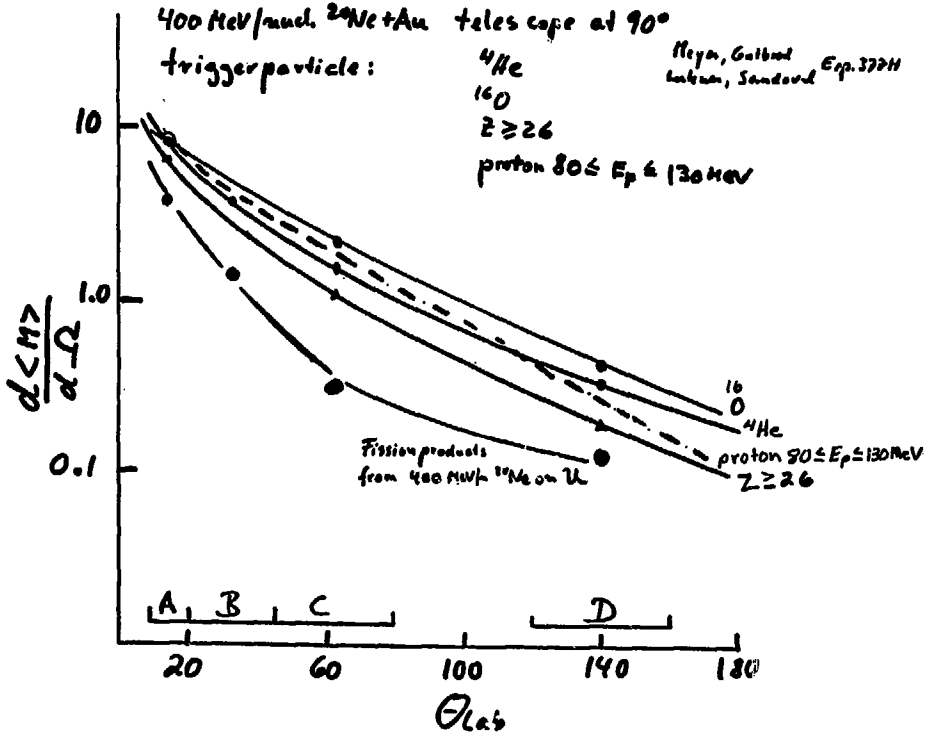
400 MeV/nucl. ^{20}Ne + Au telescope at 90°
trigger particle:
^{4}He
^{16}O
$Z \geq 26$
proton $80 \leq E_p \leq 130$ MeV
Meyer, Galbert, Lukasiak, Sandoval Exp. 377H
10
1.0
0.1
$\frac{d\langle M\rangle}{d\Omega}$
^{16}O
^{4}He
proton $80 \leq E_p \leq 130$ MeV
$Z \geq 26$
Fission products from 400 MeV/n ^{20}Ne on U
A
B
C
D
20
60
100
140
180
Θ_{Lab}

Fig. 1.26

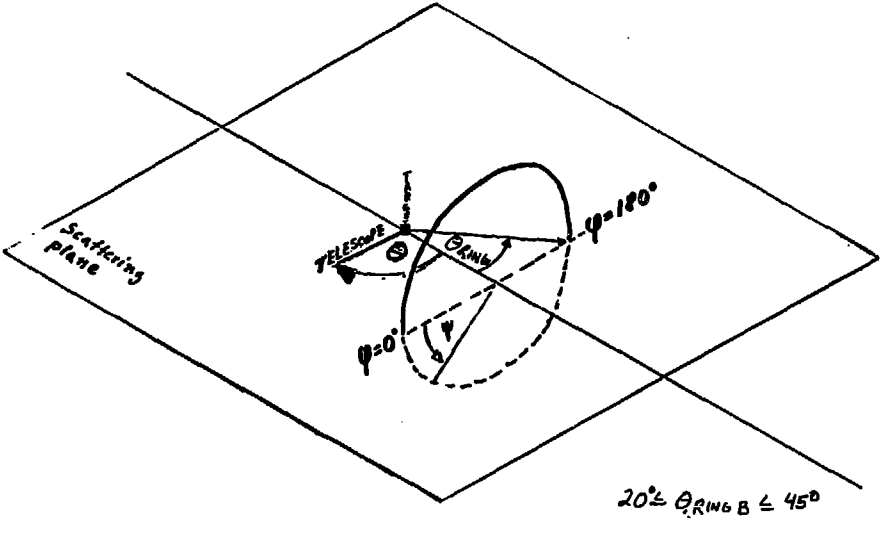

Fig. 1.27

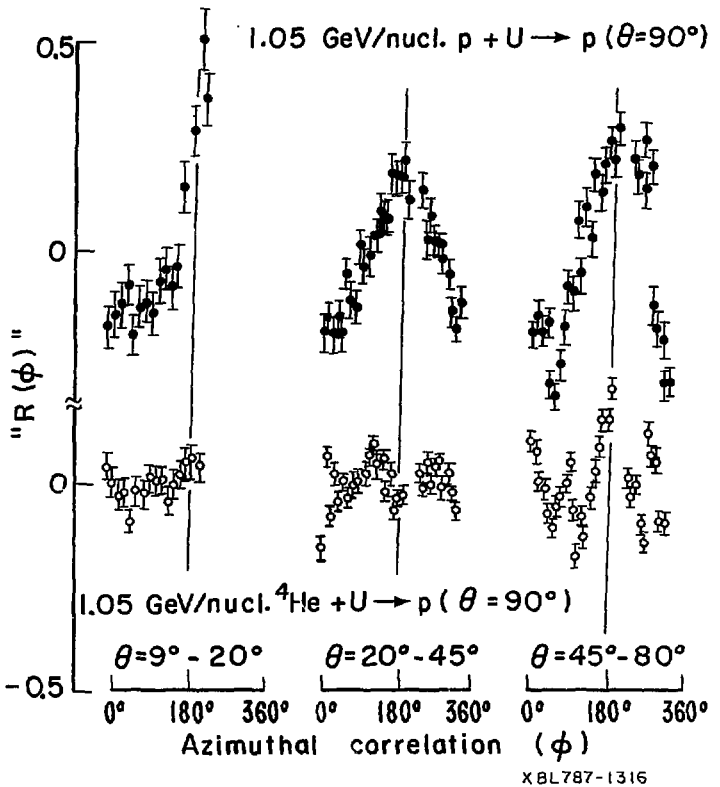
1.05 GeV/nucl. p + U → p (θ=90°)
0.5
0
0
-0.5
"R (φ) "
1.05 GeV/nucl. ⁴He + U → p (θ = 90°)
θ=9° - 20°
θ=20°-45°
θ=45°-80°
0° 180° 360°
0° 180° 360°
0° 180° 360°
Azimuthal correlation (φ)
X8L787-1316

Fig. 1.28

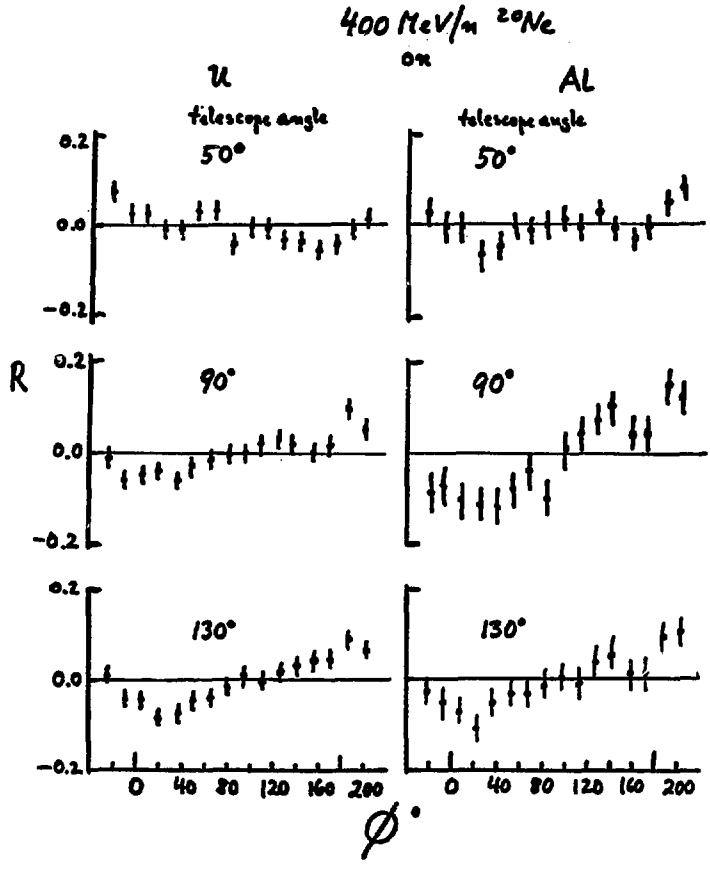
400 MeV/n ²⁰Ne
on
U
Al
telescope angle
telescope angle
50°
50°
90°
90°
130°
130°
R
0.2
0.0
-0.2
0
40
80
120
160
200
Ø°
trigger particle proton (35 ≤ Eₚ ≤ 200)

Fig. 1.29

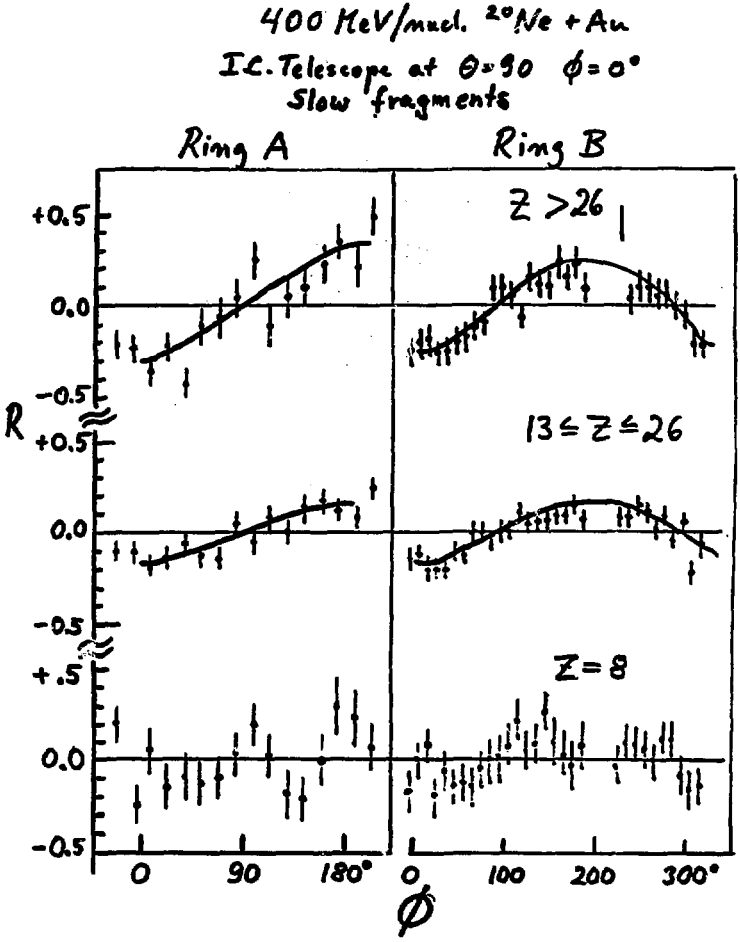
400 MeV/nucl. 20Ne + Au
I.C. Telescope at θ=90 φ=0°
Slow fragments
Ring A
Ring B
Z >26
13≤Z≤26
Z=8
R
+0.5
0.0
-0.5
+.5
0
90
180°
100
200
300°
φ

Fig. 1.30

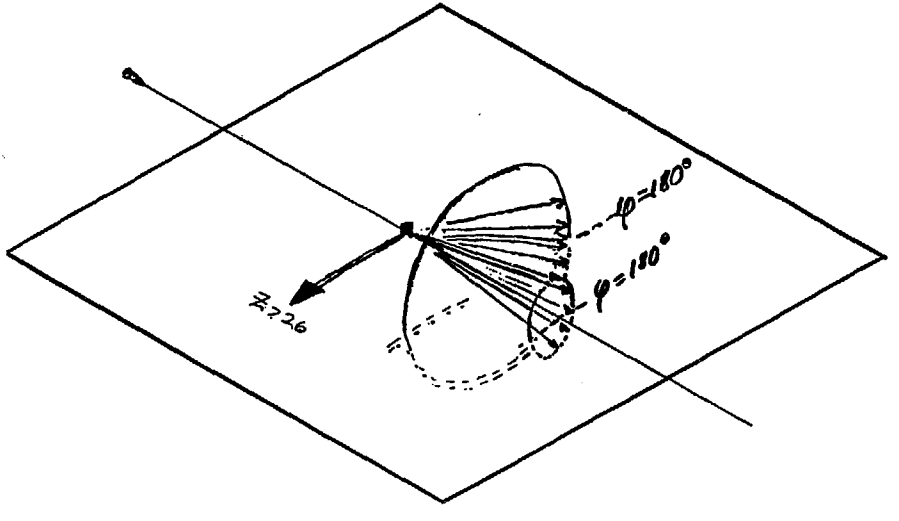

Fig. 1.31

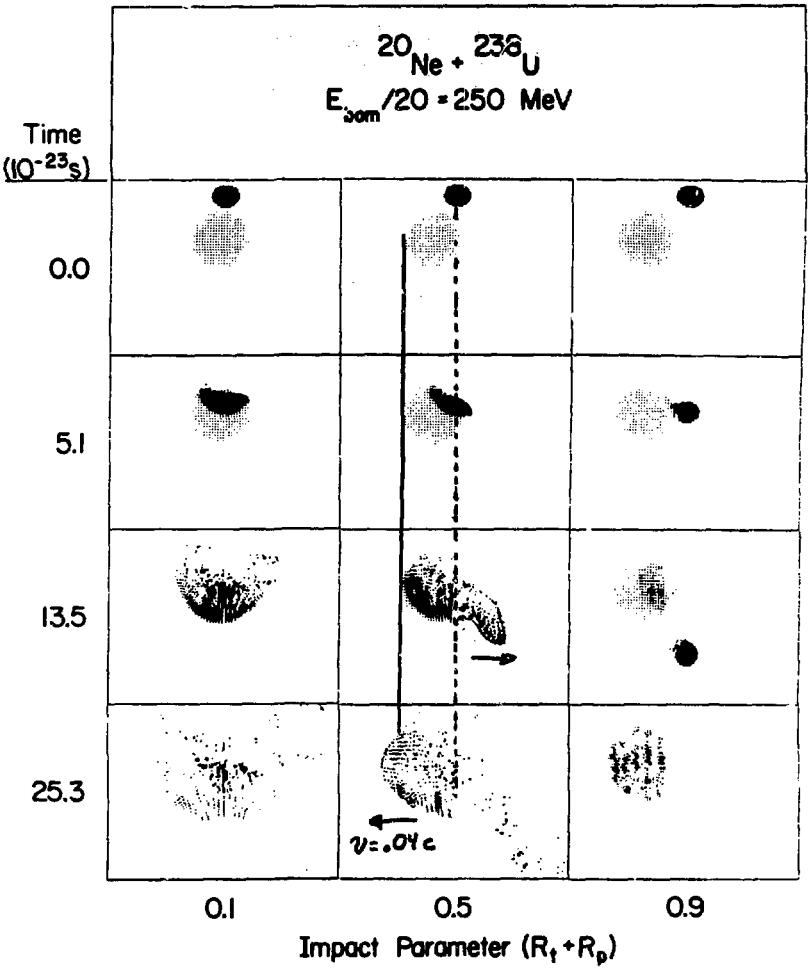
$^{20}Ne + ^{238}U$
$E_{lab}/20 = 250$ MeV
Time
$(10^{-23}s)$
0.0
5.1
13.5
25.3
$v = .04c$
0.1
0.5
0.9
Impact Parameter $(R_t + R_p)$

Fig. 1.32

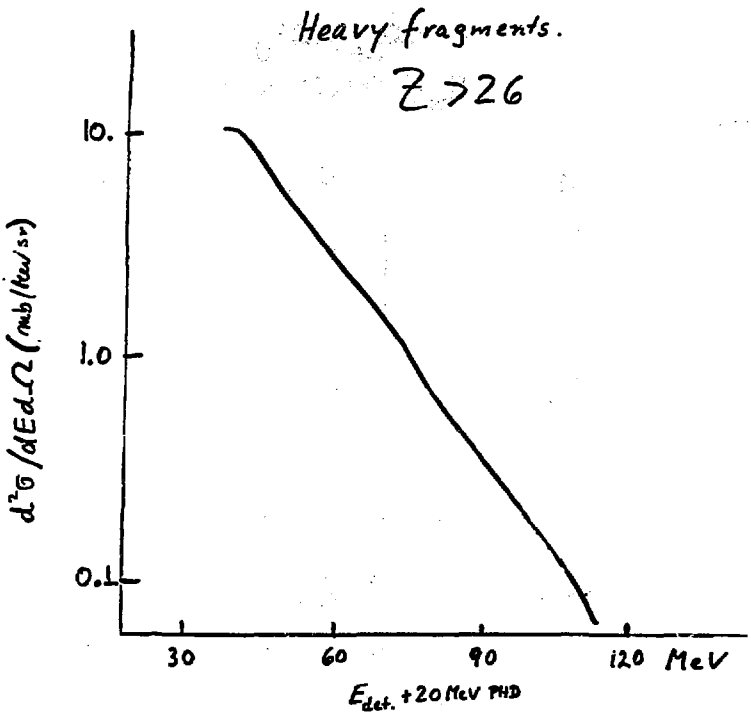
Heavy fragments.
Z >26
10.
1.0
0.1
d²σ/dEdΩ (mb/MeV sr)
30
60
90
120 MeV
E det. +20 MeV PHD

Fig. 1.33

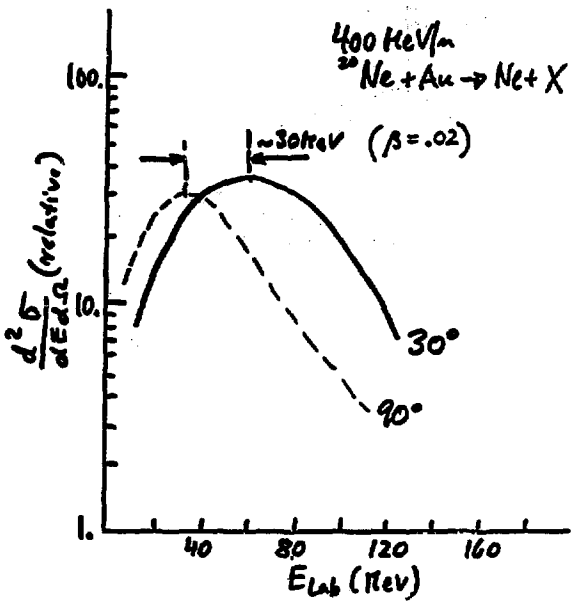
400 MeV/n
$^{20}Ne + Au \rightarrow Ne + X$
~30MeV (β = .02)
100.
10.
1.
$\frac{d^2\sigma}{dE d\Omega}$ (relative)
30°
90°
40
80
120
160
E_{Lab} (MeV)

Fig. 1.34

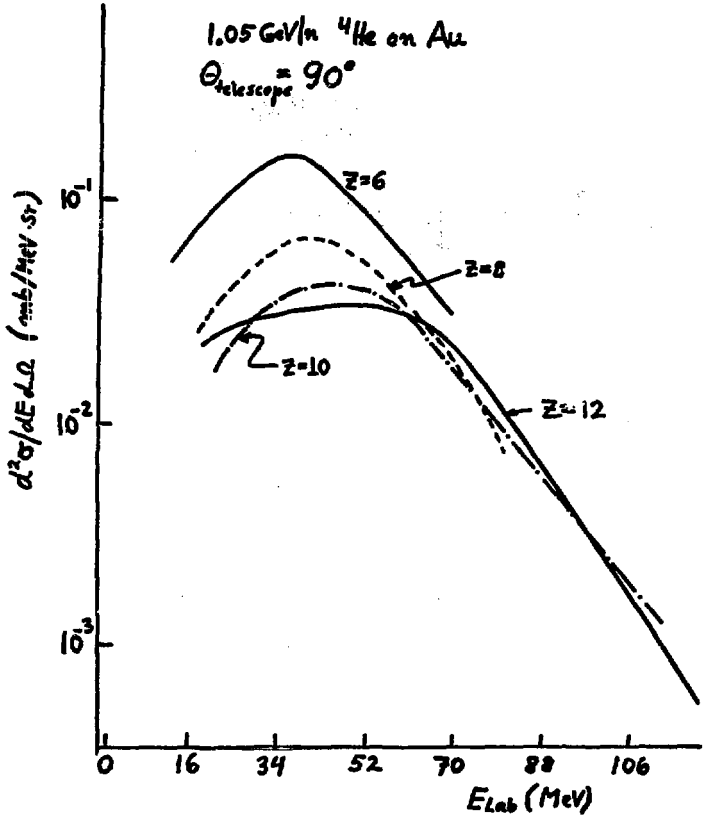
1.05 GeV/n 4He on Au
θtelescope = 90°
Z=6
Z=8
Z=10
Z=12
d²σ/dE dΩ (mb/MeV sr)
10⁻¹
10⁻²
10⁻³
0
16
34
52
70
88
106
ELab (MeV)

Fig. 1.35

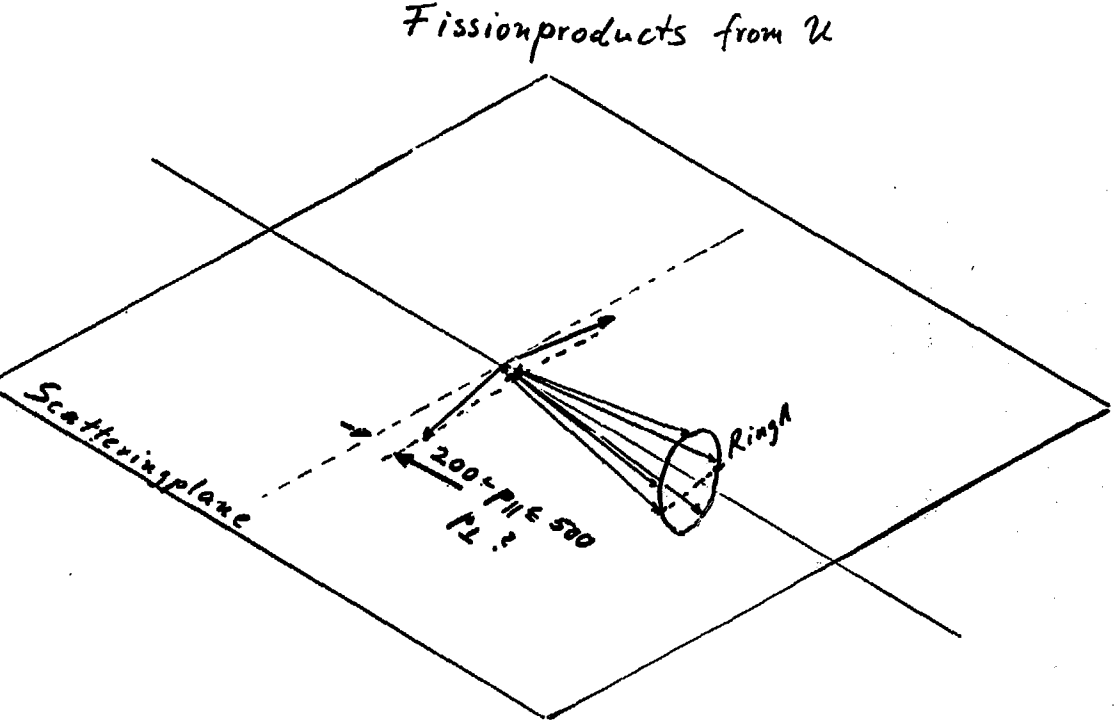

Fig. 1.36

$P_{\parallel}$ in peripheral reactions leading to fission of the spectator

Reaction	$P_{\parallel}$ (MeV/c)
400 MeV/n ^{20}Ne+U	500
400 MeV/n ^{4}He+U	480
1050 MeV/n ^{4}He+U	430
2100 MeV/n ^{4}He+U	220

Fig. 1.37

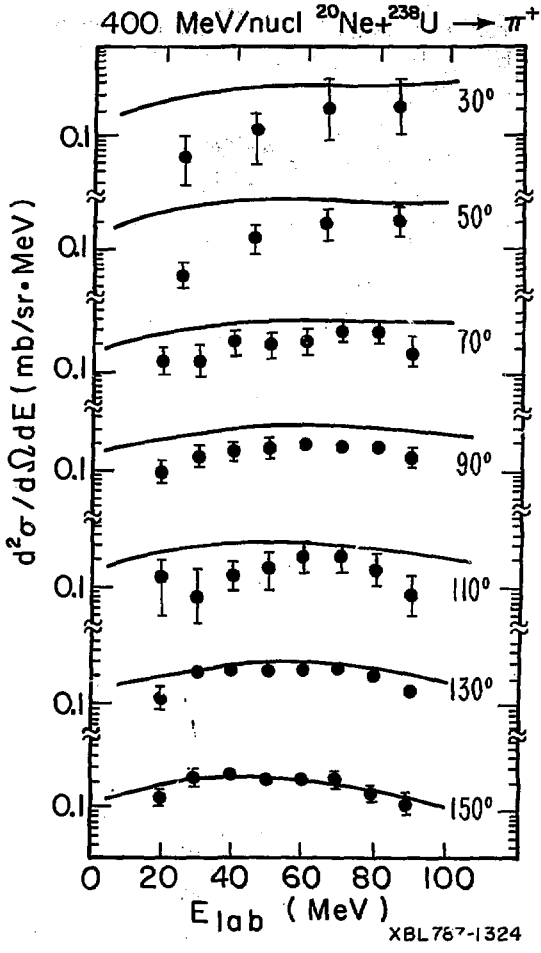
400 MeV/nucl $^{20}Ne+^{238}U \rightarrow \pi^+$
$d^2\sigma/d\Omega dE$ (mb/sr•MeV)
0.1
30°
50°
70°
90°
110°
130°
150°
0
20
40
60
80
100
E_{lab} (MeV)
XBL767-1324

Fig. 1.38

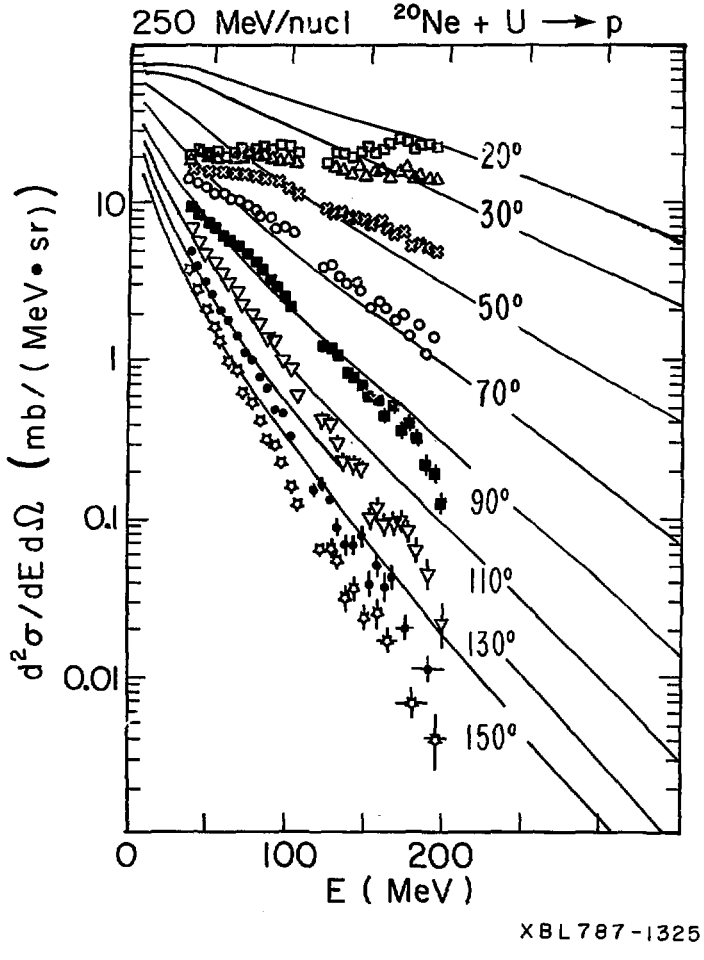
250 MeV/nucl ^{20}Ne + U → p
20°
30°
50°
70°
90°
110°
130°
150°
10
1
0.1
0.01
$d^2\sigma/dE\,d\Omega$ (mb/(MeV • sr))
0
100
200
E (MeV)
XBL787-1325

Fig. 1.39

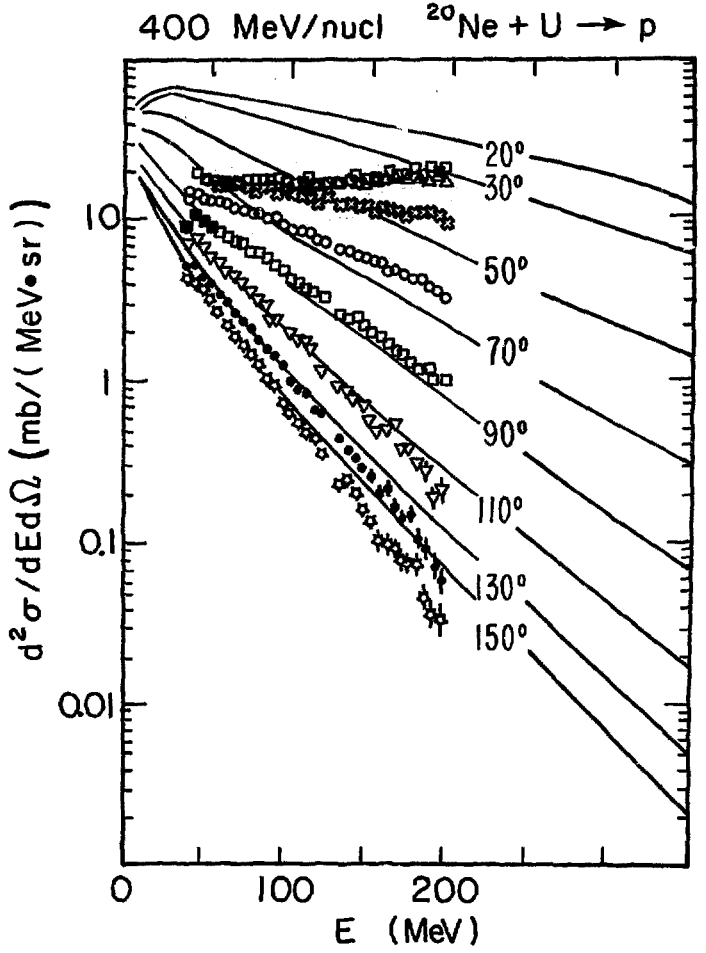
400 MeV/nucl $^{20}Ne + U \rightarrow p$
20°
30°
50°
70°
90°
110°
130°
150°
10
1
0.1
0.01
$d^2\sigma/dEd\Omega$ (mb/(MeV•sr))
0
100
200
E (MeV)
XBL787-1326

Fig. 1.40

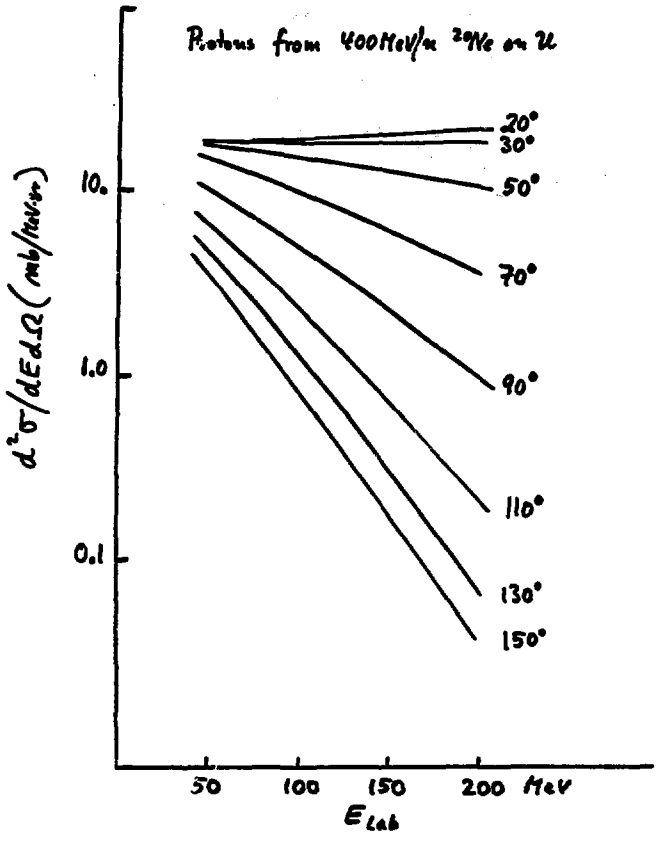
Protons from 400MeV/u 20Ne on U
20°
30°
50°
70°
90°
110°
130°
150°
10.
1.0
0.1
d²σ/dEdΩ (mb/MeV sr)
50
100
150
200 MeV
E Lab

Fig. 1.41

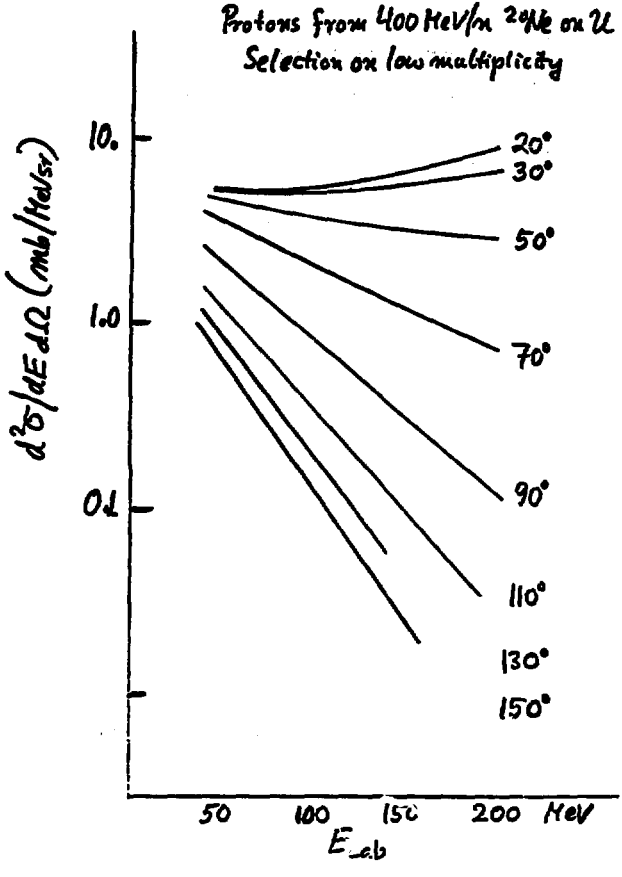
Protons from 400 MeV/n 20Ne on U
Selection on low multiplicity
d²σ/dE dΩ (mb/MeV/sr)
10.
1.0
0.1
20°
30°
50°
70°
90°
110°
130°
150°
50
100
150
200 MeV
E_lab

Fig. 1.42

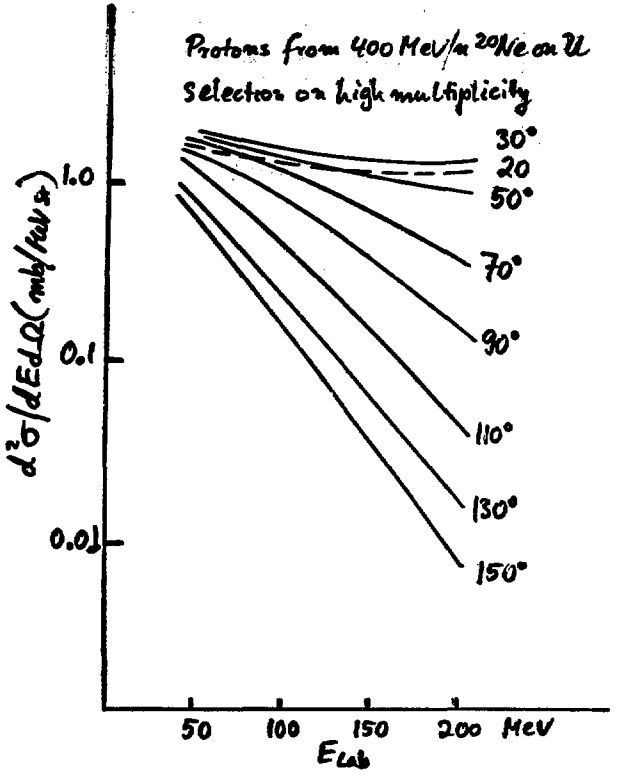
Protons from 400 MeV/n 20Ne on U
Selector on high multiplicity
30°
20
50°
70°
90°
110°
130°
150°
1.0
0.1
0.01
d²σ/dEdΩ (mb/MeV sr)
50
100
150
200 MeV
E Lab

Fig. 1.43

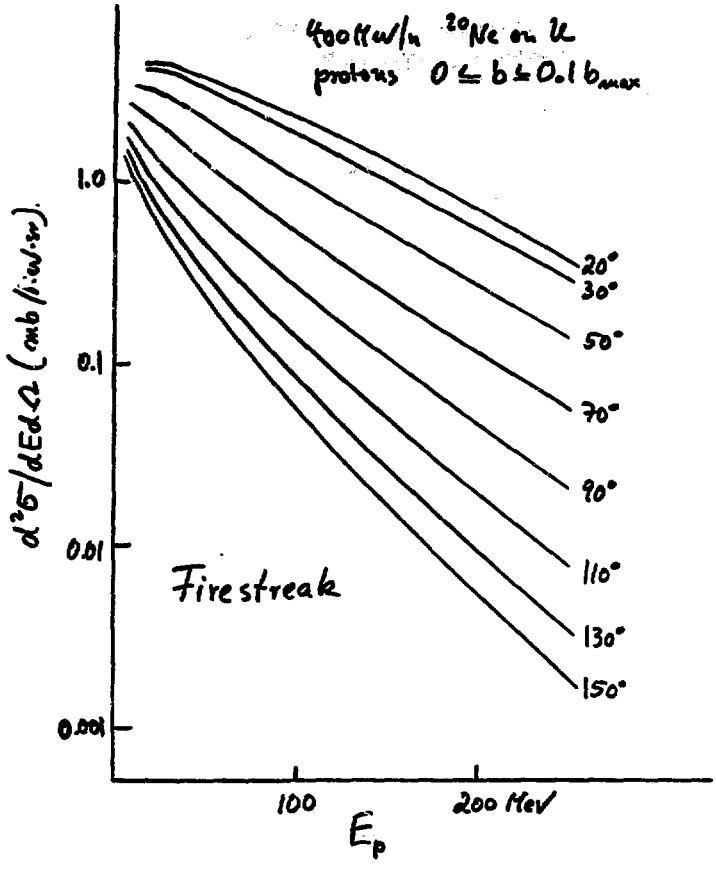
400 Mev/n ^{20}Ne on U
protons $0 \leq b \leq 0.1\, b_{max}$
20°
30°
50°
70°
90°
110°
130°
150°
1.0
0.1
0.01
0.001
Firestreak
100
200 Mev
E_p
$d^2\sigma/dE d\Omega$ (mb/l.n.s.r.)

Fig. 1.44

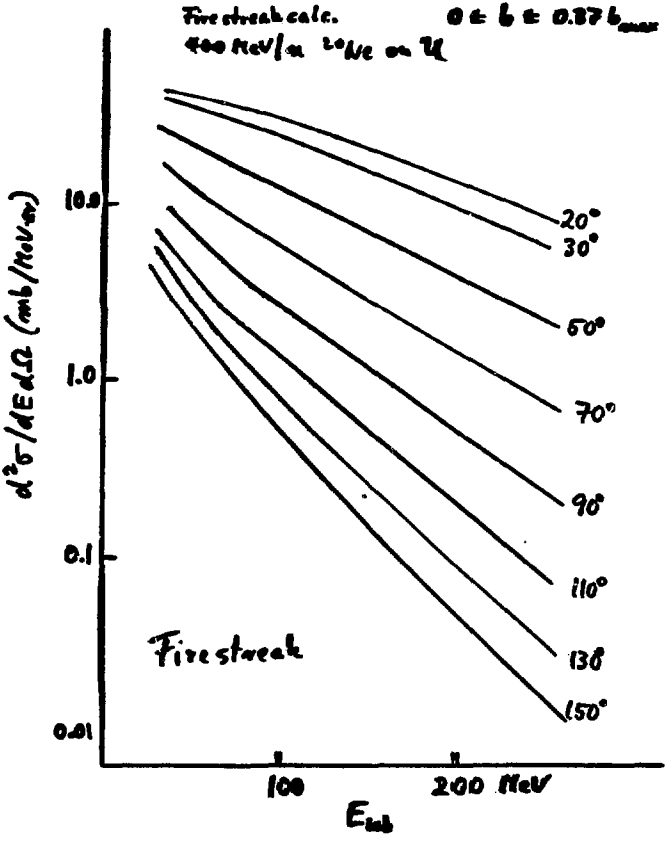
Fire streak calc.
0 ≤ b ≤ 0.87 b_max
400 MeV/u ²⁰Ne on U
10.0
1.0
0.1
0.01
d²σ/dEdΩ (mb/MeV sr)
20°
30°
50°
70°
90°
110°
130°
150°
Fire streak
100
200 MeV
E_lab

Fig. 1.45

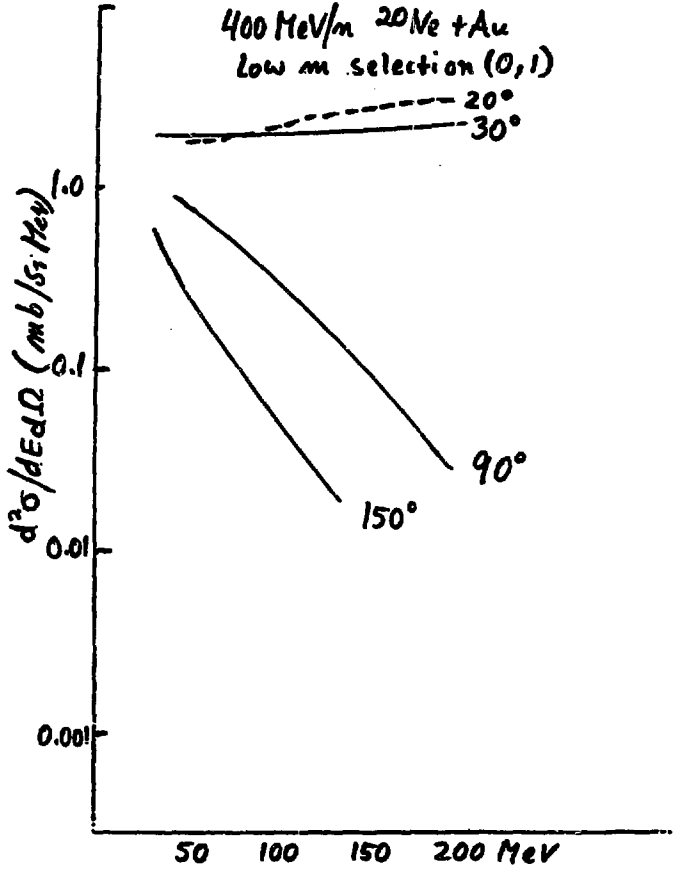
400 MeV/n 20Ne + Au
Low m selection (0,1)
20°
30°
90°
150°
1.0
0.1
0.01
0.001
d²σ/dEdΩ (mb/Sr·MeV)
50
100
150
200 MeV

Fig. 1.46

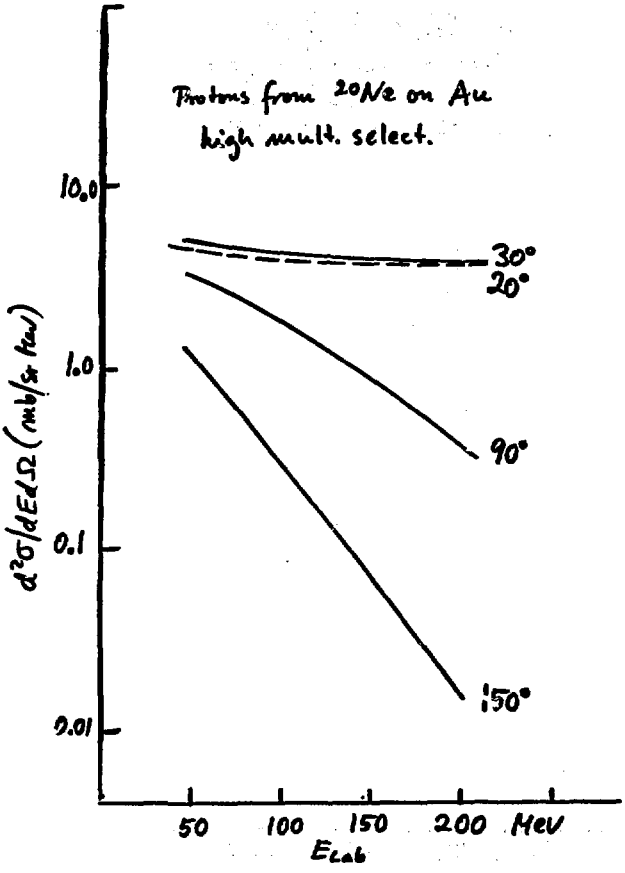
Protons from 20Ne on Au
high mult. select.
10.0
1.0
0.1
0.01
d²σ/dEdΩ (mb/sr MeV)
30°
20°
90°
150°
50
100
150
200 MeV
E_Lab

Fig. 1.47

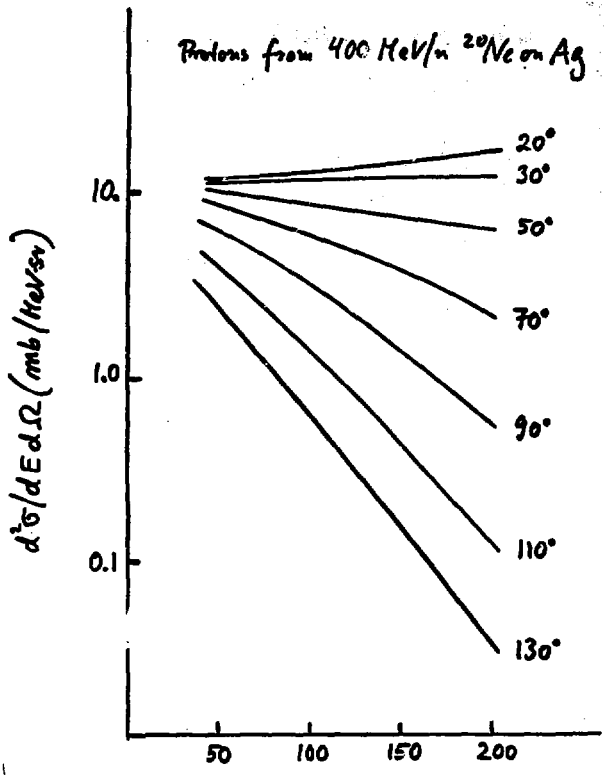
Protons from 400 MeV/n ^{20}Ne on Ag
$d^2\sigma/dE\,d\Omega$ (mb/MeV sr)
10.
1.0
0.1
20°
30°
50°
70°
90°
110°
130°
50
100
150
200

Fig. 1.48

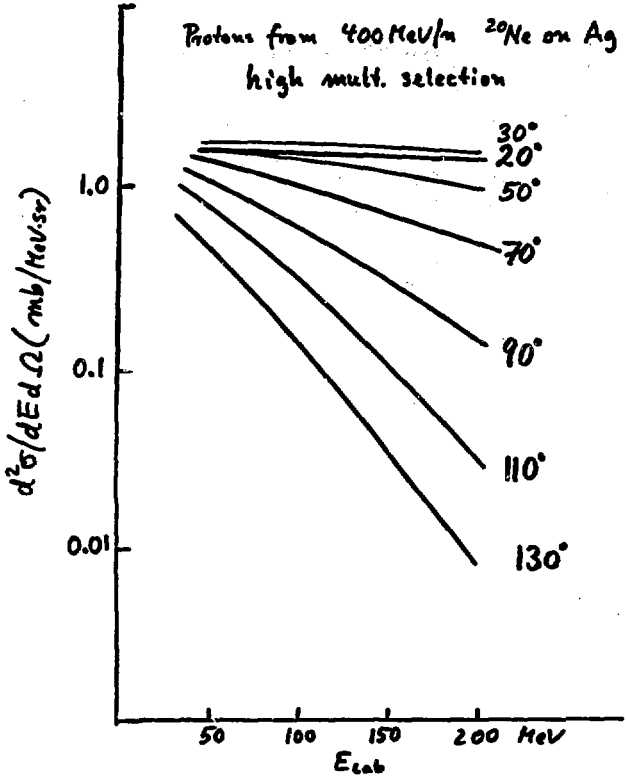
Protons from 400 MeV/n ^{20}Ne on Ag
high mult. selection
30°
20°
50°
70°
90°
110°
130°
1.0
0.1
0.01
$d^2\sigma/dE\,d\Omega$ (mb/MeV·sr)
50
100
150
200 MeV
E_{cab}

Fig. 1.49

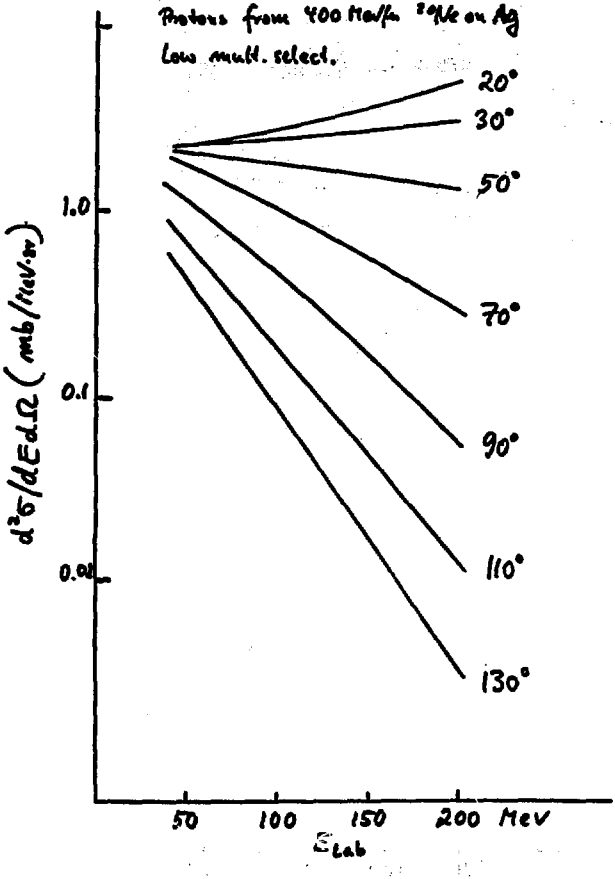
Protons from 400 Mev/a ^{20}Ne on Ag
Low mult. select.
20°
30°
50°
70°
90°
110°
130°
1.0
0.1
0.01
$d^2\sigma/dE d\Omega$ (mb/Mev.sr)
50
100
150
200 Mev
E_{Lab}

Fig. 1.50

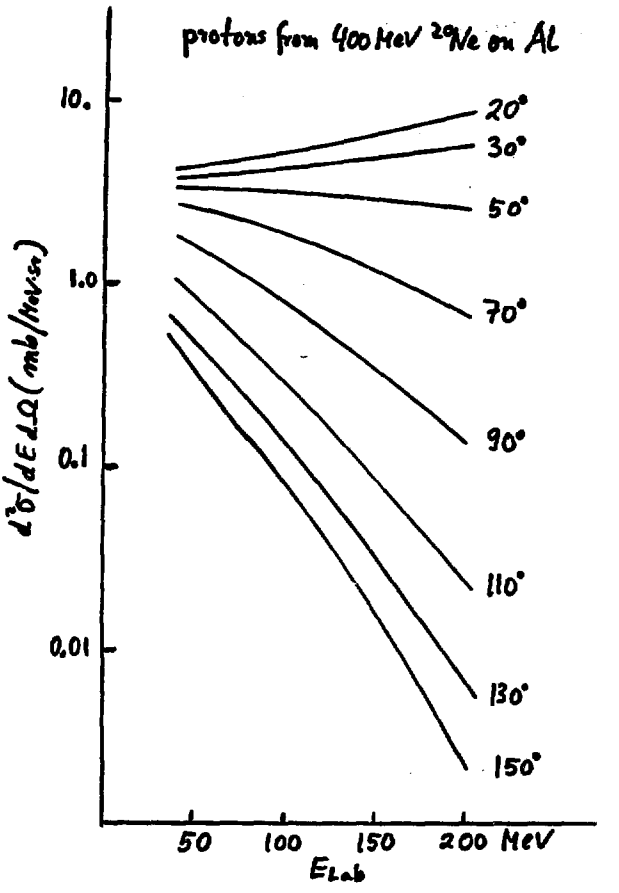
protons from 400 MeV 20Ne on Al
10.
1.0
0.1
0.01
d²σ/dEdΩ (mb/MeV sr)
20°
30°
50°
70°
90°
110°
130°
150°
50
100
150
200 MeV
ELab

Fig. 1.51

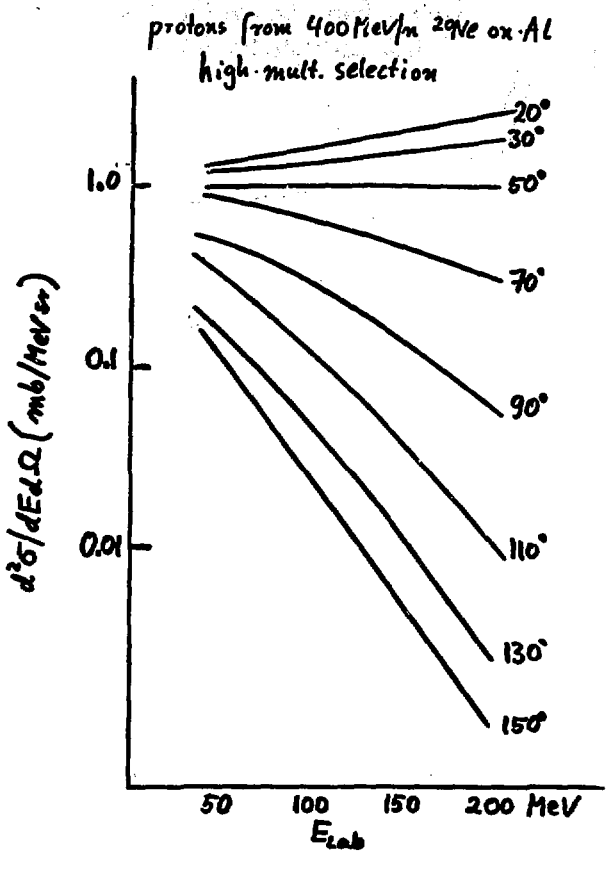
protons from 400 MeV/n ^{20}Ne on Al
high mult. selection
20°
30°
50°
70°
90°
110°
130°
150°
1.0
0.1
0.01
$d^2\sigma/dE\,d\Omega$ (mb/MeVsr)
50
100
150
200 MeV
E_{Lab}

Fig. 1.52

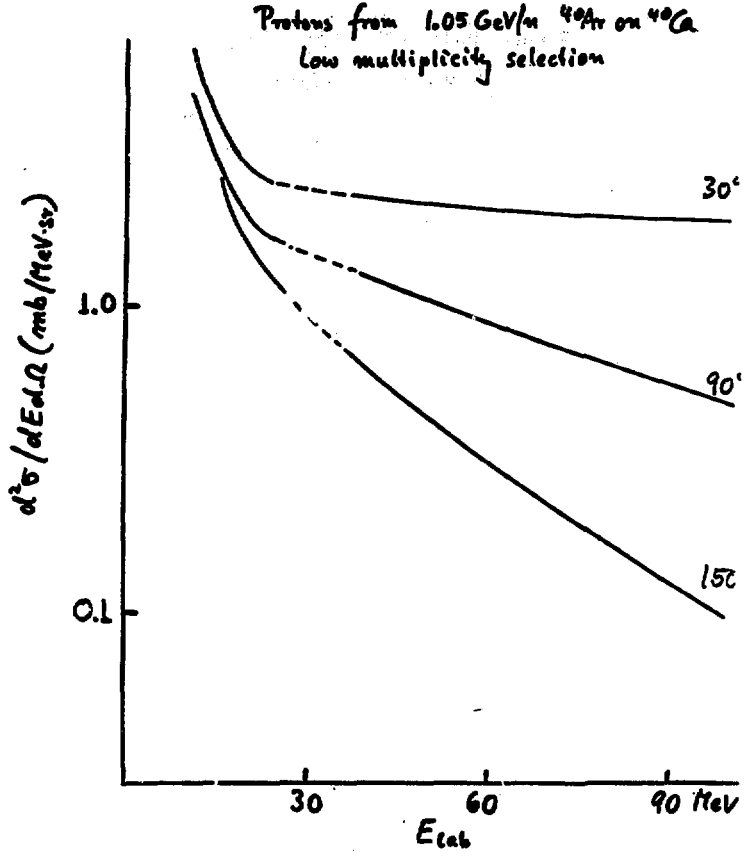
Protons from 1.05 GeV/n 40Ar on 40Ca
Low multiplicity selection
30°
90°
15°
1.0
0.1
d²σ/dEdΩ (mb/MeV·sr)
30
60
90 MeV
E lab

Fig. 1.53

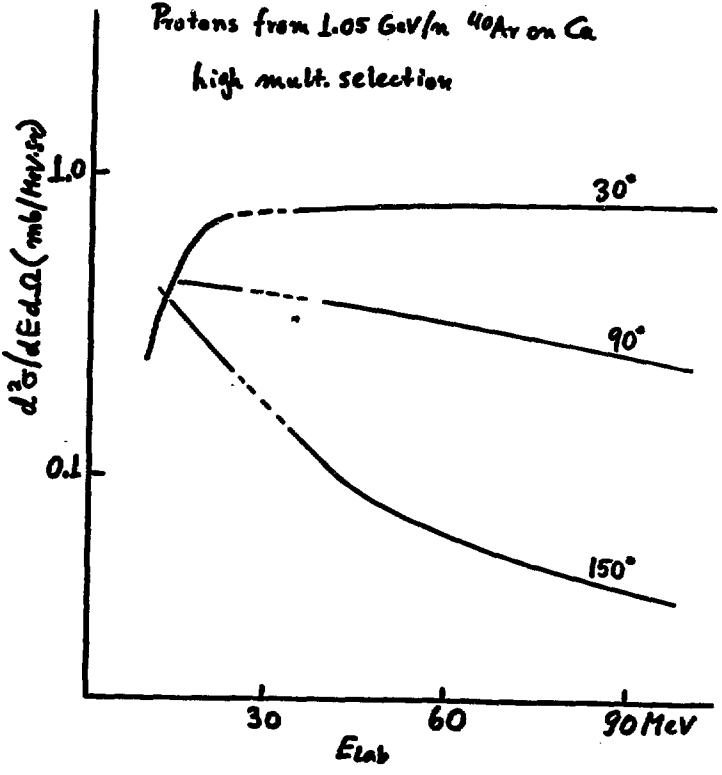
Protons from 1.05 GeV/n 40Ar on Ca
high mult. selection
d²σ/dEdΩ (mb/MeV/sr)
1.0
0.1
30°
90°
150°
30
60
90 MeV
Elab

Fig. 1.54

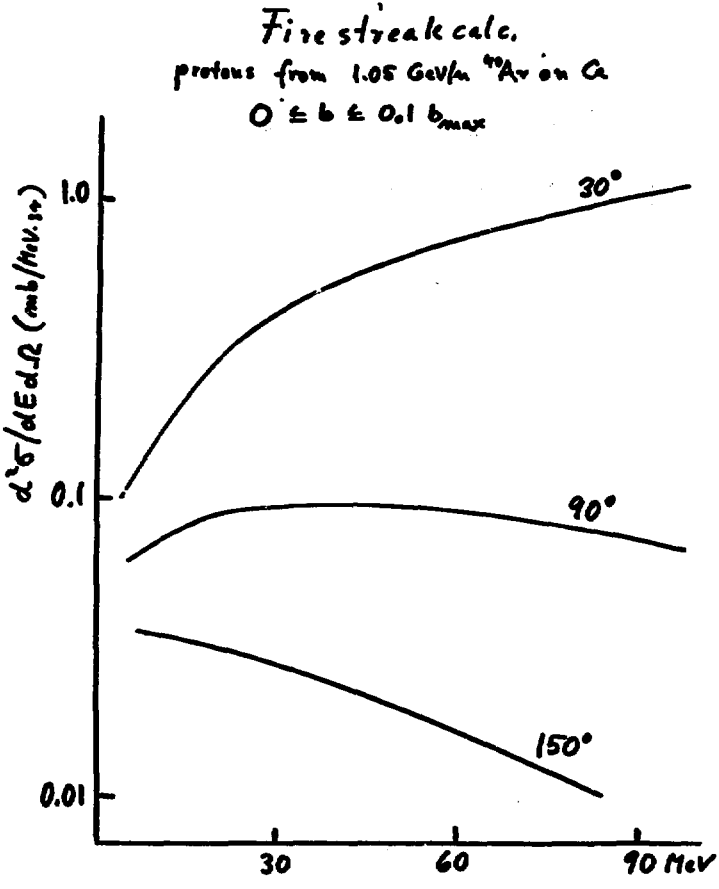
Fire streak calc.
protons from 1.05 GeV/n 40Ar on Ca
0 ≤ b ≤ 0.1 bmax
d²σ/dEdΩ (mb/MeV.sr)
1.0
0.1
0.01
30°
90°
150°
30
60
90 MeV

Fig. 1.55

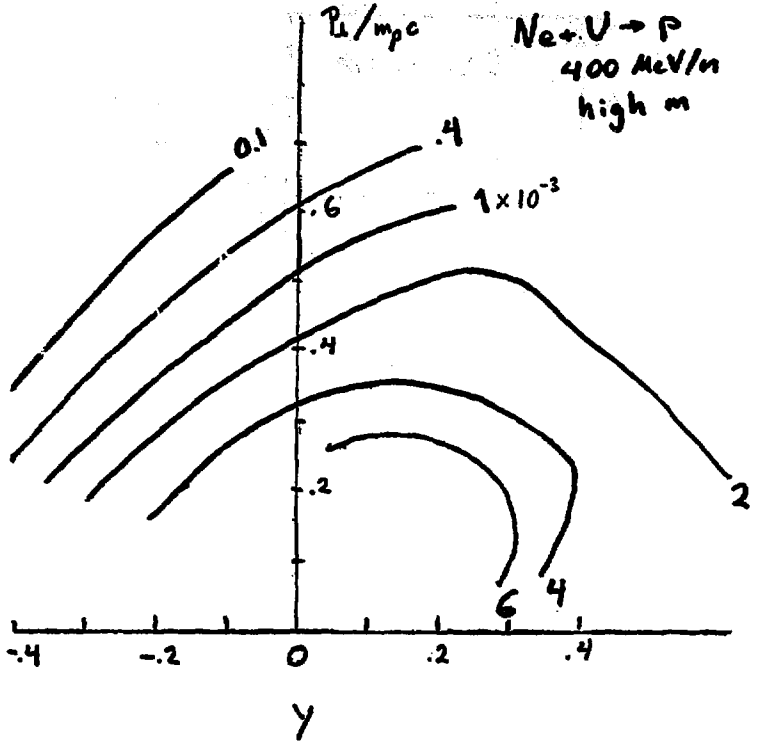

$y_B = 0.89$

Fig. 1.56

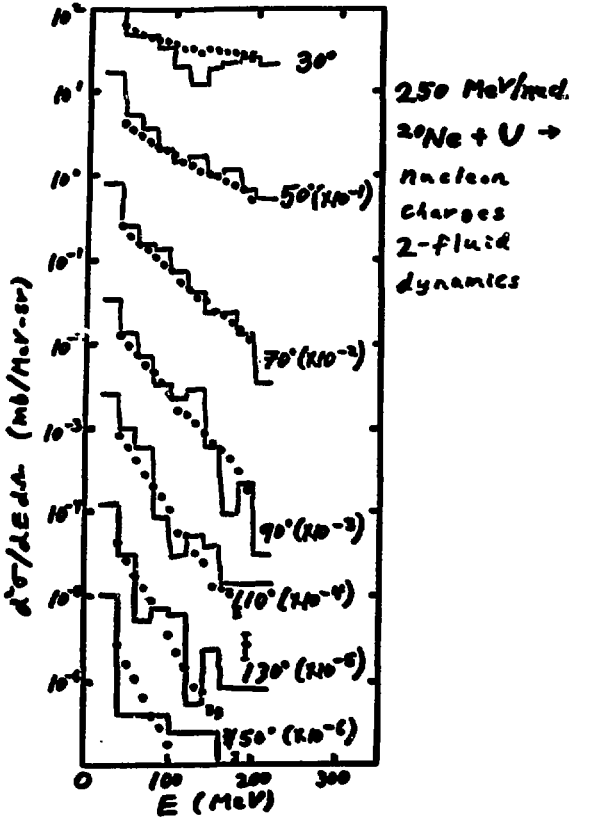
250 MeV/nucl.
20Ne + U →
nucleon
charges
2-fluid
dynamics
30°
50°(x10⁻¹)
70°(x10⁻²)
90°(x10⁻³)
110°(x10⁻⁴)
130°(x10⁻⁵)
150°(x10⁻⁶)
d²σ/dEdΩ (mb/MeV-sr)
E (MeV)
0
100
200
300

Fig. 1.57

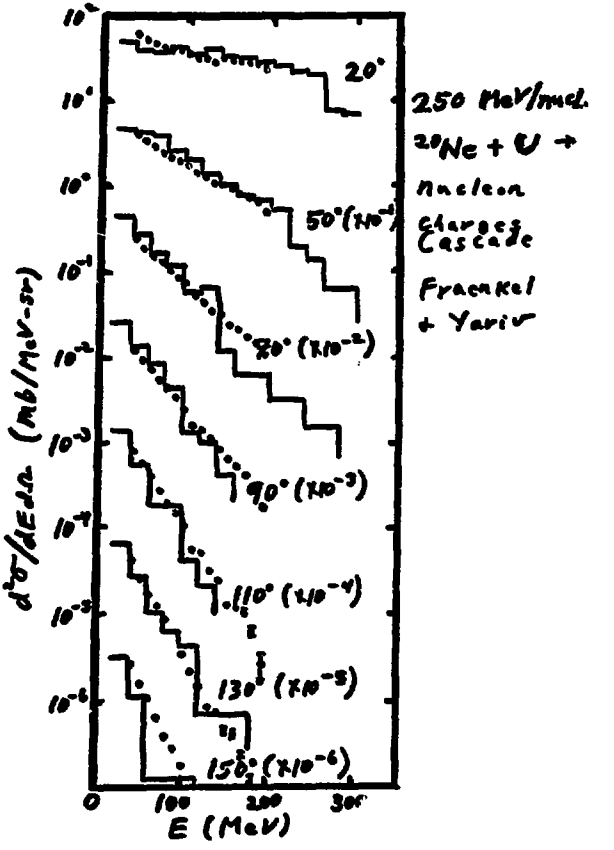
250 MeV/nucl.
$^{20}Ne + U \rightarrow$
nucleon
cleavage
Cascade
Frankel
+ Yariv
20°
50° (×10⁻¹)
90° (×10⁻²)
110° (×10⁻³)
130° (×10⁻⁴)
150° (×10⁻⁵)
d²σ/dEdΩ (mb/MeV-sr)
E (MeV)
0
100
200
300

Fig. 1.58

MEASUREMENTS OF PIONS AND HIGH ENERGY PROTONS AT LARGE ANGLES

Shoji Nagamiya

INTRODUCTION

During the past two years some new experiments have been started at the Bevalac. My talk covers mostly the results from these new experiments. Let me first introduce the groups whose work is covered in this talk. The first is our group (Fig. 2.1), which is measuring relatively high energy light fragments at large laboratory angles in order to study central collisions and high multiplicity events. Because central collisions are rather violent collisions we can expect a large momentum transfer from projectile to target, and, as a result, we can expect relatively high energy fragments to be emitted at large laboratory angles. We prepared a magnetic spectrometer to cover the high $P_{\parallel}$ region and the intermediate rapidity region between projectile and target. This magnetic spectrometer covers angles from 10 to 150° in the Lab frame and energy regions from 50 MeV to a few GeV. Another feature of central collisions is their high multiplicity. We prepared nine sets of tag counter telescopes in order to bias the measurements toward high multiplicity events. Using these counter telescopes we have also measured two or more particle correlations. So far we have measurements for 0.8 GeV/A C, Ne, and Ar, 0.4 GeV/A Ne, and 2.1 GeV/A Ne on various targets, producing π^+, π^-, protons, deuterons, etc.

The second group is Rasmussen, Nakai, and their collaborators (Fig. 2.2), who are measuring low energy pion production. Their intention is to find whether or not anomalous phenomena appear in low energy pion spectra. They prepared a range telescope for detecting the $\pi - \mu$ decay in order to identify π^+ at laboratory angles from 30 to 150° and for energies between 30 and 100 MeV. They have run at 0.8 GeV/A and 0.4 GeV/A Ne.

The third group is Schroeder and his company (Fig. 2.3) who are measuring the backward production of light fragments. In collisions between free protons there is no backward production of protons. Therefore, backward production of protons results from some kind of nuclear effect. They prepared a magnetic spectrometer to detect light fragments at 180° with energies of more than 50 MeV for protons and pions. They have measured projectile energy dependence, projectile mass dependence, and target mass dependence by using the reactions listed here (Fig. 2.3).

A common feature for all three groups is that none of the results from the work mentioned here has ever been published. Thus, all the results and interpretations are very preliminary.

The organization of my talk is as follows: I will first speak on inclusivie spectra, then cover two-particle correlations quickly, and finally use the remaining time to talk about high multiplicity events. Because of the limited time I'd like to spend most of it introducing our own results. The

results from the other two groups will be introduced in appropriate places during the talk.

INCLUSIVE SPECTRA

Let me start with inclusive measurements. We have measured inclusive spectra with a magnetic spectrometer, as shown here (Fig. 2.4). The spectrometer consists of several multiwire proportional chambers coupled to a magnet, which can rotate from 10 to 150°. Members of our group are also listed in Fig. 2.4.

Typical examples of inclusive spectra are shown in Fig. 2.5, where Lorentz invariant cross sections for proton production are plotted as a function of laboratory momentum for the case of 800 MeV/A Ar on KCl at laboratory angles from 10 to 145°. We see from this figure that very high energy protons are produced, with momentum sometimes more than twice the beam momentum per nucleon. Since, for proton beams, we never expect the emission of fragments with energies greater than the beam energy, this observation already shows one of the interesting features of heavy ion collisions.

In order to visualize these data we have plotted them in a plane of two center-of-mass variables, longitudinal momentum and transverse momentum (Fig. 2.6). Because the mass of KCl is close to that of Ar, the reaction of Ar on KCl is kinematically similar to the collision of identical nuclei. Therefore we have used the nucleon-nucleon center-of-mass frame in this plot. Each contour line connects experimental points which have the same invariant cross section. Two adjacent solid, thick curves differ by one order of magnitude in cross section. Although we don't have the data for extremely low $P_{\parallel}$ regions we can complete this figure using reasonable imagination and the results of other experiments. We then see (Fig. 2.7) two peaks at $P_{\parallel} = 0$, one located where parallel momentum is equal to projectile momentum per nucleon and the other where it is equal to target momentum per nucleon. These are projectile and target fragments. In our data we observe the effect of projectile and target fragmentation in the small $P_{\parallel}$ region, but in the regions far from these two peaks the contributions from projectile and target are very mixed up, and we observe there that the angular distribution in the CM frame is very smooth. Angular distributions of protons in the CM frame for large momentum transfers are more isotropic than those for small momentum transfers, but they are still forward and backward peaked. Isotropic distributions in this plot are indicated by semi-circular lines.

In order to give you a clear impression of the present status of the Bevalac experimental groups, I have plotted here which group covers which energy regions of proton fragments (Fig. 2.8). The Schroeder group is covering 180° while the Poskanzer/Gutbrod group is measuring a relatively low energy region. The Heckman/Greiner, Igo, and Anderson/Steiner groups are covering forward angles. Therefore, our group is really in a good location to bridge these experiments.

Next, let me show you pion spectra in the CM frame. Here (Fig. 2.9) the cross section contours for π^+ and π^- emissions are plotted for the same

reaction as we studied for protons. If I complete the figure using reasonable extrapolations, as I did for protons (Fig. 2.10), then we seen that pion emission is rather different from proton emission. For pions with CM energies around 100-200 MeV the angular distributions are forward and backward peaked, probably because of the Δ-resonance production inside the projectile or the target, but for high energy pions they are more isotropic than for the proton case. This is probably simply because the pion covers a wider kinematic region in the sense of momentum per unit mass.

For measurements of pions let me introduce again other experimental groups' activities as I did for protons (Fig. 2.11). Schroeder and his company are still measuring at 180°. The Rasmussen/Nakai group and the Poskanzer/Gutbrod group are measuring relatively low energy regions. The Igo and Anderson/Steiner groups are covering forward angles. Therefore, our group is again bridging the work of several groups.

In this talk, because of the limited time, I will concentrate mainly on proton and pion specta resulting from collisions between similar nuclei and will skip the data for complex nuclear fragments and also the data for heavier mass targets. In the case of Ar on KCl, if we look at energy spectra at CM 90°, they will be relatively free from projectile and target fragmentation. So let's concentrate for the moment on the CM 90° spectra in order to learn about central collisions.

Here I show (Fig. 2.12) three examples: 0.8 GeV/A C on C, Ne on NaF, and Ar on KCl. The horizontal axis is the kinetic energy in the CM frame. We learn several things. First, energy distributions are approximately exponential at the high energy end. The slope of the exponential decay (defined in the figure) is about 70-80 MeV, and it increases slightly as we increase target mass. Second, for low energy protons we observe a substantial deviation (suppression) of the yield from such an exponential behavior. Third, the energy integrated cross section, $d\sigma/d\Omega$, is roughly proportional to Z^2, implying that all the nucleons of both target and projectile are participating in the reaction.

How about pions? Pion spectra for the same reaction are shown in Fig. 2.13. In this case the shape of the energy spectrum is almost exponential at all energies. Target-Z dependence of $d\sigma/d\Omega$ now has a lower power of Z compared to that for protons. This is probably due to reabsorption of pions inside the nucleus. Another interesting feature is observed in the slope factor. The slope factor for pions is slightly but systematically smaller than the slope factor for protons in all cases.

Up to now we have studied target mass dependence. What about beam energy dependence? Plotted here (Fig. 2.14) are proton spectra at CM 90° in collisions of Ne on Ne at three different bombarding energies, 0.4 GeV/A, 0.8 GeV/A, and 2.1 GeV/A. The slope factor now drastically increases as we increase the beam energy. Also, it looks as though the total yield ($d\sigma/d\Omega$) stays almost constant even if we change the beam energy. In the case of pions (Fig. 2.15) the slope factor increases as we increase the beam energy, and the yield also increases. Furthermore, if we compare pions and protons, the slope factor is systematically

smaller for pions than for protons.

The energy dependences are summarized in the following two graphs. As to the yield (Fig. 2.16), the proton yield stays almost constant at the three bombarding energies, but the pion yield grows as we increase the incident beam energy. This is reasonable, because protons already exist, but we have to supply energy to produce pions. A slight decrease of the proton yield at 2.1 GeV/A is also very reasonable because at this bombarding energy the angular distribution of proton emission is very forward and backward peaked, and, therefore, there aren't as many protons left over at 90°.

As to the slope factor of the exponential decay, I have plotted here (Fig. 2.17) the slope factor as a function of incident energy per nucleon available in the CM frame. The dotted line indicates a limiting case for the fireball model where all the available energy is thermalized. I call this parameter T the slope factor and not temperature since we don't know yet if the thermal model is correct or not. We observe that the experimental value of the slope factor is monotonically increasing as a function of beam energy, and the pion slope factor is systematically smaller than the proton slope factor. Empirically, the energy dependence of the slope factor T is such that T is proportional to $\sqrt{E^*_{\beta}/A}$ instead of E^*_{β}/A where E^*_{β} is the CM kinetic energy of the projectile nucleus.

So far I have described 90° spectra only. Now, I would like to show you angular distributions. Here (Fig. 2.18) we have plotted CM energy distributions at three CM angles, 30°, 60°, and 90°, for both protons and pions produced in 0.8 GeV/A Ne on Ne reactions. For protons the yield at 30° is much higher than that at 90°, showing a forward and backward peaking. For pions, however, the yield is almost isotropic at high energies. At pion energies around 100-200 MeV we observe that the 30° yield is appreciably higher than the 90° yield. In order to complete the plot for pions on the lower energy side, we need the help of the data of the Rasmussen/Nakai group. So, at this point let me introduce their data.

Plotted here (Fig. 2.19) is the data of π^+ production for 0.8 GeV/A Ne on NaF. Black dots are our data measured by our magnetic spectrometer and open circles are their data measured by their range telescope. The two sets of data agree very well with each other.

By using their data we can complete the figure at the low energy side of pions (Fig. 2.20). Now you can see more clearly that at pion energies around 100-200 MeV the 30° yield is very high compared to the 90° yield. Also we observe that angular distribution is almost isotropic in the extremely low energy region.

Let me summarize at this point and remind you of what we have learned so far for inclusive spectra. Proton angular distributions have forward and and backward peaks, but pion angular distributions are much closer to isotropy except at the pion energies around 100 to 200 MeV. Energy distributions for protons approach exponential form for high energies while for pions they are roughly exponential at all energies. The slope factor does not linearly

increase as a function of beam energy per nucleon in the CM frame, E_B^*/A, but is approximately proportional to $\sqrt{E_B^*/A}$. We have observed that the slope factor for pions is smaller than that of protons. We have also observed non-exponential behavior for proton spectra at low energies. The proton yield is almost independent of the bombarding energy, while the pion yield is strongly dependent on it. At CM 90° the proton yield is approximately proportional to Z^2 of the target.

Now, a natural question is whether or not these typical features are explained by theories. I have about 10 different theoretical calculations available particularly for the case of 0.8 GeV/A Ne on NaF. So, I will leave this transparency (Fig. 2.20) and try to compare it with theories.

First, let me start with a naive fireball model (Fig. 2.21) where the total available energy is converted to temperature. Except for the absolute yield, this naive fireball model does not fit the data at all. The slope factor is too high and the angular distributions are not reproduced.

In order to reduce the temperature, Kapusta, et al. have taken into account the pion degrees of freedom. Furthermore, in order to reproduce forward and backward peaking observed for protons they have used the firestreak model proposed by Myers. Figure 2.22 shows their results. For protons I would say the agreement is fair. However, there is trouble with pions. In addition, if we look more carefully, we see problems even for protons. First, this firestreak model always gives exponential behavior at the high energy end and greater than exponential yield at the low energy end. Our data for the low energy end show just the opposite; we have less than exponential yield there. Second, the pion yield predicted by the model is too high compared with the data. The third problem is the slope factor. This firestreak model gives the same slope factor both for protons and pions, and therefore, the observed difference of the slope factor between protons and pions cannot be explained.

Das Gupta has recently proposed a two-fireball model (Fig. 2.23). His idea is as follows. When the nucleon number of the participant is not sufficiently large, then both projectile and target pass through each other and convert a part of the available energy into thermal energy. I think the agreement is again fair, but I should say that all the problems which we have encountered in the firestreak model still exist in this two-fireball model.

As an extension of the thermal model Siemens has proposed an explosion model (Fig. 2.24). He assumed that at the beginning of the reaction hot nuclear matter is produced. This hot matter then explodes, and part of the available energy is absorbed into expansion energy. After the system has expanded enough, it reaches a thermal equilibrium, but the temperature at this stage is much cooler than the original temperature. Unfortunately he has not calculated any absolute cross sections, and therefore the scale is arbitrary in this plot. Also, there is no relationship between the proton scale and the pion scale. Furthermore, he assumed isotropic expansion which will not explain any observed angular distributions. However, I think this model has certain good points. In the first place the observed suppression

of the proton yield at the low energy end from an exponential shape is qualitatively explained by this model. The second point is that the observed slope-factor difference between protons and pions is nicely explained. Because pions have velocities close to light in the energy region of our data, pions are relatively insensitive to the expansion velocity. On the other hand, the proton velocities are relatively small and therefore expansion flow and thermal distribution are extremely mixed up in the proton spectra. This makes the proton slope less steep than the pion slope.

A similar approach is being tried by Kitazoe and Sano, taking into account both compression and expansion. At the moment I have one calculation where only the compression effect is taken into account (Fig. 2.25). The fit is reasonable. But I don't understand why the fit is so good, since it seems to me that they have not considered the Δ-resonance effect, which I believe is very important at 800 MeV/A bombarding energy.

Up to now I have described rather macroscopic approaches based on thermal models. Another extreme approach is from the point of view of nucleon-nucleon collisions. Let's mention this type of approach next.

The most dramatic assumption of this approach is a simple, single-nucleon-nucleon, clean-knock-out collision, neglecting any multiple scatterings. Here is an example (Fig. 2.26), which was recently suggested by Koonin and Hatch. They have used the same diagram as that used by Blankenbecler and Schmidt, but have assumed an exponential-type momentum distribution of nucleons inside the nucleus [more strictly speaking, they have assumed the form of $(P/P_0)\sinh(P/P_0)$]. I would say the agreement is surprisingly good, expecially for this kind of very simple approach. The fireball model played a fundamental role in the development of thermal-type approaches. In the same way, I think this single-nucleon-nucleon model is important among various approaches of nucleon-nucleon type models. To me there is still one question remaining in this model. Namely, are multiple scattering effects really neglected in this model? They have assumed a priori the exponential-type momentum distribution of nucleons. It seems to me that this exponential-type momentum distribution may effectively involve multiple scattering effects.

Pirner and Schürmann have extended the nucleon-nucleon-type approach. They started from a single nucleon-nucleon scattering, and they treat the multiple-scattering effect by means of transport theory (Fig. 2.27). A crucial question regarding this model is whether or not the observed high momentum tail can be explained by this transport theory. I think they have succeeded in reproducing proton spectra, but not for pions. The actual multiple scattering is greater than their calculations indicate.

The extreme end of the nucleon-nucleon type approach is the cascade model. One of the disadvantages of cascade calculations is their complexity and their need for a large amount of computer time. Therefore some people have tried actual calculations under several approximations. Here I show an example by Randrup (Fig. 2.28). He did slab-slab cascade calculations. The agreement is fair for protons, but unfortunately I don't have his results for pions.

Consider now some real cascade calculations. Cascade #1 is by Smith and Danos (Fig. 2.29). The agreement between data and theory is the best among all the calculations available right now. Various features that cannot be explained by other models are now nicely explained. One unfortunate point is that there are no calculations for the high momentum tails simply because of the vanishing statistics of the calculations.

Cascade #2 is by Fraenkel et al. (Fig. 2.30). Agreement is pretty good for protons, but calculations give more pions at 30° than observed. I don't know the reason for this, but perhaps they have taken into account too great a Δ-resonance effect in their calculations.

I have not compared our data with other approaches. The pure hydrodynamic approach, the classical cascade calculation, the Boltzman-equation-type approach, and several others are glected. This is simply because I don't have the results in hand.

Now, let me summarize the model comparisons. I am always thinking that even the experimentalist should not behave as a consumer of theories. Therefore, I'm really ashamed to show you the two transparencies that I'm hiding here; they are kind of a consumer report. If some of you are interested in looking at them, please contact me privately. Summarizing several models, I think major featurea of the data are rather well explained by the models, but I would like to criticize a few points of the various approaches. As for the thermal models, non-exponential behavior observed for low energy protons is not explained. For pions, thermal models always give higher yields than observed. Furthermore, the observed slope difference between protons and pions is difficult to explain by any thermal model. How about compression/explosion models? Personally I like the hydrodynamic approach including compression and explosion. But I feel that we need more complete formulations. Taking the single nucleon-nucleon model, I think the approach by Koonin and Hatch has to be thoughtfully evaluated, but we should consider more carefully the effect of multiple scatterings. And, finally, considering the cascade model, agreement between the data and this model is the bes : the moment. Major questions, however, are: 1) how can we efficiently ra. e the statistics and 2) how should we extract physics out of the calculations?

I have not yet mentioned anything about "scaling". We have made some effort to find a good scaling variable in order to explain the beam-energy dependence of proton and pion emissions. But I will not describe this, since time is very limited. Instead, I would like to introduce at this point the results of backward π^- production measured by the Schroeder group, since there is a good approach toward scaling being investigated by this group.

Here I show (Fig. 2.31) laboratory momentum distributions of π^- produced in collisions of 2.1 GeV/A C on various targets. The shape of the pion spectrum is approximately exponential in momentum and the slope factor, p_0, slowly increases as the mass of the target increases.

When we change the projectile mass (Fig. 2.32), we again observe exponential-type momentum distributions. The change in p_0 for several projectile

masses is not dramatic. Then, what about beam energy dependence?

This graph (Fig. 2.33) shows π^- spectra produced in collisions of p on C at three different bombarding energies: 1.05, 2.1, and 4.9 GeV. Invariant cross sections are plotted vs. the traditional scaling variable x' defined by CM momentum, divided by the maximum CM momentum allowed by the kinematics. We do not observe any "scaling" as a function of this x'. The formula derived by Blankenbecler and Schmidt is $\sigma \propto (1-x')^n$, and, according to their prediction, we expect n to be about 350. However, the actual value of n changes from 20 to 60.

Then what is a good scaling variable? They found a very intereting thing (Fig. 2.34). Namely, if we plot the slope factor p_0 in the laboratory frame as a function of p_{max}, where p_{max} is the maximum pion momentum, defined in the lab, for the process projectile nucleus + proton + π^-, then there is an interesting relationships between the two quantities, p_0 and p_{max}. All the experimental points including the Schroeder and Russian results fall on a straight line. This observation, $p_0 \propto p_{max}$, strongly suggests that for backward pion production it may be better to use (p/p_{max}) defined in the lab as a scaling variable, instead of (p/p_{max}) defined in the center of mass.

TWO-PARTICLE CORRELATIONS

Let me talk next about two-particle correlations. We have done two-particle correlation measurements in the following way (see Fig. 2.35): We prepared three counter telescopes in addition to the already existing spectrometer. These counter telescopes were set up, down, and right with respect to the beam. In azimuthal angles, if we define ϕ of the spectrometer to be 0, then we have the telescopes at $\phi = +90°$, $-90°$, and $180°$. Normally we set these three telescopes at polar angle 40° and we move the spectrometer polar angle only.

We define the ratio C as the coincidence rate between the spectrometer and right counter divided by the coincidence rate between the spectrometer and up or down counter. The ratio has the following meaning. If C is greater than 1, then a co-planar-type two-particle emission is favored. If the ratio C is less than 1, two particles tend to be emitted to one side in an azimuthal direction. So we call this ratio the degree of co-planarity. In thermal equilibrium we expect the ratio to be approximately 1. Therefore, we can test whether or not the thermal model holds. We have measured this ratio C as a function of the spectrometer angle, θ_{sp}, namely, as a function of the opening angle between the two particles.

Typical results are shown here (Fig. 2.36) where we have plotted the ratio C as a function of spectrometer angle. Let me first discuss the case of carbon on carbon. The value of C, the degree of co-planarity, is more than 1 and it peaks around 40°. Because we set our tag counters at 40°, the peaking at 40° implies that when two particles have an opening angle of about 80° their emission is favored. This is consistent with the kinematics of two-proton quasi-elastic scattering. In fact, if we look at the proton energy spectrum at $\theta_{sp} = 40°$, we observe a nice peak at the expected energy of the p-p quasi-

elastic scattering. So this shows clearly that there is direct emission from a carbon-carbon reaction and thermal equilibrium is not reached in that system.

Next let me study the C + Pb or Ar + Pb reactions (Fig. 2.37). In the case of heavier-mass targets the ratio is even less than 1. What does that mean? This is probably simply because of the shadowing effect as illustrated in Fig. 2.38. If we detect the first particle at a certain angle, then the reaction region is effectively biased toward the shaded hemisphere shown in the figure. In this case, it is rather difficult for the second particle to be emitted in the opposite direction of the first particle, because it has to penetrate thick nuclear matter. On the other hand, it is not so difficult for the second particle to be emitted toward the up or down direction. This means that the coincidence rate between the spectrometer and right counter is less than the coincidence rate between the spectrometer and the up or down counter in the presence of the shadowing effect. In other words, the shadowing induces $C < 1$. When the target mass number is large, I think this shadowing effect becomes important, as data for C + Pb or Ar + Pb suggest.

Next let me discuss the final combination, Ar + KCl, in Fig. 2.36 (or Fig. 2.37). Here we observe less evidence of coplanar emission than in the C + C case. Does this mean thermal equilibrium is reached in this case? I think the answer is probably simply that the higher multiplicities in Ar + KCl collisions compared to C + C collisions wash out the evidence of coplanarity of two particles. In order to illustrate this, I would like to show here (Fig. 2.39) the beam energy dependence of the ratio C, at two bombarding energies, 0.4 GeV/A and 2.1 GeV/A, in collisions of Ne on NaF. At 400 MeV/A we observe still a sharp peak associated with p-p quasi-elastic scattering, but at 2.1 GeV/A we do not. It is hard to believe that thermal equilibrium takes place at 2.1 GeV/A and not at 400 MeV/A. Since the event multiplicity is much higher at 2.1 GeV/A than at 400 MeV/A, this comparison suggests that high multiplicity smears out the two-particle coplanarity even if direct emission is important. Of course, at 2.1 GeV/A there are some other effects; for example p-p inelastic processes become important and therefore two-proton coplanarity is smeared out even for pp collisions. In this sense, we cannot immediately conclude that the reduction of the ratio C is totally due to high multiplicity.

Let me summarize two-particle correlations. We have seen clear evidence of direct emission, at least for light-mass targets, and therefore no thermal equilibrium for light-mass systems. For a heavier-mass target we have observed nuclear shadowing. Although I've not mentioned anything about the third point, we have data which may suggest evidence of p-d quasi-elastic scatterings.

HIGH MULTIPLICITY EVENTS

Let me go to the third topic, high multiplicity events. In addition to the spectrometer, we have prepared nine tag counter telescopes (see Fig. 2.40) and placed them as azimuthally symmetrically as possible. Normally these nine tag counter telescopes are placed at polar angles around 40°. The main purpose of these telescopes is to bias the measurements toward head-on collisions

rather than to measure the multiplicity itself. The total solid angle covered by these telescopes is only 3.6% of 4π. However, if we detect, for example, four particles with these counters, we already have a strong bias toward high multiplicity events. Typically, if we detect 4 out of 9, the average total multiplicity is around 30 or more. With the bias of these tag counters we have measured particle energy and angular distributions with the magnetic spectrometer. We call this type of measurement an inclusive measurement for high multiplicity. Each counter telescope is rather complicated, as shown in the figure. By combining counters, absorbers, and a Cerenkov counter we can roughly separate particle energies and masses.

Here (Fig. 2.41) I show a typical example of proton angular distributions in collisions of 0.8 GeV/A Ar + Pb, for different number of counts in the tag counters. The inclusive angular distribution is forward peaking, but for high-multiplicity events the forward emission is highly suppressed. This situtation becomes more clear if we take the ratio between high multiplicity events and inclusive events (Fig. 2.42); the higher the multiplicity the greater the suppression of forward emission. What happens in the case of Ar on Ar (Fig. 2.43)? We see that again forward emission is suppressed, but at the same time the backward emission is also suppressed. In other words, for high-multiplicity events, the protons are likely to be emitted at around 50° in the laboratory frame.

In order to discuss these observations, we have to study in a bit more detail which kinematical region each point covers. Let's try to study energy spectra at a forward angle, at a backward angle, and at some intermediate angle such as 50°. Here we have plotted the ratio of the lab momentum spectrum for high-multiplicity events to that for inclusive events. Figure 2.44 is for Ar + Pb collisions and Fig. 2.45 is for Ar + KCl collisions. The high-multiplicity events quoted here are those events where 4 or more particles, with energies more than 100 MeV, fired the tag counters. Because we expect higher multiplicities for Ar + Pb than for Ar + KCl, the condition of detecting 4 particles is more strict in the case of Ar + KCl than in that of Ar + Pb. We observe that these high-multiplicity events constitute about 1% of the total events in the case of Ar + KCl and about 6% in the case of Ar + Pb. In our present measurements we can easily detect and momentum-analyze the events at a level of 0.5% of the total yield, but at a level of less than 0.1% it becomes difficult because of statistics.

Now what do we learn? For Ar + Pb we observe two things. At forward angles we see that high momentum protons are suppressed from 6% down to 2%. However, at large angles high-momentum yields are enhanced. In the case of Ar + KCl, however, there is no significant change observed either at forward or backward angles. Instead, the enhancement of the high-momentum yield is very remarkable at 50°.

Let me first try to explain the forward suppression observed in Ar on Pb. This is probably simply because of nuclear shadowing as illustrated in Fig. 2.46. If we detect higher multiplicities, collisions are more biased toward smaller impact parameters. In head-on collisions if the target is big, then it's rather difficult for particles to penetrate the thick nuclear matter, and

thus it is very difficult for particles to be emitted at forward angles. However, if the target nucleus is small, it is not necessary for the particles to penetrate much material, and we can expect less of a shadowing effect. I think this is why we observe strong forward suppression for the Pb target but no significant suppression for the KCl target. Forward suppression for Pb is more significant at higher laboratory momentum. This is also understandable, because low energy particles come mostly from evaporation of the target, and we don't expect any correlations for these events. In fact, if we plot angular distributions for low energy fragments only, we observe that the angular distribution for low multiplicity events is not so different from the angular distribution for high multiplicity events.

Our next obvious interest is in why the high-momentum yields are enhanced at large angles, and why such enhancements are observed at only 50° for Ar + KCl and at both 50° and 110° for Ar + Pb. In examining this point, let me start with the case of Ar + KCl. Here (Fig. 2.47) we have plotted the ratio of proton yields for high-multiplicity events to those for inclusive events, as a function of center-of-mass angle at several different CM proton fragment momenta. As we increase the CM momentum, proton emission at 90° is more likely for high multiplicity events than for inclusive events. In other words, proton emission at 90° is enhanced for high multiplicity events, and this enhancement is greater for higher energy protons in the CM frame. Is this really an anomalous effect?

In order to make this clearer, I show contour plot of cross sections for high-multiplicity events in a plane of $p_{\parallel}^*$ and $p_{\perp}^*$ (Fig. 2.48). If I superimpose on this contour plot of inclusive spectra (Fig. 2.49), then we see that for high-multiplicity events, angular distributions are more isotropic than those for inclusive spectra, and, furthermore, the interval between two adjacent contours is wider. If the contour lines for high multiplicity events are outside the contour lines for inclusive ones, then the yields for high multiplicity events are enhanced compared to those for inclusive events. At CM 90° contour lines for high multiplicity events are always outside those for inclusive events, and thus we observe an enhancement of the 90° yield for high multiplicities. Emission of protons at CM forward and backward angles is, on the other hand, suppressed for high multiplicity events when compared to that for inclusive events.

In this diagram the laboratory angles 15°, 50°, and 110° are expressed by three lines in Fig. 2.50. CM 90° is close to lab 50°. We have not observed any drastic change at laboratory angles 15° and 110°, but at laboratory angle 50° the yield is greatly enhanced for high multiplicty events on the high-momentum side.

Thus we have learned two things. First, for high multiplicity events the angular distributions tend to be more isotropic in the CM frame than those for inclusive events. This is reasonable because, as collisions become more violent, there is a tendency to lose the initial memory of the beam direction. Second, the incidence of high-transverse-momentum events is enhanced for higher multiplicities. This is also reasonable, since when collisions become more violent, multiple collisions, which spray out higher-energy fragments at large

angles, become more prevalent. In other words, for inclusive spectra we observed forward and backward peaking in angular distributions. This is because the parallel momenta carried by the projectile and target are at least in part carried off by the fragments. However, when collisions become more violent, the emitted fragments have more of a tendency to lose their initial memory of the parallel momenta carried by the projectile and the target, and, as a result, emission of high $P_{\parallel}$ fragments is favored simply because of energy conservation in the total system.

Now, let me come back to the case of Ar on Pb (Fig. 2.44). In this case the effective center-of-mass shifts more toward the target velocity. So, even at 110° we still expect a higher yield for high multiplicity events than for inclusive events. I think that if we measure the data at 160° or 170° in the lab the yield there will go down for higher multiplicities.

Up to now I have concentrated on proton spectra and not on pions. So far we have not observed a clear difference in pion production between high multiplicity and inclusive events. Here (Fig. 2.51), I show energy spectra of both protons and pions detected at CM 90° in higher-multiplicity events. As for pions, the shape of the spectra is not very different from that for inclusive events. Maybe there is a slight enhancement of low energy pion yield in higher multiplicity events, but this is statistically not very significant. For protons the slope factor of the exponential tail is larger for higher multiplicities and, in addition, nonexponential behavior at the low energy end becomes more significant for higher multiplicities. This is qualitatively in agreement with the prediction by Siemens in his explosion model.

Let me summarize high multiplicity events. For high multiplicity events proton angular distribution comes closer to isotropy in the CM frame at least for A-A collisions. As for energy distributions, we have observed an enhancement at high transverse momentum for protons but so far we have not observed any drastic change for pions. We have also observed forward shadowing for very heavy target nuclei.

Before finishing my talk I would like to show you one more transparency (Fig. 2.52). This is a very personally biased picture, but it is my favorite picture for describing heavy ion collisions. At the beginning of a collision some energy goes to a compression and the remaining energy goes into the reaction. After the system is highly compressed, some energy goes into an explosion and the rest goes to the reaction products. Of course, at present everyone must be careful about using a single model unless the experimental data lead to a single conclusion which otherwise cannot be explained. In this sense, the compression-explosion model is not at all uniquely suited to our data. However, it is also true that so far no experimental data disagree with this picture.

1. High energy light fragments at large angles - central collisions & high multiplicity events. (Our Group)

- Magnetic spectrometer
  - to cover high $P_{\parallel}$, intermediate rapidity $10° \leq \theta_{lab} \leq 150°$, 50 MeV $\leq E_p$, E_π < 3 GeV
- Tag counter telescopes
  - to bias toward head-on collision
  - 2 or more particle correlations
- $\left(\begin{array}{l}\text{0.8 GeV/A C , Ne, Ar}\\ \text{0.4 GeV/A Ne}\\ \text{2.1 GeV/A Ne}\end{array}\right) + \left(\begin{array}{l}\text{C}\\ \text{NaF}\\ \text{KCl}\\ \text{Cu}\\ \text{Pb}\end{array}\right) \rightarrow \left(\begin{array}{l}\pi^{\pm}\\ \text{p}\\ \text{d}\\ \text{t}\\ {}^3\text{He}\\ \alpha\end{array}\right)$

Fig. 2.1

2. Low energy pion production.
J.O. Rasmussen, K. Nakai et al.

- π - μ Range Telescope (π^+)
  $30° \leq \theta_{lab} \leq 150°$, 30 MeV $\leq E_{\pi^+} \leq$ 100 MeV

- $\begin{pmatrix} 0.8 \text{ GeV/A} & Ne \\ 0.4 \text{ GeV/A} & Ne \end{pmatrix} + \begin{pmatrix} C \\ NaF \\ Cu \\ Pb \end{pmatrix} \rightarrow (\pi^+)$

Fig. 2.2

3. Backward production of light fragments. L. Schroeder et al.

- Magnetic spectrometer
  $\theta_{lab} = 180°$, E_p, $E_\pi > 50$ MeV

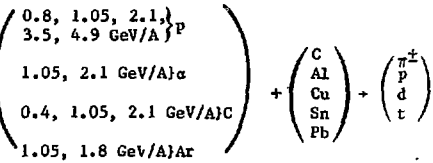

Fig. 2.3

Inclusive Measurements

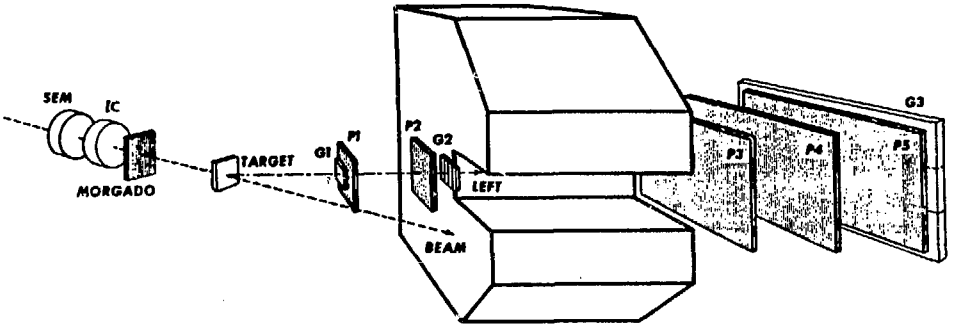

O. Chamberlain, M.C. Mallet-Lemaire, S. Nagamiya
S. Schnetzer, G. Shapiro, H. Steiner, I. Tanihata

Fig. 2.4

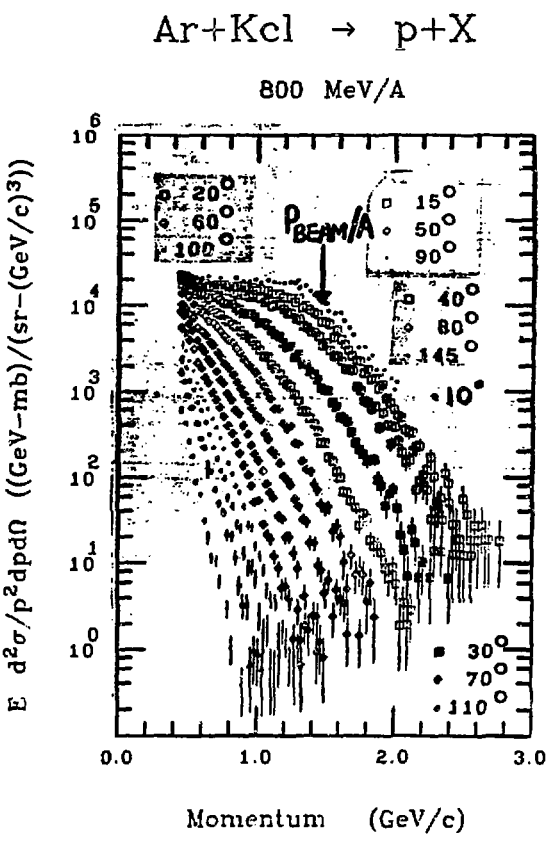
Ar+Kcl → p+X
800 MeV/A
E d²σ/p²dpdΩ ((GeV-mb)/(sr-(GeV/c)³))
Momentum (GeV/c)
P_BEAM/A
20°
60°
100°
15°
50°
90°
40°
80°
145°
10°
30°
70°
110°
0.0
1.0
2.0
3.0

Fig. 2.5

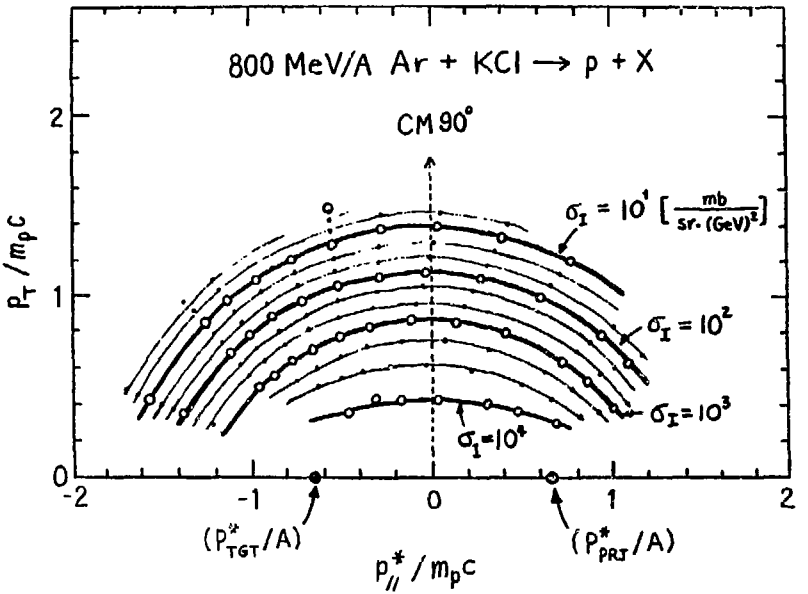
800 MeV/A Ar + KCl → p + X
CM 90°
$\sigma_I = 10^1 \left[\frac{mb}{sr.\,(GeV)^2}\right]$
$\sigma_I = 10^2$
$\sigma_I = 10^3$
$\sigma_I = 10^4$
$P_T / m_p c$
$p_{//}^* / m_p c$
(P^*_{TGT}/A)
(P^*_{PRJ}/A)
2
1
0
-2
-1
0
1
2

Fig. 2.6

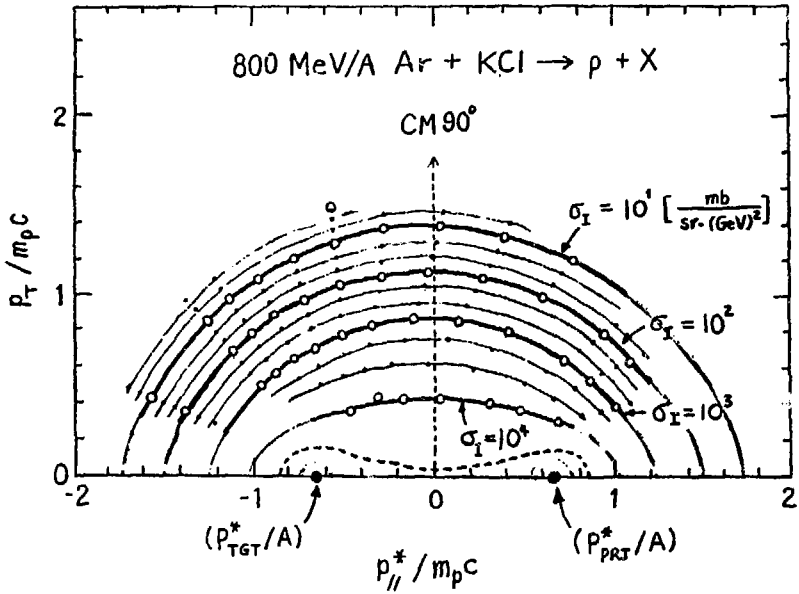
800 MeV/A Ar + KCl → p + X
CM 90°
$\sigma_I = 10^1 \left[\frac{mb}{sr\cdot(GeV)^2}\right]$
$\sigma_I = 10^2$
$\sigma_I = 10^3$
$\sigma_I = 10^4$
$p_T / m_p c$
$p_{//}^* / m_p c$
(p^*_{TGT}/A)
(p^*_{PRJ}/A)
0
1
2
-1
-2

Fig. 2.7

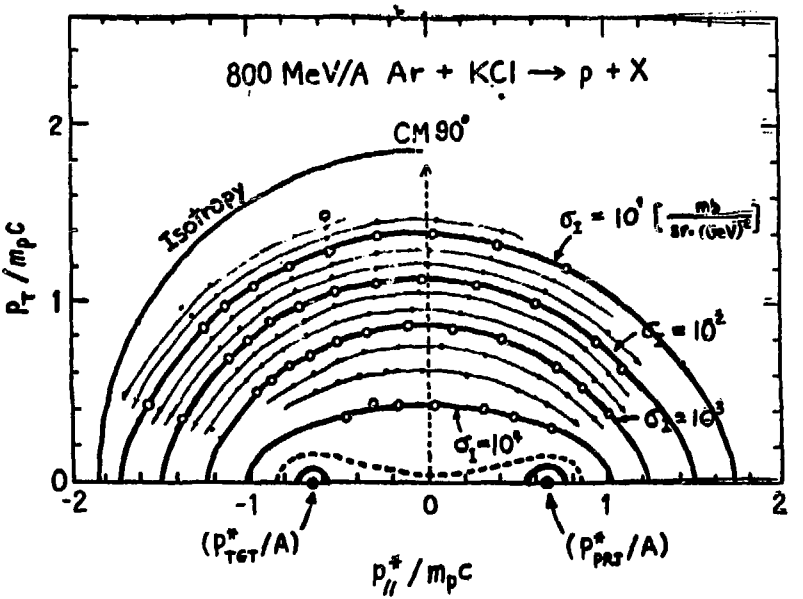
800 MeV/A Ar + KCl → p + X
CM 90°
Isotropy
$\sigma_1 = 10^0$ [mb/sr.(GeV)²]
$\sigma_2 = 10^{-1}$
$\sigma_3 = 10^{-2}$
$\sigma_4 = 10^{-3}$
$\sigma_5 = 10^{-4}$
$P_T / m_p c$
$p_{//}^* / m_p c$
(p^*_{TGT}/A)
(p^*_{PRJ}/A)
2
1
0
-2
-1
0
1
2

Fig. 2.8

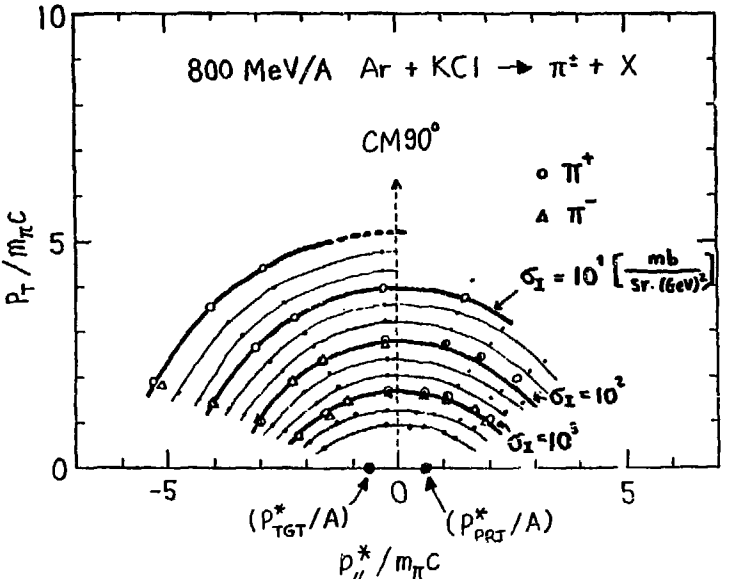
800 MeV/A Ar + KCl → π± + X
CM90°
o π+
Δ π−
σI = 10⁴ [mb / Sr. (GeV)²]
σI = 10³
σI = 10²
σI = 10
σI = 1
σI = 10⁻¹
σI = 10⁻²
σI = 10⁻³
σI = 10⁻⁴
σI = 10⁻⁵
P⊥ /mπc
p// * /mπc
(p*TGT/A)
(p*PRJ/A)
10
5
0
-5
0
5

Fig. 2.9

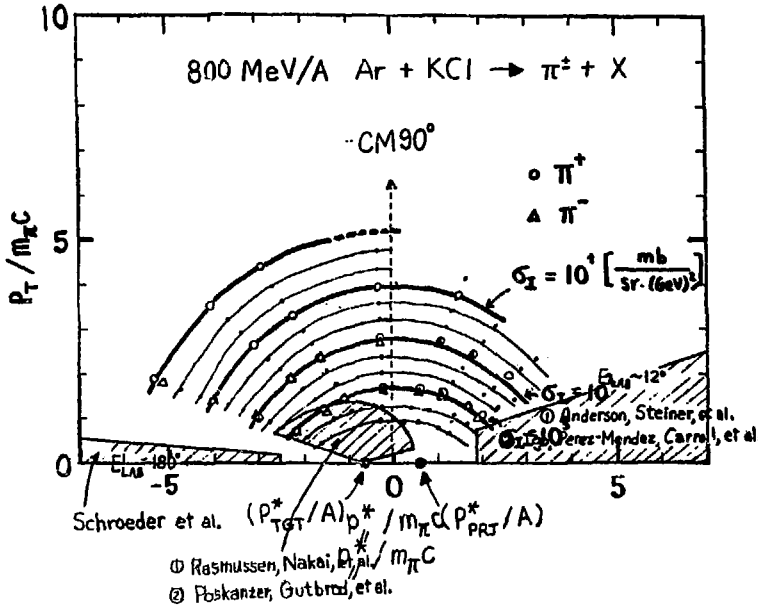
800 MeV/A Ar + KCl → π± + X
CM 90°
π+
π−
$\sigma_I = 10^4 \left[\frac{mb}{sr\cdot(GeV)^2}\right]$
$\sigma_I = 10^3$
$\sigma_I = 10^2$
E_{LAB} ~12°
E_{LAB} ~180°
① Anderson, Steiner, et al.
② Perez-Mendez, Carroll, et al.
$P_T / m_\pi c$
10
5
0
-5
0
5
Schroeder et al.
(p^*_{TGT}/A)
$p^*_{//} / m_\pi c$
(p^*_{PRJ}/A)
① Rasmussen, Nakai, et al.
② Poskanzer, Gutbrod, et al.

Fig. 2.10

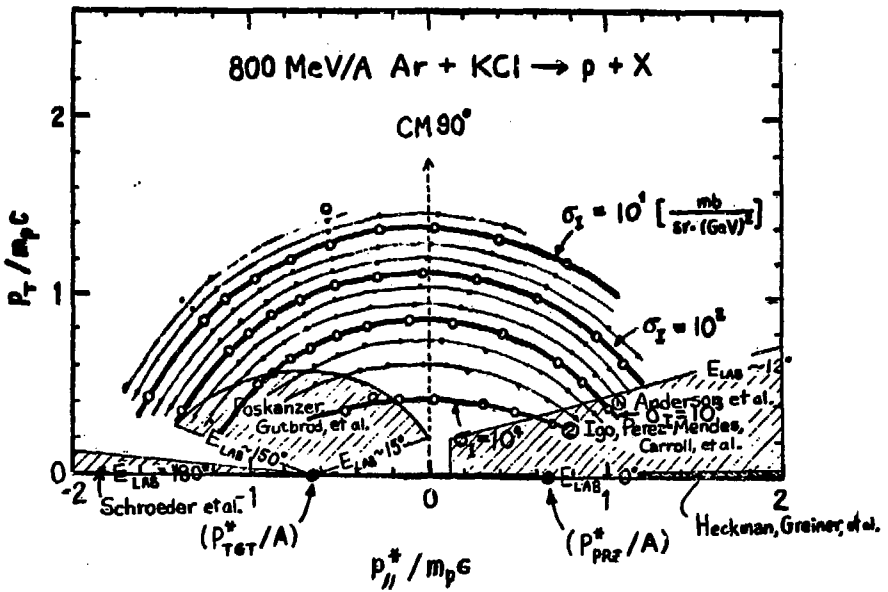
800 MeV/A Ar + KCl → p + X
CM 90°
$\sigma_I = 10^4 \left[\frac{mb}{Sr\cdot(GeV)^2}\right]$
$\sigma_I = 10^2$
P_T/m_pc
$p^*_{//}/m_pc$
Poskanzer, Gutbrod, et al.
Andersen et al.
Igo, Perez-Mendez, Carroll, et al.
Schroeder et al.
Heckman, Greiner, et al.
E_{LAB} ~12°
E_{LAB} ~150°
E_{LAB} ~15°
E_{LAB} ~180°
E_{LAB} 0°
$\sigma_I = 10^3$
$\sigma_I = 10^2$
(P^*_{TGT}/A)
(P^*_{PRJ}/A)

Fig. 2.11

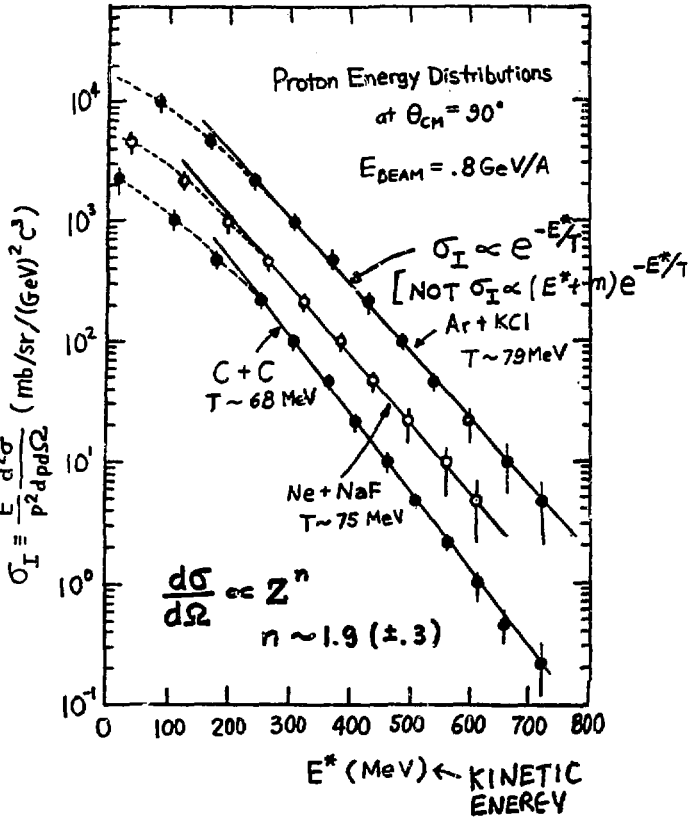
Proton Energy Distributions
at $\theta_{CM} = 90°$
$E_{BEAM} = .8$ GeV/A
$\sigma_I \propto e^{-E^*/T}$
[NOT $\sigma_I \propto (E^* + m)e^{-E^*/T}$
Ar + KCl
T ~ 79 MeV
C + C
T ~ 68 MeV
Ne + NaF
T ~ 75 MeV
$\frac{d\sigma}{d\Omega} \propto Z^n$
$n \sim 1.9\ (\pm .3)$
$\sigma_I \equiv \frac{E}{p^2}\frac{d^2\sigma}{dp d\Omega}$ (mb/sr/(GeV)^{2}c^3)
10^4
10^3
10^2
10^1
10^0
10^{-1}
0
100
200
300
400
500
600
700
800
E^* (MeV) ← KINETIC ENERGY

Fig. 2.12

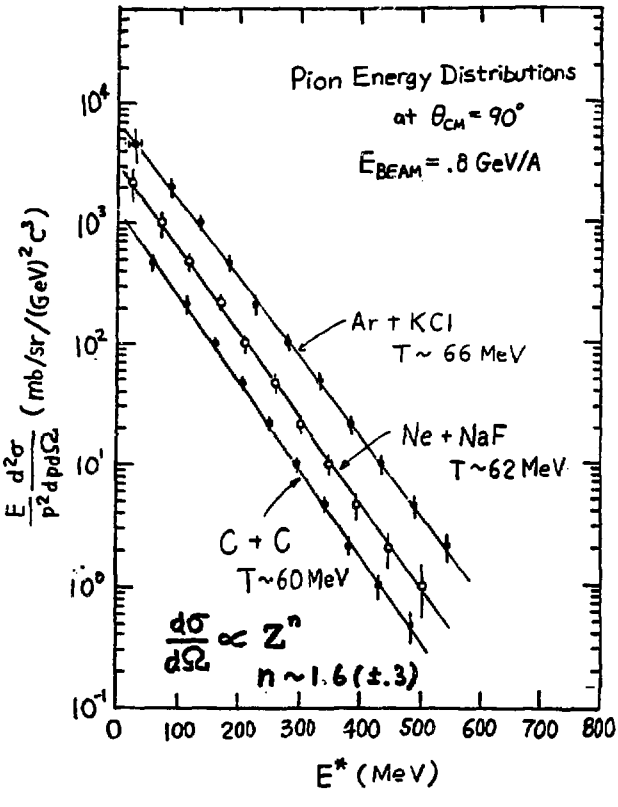
Pion Energy Distributions
at $\theta_{CM} = 90°$
$E_{BEAM} = .8$ GeV/A
Ar + KCl
T ~ 66 MeV
Ne + NaF
T ~ 62 MeV
C + C
T ~ 60 MeV
$\frac{d\sigma}{d\Omega} \propto Z^n$
$n \sim 1.6 (\pm .3)$
$\frac{E}{p^2} \frac{d^2\sigma}{dp d\Omega}$ (mb/sr/(GeV)^{2}c^3)
10^4
10^3
10^2
10^1
10^0
10^{-1}
0
100
200
300
400
500
600
700
800
E^* (MeV)

Fig. 2.13

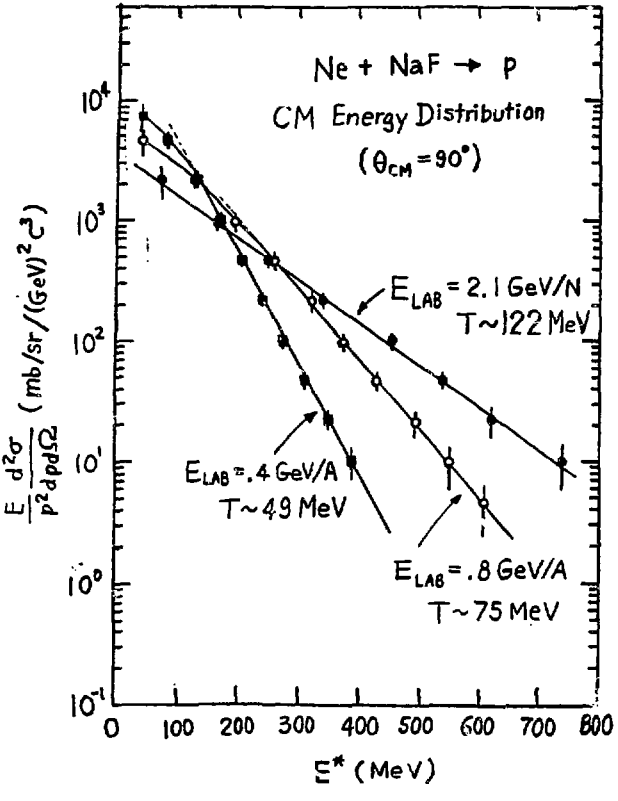
Ne + NaF → p
CM Energy Distribution
(θ_{CM}=90°)
E_{LAB} = 2.1 GeV/N
T~122 MeV
E_{LAB} = .4 GeV/A
T~49 MeV
E_{LAB} = .8 GeV/A
T~75 MeV
$E\frac{d^2\sigma}{p^2dpd\Omega}$ (mb/sr/(GeV)^{2}c^3)
10^4
10^3
10^2
10^1
10^0
10^{-1}
0
100
200
300
400
500
600
700
800
Ξ^* (MeV)

Fig. 2.14

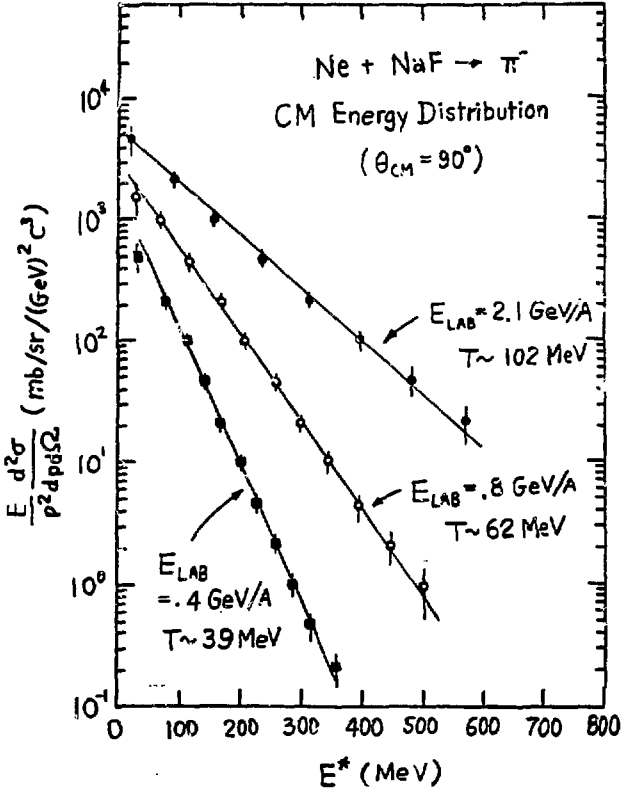
Ne + NaF → π⁻
CM Energy Distribution
(θCM = 90°)
ELAB = 2.1 GeV/A
T~ 102 MeV
ELAB = .8 GeV/A
T~ 62 MeV
ELAB = .4 GeV/A
T~ 39 MeV
E d²σ / p² dpdΩ (mb/sr/(GeV)² c³)
E* (MeV)
10⁴
10³
10²
10¹
10⁰
10⁻¹
0
100
200
300
400
500
600
700
800

Fig. 2.15

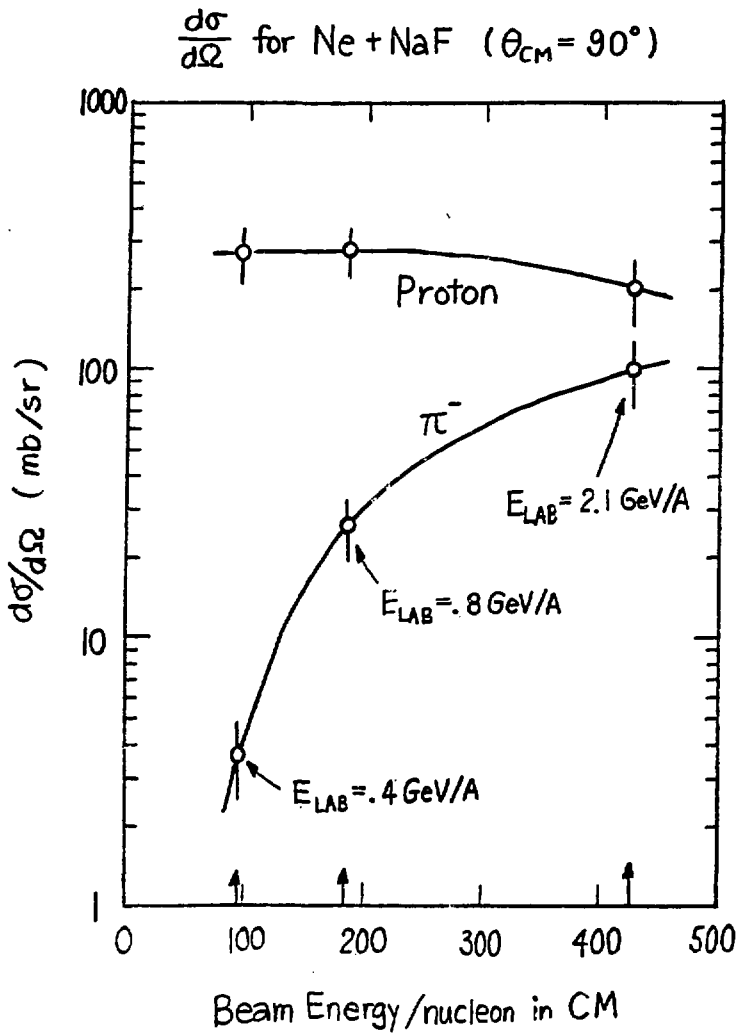
dσ/dΩ for Ne + NaF (θCM = 90°)
1000
100
10
1
dσ/dΩ (mb/sr)
Proton
π⁻
ELAB = 2.1 GeV/A
ELAB = .8 GeV/A
ELAB = .4 GeV/A
0
100
200
300
400
500
Beam Energy/nucleon in CM

Fig. 2.16

Slope Factor

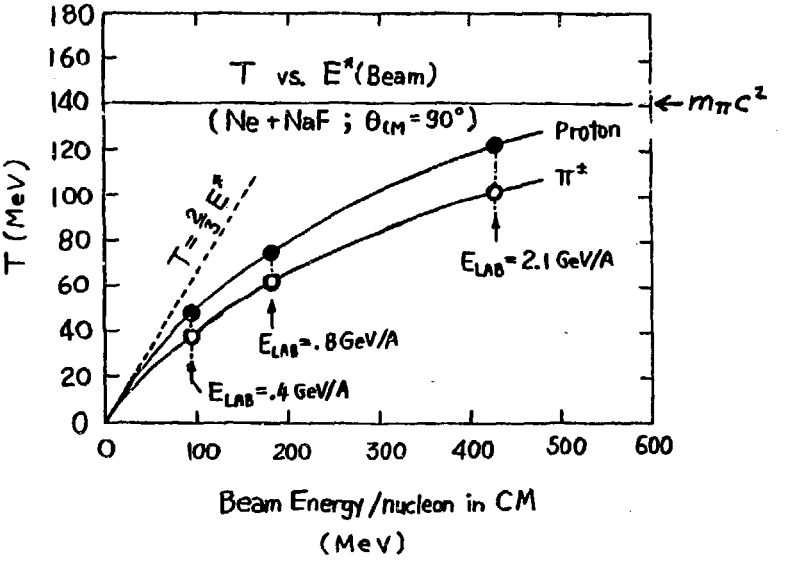

Fig. 2.17

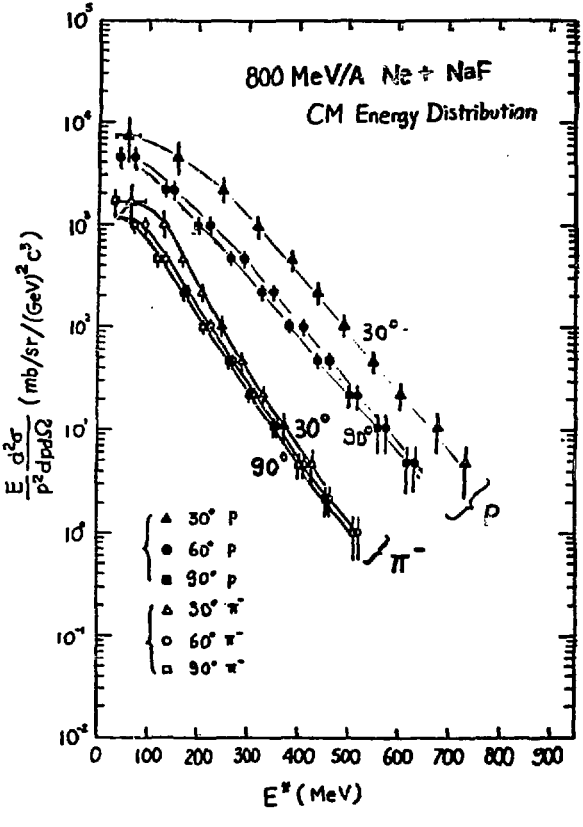
800 MeV/A Ne + NaF
CM Energy Distribution
$\frac{E}{p^2}\frac{d^2\sigma}{dpd\Omega}$ (mb/sr/(GeV)^{2}c^3)
E* (MeV)
30°
90°
30°
90°
p
π⁻
30° P
60° P
90° P
30° π⁻
60° π⁻
90° π⁻

Fig. 2.18

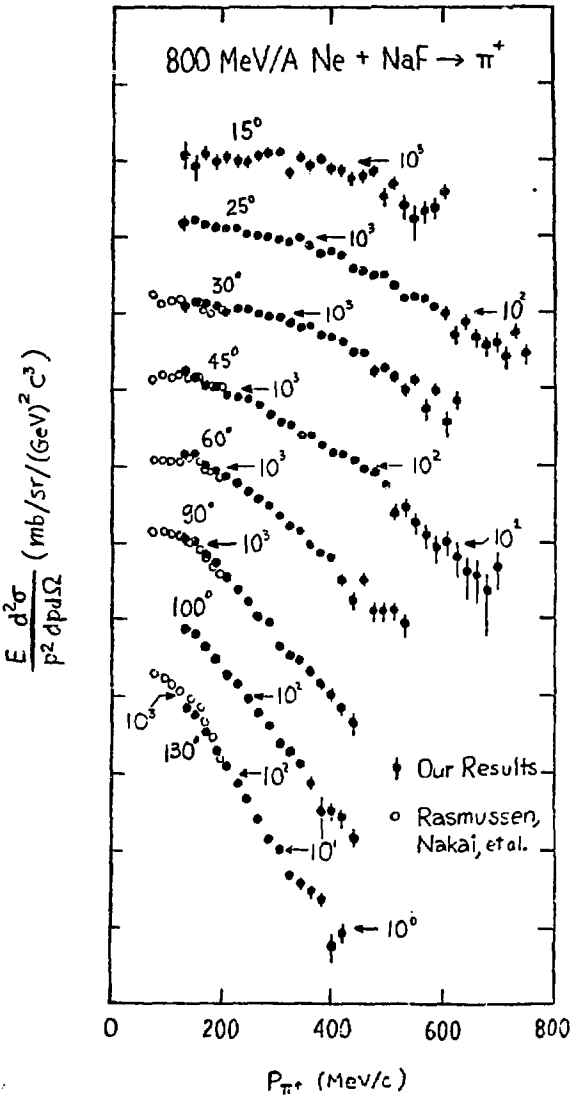
800 MeV/A Ne + NaF → π+
15°
25°
30°
45°
60°
90°
100°
130°
Our Results
Rasmussen, Nakai, et al.
0
200
400
600
800
Pπ+ (MeV/c)
E d²σ/p²dpdΩ (mb/sr/(GeV)² c³)

Fig. 2.19

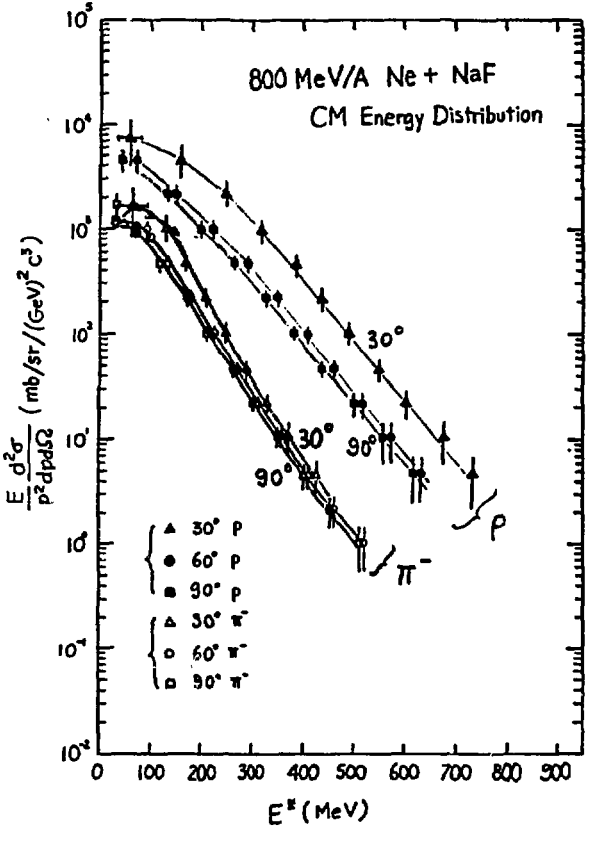
800 MeV/A Ne + NaF
CM Energy Distribution
$\frac{E}{p^2}\frac{d^2\sigma}{dpd\Omega}$ (mb/sr/(GeV)^2 c^3)
E^K (MeV)
30°
90°
30°
90°
p
π^-
30° p
60° p
90° p
30° π^-
60° π^-
90° π^-

Fig. 2.20

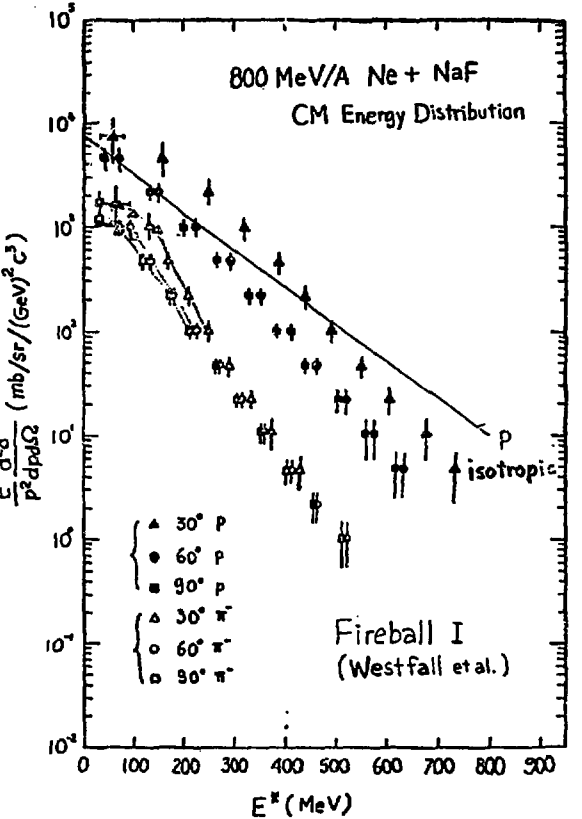
800 MeV/A Ne + NaF
CM Energy Distribution
p
isotropic
30° p
60° p
90° p
30° π⁻
60° π⁻
90° π⁻
Fireball I
(Westfall et al.)
$\frac{E\,d^2\sigma}{p^2 dp d\Omega}$ (mb/sr/(GeV)^{2}c^3)
E^* (MeV)

Fig. 2.21

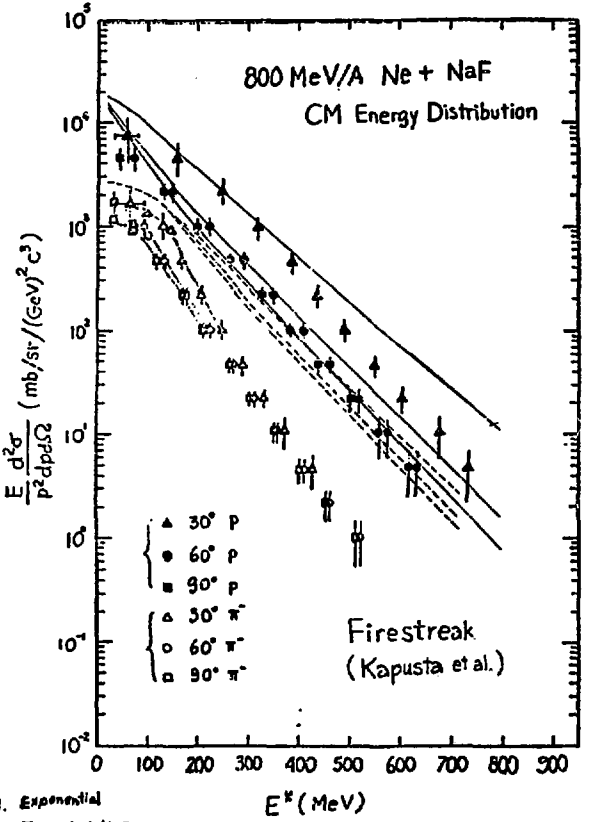
800 MeV/A Ne + NaF
CM Energy Distribution
$\frac{E\,d^2\sigma}{p^2 dp d\Omega}$ (mb/sr/(GeV)^{2}c^3)
E^* (MeV)
30° P
60° P
90° P
30° π⁻
60° π⁻
90° π⁻
Firestreak
(Kapusta et al.)
1. Exponential
2. Too high yield π
3. T(s<T(p)

Fig. 2.22

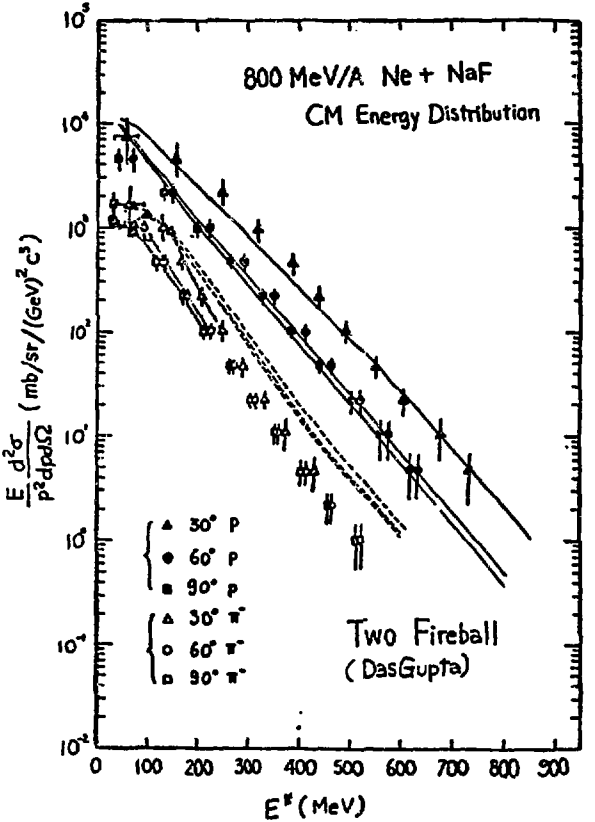
800 MeV/A Ne + NaF
CM Energy Distribution
$\frac{E\,d^2\sigma}{p^2 dp d\Omega}$ (mb/sr/(GeV)^{2}c^3)
30° p
60° p
90° p
30° π⁻
60° π⁻
90° π⁻
Two Fireball
(DasGupta)
E^* (MeV)

Fig. 2.23

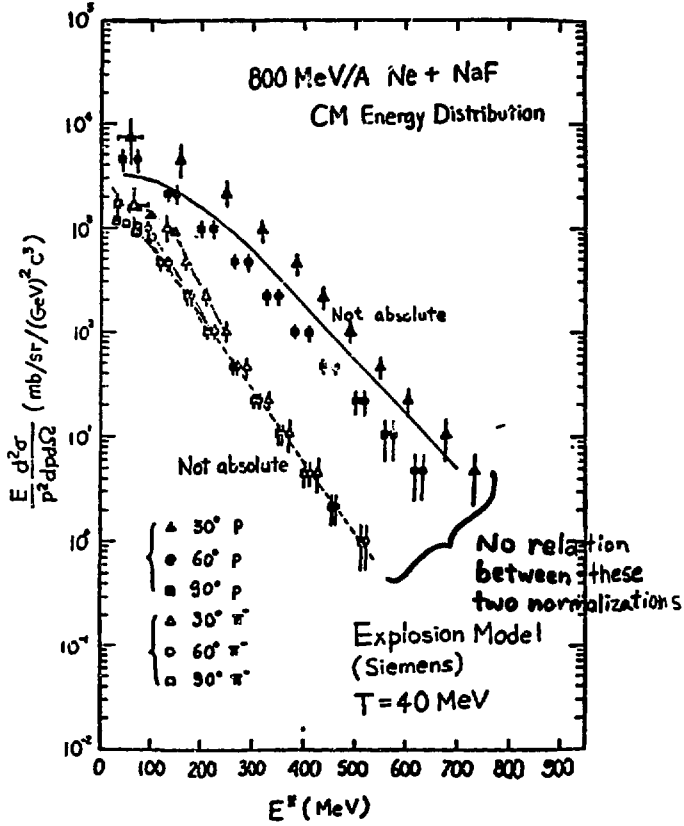
800 MeV/A Ne + NaF
CM Energy Distribution
Not absolute
Not absolute
30° p
60° p
90° p
30° π⁻
60° π⁻
90° π⁻
No relation between these two normalizations
Explosion Model (Siemens)
T = 40 MeV
E/p²dpdΩ d²σ (mb/sr/(GeV)² c³)
E^π (MeV)

Fig. 2.24

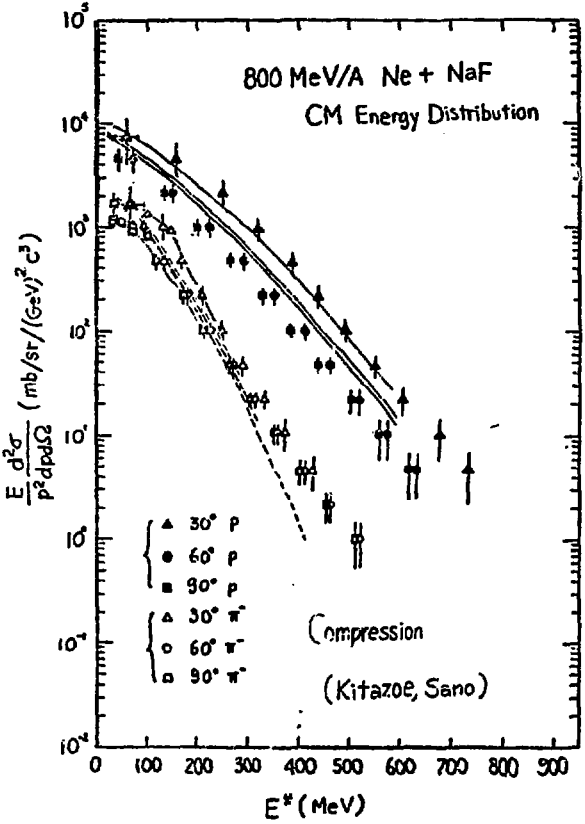
800 MeV/A Ne + NaF
CM Energy Distribution
$\frac{E\,d^2\sigma}{p^2 dp d\Omega}$ (mb/sr/(GeV)^2 c^3)
30° p
60° p
90° p
30° π⁻
60° π⁻
90° π⁻
Compression
(Kitazoe, Sano)
E* (MeV)

Fig. 2.25

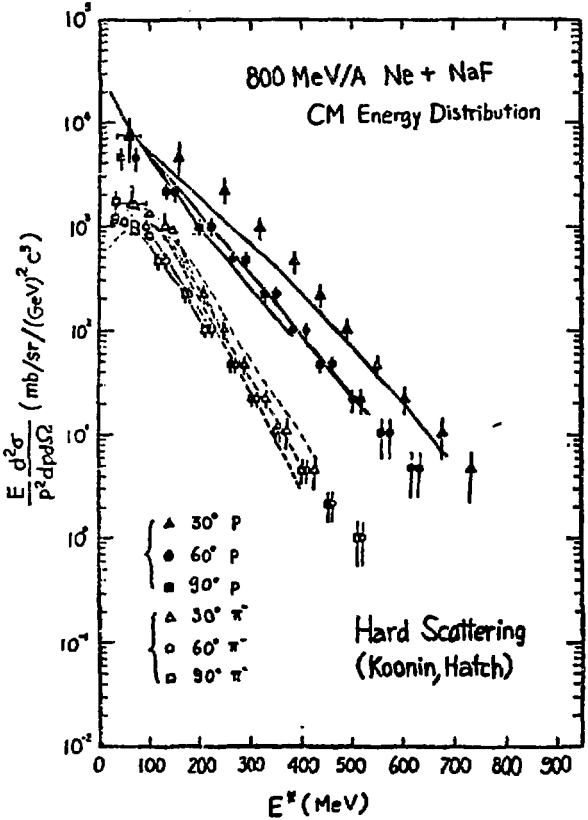
800 MeV/A Ne + NaF
CM Energy Distribution
$\frac{E}{p^2}\frac{d^2\sigma}{dpd\Omega}$ (mb/sr/(GeV)^2 c^3)
E^* (MeV)
30° P
60° P
90° P
30° π⁻
60° π⁻
90° π⁻
Hard Scattering
(Koonin, Hatch)

Fig. 2.26

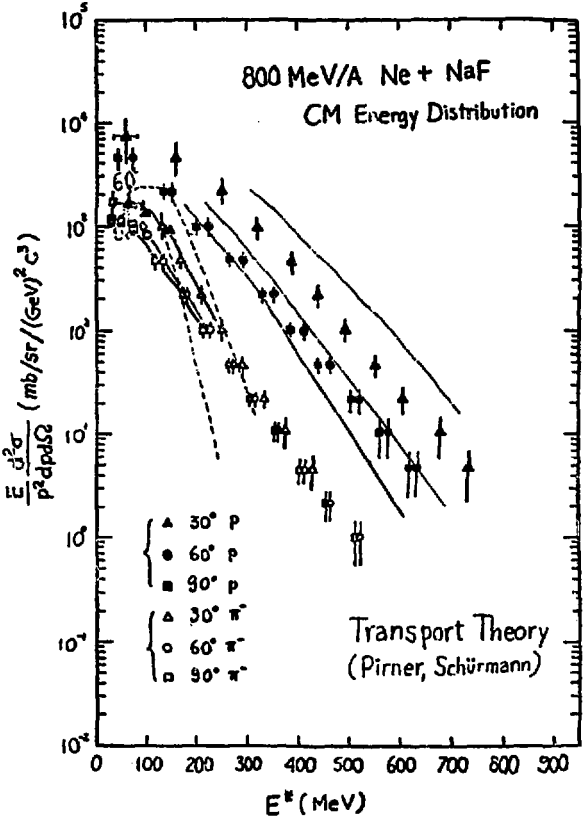
800 MeV/A Ne + NaF
CM Energy Distribution
$E\frac{d^3\sigma}{p^2dpd\Omega}$ (mb/sr/(GeV)^{2}c^3)
30° P
60° P
90° P
30° π⁻
60° π⁻
90° π⁻
Transport Theory
(Pirner, Schürmann)
E^* (MeV)

Fig. 2.27

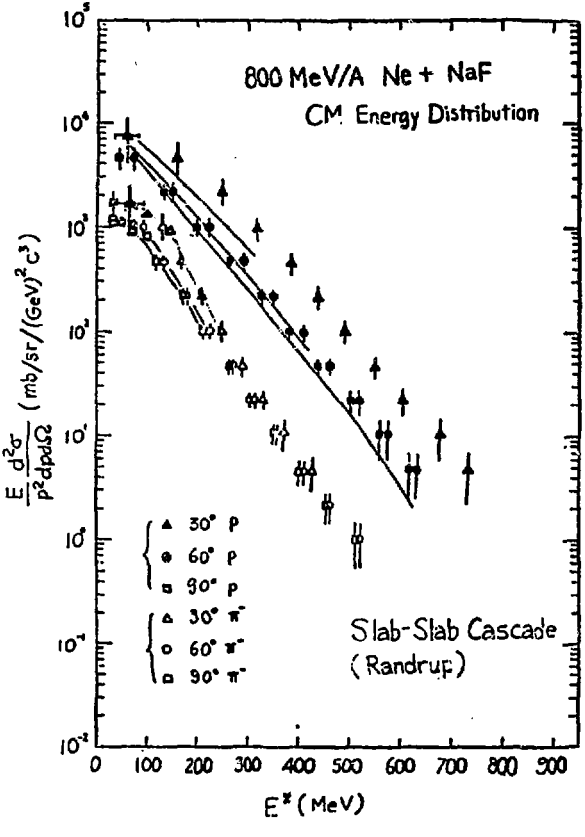
800 MeV/A Ne + NaF
CM Energy Distribution
$\frac{E\,d^2\sigma}{p^2 dp d\Omega}$ (mb/sr/(GeV)^2 c^3)
30° p
60° p
90° p
30° π⁻
60° π⁻
90° π⁻
Slab-Slab Cascade
(Randrup)
E^* (MeV)

Fig. 2.28

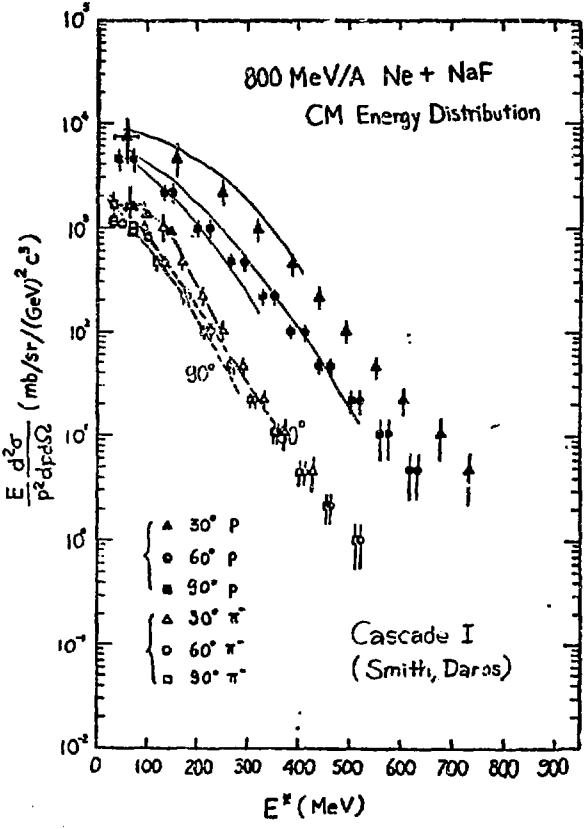
800 MeV/A Ne + NaF
CM Energy Distribution
$\frac{E\,d^2\sigma}{p^2 dp d\Omega}$ (mb/sr/(GeV)^{2}c^3)
90°
90°
▲ 30° P
● 60° P
■ 90° P
△ 30° π⁻
○ 60° π⁻
□ 90° π⁻
Cascade I
(Smith, Daros)
E* (MeV)

Fig. 2.29

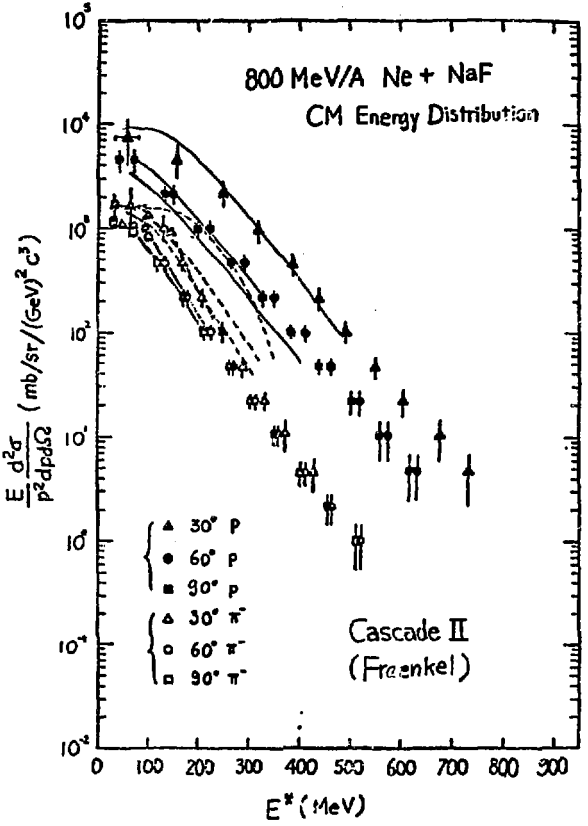
800 MeV/A Ne + NaF
CM Energy Distribution
$\frac{E\,d^2\sigma}{p^2 dp d\Omega}$ (mb/sr/(GeV)^{2}c^3)
30° p
60° p
90° p
30° π⁻
60° π⁻
90° π⁻
Cascade II
(Fraenkel)
E* (MeV)

Fig. 2.30

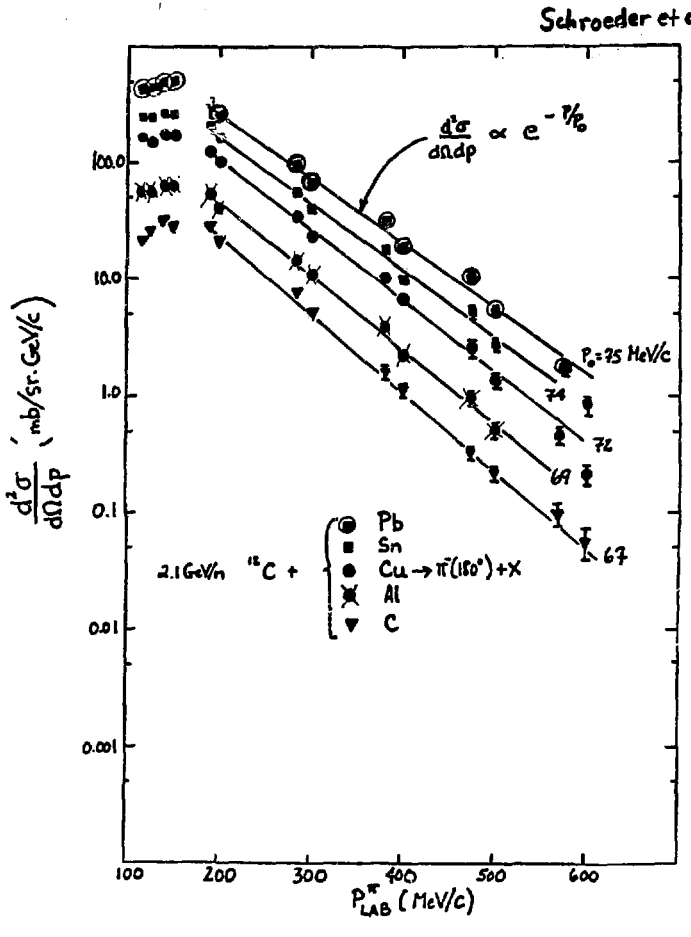
Schroeder et al.
$\frac{d^2\sigma}{d\Omega dp} \propto e^{-p/p_0}$
P_0=75 MeV/c
74
72
69
67
Pb
Sn
Cu → π⁻(180°)+X
Al
C
2.1 GeV/n ¹²C +
$\frac{d^2\sigma}{d\Omega dp}$ (mb/sr·GeV/c)
100.0
10.0
1.0
0.1
0.01
0.001
100
200
300
400
500
600
P^{π}_{LAB} (MeV/c)

Fig. 2.31

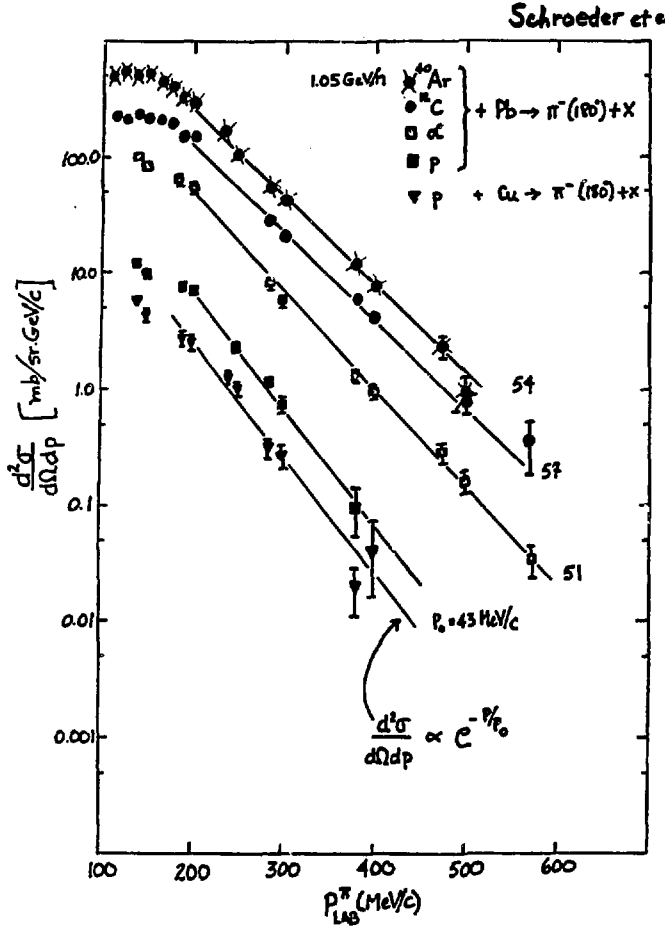
Schroeder et al.
1.05 GeV/n
40Ar
C
Al
P
+ Pb → π⁻(180°)+X
P + Cu → π⁻(180°)+X
100.0
10.0
1.0
0.1
0.01
0.001
d²σ/dΩdp [mb/sr·GeV/c]
54
57
51
P₀=43 MeV/c
d²σ/dΩdp ∝ e^(-P/P₀)
100
200
300
400
500
600
P_LAB^π (MeV/c)

Fig. 2.32

Schroeder et al.

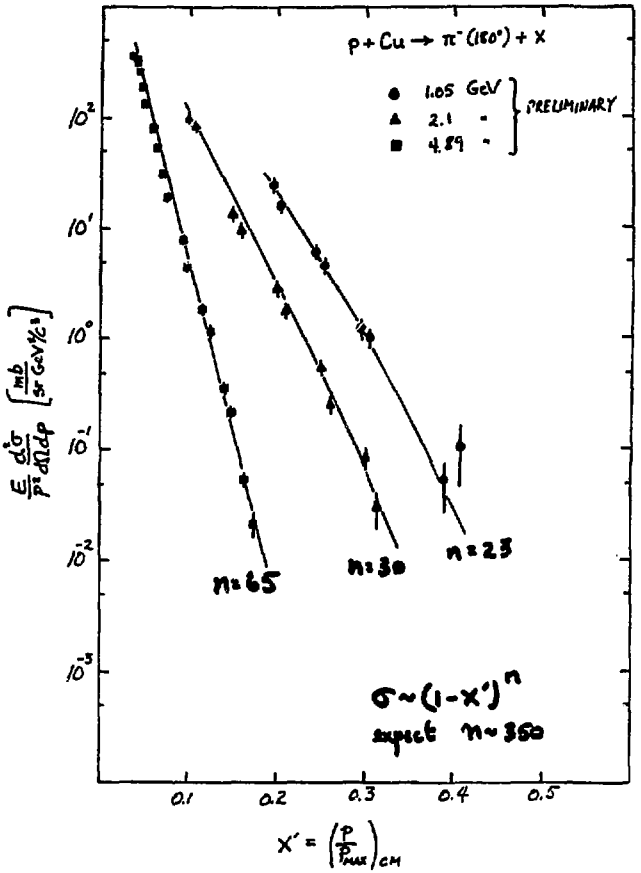

Fig. 2.33

Schroeder et al.

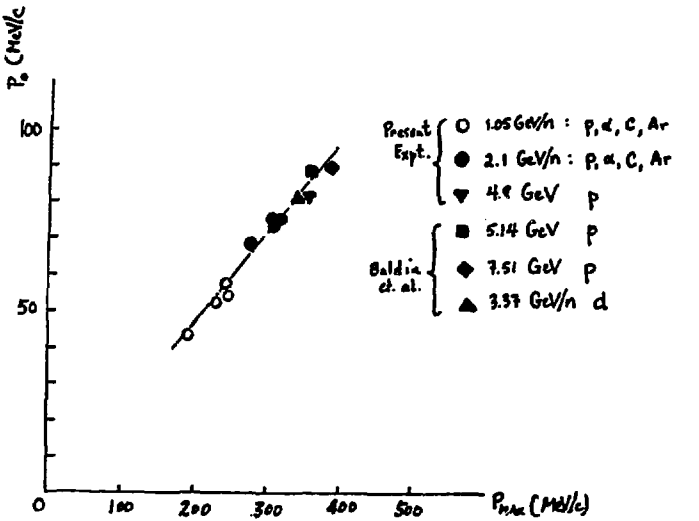

P_o = parameter from $\frac{d^2\sigma}{d\Omega dp} \propto e^{-p/P_o}$

P_{max} = max. pion momentum allowed in process : Proj. + P $\longrightarrow \pi^-(180°) + X$

Fig. 2.34

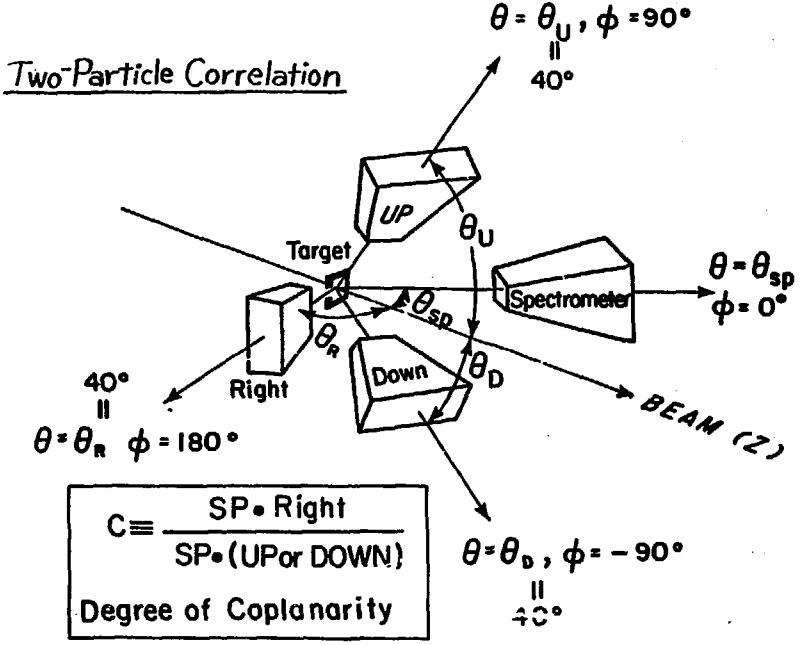

XBL788-1582

Fig. 2.35

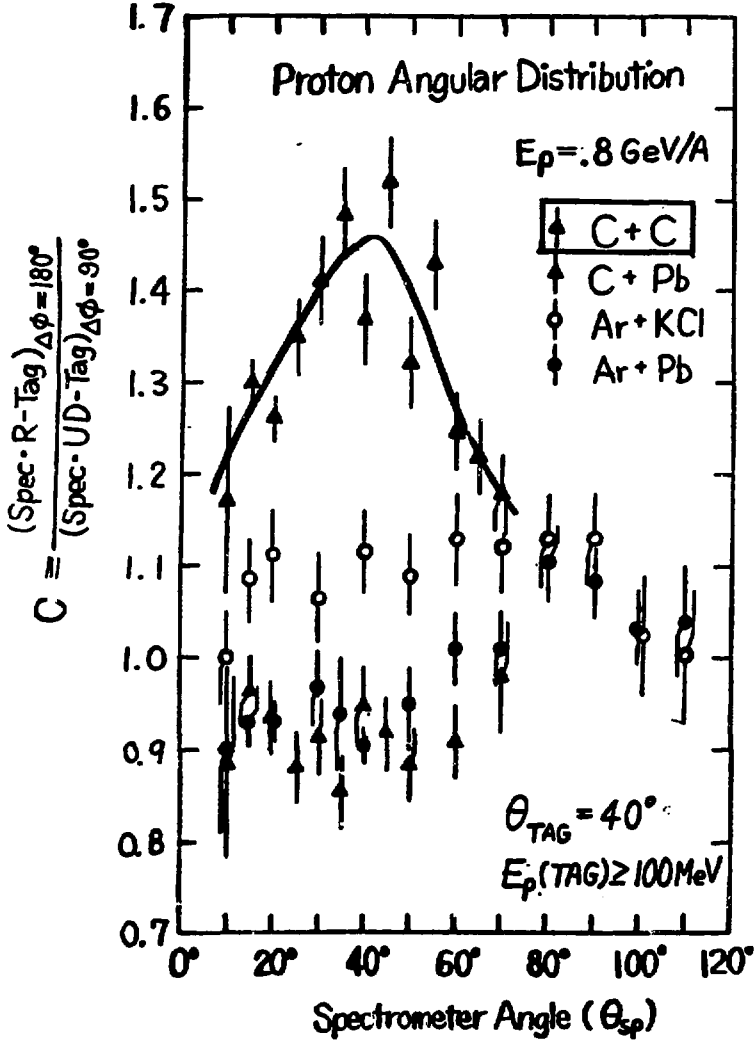
Proton Angular Distribution
Ep=.8 GeV/A
C + C
C + Pb
Ar + KCl
Ar + Pb
θTAG = 40°
Ep(TAG) ≥ 100 MeV
C ≡ (Spec·R-Tag)Δφ=180° / (Spec·UD-Tag)Δφ=90°
Spectrometer Angle (θsp)
1.7
1.6
1.5
1.4
1.3
1.2
1.1
1.0
0.9
0.8
0.7
0°
20°
40°
60°
80°
100°
120°

Fig. 2.36

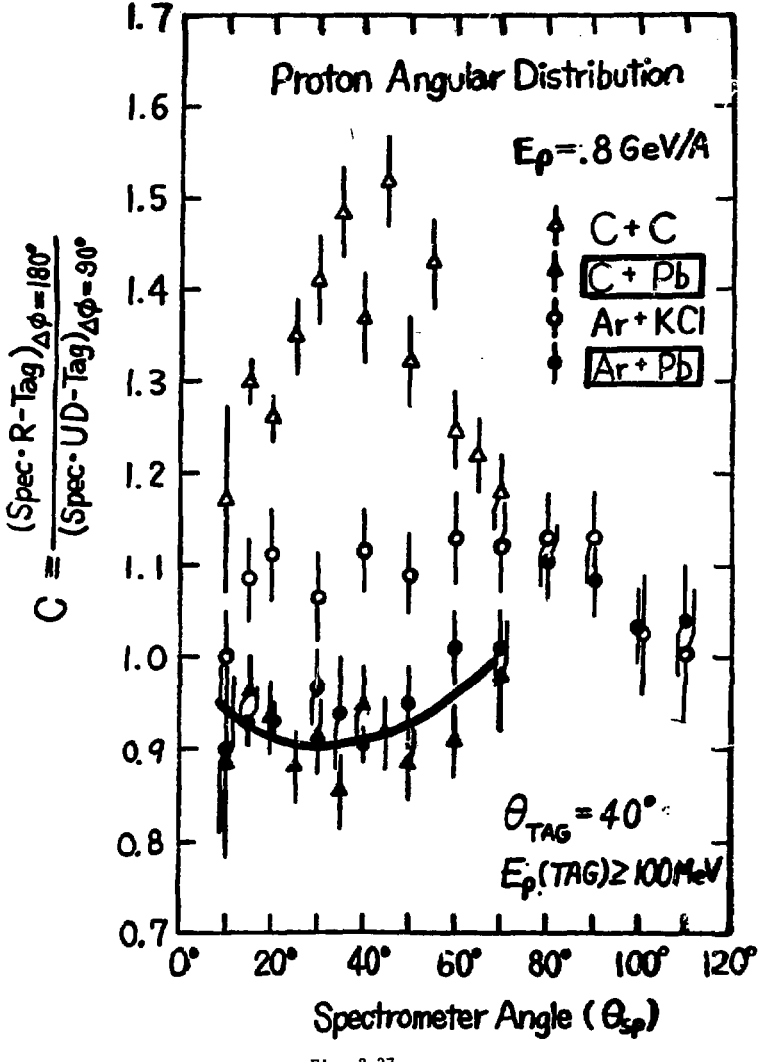
Proton Angular Distribution
E_p=.8 GeV/A
C+C
C+Pb
Ar+KCl
Ar+Pb
θ_{TAG}=40°
E_p(TAG)≥100MeV
$C \equiv \frac{(Spec \cdot R-Tag)_{\Delta\phi=180°}}{(Spec \cdot UD-Tag)_{\Delta\phi=90°}}$
1.7
1.6
1.5
1.4
1.3
1.2
1.1
1.0
0.9
0.8
0.7
0°
20°
40°
60°
80°
100°
120°
Spectrometer Angle (θ_{sp})

Fig. 2.37

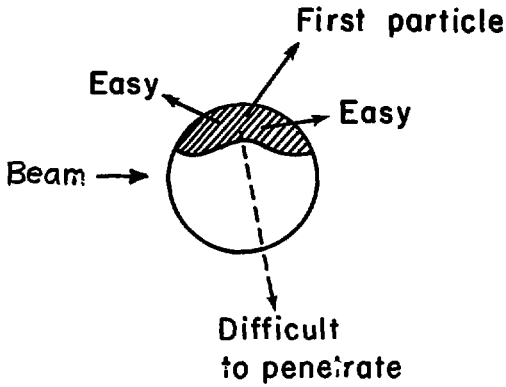

Shadowing observed in
two-particle correlation

Fig. 2.38

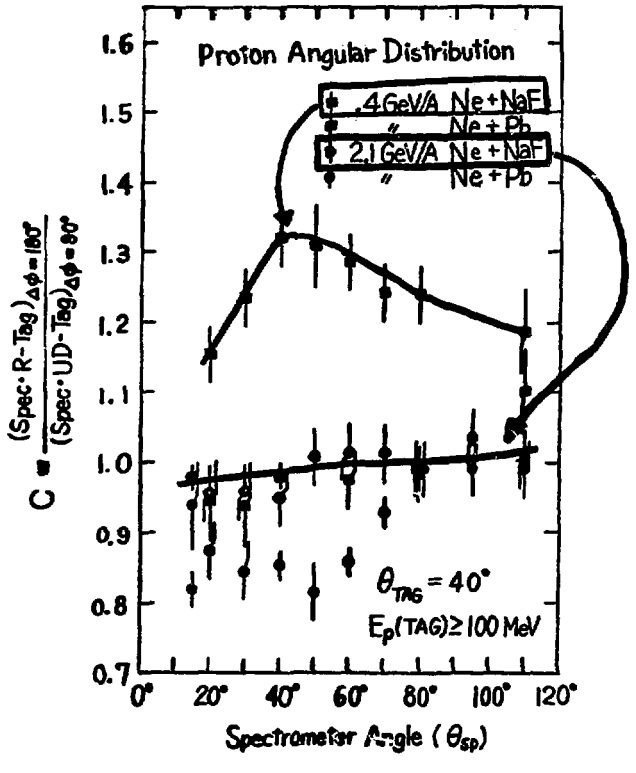
Proton Angular Distribution
.4 GeV/A Ne+NaF
" Ne+Pb
2.1 GeV/A Ne+NaF
" Ne+Pb
$C = \frac{(Spec \cdot R-Tag)_{\Delta\phi=180°}}{(Spec \cdot UD-Tag)_{\Delta\phi=90°}}$
$\theta_{TAG} = 40°$
$E_p(TAG) \geq 100$ MeV
Spectrometer Angle (θ_{sp})
1.6
1.5
1.4
1.3
1.2
1.1
1.0
0.9
0.8
0.7
0°
20°
40°
60°
80°
100°
120°

Fig. 2.39

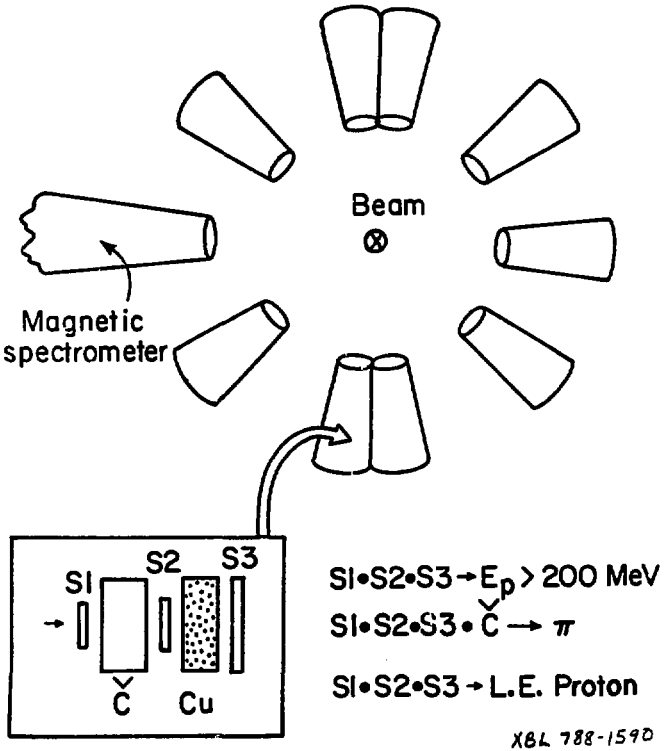
High Multiplicity Events
Beam
Magnetic spectrometer
S1
S2
S3
C
Cu
S1•S2•S3→E_p > 200 MeV
S1•S2•S3•C̄→π
S1•S2•S3→L.E. Proton
XBL 788-1590

Fig. 2.40

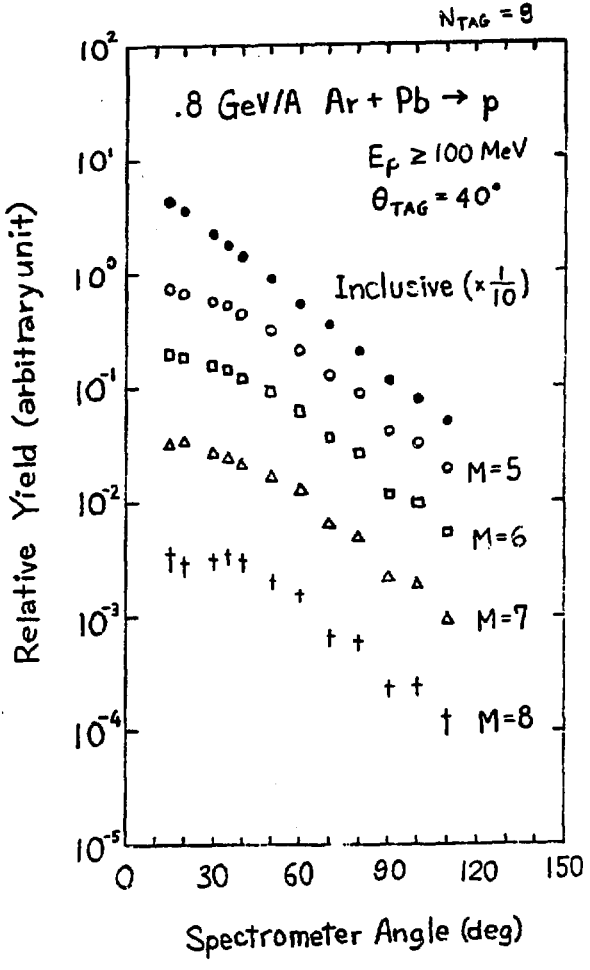
$N_{TAG} = 9$
.8 GeV/A Ar + Pb → p
$E_p \geq 100$ MeV
$\theta_{TAG} = 40°$
Inclusive ($\times \frac{1}{10}$)
M=5
M=6
M=7
M=8
Relative Yield (arbitrary unit)
Spectrometer Angle (deg)
10^2
10^1
10^0
10^{-1}
10^{-2}
10^{-3}
10^{-4}
10^{-5}
0
30
60
90
120
150

Fig. 2.41

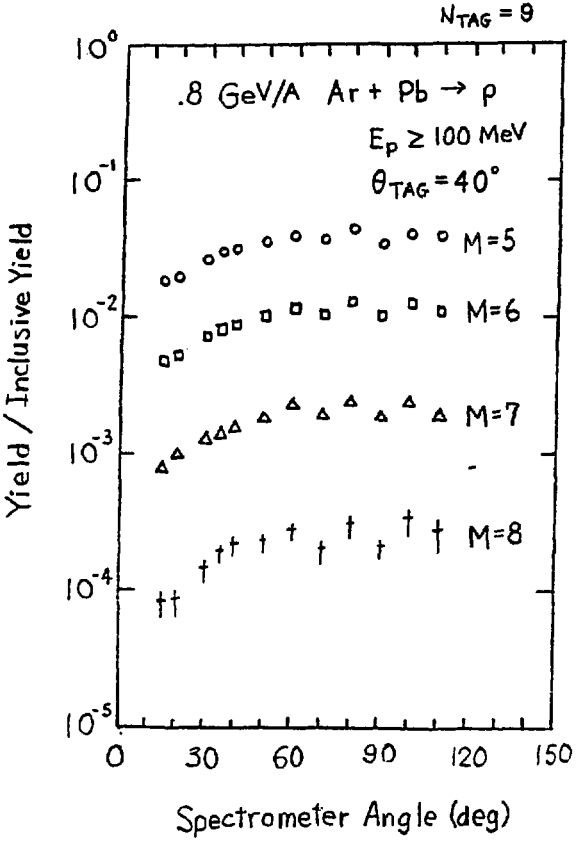
$N_{TAG} = 9$
.8 GeV/A Ar + Pb → p
$E_p \geq 100$ MeV
$\theta_{TAG} = 40°$
M=5
M=6
M=7
M=8
Yield / Inclusive Yield
10^0
10^{-1}
10^{-2}
10^{-3}
10^{-4}
10^{-5}
0
30
60
90
120
150
Spectrometer Angle (deg)

Fig. 2.42

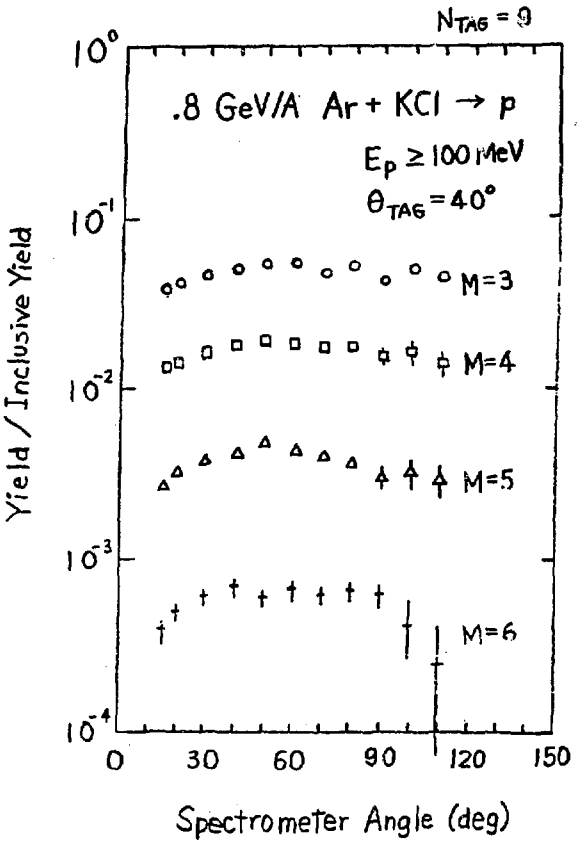
$N_{TAG} = 9$
.8 GeV/A Ar + KCl → p
$E_p \geq 100$ MeV
$\theta_{TAG} = 40°$
M=3
M=4
M=5
M=6
Yield / Inclusive Yield
10^0
10^{-1}
10^{-2}
10^{-3}
10^{-4}
0
30
60
90
120
150
Spectrometer Angle (deg)

Fig. 2.43

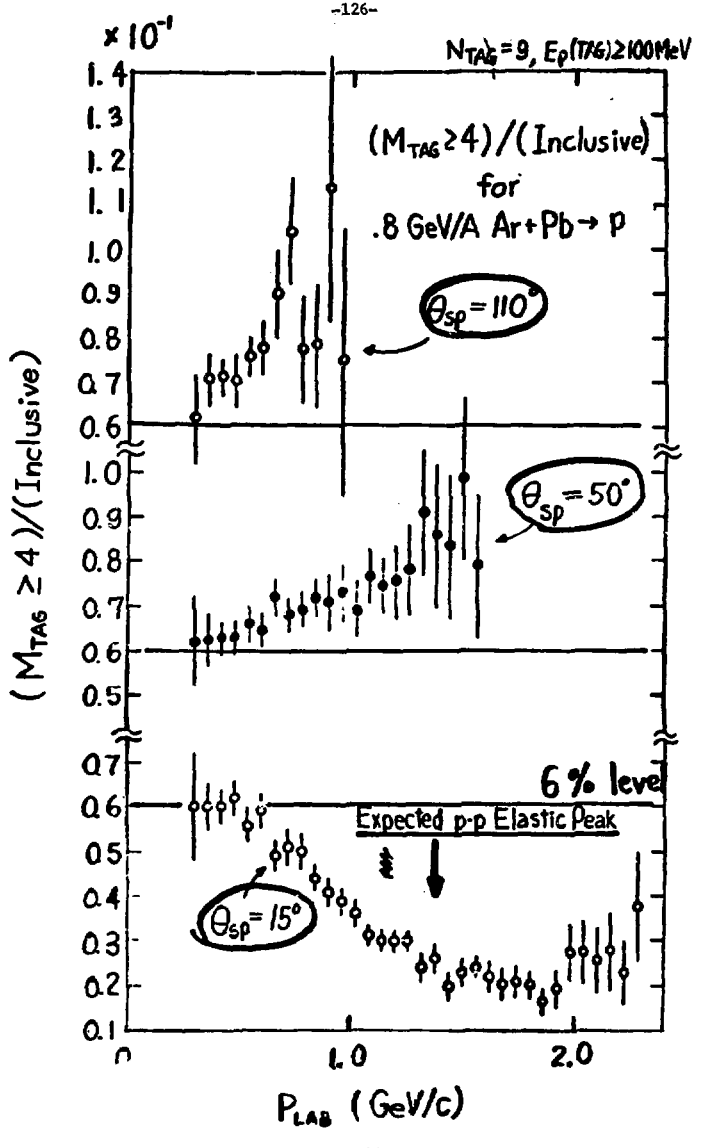
× 10⁻¹
N_TAG = 9, Eₚ(TAG) ≥ 100 MeV
(M_TAG ≥ 4)/(Inclusive)
for
.8 GeV/A Ar+Pb → p
θ_sp = 110°
θ_sp = 50°
θ_sp = 15°
6 % level
Expected p-p Elastic Peak
(M_TAG ≥ 4)/(Inclusive)
P_LAB (GeV/c)

Fig. 2.44

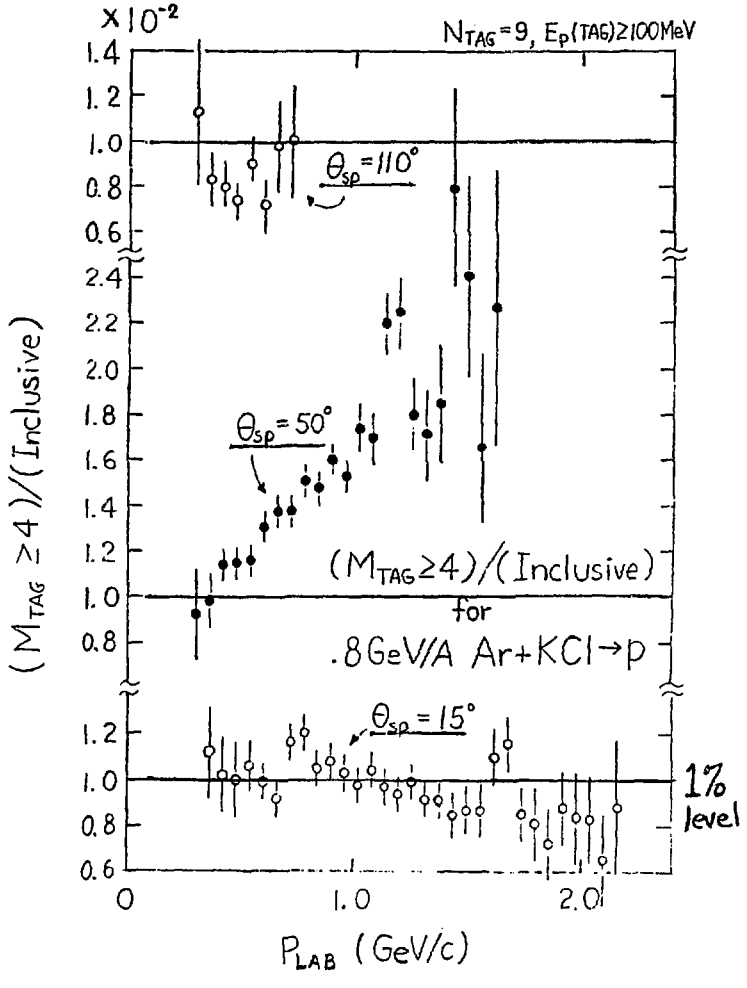
X 10⁻²
N_TAG = 9, E_p(TAG) ≥ 100MeV
θ_sp = 110°
θ_sp = 50°
θ_sp = 15°
(M_TAG ≥ 4)/(Inclusive)
for
.8GeV/A Ar+KCl→p
1% level
(M_TAG ≥ 4)/(Inclusive)
P_LAB (GeV/c)

Fig. 2.45

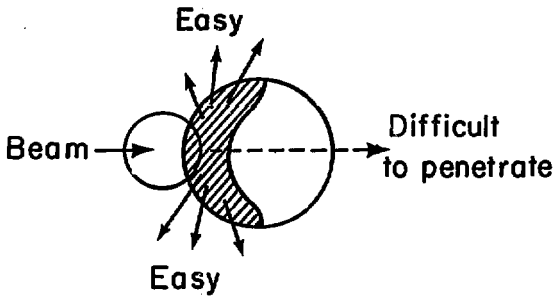

Shadowing observed in
high multiplicity events

XBL788-1585

Fig. 2.46

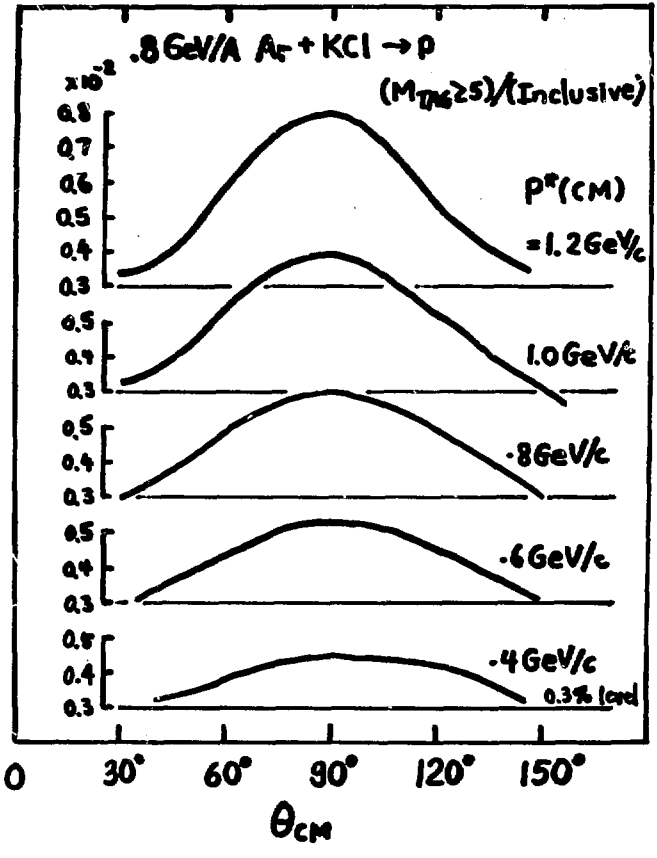
.8 GeV/A Ar + KCl → p
(M_TMC≥5)/(Inclusive)
x10^-2
0.8
0.7
0.6
0.5
0.4
0.3
p*(cm)
=1.2GeV/c
1.0GeV/c
.8GeV/c
.6GeV/c
.4GeV/c
0.3% level
0
30°
60°
90°
120°
150°
θcm

Fig. 2.47

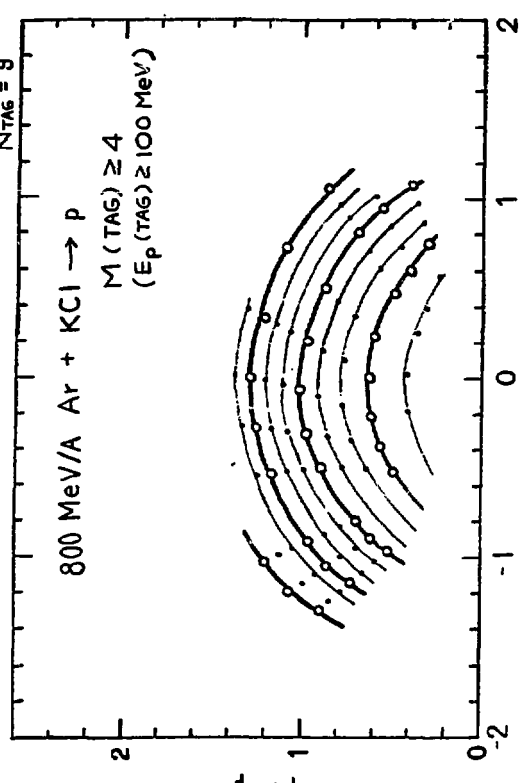
N_TAG = 9
800 MeV/A Ar + KCl → p
M (TAG) ≥ 4
(E_p (TAG) ≥ 100 MeV)
P_T /m_p c
p*_II /m_p c
2
1
0
-1
-2

Fig. 2.48

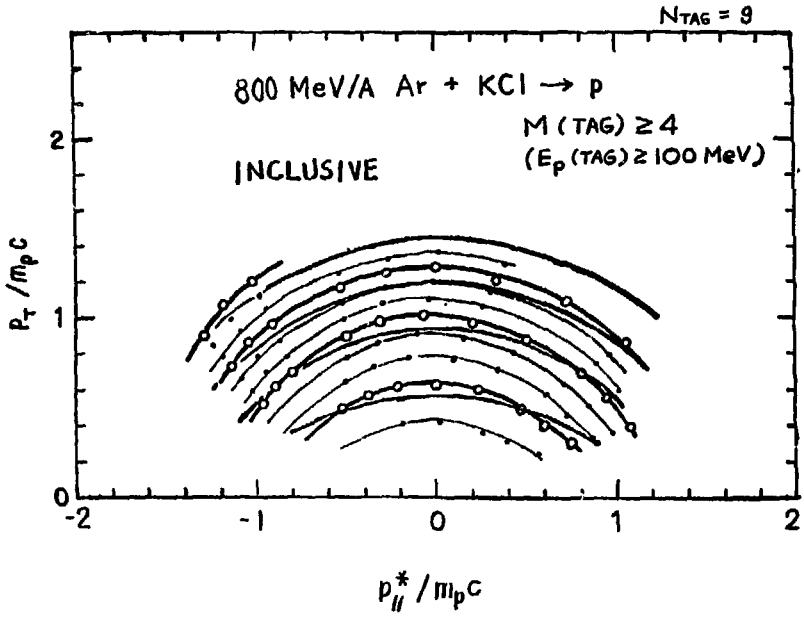
N_TAG = 9
800 MeV/A Ar + KCl → p
M (TAG) ≥ 4
(E_p (TAG) ≥ 100 MeV)
INCLUSIVE
P_T /m_p c
p*_// /m_p c
2
1
0
-2
-1
0
1
2

Fig. 2.49

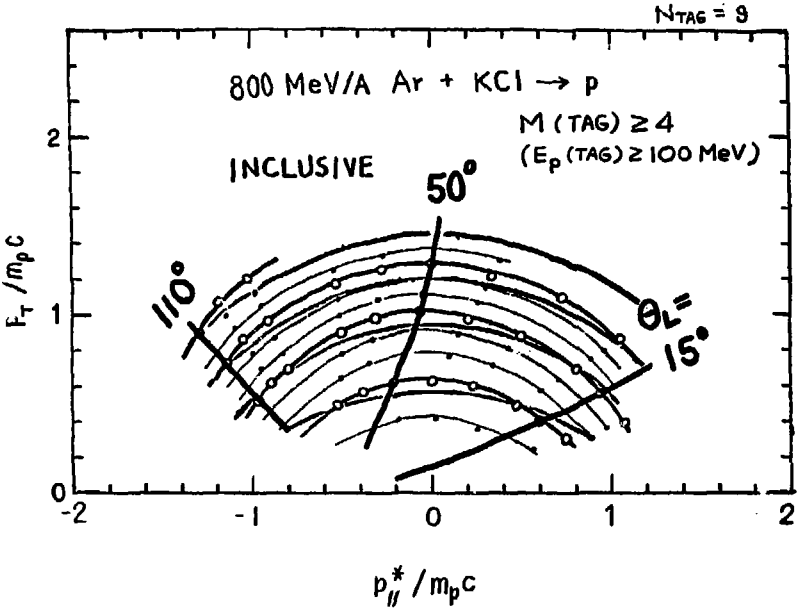
$N_{TAG} = 9$
800 MeV/A Ar + KCl → p
M (TAG) ≥ 4
(E_p (TAG) ≥ 100 MeV)
INCLUSIVE
50°
110°
θ_L = 15°
$E_T / m_p c$
$p_{//}^* / m_p c$
2
1
0
-2
-1
0
1
2

Fig. 2.50

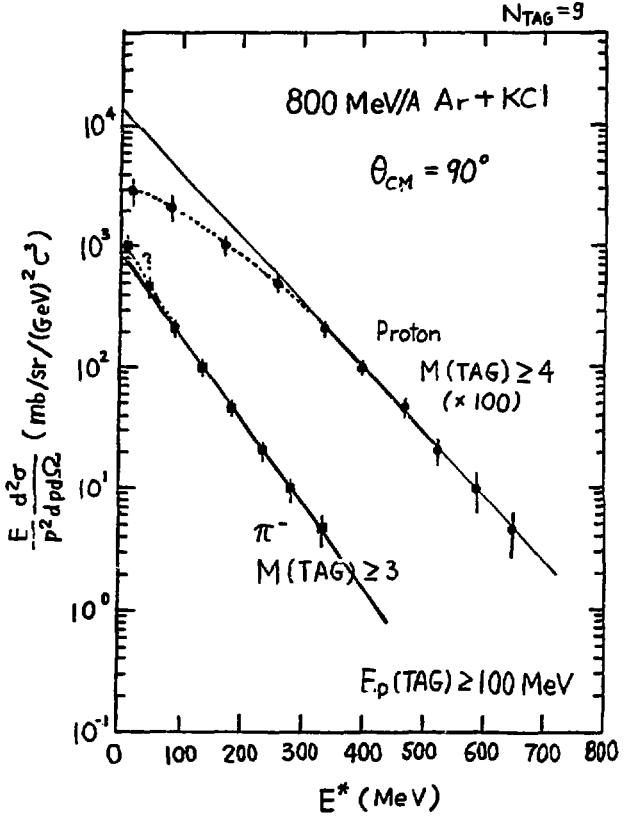
$N_{TAG}=9$
800 MeV/A Ar + KCl
$\theta_{CM} = 90°$
Proton
M (TAG) ≥ 4
(× 100)
π^-
M (TAG) ≥ 3
E_p (TAG) ≥ 100 MeV
$\frac{E}{p^2}\frac{d^2\sigma}{dp d\Omega}$ (mb/sr/(GeV)^{2}c^3)
10^4
10^3
10^2
10^1
10^0
10^{-1}
0
100
200
300
400
500
600
700
800
E* (MeV)

Fig. 2.51

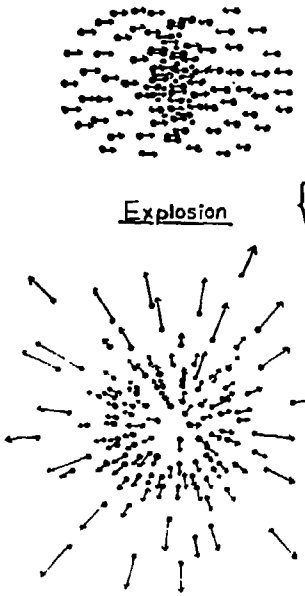
Compression
Experiment
• Energy
→ Compression
→ Reaction
(Pion Production etc.)
• Temporary High Density
• Y(π) less than any Thermal Models
Explosion
• nucleon
• pion
• Energy
→ Explosion
→ Reaction Products
• Explosion Flow
→ sensitive to protons
→ insensitive to pions
• Non-Exponential Behavior of Proton Spectra
• Pion Slope (in Energy Spectra) Steeper than Proton Slope

Fig. 2.52

APPROACH TO EQUILIBRIUM BASED ON MICROSCOPIC MODELS OF NUCLEAR COLLISIONS

Jörg Hüfner

Two years ago at the summer study we were presented with the first experimental data on inclusive proton, pion, and composite particle spectra. At that time nobody understood the underlying physics, and therefore Miklos Gyulassy handed out a homework problem: calculate the inclusive proton spectrum for 250 MeV/A neon on uranium. The first solution to the homework problem was handed in a few weeks later — it was the fireball model. It was handed in by experimentalists, which again shows that they have a better sense of physics. About half a year later theoreticians came up with a number of solutions and the variety is really bewildering — models with openly contradictory assumptions fit the data.

Let me show you, as a kind of introduction to the present status, two extreme solutions. Most of the solutions are found in between these two extremes (Fig. 3.1).

The latest measurements of 250 MeV/A Ne + U → p + X are the data of the Gutbrod-Poskanzer-Stock group. The double differential cross section is plotted against the energy of the outgoing proton. I have selected only a few data points, to avoid confusing the picture. On the left side the data are compared with the extreme thermal assumption, the firestreak model, which is a further development (by Myers) of the fireball model. It assumes that the nuclear matter in the two colliding nuclei comes to complete thermal equilibrium. On the right-hand side is a calculation by Steve Koonin, who assumes that one nucleon from the projectile interacts once (at the most) with one nucleon from the target. This is a direct interaction mechanism. In the language of low energy physics, Myers' model corresponds to a compound model while the other is a direct interaction mechanism.

When I saw these two opposing fits it reminded me of the story of two people who quarrel: since they don't come to an agreement they go to court. The first person presents his case to the judge and the judge says, "Well, you are right." Then the second person presents his, of course, opposing view of the case and the judge says again, "Well, you are right." And finally some spectators from the audience feel uneasy and ask the judge, "How can you say 'You are right' to both of them? They cannot both be right." And the judge says, "Yes, you are right."

That is the kind of situation we are in - two people present their calculations and the experiment says, "Yes, you are right" to both. But if you look a little more closely you see, for instance, that the firestreak model is very good in the backward direction, but somehow misses in the forward direction, because the slope is not well reproduced. Where the firestreak model fails, the direct interaction model seems to work, namely, the slope is well reproduced.

In order not to add to the confusion, I will be extremely simple in my talk, which will probably allow a lot of criticism. I think, however, that we have to disentangle the whole thing in order to come to the physics. Let me start by trying to divide the single-particle inclusive cross section into two aspects, the geometry and the dynamics. Since the geometry is always easier, let me start with it (Fig. 3.2).

The geometry is already present in the fireball model, and I think it is essentially present in all the models I will talk about. In this geometry all nucleons are separated into participants and spectators. Before the collision there are the approaching projectile and the target nucleus. The straight-line motion of the projectile defines an overlap zone; nucleons in that zone are called participants and those outside are spectators. The basic assumption of the geometry is that: only the participants eventually arrive at the counter. The reason for this may be that the counter doesn't accept low energy nucleons or that it looks at angles where you don't see nucleons coming from outside the overlap zone. The model is clearly defined, maybe overly simplistic compared to nature, and we can draw some numerical conclusions. Let's define the double-differential cross section as in Fig. 3.2. The geometry gives us a sum rule: the total integrated one-nucleon cross section is simply related to the number of nucleons in the target and projectile and to the area of each as seen by the other. You don't have to say anything about the dynamics — the only assumption is that you observe the participants.

How well does this sum rule work? I have made one comparison: I looked at the multiplicity, which is the integrated one-nucleon cross section divided by the total reaction cross section. That cross section is taken to be the geometric one, which is the sum of $r^2\pi$. I've drawn the relation between the theoretical multiplicity, $\langle M \rangle_{th}$, which is just a function of Z and A of the participant projectile and target, and the experimental mean multiplicity, which has been taken from streamer chamber exposures by the Poe-Schroeder group. The circles are for carbon as the projectile, the crosses are for argon as the projectile. The targets are labelled. The straight line is the prediction from the participant geometry. The agreement is not very good. It's best for barium and it's worst for lithium, but one has the impression that there is some correlation between the theoretical and the experimental multiplicity. In fact, I think the deviations are very pleasing because all the experimental values are above the theoretical prediction, which means you probably get nucleons from outside the overlap zone, as we expected. And the streamer chamber should see a lot of spectator nucleons because the trigger conditions are rather low. Furthermore, the deviations are largest for light systems like lithium and sodium. You wouldn't think that if you pulled off, say, three nucleons from a lithium, the remaining three nucleons would remain intact. So, it's comforting that the light nuclei obey this geometric rule less well than the heavy one, Bal. I think the discrepancy for the lead is due to the oxygen, but this has to be proven.

Figure 3.2 shows, I believe, that there is something true in the basic geometric assumption. And since this assumption gives you a sum rule (pure geometry - no dynamics), every "decent" model that has this sum rule in it,

either disguised or openly, should reproduce the absolute magnitude of the cross section. The absolute magnitude of the inclusive cross section does not contain a lot of physics. If you find that the absolute normalization is correctly found in a theory, that doesn't necessarily mean that the theory is very good. That's just as a warning.

For me, there remain at least two questions concerning geometry. How clean is the geometric cut and how does it change with energy? It may not be a clean straight line cut — presumably it's more like a trumpet, opening up. These are questions I don't know how to solve. I also feel uneasy about the shadowing. Do we see the shadow, and how much is it there? That could tell us something about the "hot ball" where we think the main physics happens.

I would like to discuss the dynamics in terms of two extreme situations, a direct interaction and a thermal event (Fig. 3.3). I want to estimate how much of the inclusive cross section comes from a direct event and how much from a thermal event. Of course, in order to make an estimate, "direct" and "thermal" must be defined. For the direct interaction this is simple: We assume that only one nucleon from the projectile interacts once with one target nucleon. There is no interaction before and no interaction afterwards. It's a one-on-one collision. A thermal event is somewhat more complicated: we have to put in one number, a magic number, that tells how many collision rounds it takes to get to thermal equilibrium. This thermal number, $n_{thermal}$, will be discussed later. For now, I will assume it to be three. In order to make this estimate I go back to an even simpler geometry, the geometry of one dimension, of streaks, or rows, or tubes. So I look at something like this row or tube of nucleons in the target and one in the projectile and I say that only one tube in the projectile interacts with its corresonding tube in the target. If there is only one nucleon in the target tube and only one nucleon in the projectile tube I will call it a direct interaction. If there are three or more in the projectile tube interacting with three or more in the target tube I call it a thermal event. It's just a simple counting problem to find out how many of the events are direct and how many are thermal — except that you need this magic number of three.

Taking this for granted, I come to the following estimates. Don't take them too seriously, don't quote them. They are extremely simplistic (for instance, based on uniform density), but I think they make the point.

Let's take Ne + U or C + C (Fig. 3.4). "$\int_1 d^2b$" means the one-nucleon inclusive cross section without any biases. And below (b=0) it is for a central collision. For Ne + U the direct component is less than a percent; the thermal component, the way I've defined it, is 40%, and the intermediate — those events that do not fit in either of the two — is 60%. I think this is a warning: although a considerable part of the interaction goes thermal, one half is not thermal even in a collision like Ne + U. And if you go to central collisions you may increase the amount of thermal events, but not by 100%. I think that is the message. And for C + C it's even worse. About 4% is direct, and a corresponding amount is thermal, and everything else — 90% — is in between, and doesn't fit either model. In a central collision you would expect an increase in the thermal component, but this is not true.

Here the thermal component increases, but the direct component also increases because the nucleons on the rim interact, and because one nucleon is usually on the rim hitting another nucleon on the rim. Therefore there is a lot of direct interaction even in a central collision. So the separation of direct interaction and thermal events is by no means easy.

To give some evidence for the direct interaction I want to show a picture that Shoji Nagamiya showed yesterday (Fig. 3.5). An evidence for direct interaction — or, to be safe, an evidence against its being a thermal event — is the two-nucleon correlation. Instead of looking at just one nucleon, you tag one and look at the second, and make an in-plane and out-of-plane correlation. Direct interaction mechanism should favor the in-plane events, and there should be nothing out-of-plane. In a thermal event there should be no correlation between the in-plane and out-of-plane. We see here the in-plane to out-of-plane correlation for C + C → p + X, as a function of the momentum of the outgoing nucleon. The quasi-elastic peak, which corresponds to a direct nucleon-nucleon event, is expected, and indeed you see something in the correlation function. If you want to make the comparison these may be somehow connected with the 4%. If you go to a heavy system, C + Pb, roughly Ne + U, the correlation vanishes; this may be due to the reduction from 4% to 0.4%. I'm not completely sure whether that is true, but at least experiment does not contradict the suggestion. If we take the same reasoning to the data that Hans Gutbrod showed yesterday, namely, the similar correlations for p + U and ^{4}He + U, there is a strong correlation for the former but there is none for the latter. If you take the geometry argument, which gave us the factor of 10, and apply it to the proton and ^{4}He ratio, you come out with a factor of 2.5, and therefore ^{4}He should be lower by a factor of 2.5 than the proton. But experiment is certainly lower than that. So there must be something in addition to this pure geometric argument and my guess, which I cannot substantiate it by any calculation, is that there is Fermi motion. Fermi motion also washes out a certain correlation, and that has to be investigated.

This introduction explains that in order to describe the data in a quantitative fashion you have to have approaches that can account for the transitions from direct interactions to thermal equilibrium. There are many models that do that. Essentially all have in common the fact that they solve the Boltzmann equation, which describes the approach to equilibrium for a classical system and for a system of low density as well. As Hans Gutbrod said yesterday, we're dealing with hot air. The most complicated solution to the Boltzmann equation is the cascade calculation. I don't want to go into details, since they are extremely complicated. But there are three calculations that essentially agree: an approach by Z. Fraenkel and Y. Yariv, another by K. Smith and M. Danos and a third by J. Bondorf, E. Halbert and C. Noack. Then there are some approximate solutions: among others, the rows on rows model, which J. Knoll and I have developed in Heidelberg with improvements by J. Randrup, H. Pirner and B. Schurmann; and the approximate solution by R. Malfliet; the hydrodynamics approach by Nix and collaborators; and finally the equations of motion. A. Bodmer and Panos worked on them as well as L. Wilets and collaborators. I think the input to the solutions is essentially classical physics and they are all based on the same equation, the Boltzmann equation, for the approach to equilibrium. (Note: A. Bodmer pointed out that the classical

equations of motion go beyond the Boltzmann equation and also that hydrodynamics may be derived differently.) It is not surprising that they give roughly the same answer.

Since I have no cross section calculations from the classical equations of motion, I have taken examples from the first three (Fig. 3.6, 3.7). The intranuclear cascade calculation is from the Weizmann Institute, the rows on rows is from Heidelberg and the two-fluid hydrodynamics is by Nix. The data are 250 MeV/A Ne + U → charged particle + X, and the dots are a kind of mock-up experiment. They are not the actual proton data, but all charged particle data have been put together, because none of the approaches can handle the composite particles. There is no normalization constant applied — these are absolute fits. I think it was very good that in the beginning the experiments were not right in the absolute magnitude because this tested the honesty of the calculations. I think it's fair to say, therefore, that within the present range of experimental data all three approaches, and they stand for many more, do fit the data. In the rows on rows model there is a clear discrepancy of a factor of 2, 3, or 4, which also shows up in the cascade calculation. Certainly the two-fluid model predicts a strong forward peak, which neither of the other two models predicts — we have to see what experiment has to say. It's also fair to say that most of the calculations, i.e., the cascade calculation as well as the hydrodynamic calculation, are extremely complicated. That is what is good about ours — it can be done in an afternoon on a desk calculator. I don't want to say that this is therefore better, but we may get more physical insight if we look at a very simple theory. If you want to compare with experiment later, then you should do the best numerical solution possible.

Let me show you an example of what kind of physics we can expect and what we can learn. I want to show this to explain the magic number of how many collisions it takes to come to equilibrium. Let's take a typical nucleon-nucleon event, which is part of the whole cascade (Fig. 3.8). One is a nucleon from the target nucleus, the other from the projectile -- they collide and scatter into some other directions. The brackets denote the mean momenta of the two nucleons and the primes refer to the mean momenta of the outgoing nucleons. Whatever the distribution is, whether thermal or not, the mean momenta before and after the collision are related in an extremely simple nonrelativistic fashion. The projectile momentum loses a fraction, α, in the scattering process, and the target nucleon adds a fraction, α, in the scattering process. On the average, momentum conservation is fulfilled. It is this α, obviously, which shows how quickly the two momenta approach each other. Alpha is connected with the nucleon-nucleon cross section. Essentially the whole nucleon-nucleon cascade depends only on the value of α, and not on any other details of the nucleon-nucleon cross section. Alpha is a dimensionless quantity and governs the approach to momentum equilibration. Therefore, we would call the inverse of α the number of collisions until complete equilibration of the momenta. For an isotropic nucleon-nucleon cross section, $\alpha = 1/4$. That means $n_{thermal}$ is about 4, which is in fairly good agreement with the number 3 that we had. Incidentally, in the appendix of Kittel's book on the theory of heat, there is a numerical study about gas in which 100 particles are put in some corner of the phase space and let go. It takes

three collisions until the system comes to equilibrium. It's a gas of billiard balls, that is, hard-sphere scattering. If you remember that hard-sphere scattering is isotropic scattering this completely different system is again governed by something like $n_{thermal} = 4$.

But I have a few questions I would like answered. We saw data yesterday that broke up the cross section according to associate multiplicity. In the language of theory it seems that it's related to breaking up the cross section with respect to impact parameter. It's important to understand this because it changes the amount of direct interactions to thermal events, or whatever we have, so we can get a deeper understanding. One other question is what is the magic number above 1 GeV/A? There you need more than kinematics: deltas, pions, and maybe higher resonances have to be included. There are indications that the magic number is somewhat higher, maybe 6 or 8. But I think this has to be investigated. It's extremely important because it has a lot of bearing on what N. Glendenning proposes in the model of highly compressed hadronic matter.

Then there is work for theorists on the Boltzmann equation. We should have better solutions, not only in the sense of numerics, but also of transparency. And we have to get away from the classical dilute gas because it's hot air, and who likes to investigate hot air? We have to see where quantum effects enter; we have to see on which level nucleon-nucleon correlations enter; we have to cope somehow with the high density; we have to see how, say, phase transitions come into these equations, because somehow they have to be put in. It's a long way to go, but we must find out what the signatures are in order to do meaningful experiments. So I think we're just at the beginning —we've had a glimpse at what can possibly happen.

I would now like to discuss the composite particles (Fig. 3.9), not because I understand very much about them, but in order to draw your attention to the fact that there are many other questions that need to be answered. Let me try to describe the situation for composite particle production, using the deuteron as an example. Projectile plus target gives deuteron plus X, and again, in two years we have seen two complementary models, namely, the direct model and the thermal model.

The direct model is called the coalescence model. Its basic idea is that when two nucleons from the expanding participant volume have nearly equal momenta they coalesce to a deuteron. The other model, of chemical equilibrium, was developed by A. Mekjian. It is based on the assumption that the participants in the participant volume come to a chemical equilibrium. The system expands and at the end there is a certain freeze-out time when the objects in the hot blob do not interact anymore, and the observed deuteron spectrum reflects the chemical equilibrium at the freeze-out density. The two models predict that the deuteron cross section should be related to the square of the proton cross section with a constant that, in the coalescence model, depends on p_o, the momentum in phase space, and on the freeze-out density for the chemical equilibrium. Typical values come out very reasonably in both modes: p_o = 200 MeV/c for the coalescence model and the freeze-out density is roughly half of the nuclear matter density.

How well is this relation fulfilled? I have some data from Shoji Nagamiya's group, which M. Lemaire prepared for me (Fig. 3.10). This is 400 MeV/A Ne on NaF, and shows the invariant cross section for the deuteron production plotted against the momentum at two angles, 30° and 60°. The theory, the square law (shown in Figure 3.13) is so close to the experiment that I had to mark the experimental transparency with an E to tell them apart. They just fall on top. Not only is the shape at 30° well reproduced, but also the ratio between 30° and 60°. There is one overall normalization. It's amazing how well this square law works, especially when you look for the basis of this law. It just shouldn't happen; this relation shouldn't even hold. You should break up cross sections as a function of impact parameter and then take the square and sum them.

I think the situation for composite particles is even more confusing. The shape of the cross section is not a way to distinguish between two models, so its's only the constant. And nobody can calculate it so accurately as to exclude one or the other (Fig. 3.12). Is the time sufficient for reaching chemical equilibrium, or do we stop somewhere in between with a pre-equilibrium situation? I don't want to go very much into the expanding fireball and estimate times and lengths, and so on, but I want to draw your attention to one thing. If you look at the mean free path for one nucleon — for the reaction N+N → N+N — then because this nucleon needs only one other nucleon to collide, the mean free path is just a function of the density. Here all the quantities are taken as a function of time, because you are looking at the expanding fireball. If you look at the deuteron formation, you need a third partner to conserve energy and momentum, and because of the third partner the mean-free path for this reaction goes as the density squared. That is in A. Mekjian's paper. Because of these two different powers of the density, the freeze-out point — when the mean free path is equal to the radius of the fireball — is different for the different reactions. If you calculate it you find that a nucleon may have a few collisions, 1 to 3 collisions until the freeze-out point, but there seems only time for one collision, n+p → d. It's by no means clear to me whether we really come to a chemical equilibrium. I think we should do some more work on this.

I have one proposal that needs to be done to come closer to the answer (Fig. 3.13). Since no one can calculate this constant accurately, we have to look for relative changes, that is, changes with respect to the energy. I would think that the chemical equilibrium constant may depend on the temperature, and therefore on the energy of the incoming particle. I wouldn't think the coalescence model should differ between 250 and 400 MeV/A because the p_o constant in momentum space should be just the same. But if you look at target/projectile dependences you would think the chemical equilibrium is not so dependent on the size of the interaction zone as it may be for the coalescence model, where somehow you need the distance in phase space. I think in such investigations we may come closer to separating the two mechanisms.

In the nucleon inclusive spectra, the composite particle spectra, and also in the pion spectra, the heavy ion reactions span the whole range between the direct and the thermal mode. We must understand to which degree one or the

other or the intermediate situation is realized. This is an important task for both experimentalists and theoreticians for the next two years. Does the time for formation and expansion of the fireball suffice to reach chemical equilibrium?

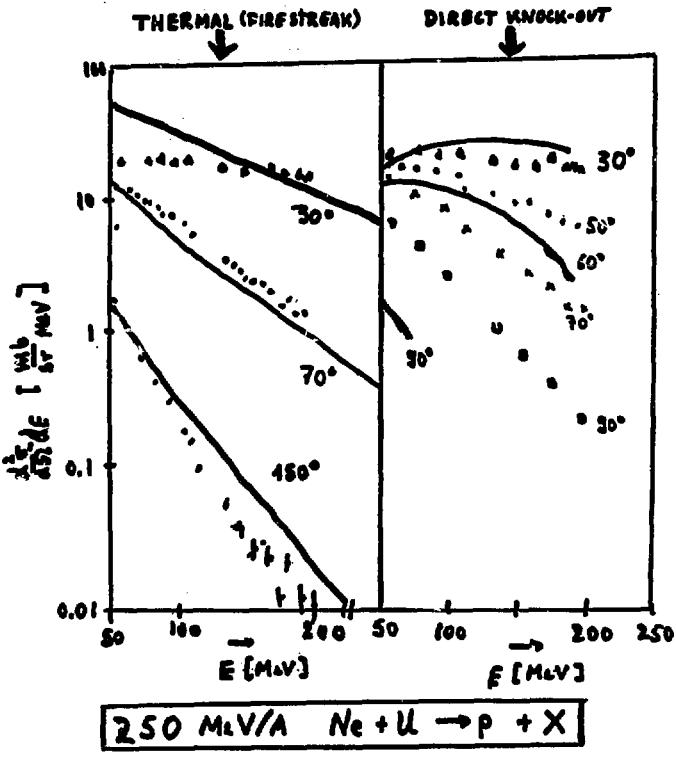
THERMAL (FIRESTREAK)
DIRECT KNOCK-OUT
100
10
1
0.1
0.01
30°
70°
150°
30°
50°
60°
70°
90°
90°
50
100
200
50
100
200
250
E [MeV]
E [MeV]
250 MeV/A Ne + U → p + X

Fig. 3.1

The geometry of participants and spectators

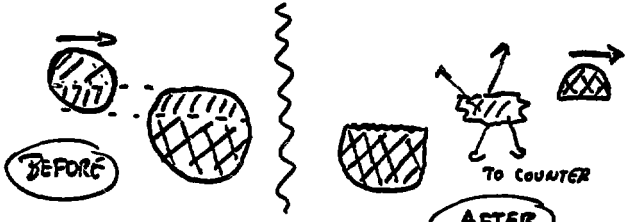

//// "PARTICIPANTS"

XXX "SPECTATORS"

$\frac{d^3\sigma_p}{dp^3}$: Projectile + Target → p + X

FROM ABOVE GEOMETRY

$$\int d^3p \frac{d^3\sigma_p}{dp^3} = Z_p \pi R_T^2 + Z_T \pi R_p^2$$

AND MULTIPLICITY

$$\langle M \rangle_{th} = \frac{Z_p A_T^{2/3} + Z_T A_p^{2/3}}{(A_T^{1/3} + A_p^{1/3})^{2/3}}$$

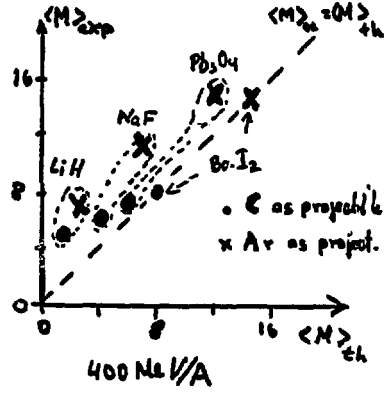

Fig. 3.2

THE DYNAMICS OF THE PARTICIPANTS

direct knockout -vs. thermalization.

Definition: "direct": a projectile and a target nucleon scatter and leave the nucleus. There is no other interaction of these nucleons before or after this event.

Definition: "thermal": Nucleons from projectile and target scatter by each other at least $\nu_{thermal}$ times.

Simple geometrical estimate in one-dim. geometry

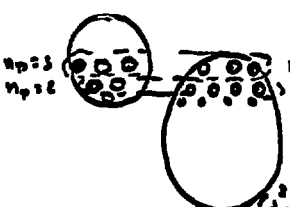

$$W(\nu_p, \nu_T) = \frac{\int d^2p \; \frac{d^2\sigma_p}{d\rho^2}(\nu_p, \nu_T)}{\int d^2p \; \frac{d^2\sigma_p}{d^2p}}$$

"DIRECT" $\nu_p < 1.5$ & $\nu_T < 1.5$

"Thermal" $\nu_p > 2.5$ & $\nu_p > 2.5$ if $\nu_{thermal} = 3$

Fig. 3.3

		"direct"	intermediate	"thermal"
Ne + U	$\int d^2b$	0.4%	60%	40%
	$b=0$	0%	40%	60%
C + C	$\int d^2b$	4%	89%	7%
	$b=0$	20%	50%	30%

Evidence for direct : azimuthal correlations (in-plane $\phi = 180°$ to out-of-plane $\phi = 90°$)

Models which account for the transition direct to thermal

(1) Cascade calculations

(2) Approximate solutions of the Boltzmann eq.

(3) Hydrodynamic approach

(4) Classical eqs. of motion.

THE BOLTZMANN EQ. DESCRIBES THE APPROACH TO EQUILIBRIUM FOR A DILUTE CLASSICAL MANY-BODY SYSTEM.

Fig. 3.4

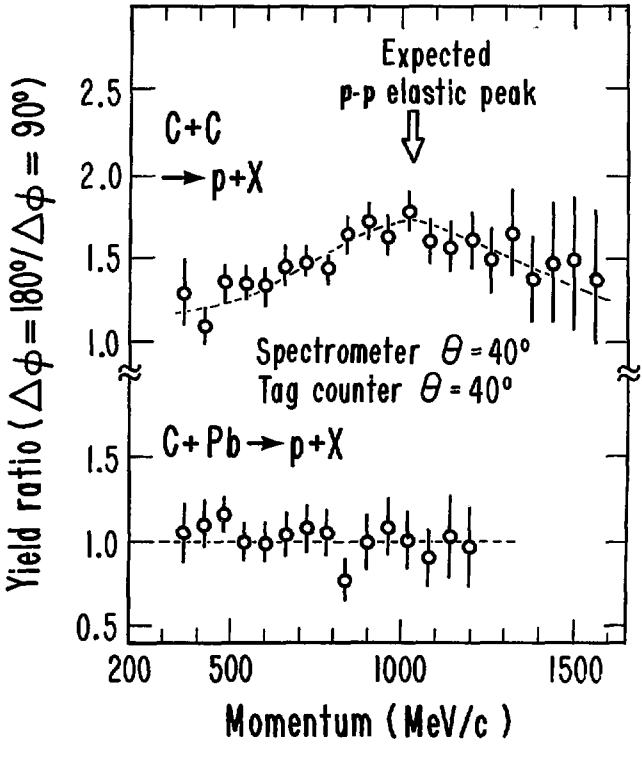
Expected
p-p elastic peak
C+C
→ p+X
Spectrometer θ = 40°
Tag counter θ = 40°
C+Pb → p+X
Yield ratio (Δφ = 180°/Δφ = 90°)
2.5
2.0
1.5
1.0
1.5
1.0
0.5
200
500
1000
1500
Momentum (MeV/c)
XBL779-1882

Fig. 3.5

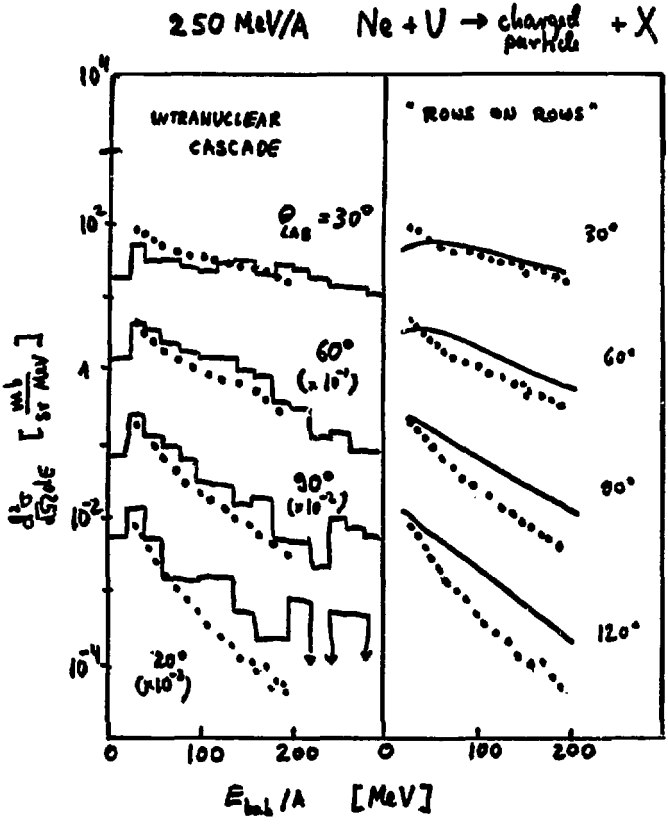
250 MeV/A Ne + U → charged particle + X
INTRANUCLEAR CASCADE
"ROWE ON ROWS"
θ_LAB = 30°
60° (×10⁻¹)
90° (×10⁻²)
120° (×10⁻³)
30°
60°
90°
120°
d²σ/dΩdE [mb/sr MeV]
E_kin/A [MeV]
0
100
200

Fig. 3.6

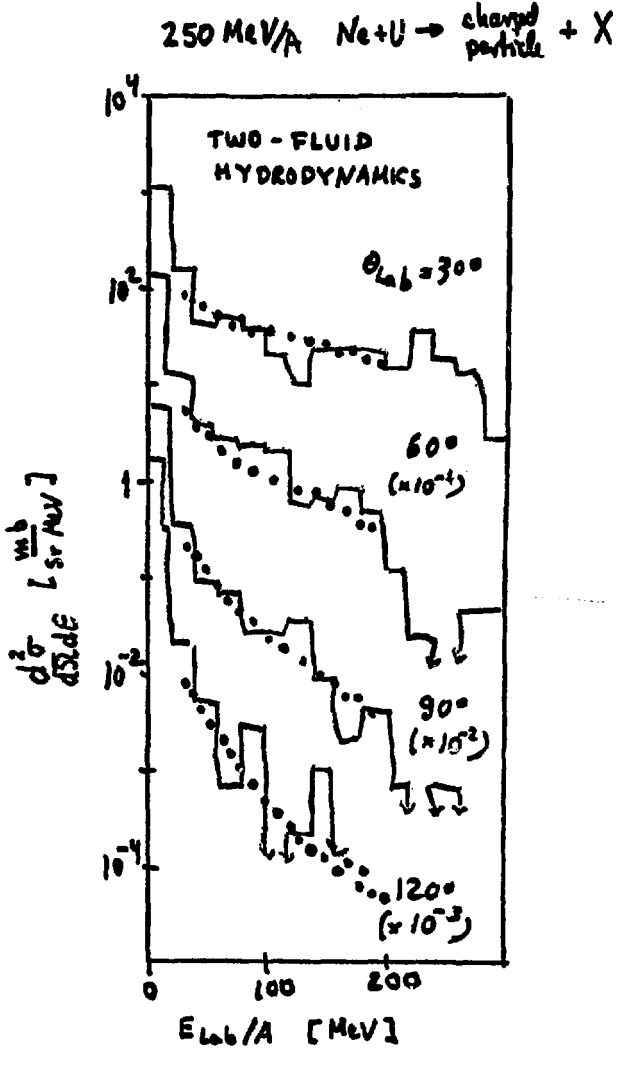
250 MeV/A Ne+U → charged particle + X
TWO - FLUID
HYDRODYNAMICS
θLab = 30°
60°
(×10⁻¹)
90°
(×10⁻²)
120°
(×10⁻³)
d²σ/dΩdE [mb/sr MeV]
ELab/A [MeV]
0
100
200

Fig. 3.7

Estimate of n_{th}

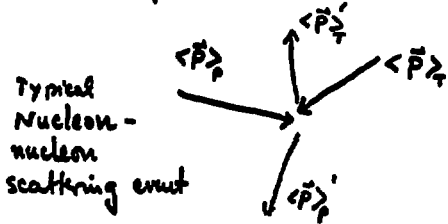

Typical Nucleon-nucleon scattering event

$\langle \vec{p} \rangle$: mean momentum

$\langle \vec{p} \rangle_p' = (1-\alpha) \langle \vec{p}_p \rangle_p + \alpha \langle \vec{p} \rangle_t$ (non-relativist.)

$\langle \vec{p} \rangle_t' = \alpha \langle \vec{p} \rangle_p + (1-\alpha) \langle \vec{p} \rangle_t$

$\alpha = \langle \sin^2 \theta_{cm} \rangle_{NN}$

$n_{th} \simeq \frac{1}{\alpha}$

For isotropic NN cross section $\alpha = \frac{1}{4} \rightarrow n_{th} \simeq 4$

Fig. 3.8

COMPOSITE PARTICLES

eg. Projectile + target $\longrightarrow$ $d + X$

direct mechanism ("coalescence model"):

a proton and a neutron on their way out of the collision zone form a deuteron if their momenta a very close

$$|\vec{p}_p - \vec{p}_n| < p_0$$

equilibrium mechanism ("chemical equilibrium")

The participants come to chemical equilibrium ($n + p \rightleftarrows d$), the observed deuterons arise reflect this equilibrium at the "freeze-out" density $\rho_{F.O.}$

Both predict

$$\frac{d^3\sigma_d}{d^3p_d{}^2} = C \left(\frac{d^3\sigma_p}{d\,p_p^3}\right)^2 \quad \text{for } d.$$

$C(p_0)$ (coalescence model) fit with $p_0 \simeq 200$ MeV/c

$C(\rho_{F.O.})$ (chemical equilibr.) fit with $\rho_{F.O.} \simeq \frac{1}{2}\rho_{n.m.}$

Fig. 3.9

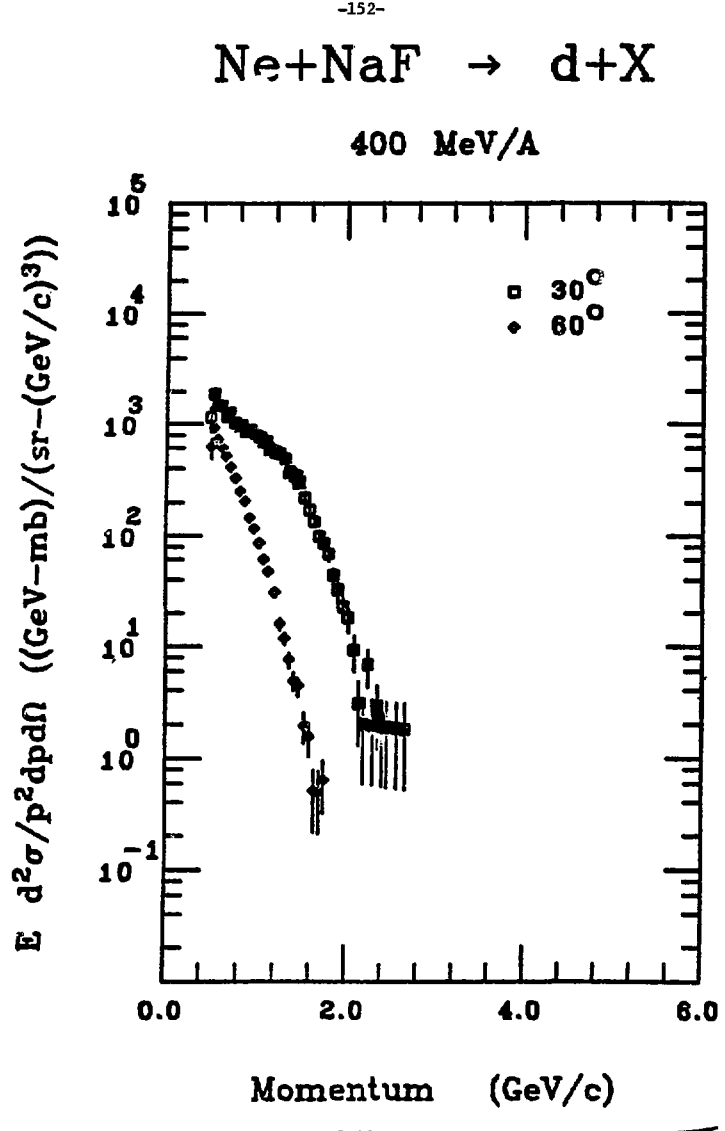
Ne+NaF → d+X
400 MeV/A
30°
60°
E d²σ/p²dpdΩ ((GeV−mb)/(sr−(GeV/c)³))
10⁵
10⁴
10³
10²
10¹
10⁰
10⁻¹
0.0
2.0
4.0
6.0
Momentum (GeV/c)

Fig. 3.10

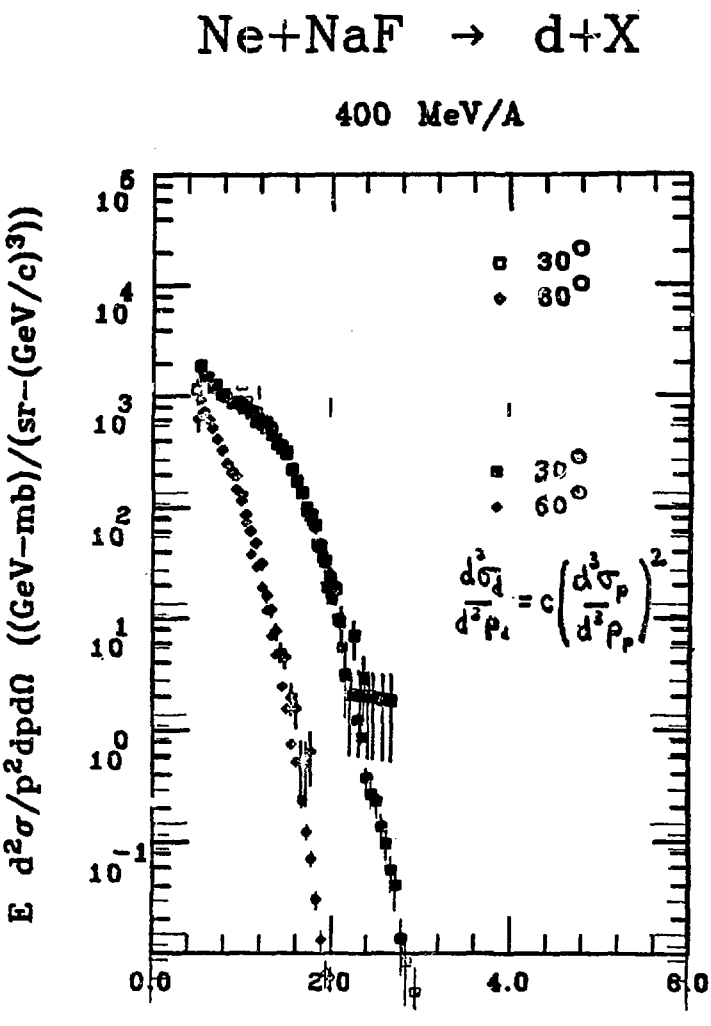
Ne+NaF → d+X
400 MeV/A
E d²σ/p²dpdΩ ((GeV−mb)/(sr−(GeV/c)³))
30°
60°
30°
60°
d²σd/d³pd = C(d³σp/d³pp)²
10⁵
10⁴
10³
10²
10¹
10⁰
10⁻¹
0.0
2.0
4.0
6.0

Fig. 3.11

Does the time for formation and expansion of the fireball suffice for to reach chemical equilibrium ?

At time $t=0$ there is a fireball with radius $R(0)$ and density $\rho(0)$ and expanding with velocity v. The mean free path

$\lambda_N(t)$ for $N+N \to N+N$ $\quad \lambda_N(t) \propto \frac{1}{\rho(t)}$

$\lambda_d(t)$ for $N+N+N \to d+N$ $\quad \lambda_d(t) \propto \frac{1}{\rho^2(t)}$

Freeze-out for "N" degree $\quad \lambda_N(t_N^{f.o.}) = R(t_N^{f.o.})$

" " "d" degree $\quad \lambda_d(t_d^{f.o.}) = R(t_d^{f.o.})$

in general different freeze-out densities.

Number of collisions until freeze-out

$$N_c = \int_0^{t_{f.o.}} \frac{v\,dt}{\lambda(t)}$$

for $t=0$: $\rho(0) = 3\ \rho_{n.m.}$; $\lambda_N(0) = \lambda_d(0) = \frac{2}{3}\ fm$; $\rho(0) \approx 6\ fm$

$\to$ $N_c^{(N)} \approx 3$ $\qquad N_c^{(d)} \approx 1$

$\rho_{f.o.}^{(N)} \approx \frac{1}{5}\ \rho(0)$ $\qquad \rho_{f.o.}^{(d)} \approx \frac{1}{2}\ \rho(0)$

Fig. 3.12

I think (based on this crude estimate) that chemical equilibrium is not completely reached. Probably again an intermediate situation (at least for heavy systems) prevails.

Q6: How does the proportionality constant C (in $\frac{d\sigma_d}{d^3p_d} = C\left(\frac{d^3\sigma_p}{d^3p_p}\right)^3$) vary with incident energy and target-mass projectile combination. For the coalescence model I would expect energy independence (but dependence on Projectile - target). Chemical equilibrium should depend on Temperature (energy).

Fig. 3.13

LIGHT FRAGMENT PRODUCTION AND ASSOCIATED MULTIPLICITIES FROM COLLISIONS OF 1.85 GeV/Nucleon ^{40}Ar

Jim Carroll

I'm here this morning to give a progress report on a research program that's been in progress on at the Bevalac for about three years. The work is a collaboration between two groups, one from UCLA under the direction of George Igo, and a local group from LBL under the direction of Victor Perez-Mendez (see Fig. 4.1 for a full list of collaborators). The work is part of a continuing collaboration that originally concentrated on a series of elastic scattering experiments designed to study the wave functions of light nuclei in the GeV region. From the elastic scattering program we got a large magnetic spectrometer, which was the basic instrument used in the light fragment production study, but our primary commitment to the elastic experiments has delayed the complete analysis of the light fragment data.

Since I am acting as a spokesman, with much (if not most) of the work being done by others, let me give a few specific credits - to G. Igo, who wrote the original proposal; to M. Gazzaly, whose thesis work yielded the data to be presented today; to A. Sagle, who supervised the analysis; and to F. Brochard, from Strasbourg, who is converting our analysis program to run on the CDC 7600.

The motivation for this experiment was the tempting opportunity of looking for the new physics of hot, compressed nuclear matter. The exciting signature at the time we started — when the proposal was written — was the shock wave, as apparently seen in the data of W. Greiner and his collaborators. I will mention it just briefly, although shock waves are slightly out of fashion at the moment — for presumably good reasons. Fig. 4.2 is a classical picture of a shock wave with the shock front emitting particles. The idea at that time was to run the interaction backwards, bring a heavy projectile in onto a light target and use the resulting favorable kinematics to make detection of the resulting fragments easier. It turns out that the particles ejected by the shock fronts are folded over in the lab into the forward direction and they turn out to be peaks in momentum rather than in angle. The idea also was that this way you detect the fragments, which have low energies in the projectile rest frame, rather easily in the lab where they have much higher energies. The shock-wave idea led us to the desire for a central collision trigger to emphasize the symmetry of the situation, so we thought we would look for a high multiplicity associated with such events. (Rather than actually use it as a trigger, we would simply record all the data and post-select for events with high multiplicities.) Because of the inherent symmetry at small impact parameters, we desired a measurement of the azimuthal distributon of the multiplicity, because that way we could presumably select the symmetry of the events. We could then reject the type of event in which the two nuclei scatter at some moderate momentum transfer and then evaporate, resulting in large, but asymmetric multiplicities. Having such a detector, then, permits you to think about making correlations between the particles detected in the array and the inclusive particle detected in the spectrometer. One can also look at correlations within the array itself, where one might

find "jets", or groups or clumps, of particles of some kind coming off together.

The detector that we constructed as a multiplicity array is rather simple in principle (see Fig. 4.3). It's 30 elements each 11.25° in azimuth - which cover roughly 5° out to 12° in polar angle for most of the data I'm going to talk about today. By moving the detector toward and away from the target, that included angle can be changed rather readily but the original hole size was designed to be about twice the width of the $P_\perp$ distributions that have been seen in projectile fragmentation. We did not want to include in this array of particles anything that comes from projectile fragmentation of the peripheral reaction type.

The set-up is rather simple in principle (but turns out to be complicated in practice, see Fig. 4.4). There's a target, the multiplicity array; the beam goes through the center of the hole, the gap in the azimuthal counters is left so that the charged particles to be detected in the spectrometer have a free passage and then there is a rather straightforward magnetic spectrometer, no focusing, wire chambers and scintillators upstream, wire chambers and scintillators downstream. Time-of-flight over a 9.5 m path, and pulse height information for each event, are recorded in addition to the trajectory data, so we can do particle identification of the forward particle. The properties of the multiplicity array were chosen so that they would not be sensitive to fragments from the target because if you use a heavy target you can get swamped. The velocity threshold of this device is 0.7C (it's a lucite counter) and that puts you well above fragments coming from the target but permits you to detect fragments coming from the projectile or even well down into the mid-rapidity region. So if there were fragments coming from some kind of fireball they would be easily picked up by this device. You find listed here (Fig. 4.4) the projectiles, targets, and fragments for which data have been taken. We simply don't see any heavier fragments in this momentum transfer range. Even the charge-2 states are suppressed because, at any given angle, the P/Z selection of the spectrometer requires that they have twice the $P_\perp$ of the singly charged particles.

Now let me show you the kinematic region in which we are working. (See Fig. 4.5). This is the plot Shoji presented yesterday, with our area in the lower right. We go down fairly near the mid-rapidity region (some recent data extend below the mid-rapidity region for some of the fragments). Figure 4.6 is essentially the same thing on an expanded scale, but I now plot $P_\perp$ vs Y. The beam rapidity is indicated; the target rapidity is slightly off to the left. This is the span of the data showing the regions for protons, deuterons tritons, ^{3}He, and ^{4}He. Spectrometer settings were chosen so that the edges of the acceptance regions were adjacent to each other. Thus the bounded areas are filled with a continuum of data. I'm going to present today only data along the edges. Line A-A represents measurements at a large constant angle; line B-B at a small constant angle. I shall concentrate on data showing proton and deuteron fragments.

Figure 4.7 shows the basic raw data, which I'm not going to dwell on. (I apologize to the local people who have seen this several times already.) This is all at high energy. We have concentrated our experiments on the

highest energy of the machine because, first of all, for shock waves you want the high velocity. Secondly, we have always had the feeling that high energy was the unique characteristic of the machine, and that was probably where the interesting physics was. This is ^{40}Ar at 1.85 on Cu and Be, protons, deuterons, and tritons. You see data at 5° showing the remnants of the projectile fragmentation in both the copper and beryllium data and then two larger angles at 12° and 14.7° where the indication of the projectile fragmentation peak has disappeared, similarly for the deuterons and tritons. We don't really go out far enough to get the entire triton peak. When we designed the multiplicity array we tried to make it so that it would not, in fact, include the projectile fragmentation region but its minimum angle is 5° and you see there is still a fair amount of projectile fragmentation in that cone -- the velocity threshold is down here somewhere (see Fig. 4.8). That will prove to be significant later on.

Now to give you some idea of what the charge-2 data looked like, let me show you Fig. 4.8 -- at the smallest angle -- the black circles are ^{4}He, the white are ^{3}He; at this angle you still see some remnants of the projectile fragmentation, but the cross section is down. I'm really not going to speak any more about the charge-2 data today.

Let me show you now something that even the local people haven't seen (Fig. 4.9a). We were asked to make contour plots and I was pleased to see that, even having only the data from the extreme angles, one could draw fairly nice plots. Again I'm plotting y, the beam rapidity against $P_\perp$. This is Ar + Cu going to protons. This is 14.7°, the physical limitation of our spectrometer, and we run into a shielding wall. Below 4° we run into the beam. The little light dots represent a third of a decade (it's a log plot) the solid line is 10^1 invariant cross sections in $\frac{\text{barns}\cdot\text{steradians}}{\text{GeV}/c^2}$. Then the other lines are each down an order of magnitude. These are measurements along constant angle, as I described before. I'll show you now what happens when we draw the contours (see Fig. 4.9b). I showed you Fig. 4.9a so you know I wasn't really cheating in drawing the contours. There is a hump around the projectile and it is fading fairly rapidly into something that is clearly becoming more and more isotropic. One of the things we have discovered is that in paying attention mostly to shock waves we have not gone down as far as we could in the earlier data acquisition. There are more data coming in the area that goes down for protons into the mid-rapidity region.

Now I'm going to show you Ar + Be going to protons (see Fig. 4.10). I haven't bothered to show you all the little fold-overs because it's fairly straightforward to draw these contour lines. I would like to call your attention to a comparison between these two sets of data; there seems to be a slightly larger persistence of the projectile association for the Be than for the Cu. In other words, if you go out to an equivalent momentum transfer ($P_\perp$) the copper data do not bend over as much as the beryllium data. We have other evidence to support this, which I'll get to in a few minutes.

The situation is similar for deuterons, i.e., Ar on Be and Ar on Cu (Figs.

4.11 and 4.12). These data show that the projectile association is even stronger for the deuterons. This is not actually very new news because it has been seen before in other data. It says that, if you look at the cross section at constant $P_\perp$ as a function y, there is a bigger valley for deuterons than for protons. That presumably has something to do with the coalescence or the composite particle relation, which is exactly what you'd expect in that kind of situation.

Fig. 4.13 is the ratio of argon on copper to argon on beryllium as a function of rapidiity at extreme angles. We show here just the target dependence you'd expect if things went like $A_T^{1/3}$ $A_T^{2/3}$. Notice that, in the deuteron data, as you go down to the mid-rapidity region, the target dependence increases up to about A, possibly indicating that there's a very strongly central collision.

I'll try to go very briefly through the multiplicity data. (See Fig. 4.14). This is simply the multiplicity distribution, with an average value of 6.9 (we see averages up to about 8). Notice how much room there is in the detector for higher multiplicities and low saturation.

Figure 4.15 shows the ratio of cross section measured with a requirement of large multiplicity (m=7) to cross section measured with no multiplicity requirement. In this way we tried to get away from a simple inclusive measurement, and to increase the fraction of central collisions. The most striking feature of these data is the absence of any structure at all. Even when a requirement of large and symmetrically distributed multiplicity is imposed, no significant structure or slope is revealed. This is possibly, or probably, due to the inclusions of a significant amount of peripheral fragmentation in the multiplicity array. We have some recent data in which the minimum $P_\perp$ was increased to avoid this situation, but they have not yet been analyzed. Note that the general lack of structure implies the lack of visible shock waves.

We conclude that first there are no visible shock waves (with caveats about the particular target, projectile, trigger mode, etc.), which comes as no particular surprise; second, there is no effect from the multiplicity cut, which we found surprising, but for which there is a possible explanation; and third, there is rapidity dependence of the copper to beryllium ratio, indicating the possibility of some kind of centrality at the midway rapidity region. We find in conjunction with this that the average multiplicity we see is independent of the fragment type and of the fragment momentum. A preprint has mentioned that the average multiplicity depended on the angle of the inclusive fragment. A more careful analysis has called this conclusion into question. We find that the ratio of average multiplicities from copper to argon is smaller than the corresponding cross section ratio. The multiplicity ratio here is about 1.4; the corresponding cross section ratio is 2.6, which is a little puzzling. A preliminary analysis of the azimuthal detector indicates there are no strong azimuthal correlations.

In the future we plan to collect the intermediate-angle argon data with the same multiplicity conditions you see, a full data set from ^{12}C filling

all the phase space plots I showed. We have argon data at a small rapidity with new multiplicity conditions. As I said, the multiplicity array seems to go down too low in $P_\perp$. We have now taken data at much higher $P_\perp$'s, however, we have not yet looked at it in any detail. We will have beam and target dependence of the cross sections versus $P_\perp$ and y. We'll also have a complete analysis of multiplicity correlation information and, in a rather different vein, we will be doing a new experiment involving two-particle (two-proton) correlations at small relative momenta. This will involve the nuclear interferometry, Hanbury-Brown-Twiss phenomenon, at rapidities varying from rapidity down to the midway region and for equal mass target and projectile and for other combinations.

LIGHT FRAGMENT PRODUCTION AND ASSOCIATED MULTIPLICITIES FROM COLLISIONS OF 1.85 GeV ^{40}Ar

UCLA

6. IGO

J. CARROLL

J. McCLELLAND

J. OOSTENS

ABSENT FRIENDS

J. GEAGA

M. GAZZALY

M. NASSER

H SPINKA

LBL

V. PEREZ-MENDEZ

F. BROCHARD (STRASBOURG)

A. SAGLE

R. TALAGA

E. WHIPPLE

F. ZARBAKSH

Fig. 4.1

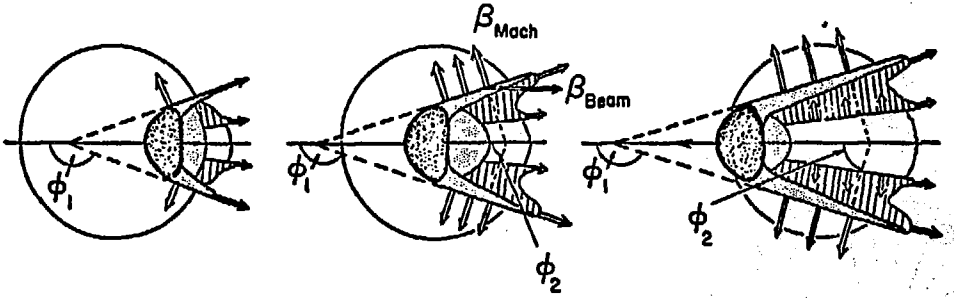

CENTRAL COLLISIONS

Fig. 4.2

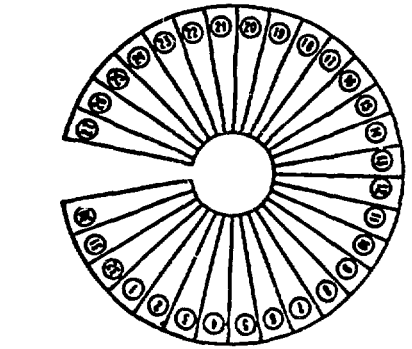

HOLE ~ $2\sigma_{P_\perp}$

A) Front View

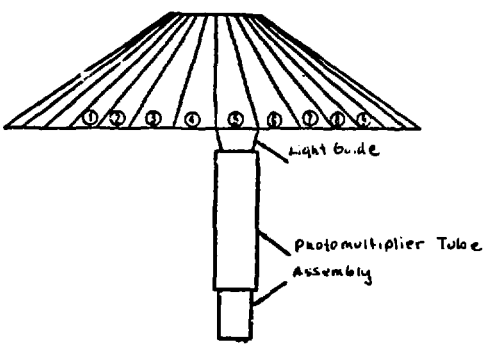

B) Top View

Fig. 4.3

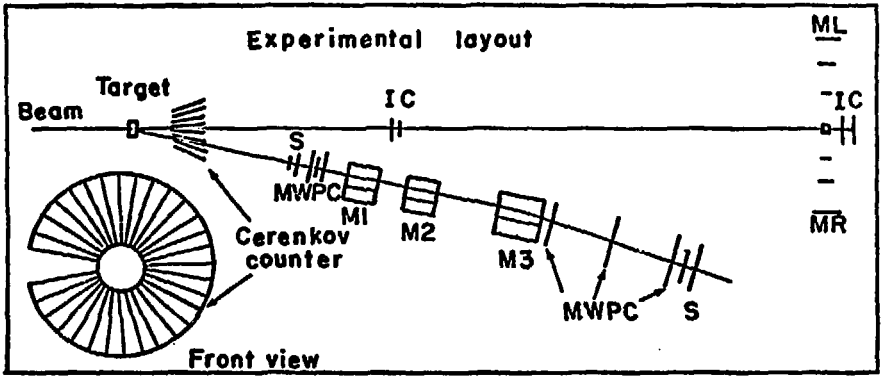

XBL762 - 169

PROJECTILES	TARGETS	FRAGMENTS	
^{40}AR - 1.85 GeV/A	Be	P	^{4}He
	Cu	P	^{3}He
^{12}C - 2.10 GeV/A	Pb	D	
		T	

Fig. 4.4

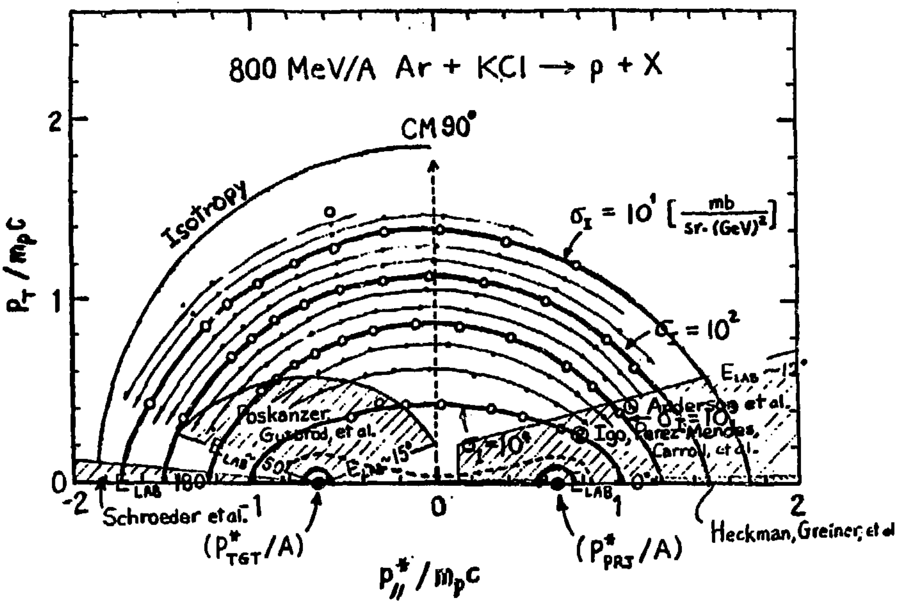
800 MeV/A Ar + KCl → p + X
CM 90°
Isotropy
$\sigma_I = 10^1$ [mb / sr·(GeV)²]
$\sigma_I = 10^2$
E_{LAB} ~12°
Anderson et al.
Igo, Perez-Mendes, Carroll, et al.
Poskanzer, Gutbrod, et al.
E_{LAB} ~15°
E_{LAB}
180
0°
Schroeder et al.
Heckman, Greiner, et al
(P^*_{TGT}/A)
(P^*_{PRJ}/A)
p_T/m_pc
$p^*_{//}/m_pc$
-2
-1
0
1
2

Fig. 4.5

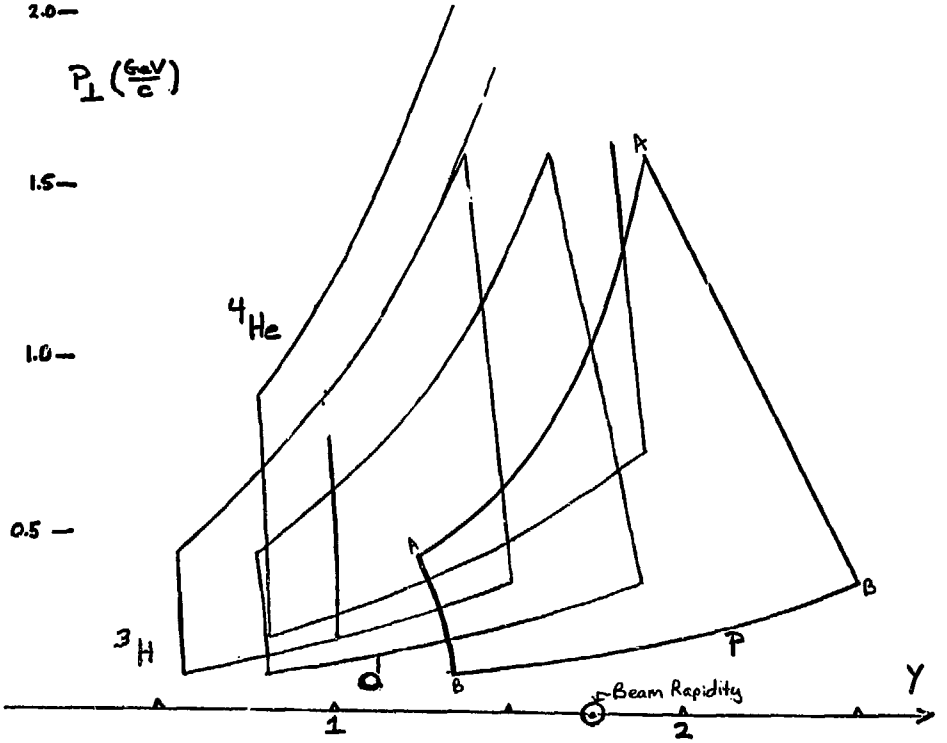
2.0
$P_\perp \left(\frac{GeV}{c}\right)$
1.5
1.0
0.5
^4He
^3H
A
A
B
B
d
p
Y
Beam Rapidity
1
2

Fig. 4.6

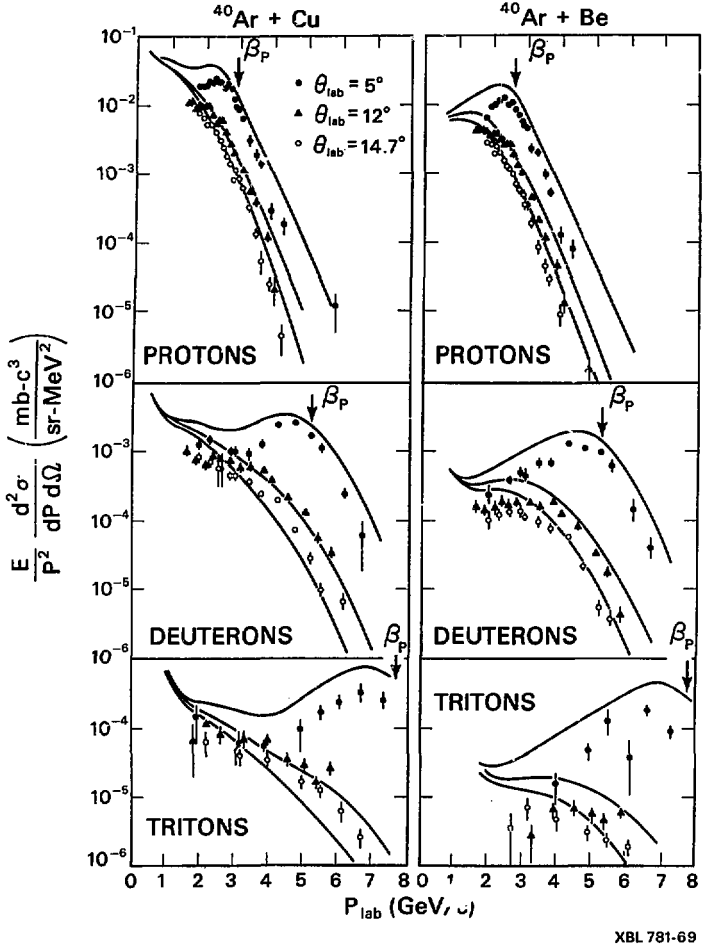
^{40}Ar + Cu
^{40}Ar + Be
β_P
θ_{lab} = 5°
θ_{lab} = 12°
θ_{lab} = 14.7°
PROTONS
DEUTERONS
TRITONS
$\frac{E}{P^2}\frac{d^2\sigma}{dP\,d\Omega}\left(\frac{mb\text{-}c^3}{sr\text{-}MeV^2}\right)$
P_{lab} (GeV/c)
XBL 781-69

Fig. 4.7

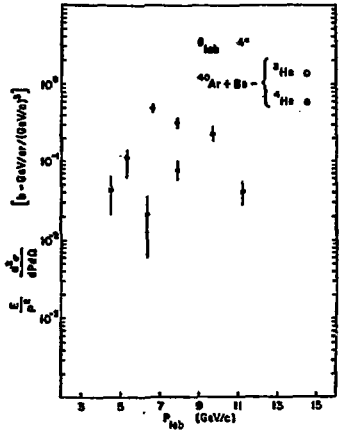
θ_{lab} 4°
$^{40}Ar + Ba$ – ^{3}He o
^{4}He e
$\frac{d^2\sigma}{dP d\Omega}$ [b-GeV/sr/(GeV/c)^2]
P_{lab} (GeV/c)

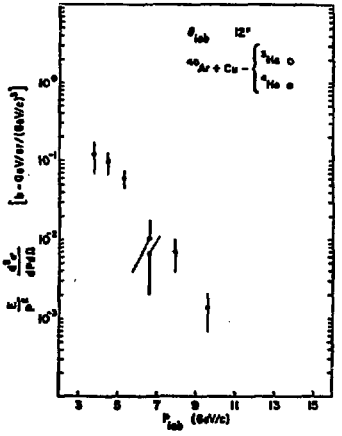
θ_{lab} 12°
$^{40}Ar + Cu$ – ^{3}He o
^{4}He e
$\frac{d^2\sigma}{dP d\Omega}$ [b-GeV/sr/(GeV/c)^2]
P_{lab} (GeV/c)

Fig. 4.8

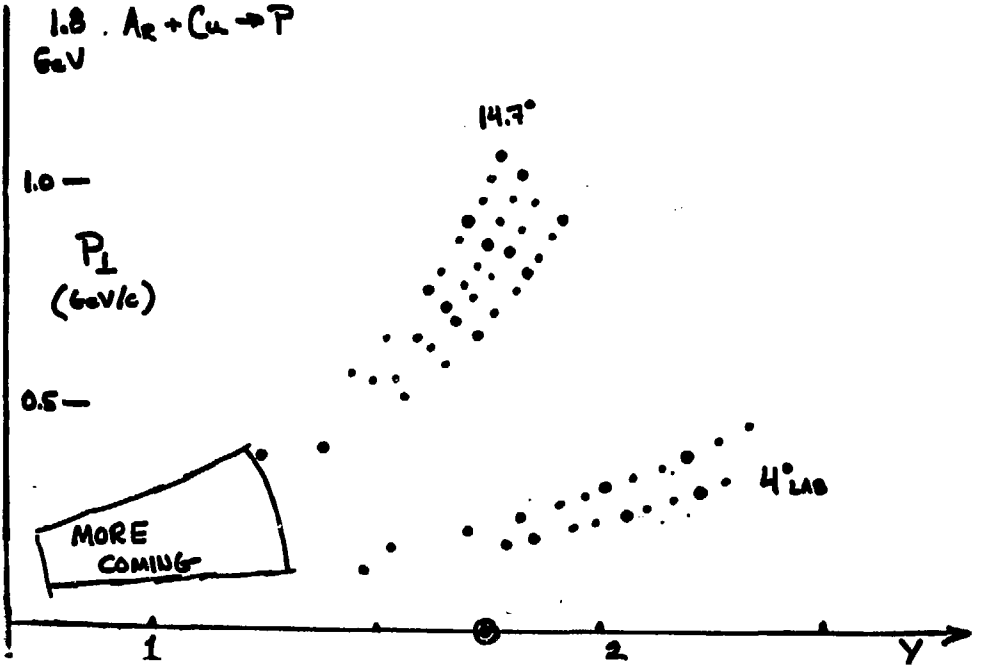

Fig. 4.9a

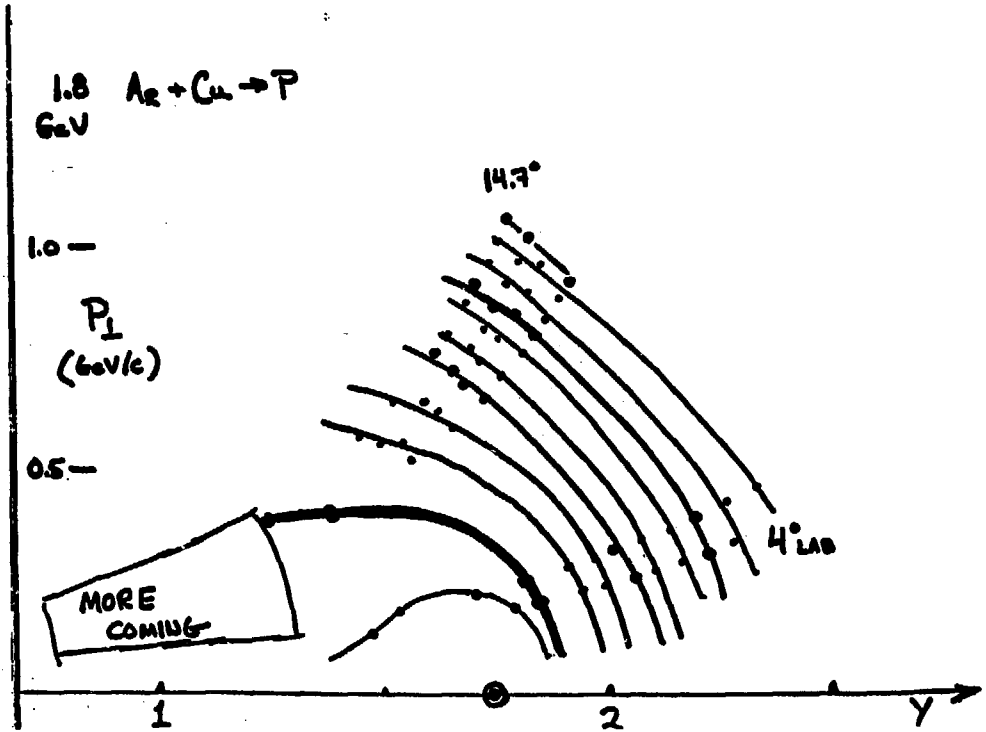

Fig. 9.9b

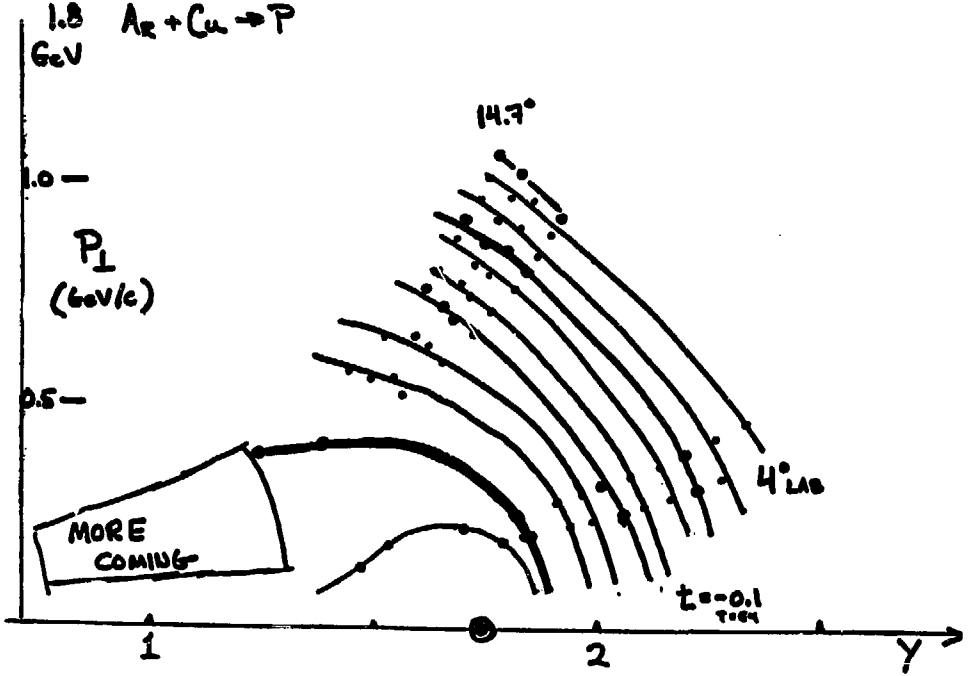
1.8 GeV
$A_R + Cu \rightarrow P$
14.7°
1.0
$P_\perp$ (GeV/c)
0.5
MORE COMING
4° LAB
t=-0.1 (GeV)²
1
2
Y

Fig. 9.4c

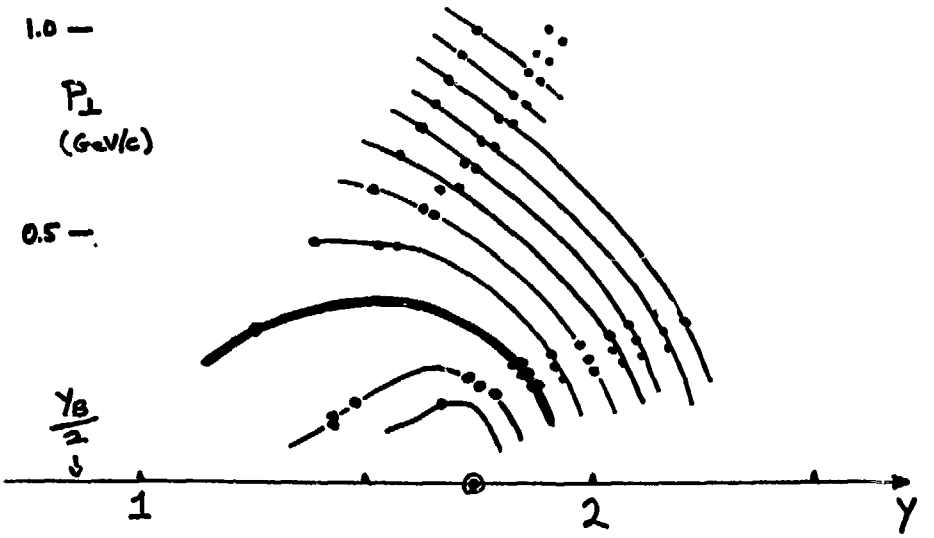

Fig. 4.10

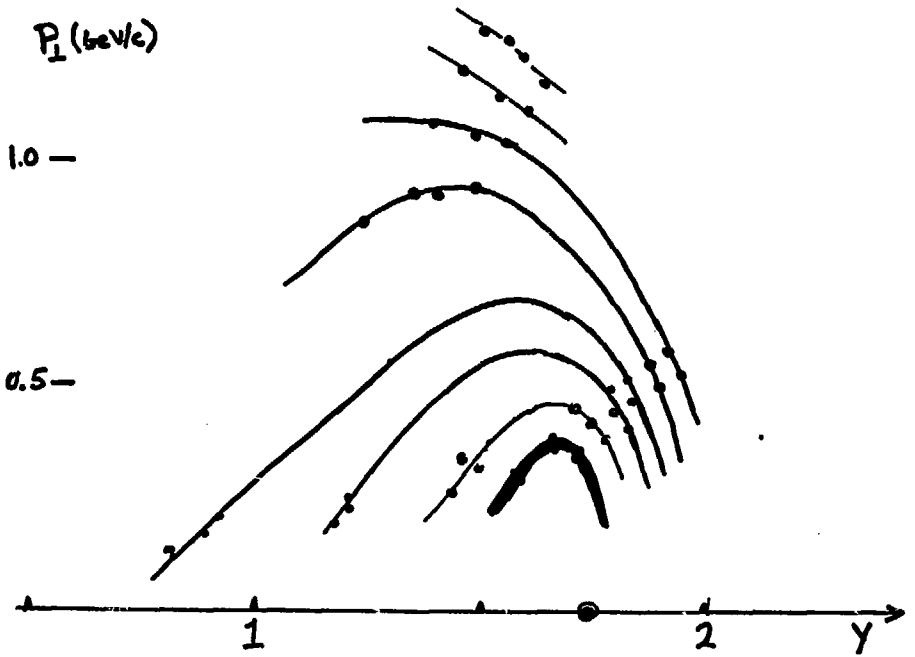

Fig. 4.11

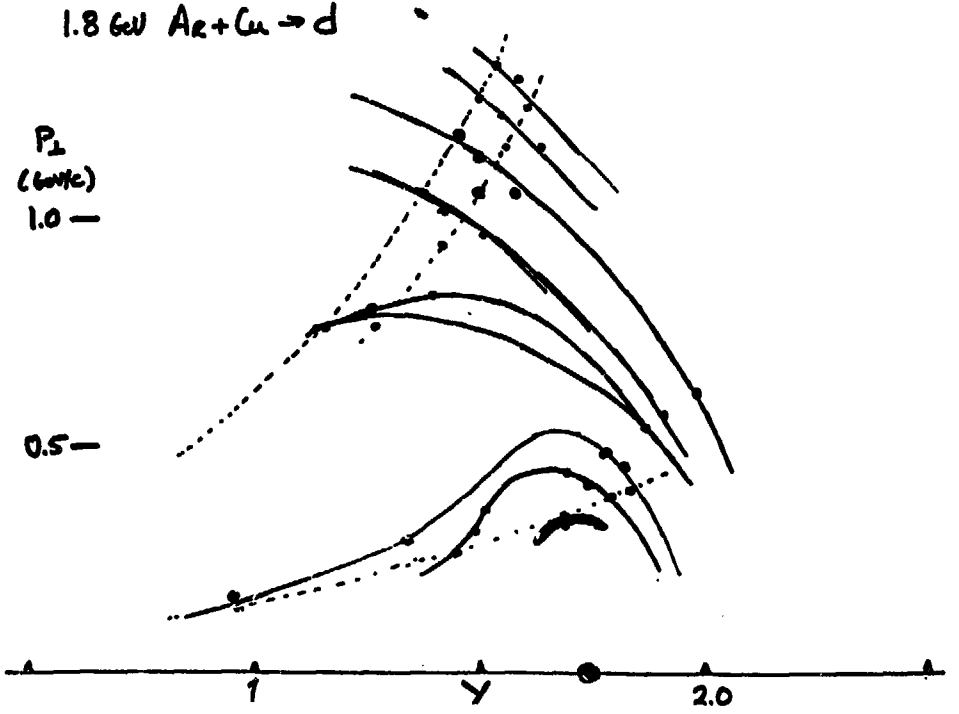

Fig. 4.12

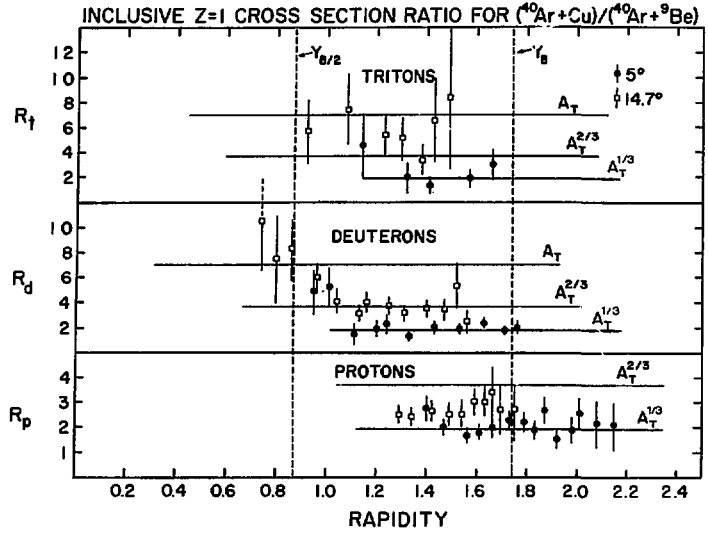

XBL 778-1632

Fig. 4.13

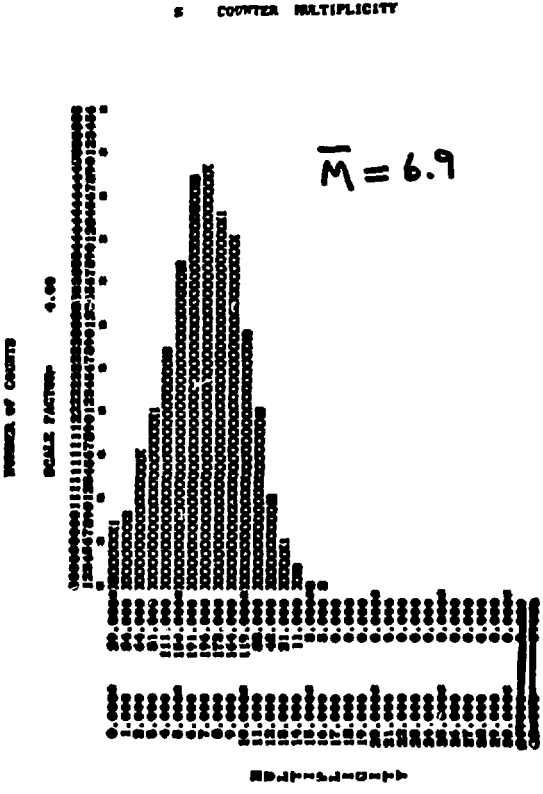

Fig. 4.14

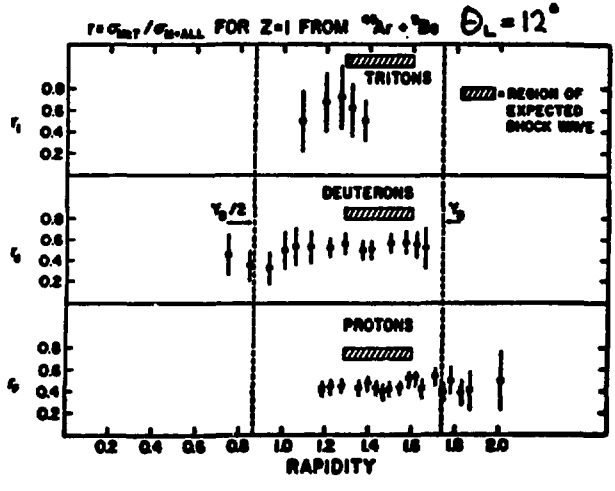

θ=12° -ALS

Fig. 4.15

SCIENTIFIC PROGRAM FOR SATURNE II

Pierre Radvanyi

THE NEW SATURNE

A few years ago, the French Government decided to start two new national programs: one in heavy ion physics, GANIL, at Caen, and the second in intermediate energy physics, the Saturne II project, at Saclay. "National" means that the two main organizations that handle basic nuclear physics in France participate in, finance, and share the two programs and the accelerators that are to be built. They are the IRF (Institute of Fundamental Research) of the C.E.A. (the Atomic Energy Authority), and the IN2P3 (National Institute for Nuclear and Particle Physics) of the C.N.R.S. (National Scientific Research Center) and the Universitites. Two agreements were established, one for the construction period, which for Saturne is now completed, and one for the starting and the operating period. A joint C.E.A. and IN2P3 governing body has been set up. The new National Laboratory Saturne was set up in January of this year. The first experiments are being prepared and we almost have our machine running.

What is Saturne? There are different possible answers: The first is shown on the first slide (Fig. 5.1). Fig. 5.2 shows the old Saturne accelerator, which was shut down at the end of March of last year. It was an N = 0 ring conventional synchrotron. Fig. 5.3 shows different parts of the new Saturne set up; we see the new ring and the injector in the background at the right. In Fig. 5.4 you see more closely a part of the ring and the quadrupoles - you can note that the magnets are smaller but the radius is larger than for the previous Saturne I. The structure of the new Saturne is shown schematically in Fig. 5.5. There are four straight sections and you can also see that there are two extractions, which we will try to use simultaneously, that is, extracting two different energies on the same pulse.

The charcteristics of the new machine are shown in Fig. 5.6, i.e., the physical radius and the energies that can be achieved, the injection energies, the minimum (by minimum we mean beams with a certain standard in optics - we could go lower if an experiment can accept a lower standard) and the maximum energies we can obtain. Also are shown the extracted intensities we hope to have (at least 10^{12} for protons) and the other values for the other particles shown here. I shall come back in a few minutes to the heavy ions and the polarized particles. Here you have the emittance of the beam at 1 GeV and the momentum resolution achieved in the extracted beam. As I said, we can have two simultaneous extractions and we expect also to have a secondary π^+ beam obtained through the indicated two-body reactions. The duty cycle and typical cyclings are also shown.

I am happy to tell you that the first protons were running in the ring last week and at present our people are very busily accelerating them. We expect to have an external beam of about 2.10^{11} protons at the end of October and we hope to have the first physics experiments going on in November of this

year. Of course, at the beginning we won't go to the maximum intensity and the first few months will be devoted partly to the machine, to the tuning, to achieve the best possible characteristics, with physics going at the same time. The normal ion source is able to produce p,t, α and also ^3He ions.

THE CRYEBIS ION SOURCE

Now, I would like to talk a little about our new ion source (shown in Fig. 5.7), which we have constructed and are in the process of setting up. This special ion source has the nice name of Cryebis which comes from cryogenic. It is an electron confinement source and you get here an idea of how it works: in the central diagram you see the ions coming in from the left (they can be also polarized particles), and you see the volume where the ions are maintained by the magnetic field radially and by the high voltage longitudinally. The electrons in the source ionize the atoms and you get fully stripped ions, which are then extracted. Cryebis works as a cyclic source. You fill the potential well with the ions and when it is filled you empty it by having the bottom of the well rise; you then inject the particles you have stocked into the linac and the ring. The original idea of such a source is from Donetz, at Dubna.

In Fig. 5.8 are given the characteristics of our ion source. Cryebis has been constructed and is presently being tested at Orsay by a group of engineers of the University. It will be set up on Saturne at Saclay next spring. The maximum number of charges we can obtain with these characteristics will be about 3×10^{11} charges per cycle. So you can calculate what is possible with this source. The expected efficiency from source to target is about 4%, and we expect a maximum of about 10^9 x $^{20}Ne^{10+}$ per cycle and 10^{10} polarized protons per cycle on the targets. These are, I think, maximum values. The first test, which was just performed in June, shows that the source is going on very well. At the bottom of Fig. 5.8 are the characteristics of the first testing; we have not yet gone to the nominal high voltage of 10 kilovolts, nor to the 2 amperes that will be used, nor the 3 teslas, but with the preliminary values we have been able to work with a confinement time of 15 milliseconds, which means that in the future we could possibly go to higher cycling. Also shown are the efficiencies achieved for the Ne^{10+}, and the source is even able to produce Xe^{35+} (35+ is a mean value). The ions with which we propose to start are indicated in Fig. 5.8.

The source being tested is shown in Fig. 5.9. The first tests have not been made on the high voltage platform, but the next tests will be made at 10 kV. The whole set-up will then be dismantled and taken up the bill to Saclay. The vacuum operation conditions in the ring are shown on Fig. 5.10. The present vacuum in the machine is 5×10^{-7}, so you can note that there is a small loss for Ne^{10+} in the machine; in order to go to the higher masses we must, in the future, improve the vacuum. The chamber is all right for that; we shall only have to buy additional pumps.

EXPERIMENTAL AREAS AND SPECTROMETERS

Let us now go to the experimental areas that are shown in Fig. 5.11. There are two extractions, SD2 and SD3. We shall start by working on the first extraction, SD2. The second extraction should be installed by next spring, approximately. One sees the locations of our spectrometers. SPES I, which is the oldest one and which has the highest energy resolution, is here in the central target area. In target area 3 at the bottom right we shall have, possibly to use for coincidence experiments, SPES II and SPES III. We shall have the possibility of a π^+ beam on target in target area 3. Target areas 4 and 5 will be used for high and low energy work, respectively. Target area 6 is the nucleon-nucleon target area; at 7, we have the 4 GeV/c spectrometer, which is a kind of SPES IV. Target areas 8 and 9 are testing areas.

Now a few words about the spectrometers. The next slide (Fig. 5.12) shows SPES I on its air cushion. This photograph was taken in its former location, which has now been changed, but of course, the spectrometer looks the same. A scheme of SPES II, which has now been at CERN for two years, is shown in Fig. 5.13. You see the two dipoles and the quadrupole of SPES II with a detection system that has been used in an experiment looking for hypernuclei. SPES III is shown on Fig. 5.14. In order to save money, we have used the old cyclotron at Saclay - it has been cut and the pole faces have been reshaped. It is not an ordinary shape. SPES III will work at 3 teslas; the yoke has been cut in order for the primary beam to get through at small angles. There are only one or two pillars to hold the magnet together. The focal plane extends into the fringing field between the coils.

Fig. 5.15 shows SPES IV, which is able to go up to 4 GeV/c (3.8 GeV/c corresponds to the maximum momentum of the protons in the ring). This spectrometer has been made out of some of the magnets of the Saturne ring. At the upper right appears the primary beam coming in. The target is at C_1 or C_2 and we change the incidence angle of the beam on the target - the spectrometer as such is fixed. The focal plane is at I_2 and we have an intermediate point of focusing (I_1) which can be used for time-of-flight measurements.

The characteristics of the four spectrometers are summarized in Fig. 5.16. Note that SPES II and SPES III have large solid angles and large momentum acceptances. SPES III will work at a fixed field; this means that everything is calculated for the corresponding momentum acceptance. Of course one could put on a lower field, but then we are not sure of the magnetic characteristics. Nevertheless, for some experiments this might be convenient. The 3.8 GeV/c spectometer has two modes of operation with different momentum acceptances, which means also, of course, different solid angles and resolutions. There are also two possible angular ranges corresponding to two different target positions (C_1 and C_2), depending on whether or not the sweeping magnet M_2 is used.

The schedule for the various operations and equipment is given in Fig. 5.17. We hope to have the first extraction operating in October, and we

should start physics in November. The second extraction should be installed in the spring of 1979. Cryebis, which gives us the possibility of starting experiments with heavy ions and polarized particles, should be working sometime next summer. SPES I, being already on the spot, will start at the very beginning, and the others as shown. The nucleon-nucleon experiments should be able to start next spring and we expect to have the π^+ beam in the winter of 1979-1980.

THE GENERAL EXPERIMENTAL PROGRAM

Now about the future experiments. Of course, I cannot report yet on experimental results from Saturne II. We have asked for proposals and letters of intent and by now we have received 36 of them, coming from 154 scientists, among them 122 nuclear physicists, which gives you an idea of the nuclear physics participation. About half come from the Atomic Energy Laboratories and half from the C.N.R.S. and the Universities. They pertain to twenty-six laboratories. Most of the proposals are collaborations between different laboratories.

I have listed in Figure 5.18 the main orientations of these various experiments. These are the first proposals and letters of intent, and, since the machine has not started yet, it is quite possible that some of these will evolve in time. Some experiments are a continuation of the work done at Saturne I. Other experiments are extrapolations to higher energies of previous work done at lower energy, while others are concerned with new kinds of problems. Our experimental committee is scrutinizing all these experiments. In Fig. 5.18 there are sometimes several experiments per line: I have tried to group them according to their objectives and domain.

The first line corresponds to the nucleon-nucleon program; we have a group of people very interested in obtaining phase shifts at energies higher than the energies well-studied until now (that is up to $\sim$ 700 MeV) and want to study the nuclear force by making precise measurements above that energy. (Since there are too many names to put down, I have indicated only the laboratories of the people involved in each category of experiments.) The second line concerns what one can call classical nuclear reactions — elastic, inelastic, and transfer reactions; the first experiment will probably be elastic scattering on ^{208}Pb with SPES I. Then you have reactions with polarized particles. Let me mention one experiment in which there will be an ion jet stream in the vacuum of the machine hitting the particles — the protons or deuterons turning around — this would have practically no interference with the main user, a permanent measurement going on of scattering cross sections and polarization. Then comes pion production in nuclei, which includes also coherent pion production (p,π^+) and other reactions of this type, and coherent pion production by composite particles — deuterons and alphas. Production of resonances in nuclei — i.e., production of Δ's and N*'s in light nuclei. Then we have more complex nuclear reactions, spallation studies, relativistic heavy ions (I will come back to that item below). As for π^+ scattering and reactions with π^+'s above 400 MeV, we have people coming from SIN who would like to continue work done with lower energy pions at SIN. Then

comes experiments of astrophysical interest, followed by space research - the calibration and testing of various equipment to be put on satellites and other space probes. Dosimetry and radiobiology, radiography and diagnostic come next; we have, for instance, in radiography, a possibility which has been developed by a Saclay-CERN-Marseille group of obtaining cuts showing the different parts of the human body, as with x-rays, but with the additional possibility of showing the hydrogen distribution. And finally there is the testing of apparatus for elementary particle work at CERN.

THE RELATIVISTIC HEAVY ION PROGRAM AT SATURNE

Let us come now to the heavy ion program (Fig. 5.19). The heavy ion program will start in about one or one and a half years. At the present stage the experimental methods are probably better defined than the physics. And clearly all physicists working at Saturne are aware of the pioneer work done here and are very eager to take into account the nice results you are obtaining at Berkeley. The first line in Fig. 5.19 concerns a study of multiple pion and proton production and correlations with a 4π detector, which will be a chamber using time projection, either the LBL-Stanford system or the Heidelberg system. Then come experiments on nucleus-nucleus and proton-nucleus correlations using SPES IV, the 3.8 GeV/c spectrometer in coincidence with other detectors. There will be also low energy fusion experiments trying to link the low energy approach to the high energy approach, going above the energy corresponding to the maximum angular momentum that can be given to the nuclei involved. Then we have experiments on cluster production by looking at quasi-elastic reactions on a hydrogen target, the inverse of the normal quasi-elastic scattering experiments. A study is also planned of pion production below 500 MeV/c with SPES III, which should be the continuation of previous work on pion production with composite particles. We also have proposals for experiments on C + C fusion, on fragment production for astrophysics (propagation of cosmic rays), and on dosimetry and radiobiology.

HEAVY IONS AT CERN AND GRENOBLE

Art Poskanzer asked me to add a few words about the heavy ion plans at CERN, and on the schedule of the Grenoble machine. At CERN in Geneva, as you know, there will be a $^{12}C^{4+}$ beam available in September of 1979 and it will have an energy of 86 MeV/nucleon and an intensity of about 10^{11} particles per second, so it will be a powerful beam. Three studies have been proposed so far, I think; there are people here involved in that work so they can correct me. These are the experiments of the Isolde collaboration, which will continue its work with Isolde and with an on-line mass spectrometer. There is an experiment proposed by physicists from Copenhagen and Lund on proton emission in central and peripheral collisions, and another experiment on projectile fragmentation and light particle emission by a group from Grenoble.

Finally let me indicate that the Grenoble afterburner should become operational in 1980 and will have heavy ion beams of 30 MeV per unit mass. The first ions to be accelerated will range from ^{12}C to ^{20}Ne.

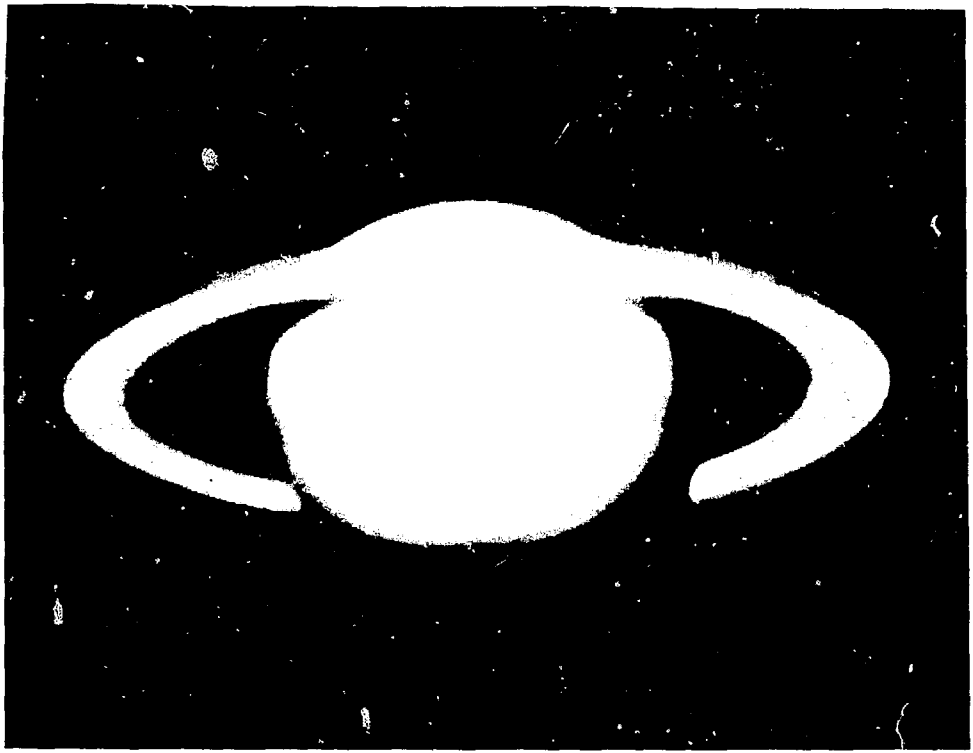

Fig. 5.1

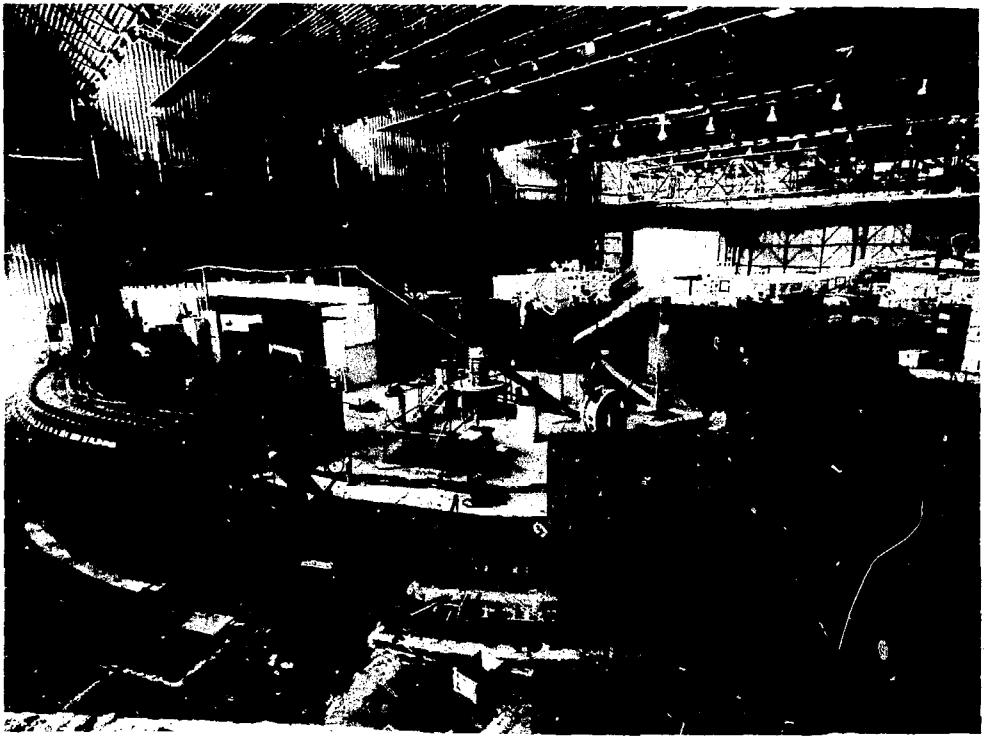

Fig. 5.2

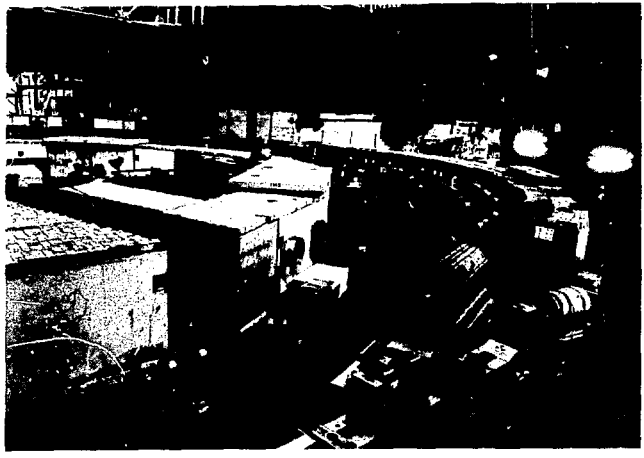

Fig. 5.3

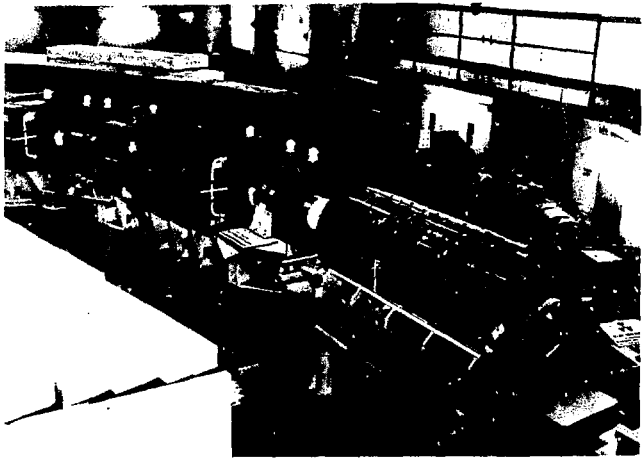

Fig. 5.4

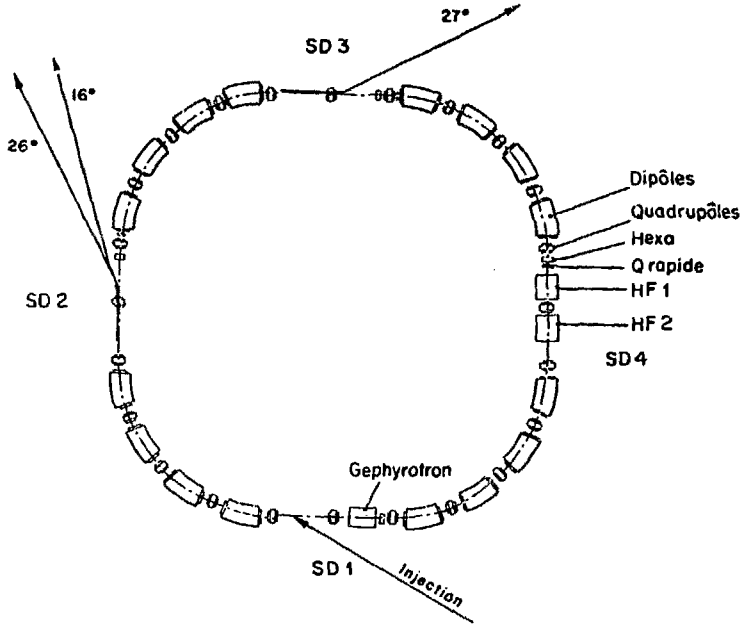

SCHEMA DE L'ANNEAU DE SATURNE II

Fig. 5.5

Saturne II

$R_{phys.} = 16.8$ m

16 dipoles 24 quadrupoles 4 straight sections

	$E_{inj.}$	E_{min}	E_{max}	$i_{extracted}$
protons	20 MeV	~ 300 MeV	3 GeV	$\gtrsim 10^{12}$/c
deuterons	10 MeV	~ 150 MeV	2.3 GeV	$\gtrsim 4 \cdot 10^{11}$
^3He	15 MeV		4.6 GeV	$\gtrsim 2 \cdot 10^{11}$
α	20 MeV		5.25 GeV	$\gtrsim 2 \cdot 10^{11}$
heavy ions	5 MeV/Amu	~ 100 MeV/Amu	1.15 GeV/Amu	$10^8 - 10^9$
$\vec{p}$, $\vec{d}$				$1 - 4 \cdot 10^9$

At $E_p = 1$ GeV $\varepsilon_H \approx 6\pi$ mm.mrad

$\varepsilon_V \approx 35\pi$ mm.mrad

Resolution $(\Delta p/p)_{extracted} \approx \pm 2.5 \cdot 10^{-4}$

Two possible simultaneous extractions at different energies

Secondary beams : $p+p \rightarrow d+\pi^+$

Parasiting

Duty cycle : 15% — 40% (depending on energy)

Typical cycling : 0.5 — 3 /sec (" " ")

Fig. 5.6

SOURCE CRYEBIS

for Heavy ions
and Polarized particles

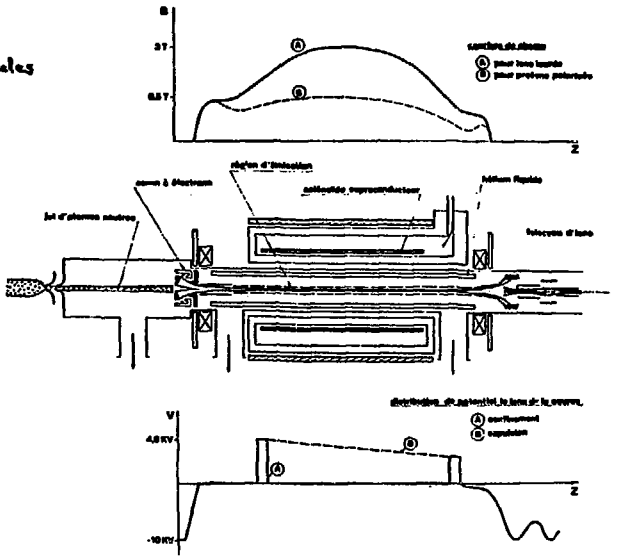

Fig. 5.7

Cryebis

Constructed and tested at Orsay
Will be set-up at Saclay on Saturne next spring

Will work with : $B = 3\ T$. mean: 750 A/cm²
density on axis : 2000 A/cm²
Source transmission : 99.98 %
inside pressure $< 10^{-10}$ torr.

$V = 10\ KV \qquad I = 2\ A$

$Q^{+}_{charges} \leq 3 \cdot 10^{11}$ per cycle

Expected efficiency from source to target : 4 %
(i.e. $\sim 10^{9}$. $^{20}Ne^{10+}$ per cycle)
$\sim 10^{10}$ $\vec{p}$ per cycle

Cyclic : injection ~ 200 μs
confinement ~ 20 - 30 ms
extraction ~ 200 μs

- First tests at : $V \leq 3.5\ KV \qquad I \leq 0.4\ A$
$B = 1.5\ T$
$\tau_e = 15$ ms.

N^{7+} - $3 \cdot 10^{8}$ Ne^{10+} (75%) Ne^{9+} (25%)
$2 \cdot 10^{7}$ Xe^{35+} (mean charge state) → Xe^{40+}

First ions to be used : ^{12}C, ^{14}N, ^{16}O, ^{20}Ne
$\vec{p}$, $\vec{\alpha}$

Fig. 5.8

Fig. 5.9

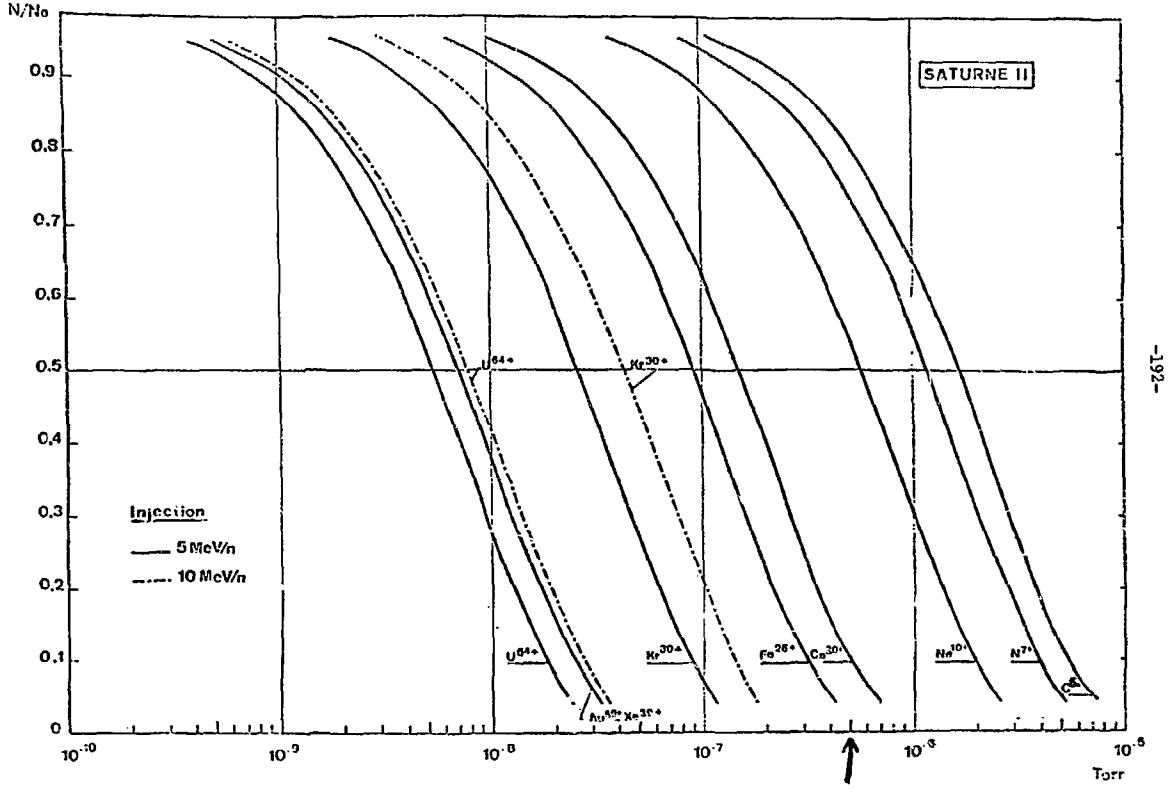
N/No
0.9
0.8
0.7
0.6
0.5
0.4
0.3
0.2
0.1
0
SATURNE II
Injection
5 MeV/n
10 MeV/n
U64+
Kr30+
U64+
Kr30+
Fe26+
Co30+
Ne10+
N7+
Ar18+ Xe30+
10-10
10-9
10-8
10-7
10-6
10-5
Torr

Fig. 5.10

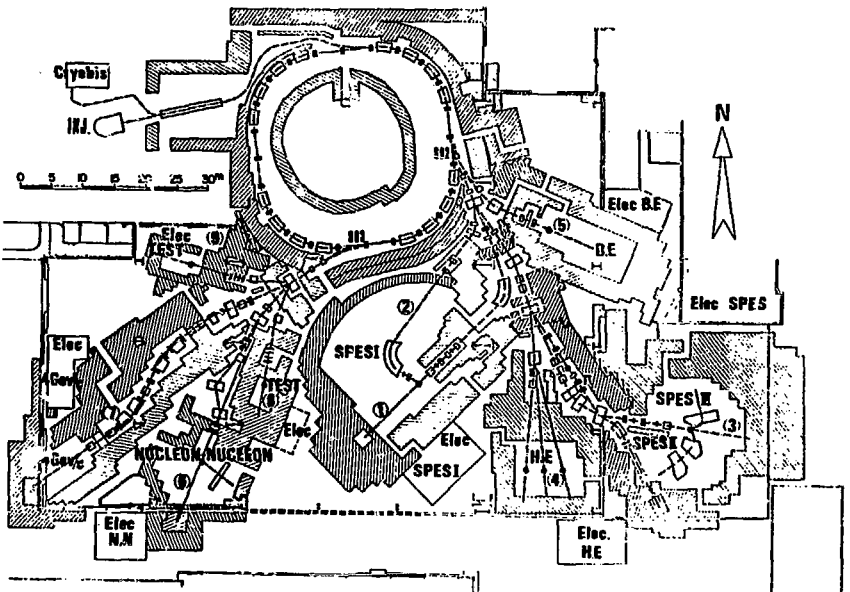
Cyclotron
INJ.
0 5 10 15 20 25 30m
Elec TEST
(6)
III
Elec B.E
(5)
D.E
N
Elec SPES
(2)
SPESI
Elec
Gen
TEST
(6)
(1)
Elec
SPESI
SPES II
(3)
SPES II
NUCLEON
NUCLEON
(7)
H.E
(4)
Elec
N.N
Elec.
H.E

Fig. 5.11

Fig. 5.12

SPES II

Focal plane : 2 m

$\rho F / \rho_c \simeq \frac{1}{4} - \frac{1}{2}$

$\rho_{max} = 750$ MeV/c

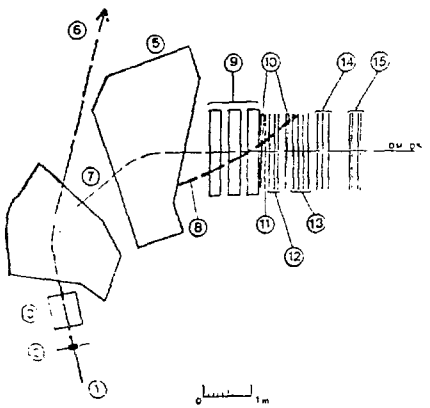

Fig. 5.13

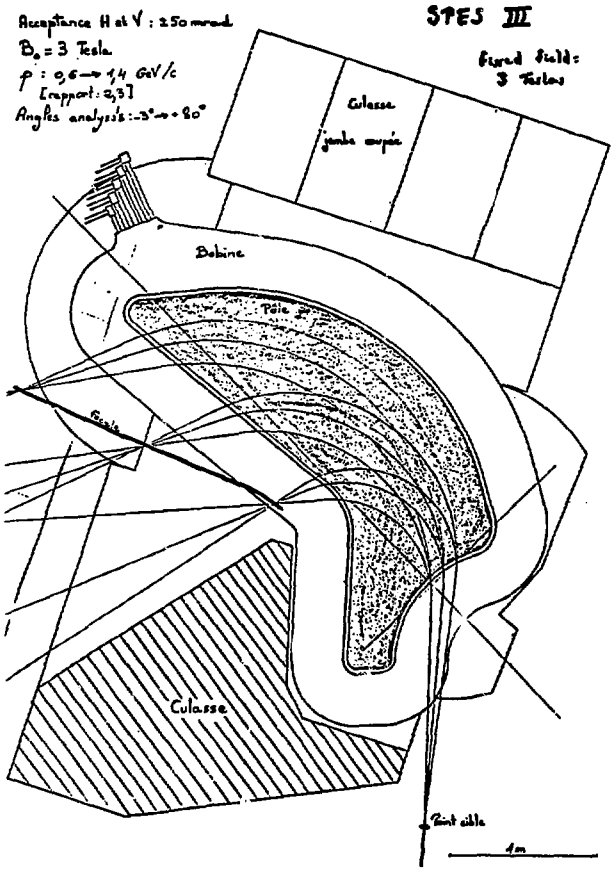
Acceptance H at V : 250 mrad
B_o = 3 Tesla
p : 0,6 → 1,4 GeV/c
[rapport : 2,3]
Angles analysés : -3° → + 80°
STES III
Fixed field : 3 Teslas
Culasse
jambe coupée
Bobine
Pôle
Culasse
Point cible
1m

Fig. 5.14

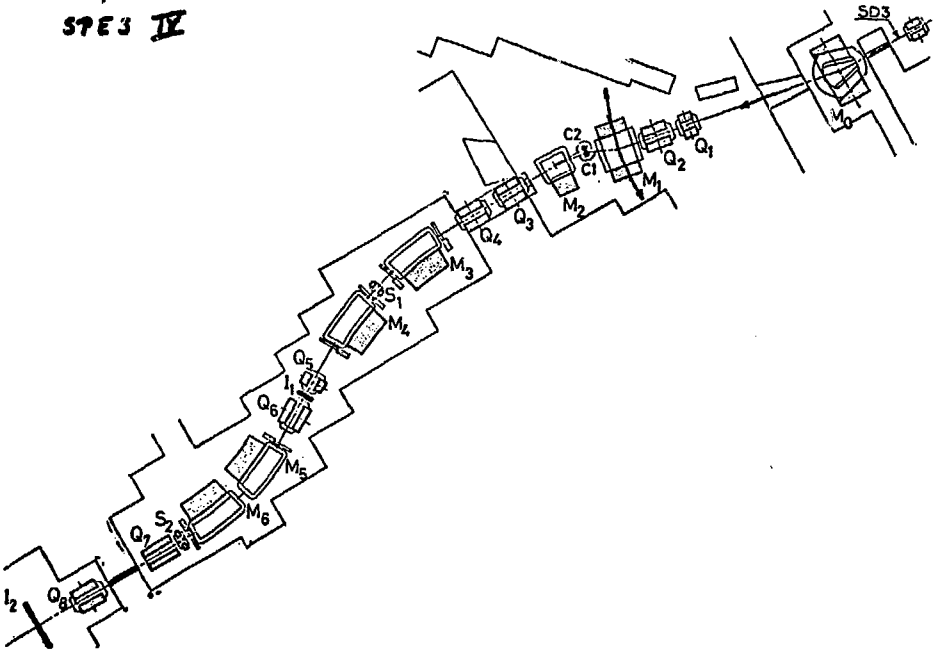
3.8 GeV/c
STE3 IV
SD3
M0
C2
C1
Q2
Q1
M1
M2
Q3
Q4
M3
S1
M4
Q5
I1
Q6
M5
M6
S2
Q7
I2

Fig. 5.15

Spectrometers

	Angular range	Solid angle	Resolution	Momentum	momentum acceptance
SPES I (100 t.)	0° – 80°	$3 \cdot 10^{-3}$ sr	$\frac{\delta E}{E} \simeq 10^{-4}$	2 GeV/c	$\Delta p/p = 3\%$
SPES II (100 t.)	0° – 60°	$2 \cdot 10^{-2}$ sr	$\frac{\delta p}{p} \simeq 3 \cdot 10^{-4}$	0.75 GeV/c	3 %
SPES III (250 t.)	−5° – +80°	10^{-4} sr	$\frac{\delta p}{p} \simeq 5 \cdot 10^{-4}$	8.4 GeV/c (Fixed field)	0.6 – 1.4 GeV/c
3.8 GeV/c (SPES IV)	+1.7° – +26.3° / −6.8° – +19.8° (with swinging magnet)	$3 \cdot 10^{-3}$ sr / $3 \cdot 10^{-4}$ sr	$\sim 1.5 \cdot 10^{-4}$ / $\sim 1.5 \cdot 10^{-3}$	4.0 GeV/c	~ 1.5 % ~ 3 %

Fig. 5.16

Schedule

Injection - Acceleration	July 1978
1st extraction ($\sim 2 \cdot 10^{11}$)	October 1978
Beginning of physics (1/3 physics - 2/3 machine)	~November 1978
2nd extraction	Spring 1979
Cryebis (heavy ions, $\vec{p}$, $\vec{d}$)	Summer 1979
SPES I	October 1978
3.8 GeV/c (SPES IV)	~Fall 1979
SPES II	~Beginning 1980
SPES III	~Fall 1980
N - N experiments	Spring 1979
π^+ beam	Winter 1979-1980

Fig. 5.17

Programme at Saturne

- Nucleon-nucleon experiments (Saclay DPhPE-DPhN/ME,Caen)
- Classical nuclear reactions (Saclay-ME, CNRS, Orsay IPN) (elastic, inelastic, transfer...)
- Reactions with polarized particles (Saclay-ME, Grenoble, SIN, Neuchâtel)
- Pion production in nuclei (Orsay IPN, Saclay ME, Strasbourg)
- Production of resonances in nuclei (Lyon-Orsay IPN-Saclay ME)
- More complex nuclear reactions (Bordeaux) (spallation...)
- Relativistic heavy ions → see below
- π^+ scattering and reactions above $\sim$ 400 MeV (Grenoble, SIN, Neuchâtel, Saclay)
- Astrophysics (Orsay CSNSM, CNRS)
- Space research (testing and calibration of apparatus) (Saclay SEP, Denmark, Kiel)
- Dosimetry and radiobiology (Fontenay, Villejuif)
- Radiography and radiodiagnostic (Saclay ME, CERN, Marseilles)
- Testing of apparatus for elementary particle physics at CERN

Fig. 5.18

Heavy Ion Program

- Multiple π and p correlations with a 4π TPC system (Saclay ME-BE-MF, Strasbourg, Clermont Fd)
- Nucleus-nucleus and p-nucleus correlations with SPES IV (Lyon-Orsay IPN, Saclay ME)
- Low energy fusion (Saclay BE)
- Cluster production by quasi-elastic and other reactions on H target with SPES IV (CNRS, Clermont Fd, Caen)
- π production below 500 MeV/Amu with SPES III (Strasbourg, Orsay IPN)
- $^{12}C + ^{12}C$ fusion (Orsay CSNSM)
- Fragment production for astrophysics (cosmic rays) (Orsay CSNSM, CNRS)
- Dosimetry and Radiobiology (Fontenay, Villejuif)

Fig. 5.19

PROPOSAL FOR DUBNA-KURCHATOV HIGH ENERGY HEAVY-ION ACCELERATOR

Alex Ogloblin

Yesterday I mentioned that a new research program was recently developed at Kurchatov Institute and this program is gradually becoming a national program in nuclear physics. The bulk of this program is high energy heavy ion collisions research with perhaps the most evident goal to study the nuclear matter equation of state and the possibility of the existence of the abnormal state of nuclear matter - I mean super dense nuclei and neutron nuclei. A detailed discussion of the requirements for an accelerator that would be necessary for such studies led to four basic requirements, which are listed here (Fig 6.1). First is that the mass of the accelerated ions should be as high as possible. This means up to uranium. Second, the energy should be at least 250 MeV/A, which allows a compression of nuclear matter of about a factor of 2. Third, the intensity should be as high as possible but from economical reasons we think the maximum is about 10^8 or 10^{10} per second. And fourth, a wide energy variation is needed because no one can say what energy region will be the most interesting. Two considerations influenced the development of the project. First was the Moscow site - at Kurchatov Institute we don't have enough space for a good high energy accelerator. Second is that the Institute in Dubna was involved in relativistic heavy ion physics for some time and Dubna has its own project for the nuclotron, which means a superconducting cyclotron that is a substitute for the existing synchrofasotron. So it was decided to combine the efforts of both institutes and to build a common accelerator on the site of the Dubna Institute.

At the present moment Dubna has a synchrofasotron (see Fig. 6.2). It is a machine with weak focusing like the Bevatron here. The main parameters of this machine at the present moment are: It can accelerate protons up to 10 GeV with intensities of about 10^{12}/pulse; deuterons, alphas and carbon at an energy of 4 GeV/A with intensities for alphas of about 10^{8}/pulse and for carbon 10^{5} or 10^{6}/pulse; beams of oxygen and neon are also obtained but with a very low intensity, which is due to bad vacuum conditions.

The schematic of this joint Dubna-Kurchatov accelerator complex is shown in Fig. 6.3. The dark line shows what already exists, the synchrofasotron with 20 MeV limit. The lighter line shows the main idea of this new accelerator. This means a heavy-ion synchrotron (HIS) and a special linac, with which it will be possible to accelerate all ions up to uranium with an energy of 10 MeV/A. But this linac will have no capabilities of a separate accelerator - it will be a pulsed linac, whose sole aim is to be an injector for this machine. A future possibility remains, which is to substitute a superconductive ring (Nuclotron) for the synchrofasotron, and to have the heavy ion synchrotron, HIS, as an injector not only for the synchrofasotron but also for the future Nuclotron.

Here are the main parameters for all the combinations of accelerators: HIS will accelerate different ions, and for uranium it is 250 MeV/A for slow

extraction mode and 350 MeV/A for fast extraction mode. After injection to the synchrofasotron this value will be 3.4 GeV/A for uranium and if, in the future, the synchrofasotron is replaced by a superconducting machine this value will be 10.7 GeV/A. For lighter ions the values are higher, 0.6 GeV/A for argon and after the synchrofasotron, 4.1 GeV/A. The intensity is estimated to be 10^{11} for the lightest ions and 10^{10} for heavy ions after HIS and two orders of magnitude less after the synchrofasotron. The cycling is 3 Hz for HIS and the existing cycling is 0.1 Hz for the synchrofasotron. Two comments should be made about these parameters. First is that the energy of uranium, 350 MeV/A, is enough for complete stripping of uranium ions so that the bare nuclei can be accelerated in the synchrofasotron; this means that no improvement of vacuum conditions should be done in the synchrofasotron. Second, at the present moment the synchrofasotron allows one to reduce the energy from 4 GeV/A down to 400 MeV/A and HIS also has the capability to come down approximately to injection energy. So the whole energy range would be covered by this machine. During the development of the project two important simplifications were found. First is that the magnetic system of the heavy ion synchrotron was chosen exactly the same as for a booster for a high energy proton synchrotron; this booster is now under construction so we don't need new magnets and can use those we already have. Second is that it is possible to put HIS inside the synchrofasotron ring (see Fig. 6.4), which means it isn't necessary to have a special new building and both beams from HIS and from the synchrofasotron would be transported to the same experimental vault, which is already built. In the second slide is shown the place where HIS will be situated (see Fig. 6.5). A man is standing at approximately the same place where the HIS ring will be and has in his hands a sheet of paper which is the exact cross section of the HIS synchrotron. The background shows the existing synchrofasotron which will be also part of the shielding for HIS.

In Fig. 6.6 I compare the proposed accelerator complex with other projects. This is a usual diagram where y is energy per nucleon and x is mass of the accelerated ions. This is HIS in Russian—THC—the line labelled THC + CΦT is the combination of HIS plus the synchrofasotron; the three lines below are for the improved Bevalac, the synchrotron in Darmstadt, and the Numatron. The dashed line represents the possible combination of HIS with the Nuclotron.

In Fig. 6.7 the comparison is done in a little different way. x is the energy of the ions and y is the compression factor, which is the compression of nuclear matter in comparison with equilibrium nuclear density. There are many different calculations of the dependence of the compression of nuclear matter on the energy of the incident ions. We use here two limits. I will call the lower curve the pessimistic approach and the upper curve the optimistic approach. The large arrows are very rough estimates of the density needed for the phase transition due to pion condensation, and due to σ meson field if that phenomenon exists. So we can see approximately what compression is needed in order to get this or that phase transition phenomenon. Here again is the energy obtained by HIS (THC) and this is for HIS and synchrofasotron (THC + CΦ) and T, D, B are Tokyo, Darmstadt, and Berkeley in Russian letters. I think it is not necessary to talk just at the moment about the scientific program. We think there will be a smooth transition between experiments that are now on at the existing synchrofasotron, and that international cooperation in this sense will be very fruitful.

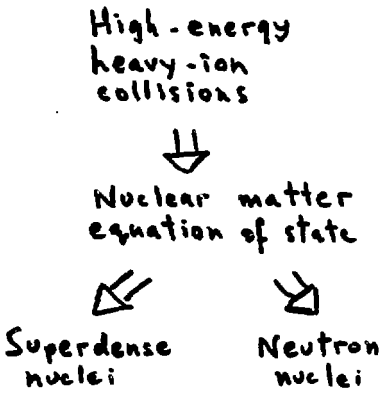

Basic requirements:

1. A : up to ^{238}U
2. E/A : at least 250 Mev/N
   $(\rho/\rho_0 \approx 2)$
3. I : $10^8 - 10^{10}$/sec
4. Energy variation

Fig. 6.1

Dubna synchrofasotron

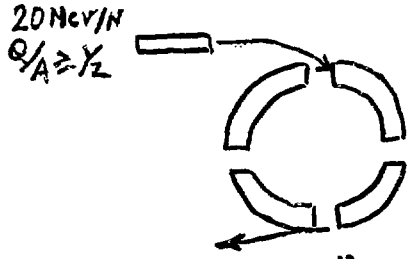

Fig. 5.2

Dubna - Kurchatov accelerator :

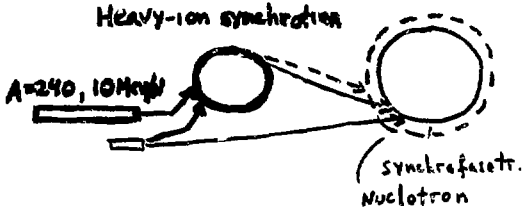

Energy, GeV/N

	HIS slow	HIS fast	SF	Nucl.
^{40}Ar	0.47	0.6	4.1	12.6
^{132}Xe	0.35	0.49	3.6	11.4
^{238}U	0.25	0.35	3.4	10.7

Intensity: 10^{11}-10^{10}/sec 10^{9}-10^{8}/sec

f : 3 Hz 0.1 Hz

Fig. 6.3

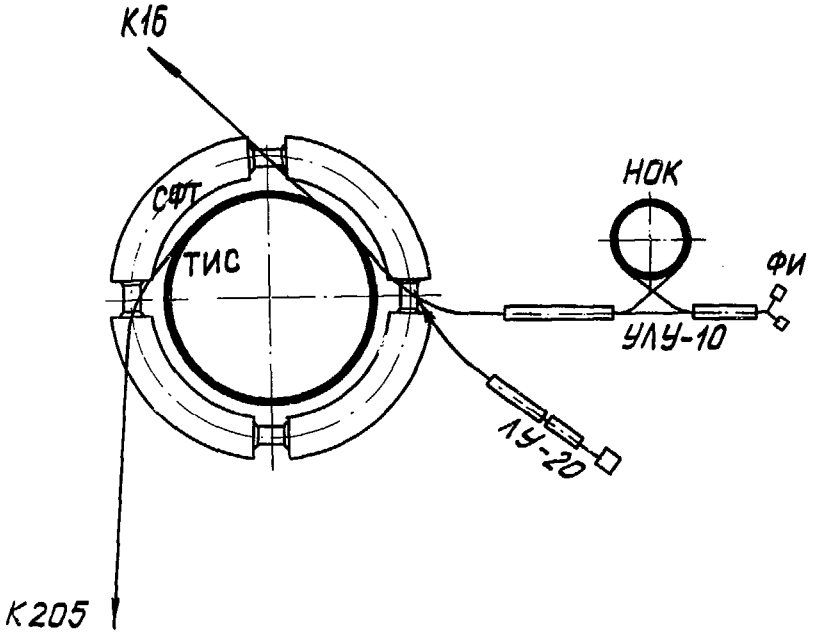

Fig. 6.4

XBL 787-9768

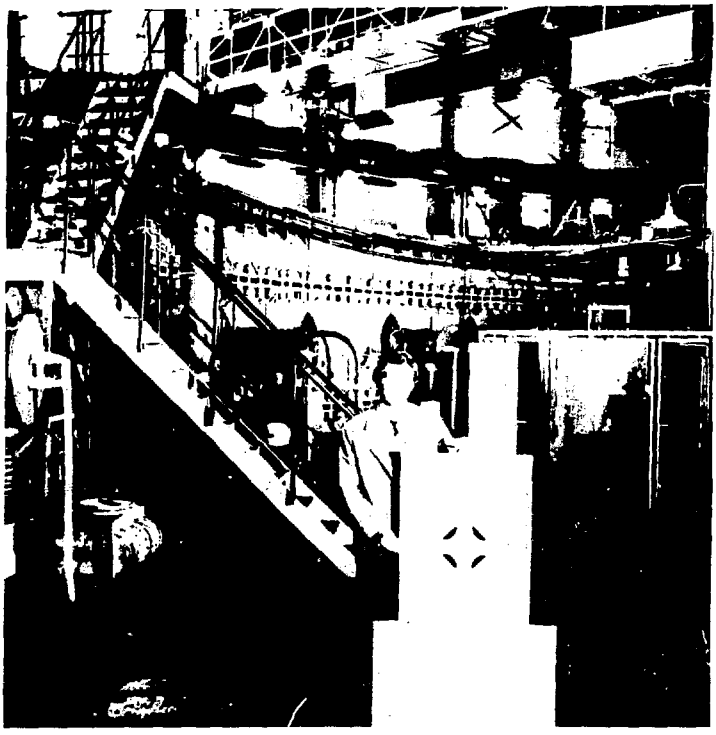

Fig. 6.5

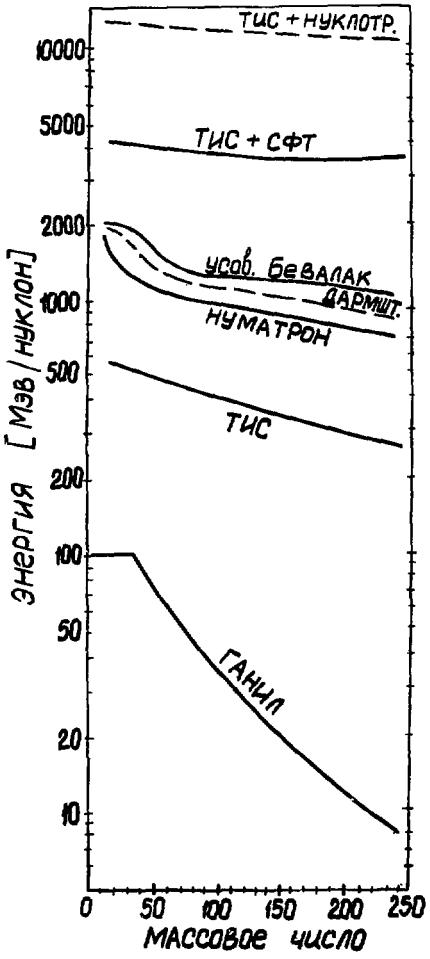

XBL 787-9766

Fig. 6.6

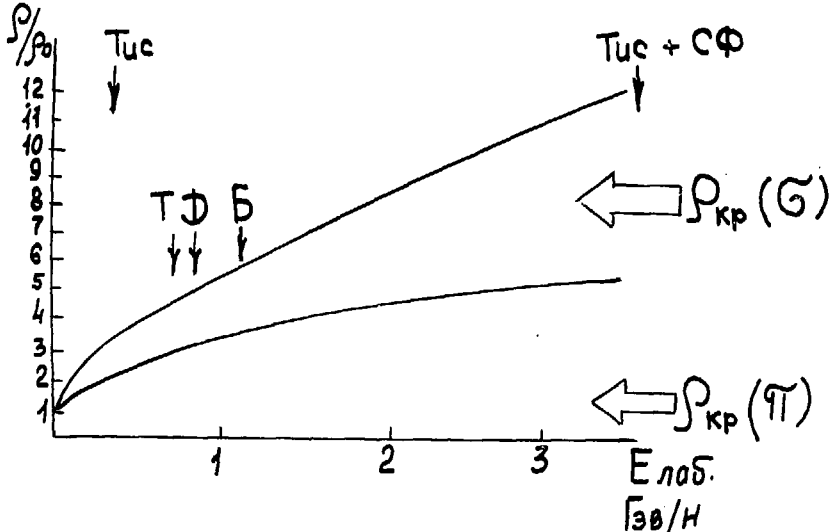

Fig. 6.7

XBL 787-9767

THE PRESENT STATUS OF THE NUMATRON PROJECT

K. Sugimoto

I would like to introduce to you, very briefly, the present status of our Numatron project in Japan, which is a high energy heavy ion physics facility designed to provide heavy ions up to U in an energy range of 100-1000 MeV/A with reasonably good intensities. (See Fig. 7.1.)

The aim of the project is to open up a new field of nuclear physics, which is just the theme of this summer study. A group of nuclear physicists in Japan has conceived plans during recent years to contract such facilities, and the Numatron project was proposed. A study group was assembled at the end of 1976 at the Institute for Nuclear Studies, University of Tokyo. The major activity of the study group has been directed so far to the detailed design studies of the accelerator and the related technological developments.

In my talk I will mention briefly the design of the proposed accelerator complex and also the present activities of the study group. The region covered by the Numatron is shown in Fig. 7.2, which shows typical threshold energies assuming U as the target.

Fig. 7.3 shows the present design of the proposed accelerator complex. The desired capability can be achieved by an accelerator complex that has a synchrotron at the final stage. Important problems in designing such an accelerator complex are how to share acceleration stages and how to get the expected beam intensities. In order to obtain an intense beam, a storage ring is installed between the injector linac and the synchrotron.

The accelerator complex consists of a Cockcroft-Walton injector followed by Wilderoe and Alvarez Linacs, between which one or two charge-stripping stages are used depending on the mass number of accelerated ions. Ions accelerated up to 10 MeV/A are injected into the storage ring and stored more than a thousand turns. RF stacking combined with multiturn injection will be used in the storage ring while a previous group of ions is accelerated in the main synchrotron and then extracted. The synchrotron is a separated-function strong-focusing type, and the average diameter is 68 m. The repetition rate is 1 Hz. In this way, intense beams can be obtained, i.e. for Xe $\sim 10^{11}$ p/s and for U $\sim 10^{9}$ p/s.

The storage ring has almost the same radius and structure as the synchrotron, and these together form a two-ring system. The system can be operated in a variety of injection and acceleration modes. Fig. 7.4 shows some of the possible variations of the time-sequence program of operation. The first operation mode shown is the basic one, and the other variations can also be considered. The choice of the mode will depend on the results of further studies, especially on what is discovered about the stacking technique of the low energy heavy ions.

Major technical problems associated with the construction of the Numatron are presently being actively pursued by the study group at INS. Among these activities, I will mention here only the test ring for heavy ion storage and acceleration, which is now under construction (see Fig. 7.5).

The aim of the test ring is to study the beam dynamics and the efficiencies of multiturn injection and storage of heavy ions. $^{14}N^{5+}$ or molecular hydrogen H_3^+ ions accelerated up to 8 MeV/A by the INS cyclotron will be injected. The diameter of the ring is 10 m. The test experiment will be started around October 1978.

Fig. 7.6 shows the anticipated time schedule. The basic studies are funded and started; however, the main project is not formally approved yet. If the project is approved, we can start the preparatory work during the next year, and the main construction will begin in 1980 and will take about four years. Before the final approval of the project we must find a new site for it, because the present INS site is unfortunately too small. However, we are hopeful that the project will soon be started and that we will be able to contribute to this new field of nuclear physics with the Numatron project.

Numatron Project

INS, Univ. of Tokyo

M. Sakai, K. Sugimoto, Y. Hirao, T. Marumori

- High-Energy Heavy-Ion Physics Facilities
  (Up to U: 0.1 ∿ 1 A/GeV)
- Proposed Accelerator Complex
  (Up to Xe: ∿ 10^{11} p/s, U: ∿ 10^{9} p/s)
- Activities of the Study Group at INS
  (Test Ring for Heavy-Ion Storage & Acc.)

Fig. 7.1

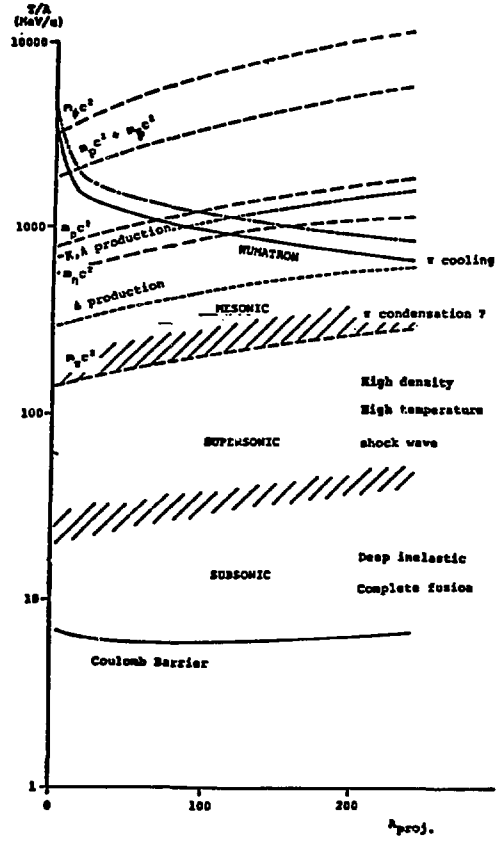

Fig. 7.2 Various phases of heavy ion interactions

The typical threshold energy of various reactions are indicated together with the energy of NUMATRON. Target is assumed to be uranium and projectile is changed over almost all elements. The bulk-production (i.e. the number of produced particles is equal to the mass number of the projectile) is considered.

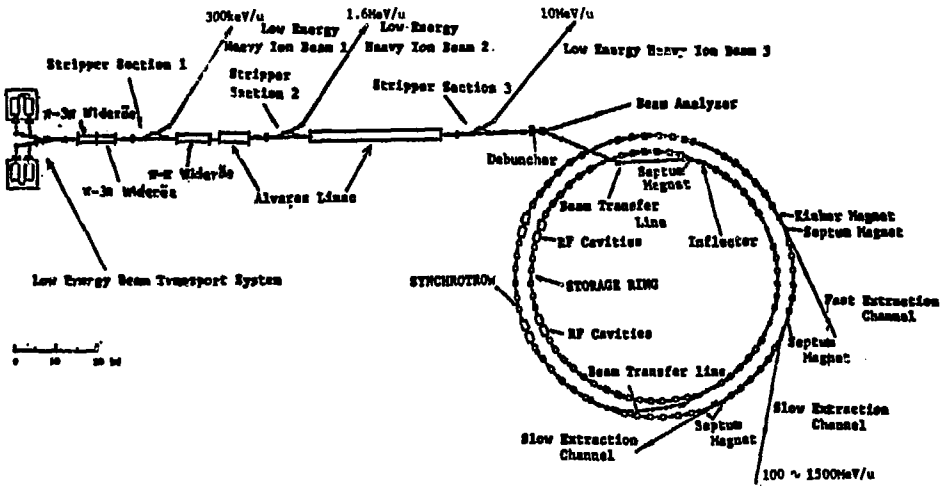
300keV/u
Low Energy
Heavy Ion Beam 1
1.6MeV/u
Low Energy
Heavy Ion Beam 2
10MeV/u
Low Energy Heavy Ion Beam 3
Stripper Section 1
Stripper
Section 2
Stripper Section 3
Beam Analyser
Debuncher
Septum
Magnet
Beam Transfer
Line
RF Cavities
Inflector
Kicker Magnet
Septum Magnet
SYNCHROTRON
STORAGE RING
Fast Extraction
Channel
RF Cavities
Septum
Magnet
Beam Transfer Line
Slow Extraction
Channel
Septum
Magnet
Slow Extraction
Channel
100 ∿ 1500MeV/u
Alvarez Linac
Low Energy Beam Transport System

Fig. 7.3

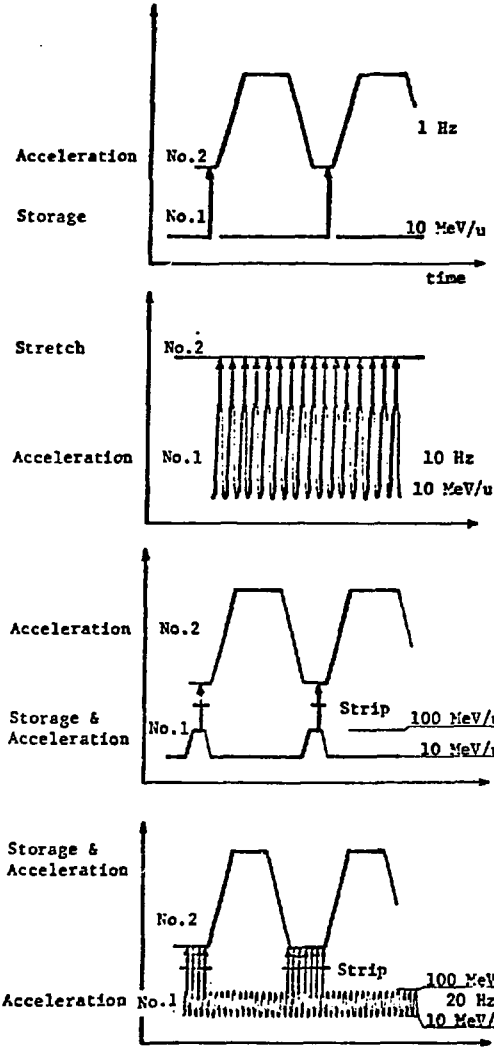

Operation Modes of two-ring Accelerator.

Fig. 7.4

Y. Mizao, A. Mizubucki, T Katayama,
S. Yamada, A. Noda, T. Matori,
S. Watanabe, M. Yoshizawa,
K. Chiba, H Tsujikawa,
T. Morimoto, K. Omata,
M. Muton, K. Kuneko,
H. Sasaki, and
A. Miyahara.

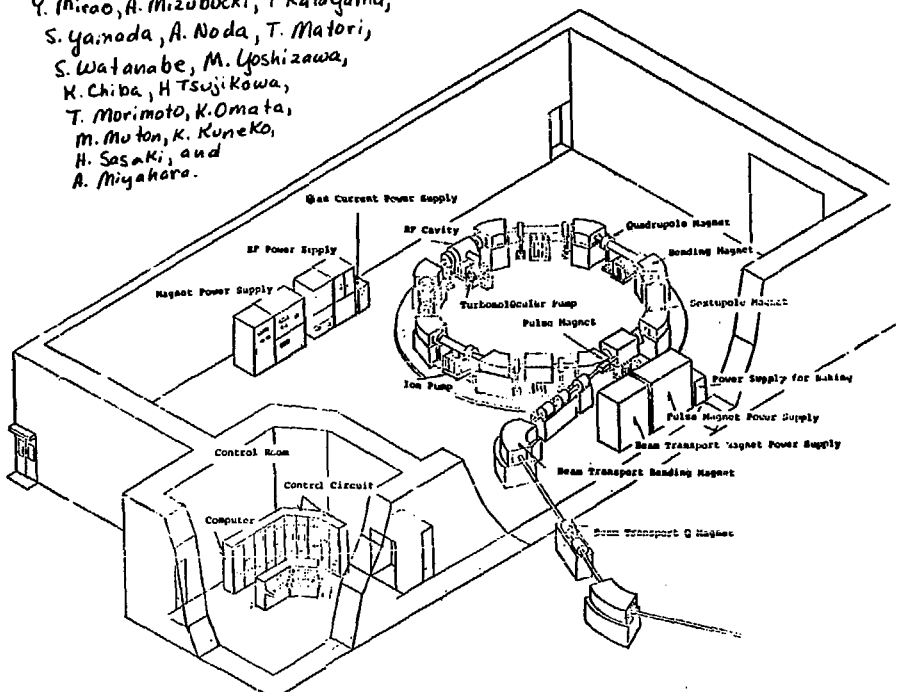

Fig. 7.5

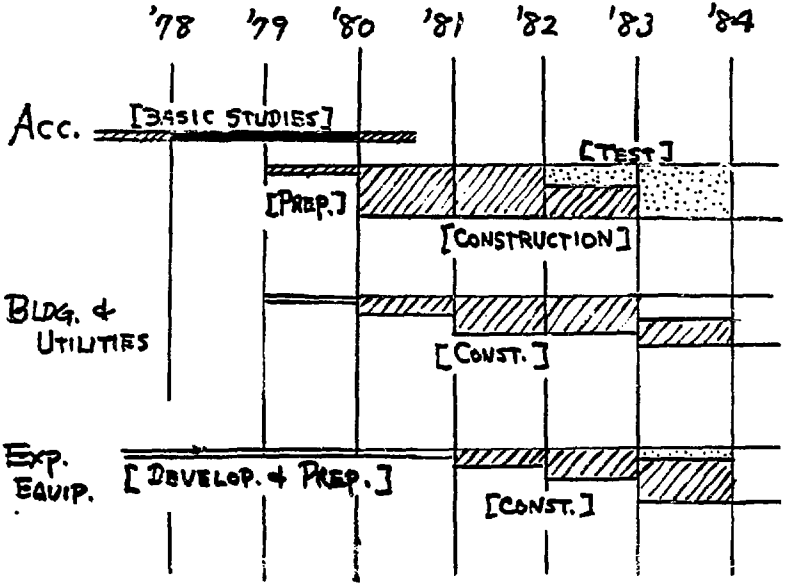
'78
'79
'80
'81
'82
'83
'84
ACC.
[BASIC STUDIES]
[TEST]
[PREP.]
[CONSTRUCTION]
BLDG. & UTILITIES
[CONST.]
EXP. EQUIP.
[DEVELOP. & PREP.]
[CONST.]

Fig. 7.6

CRITICAL REVIEW OF CRITICAL PHENOMENA IN NUCLEAR COLLISIONS

Mannque Rho

I was asked by Norman Glendenning, one of the organizers of this meeting, to discuss and review the subject of critical phenomena in nuclei. I shall, in fact, restrict myself to reviewing the overall views of this subject. I will have no difficulty in doing this. However, there was one further stipulation to the invitation: Glendenning said I should review the subject in the context of nucleus-nucleon scattering. After having heard so many talks on various aspects of nucleus-nucleon scattering, I think it would be fair to say that it would be some kind of insanity to try to discuss the experimental data in light of possible phenomena associated with the very interesting physics, e.g., the critical phenomena in nuclei. Therefore, I will veer away from the main theme of this conference and try to restrict myself to the aspects of critical phenomena that one could discuss on the grounds of experimental evidence. If it is not possible to do this, then I will try to make some general arguments that might indicate one direction or the other.

The subjects I was asked to discuss – as you notice I have taken off the nucleus-nucleus collision from my title – are actually three. The first subject is pion condensation; the second, Lee-Wick matter, which I will refer to in most of the cases as abnormal state. Since there is an abnormal state one talks in terms of the pion condensation, unless I refer to it specifically in this way. I shall mean Lee-Wick state when I refer to abnormal state. I was also asked to talk about Quark Matter. This is, of course, a logical sequence in the discussion of the critical phenomena; however, the next speaker will deal extensively with this. Therefore, I will go into the subject to the extent that it is relevant to the rest of the subject.

Let me start with a kind of dream a theorist might have of something wonderful in nuclear physics, which can be summarized with a couple of examples. Let's consider very low energy phenomena (see Fig. 8.1). By low energy I mean 10, 20, 30 MeV/A in the center of mass. Suppose we consider collisions of two ions. What one would like, of course, is to probe with this kind of nuclear interaction the equation of state that might yield some interesting information beyond the density regime known at the moment. Suppose we have a theorist's prediction of various curves corresponding to the equation of state. This is the energy per particle minus the nucleon mass plotted against the density. Now suppose that we know that the normal equation of state, in which there is nothing strange going on, is given by this dashed curve. If I do the modern-day pion condensation calculations and then plot possible phase transitions associated with the pion degrees of freedom, this turns out to be very sensitive (we will come back to this question later) to some parameter which I call g'. I won't specify yet what it is – for the moment it is only necessary to look at the relative size of these numbers, and then we'll see what the physics of all this is. Now let's say I take for g' a value of 0.45. In this case one expects to have a state at higher density which has much larger binding energy than the normal state (curve b). If I just increase this slightly within the framework of the theory given, one

finds that the equation of state moves up in this way (curve a) with much less binding energy. And, of course, if I increase it further we might get nearer this (dashed) curve. And so on.

Now the scenarios corresponding to these two curves are rather drastic. I will take the second scenario, that is, the deep binding on the system (curve b), and I will do the rather well advertised TDHF, which is probably the best on the market as far as the microscopic structure is concerned. Suppose I shoot ^{16}O on ^{16}O with 10 MeV/A in the center of mass. Then the program gives, whether realistically or not, something unusual happening: that is, that you can easily create some superdense matter. However, if you take the other scenario (curve a), there is a slightly decreased binding energy and you will find practically nothing interesting as far as the spectacular aspect is concerned.

All this is for very low energy. Let's go to higher energy. (See Fig. 8.2.) Suppose that again you look at the possible structure of the energy density curve, which has the following structure: at temperature equal to 0 plotted with the binding energy versus the nuclear matter density, ρ/ρ_0, you might have this deeply bound, superdense state (at 5) in contrast to the ordinary matter, which sits at a density of 1 and has a small binding energy. The scenario changes again very drastically whether or not this B', which refers to the binding energy, is large or small. Suppose that B' is of the order of a pion mass 140 MeV, which is very much bound. Then as a function of the laboratory energy plotted here in GeV/A, you might expect to have large π multiplicity with respect to the normal equation of state for the production of pions. Those are quite idealized calculations within the assumption that the system thermalizes completely. Of course there have been lots of discussions on whether this is possible or not. I don't want to go into any of those questions but the picture suggests that you might have some spectacular facts in certain circumstances. I just mention here that this is not valid when the nucleons make a phase transition to quark state; this will probably be discussed later on by someone else.

All right, now that is a kind of dream. It would have been wonderful, but we haven't seen it. Whether or not we have actually had such interactions occurring in the collision is not clear. What experimentalists see at the moment — whether these observations tell us something about what occurs inside — is not at all clear. I won't worry about that but will go into the subject matter in question and in depth.

Let's consider first pion condensation. (See Fig. 8.3.) I have put here π and σ as chiral partners for continuity of discussion. Now the first question that arises, if we are talking about phase transitions associated with pions, is whether or not we have some evidence that the pion plays a role in nuclei. Of course, we can always create them if we give enough energy. But does the pion play a role in nuclear physics? Up to now, I think nuclear physicists have had no difficulty in understanding most of nuclear properties — individual particle behaviors, collective behaviors, and all these things — without invoking anything about the pion or meson degrees of freedom. But if you want to consider something about the pion-induced

phase transition you have to have some idea that the pion is definitely playing a crucial role. I shall then start with a subject that may not be directly related to this conference, but will lead to some understanding of what might be going on with the pions.

Let us consider the pion degrees of freedom. In particular, do we have any evidence that somewhere along the way in the description of nuclei we definitely need pions in order to understand what goes on in the experimental observation? Let us first concentrate on the questions related to soft pions. It is very difficult to describe hard and soft pions in detail in a short talk, but soft pions are those having small energy and momentum, and in this region we are in a position to understand certain dynamics involved with pions better than in other situations, so it seems to be the natural place to start looking for the pion degrees of freedom. We will come back to the notion that pions are associated with questions of chiral symmetry, and in fact this notion plays a very important role throughout my discussions here. In particular, I would like to pose the following question: we understand very well by the electromagnetic interactions what the charge structure of the nucleus is — charge distributions and so on — but do we understand the charge distributions associated with axial charge? The axial charge that has, for instance, the pseudoscalar nature of the charge distribution, and the pion quantum number— what structure does that charge have if you compare it with the vector charge in a certain kinetmatical limit, in particular the long wave limit? We know that the charges are usually described by point charges; that has been very successful in describing much of the understanding of the electromagnetic properties of nuclei.

Now I will come to the main question, that is the axial charge, and I will make the assertion that the axial charge is quite different even if you assume that the axial charge is conserved. It has quite a different structure and axial charges cannot be described by point charges associated with each nucleon; you have to have some sharing between them. This is a kind of collective behavior one would like to see in nuclear physics. The question is how to see the sharing of this kind of charge.

Well, there is a way of seeing it, it turns out, and this evidence comes from several completely different experiments, unknown to many in the nuclear physics community, and that evidence is the following: you would like to see the pion degrees of freedom, so you would therefore like to see a nuclear state associated with the pion quantum number. It turns out that a very nice experiment could be done with a well known nucleus, ^{16}O. (See Fig. 8.4.) You have an ^{16}O ground state and put a muon in, and make a muon capture into the system, exciting it to a 0^- state in ^{16}N, which corresponds to the pion quantum number. And you can also look at the inverse decay going from the ^{16}N to the ^{16}O. Now this is a very gentle probe because it's a weak interaction; however, as is always the case in nuclear physics any of these processes depends upon nuclear structure. Particularly in a simple minded picture, the 0^- state can be regarded as some kind of particle-hole excitation with a quantum number of 0^-, and in fact if you look into the shell model structure you will find that there are a couple of such configurations, and there obviously will be dependence upon the mixing coefficients of the wave function. The nice thing

about this particular process is that if you take the ratio of the muon absorption to the beta decay it turns out to be quite sensitive to what I was talking about as the distribution of the axial charge shared between nucleons; and furthermore, it is almost model-independent. Such an experiment exists and the data are in Fig. 8.4. At the moment the error bars are rather large; however, one can use this already to see whether we understand the pion-like structure in nuclei by doing the simple minded calculations. That is, you assume that there is no sharing of the charges and that gives the upper line — that's the theoretical prediction. Now if you then introduce the sharing of charges through a pion, with a well-prescribed method based on soft pion theorems (or equivalently chiral symmetry) then you can obtain the result given by the lower line (labelled soft-pion exchange). This gives us the first clear evidence that the pion does something in nuclei, without which you cannot actually understand the very specific experiments I am talking about. It's gratifying to see that the ratio is nearly independent of η, the configuration mixing. And it is indeed so even when you introduce the meson degrees of freedom into the picture.

Having seen that there are something like pions in the system, let's go to the pion condensation. (See Fig. 8.5.) I won't go into much detail because I'm sure this has been discussed in all the conferences dealing with heavy ion physics — clearly one of the most exciting subject matters — but I will just state the things involved in this kind of game. In one description of pion condensation, the statement goes as follows: if one takes the chiral symmetry as the basis, then from the rather general considerations one can deduce the nature of a pion condensed state, ψ_c, such that the pion field develops a non-zero expectation value in the limit of the volume going to infinity. Furthermore, the condensed state has an energy less than or approximately equal to the normal nuclear matter energy. There can not be too much difference from the normal state. In consequence the parameters used in describing the pion condensation are almost identical in both phases the condensed as well as the normal phase. This is a very important issue.

Now from our understanding of pion-nuclear interaction, we know that the interaction in the s-wave is repulsive and therefore the possibility of having a pion condensation exists more in the p-wave, which is attractive. All these rather numerous discussions can be summarized in terms of effective potential, which acts between particles and holes, or Δ resonances and holes, and the effective interaction is governed by a couple of terms. There is a term corresponding to the pion exchange, which, of course, is the one that will drive the system to pion condensation. In addition there is a local repulsive interaction. Now in the pion exchange you have to use the pion-nucleon coupling, the propagator with the pion-pion interactions in the system. Then of course, since they sit inside the medium, you have to put in all the medium corrections, in particular the corrections due to virtual excitations of the Δ-hole. Therefore, the self energy of the pion is represented by this kind of thing. That is, the pion comes in, excites the Δ and hole, and then the excitation and de-excitation continue through an exchange of everything other than the pion. We would like to put in what is called irreducible self-energy term. Such effective potential has the following

structure: g' is a local repulsive interaction due, essentially, to the hard core but in any case a repulsion between the nucleons when they are together in a particular channel corresponding to the pion quantum number. If we had no such thing, it's clear that this interaction would be attractive. If the particle-hole state wave function peaks around this region, then there will be the attraction, and therefore something occurring to the system. However, because of g' we think exists (I will show that it exists later on) the attraction is diminished, depending upon the value of g' — at 0.6 it's less attractive, and at 0.8 the attraction is almost washed out. It would be very simple and nice if there were no repulsive interactions but of course nature is not that simple, and this is essentially the complication of all the physics involved. (See Fig. 8.6.) The local interaction is repulsive in the pion channel, and in Migdal's description of nuclear structure this is given as the Fermi liquid parameter corresponding to the pion channel, the spin-isospin channel, and is usually referred to in this kind of treatment as g', or if you are familiar with pion-nuclear scattering, it is essentially the Lorentz-Lorenz effect. In order to define my terminology, g' for the classical Lorentz-Lorenz effect, corresponds to exactly 1/3. So any number given should be compared with this 1/3. Since we are dealing with several variants in the system, if it's the diagonal nucleon-hole interaction I will refer to it as g_a', the nucleon-delta diagonal interaction is g_b', and the off-diagonal interaction is g_c'. The scenarios for heavy ion physics that something wonderful might occur doesn't really depend upon what we have as a relation between these quantities. Particularly if we take the point of view of Migdal and his collaborators, g_a' corresponding to the nucleon-hole, local interaction is usually taken to be greater than 1/3, whereas all the rest are taken to be approximately zero. A different point of view, taken by all but the Migdal group, is essentially that they are all the same and greater than 1/3. As a justification, they usually assign an SU(4) group to the nucleon and Δ. That is not terribly relevant but whether or not this is so has to be seen through experimental evidences.

Now what I would like to describe here is what information we can get on g' from experiments other than just the heavy-ion collisions. In fact, you can place quite a stringent limit on this and from all classical experiments. In fact, there have been many, many beautiful experiments that were done for other purposes. Now I'm going to use these in a very cheap way to tie down the crucial information on g' (Fig. 8.7). The first thing is spectra. We are talking about quantum numbers associated with the pion, and therefore the natural thing is to look at the energy spectra that correspond to the excitation with the pion quantum number, namely those quantum numbers like 0^-, 1^+, 2^-, T=1 states and also M1 transition rates which had been looked at in an extensive way. The second possibility is to look at the beta decay, for which there are enormous amounts of data available, and the third possibility is to look at the π-mesic atom.

Those are all "different" fields of nuclear physics. Now the physics involved in this kind of argument is the following: Let's consider first the spectra. Let's look at the first excited state, as an example. You can find many other examples, but the first we get as an example is the 0^- state of ^{16}O, which lies at something like 12.79 MeV, and in particular,

consider the energy difference between the ground state and the excited state. Now this, as we all know, reflects the interactions between the particles and holes and the interactions, as I have mentioned before, have two competing effects. One is attractive pion exchange and the other is repulsive g', the local interaction. Now anybody who knows Goldstone diagrams will immediately draw such graphs and then compute the energy. Since we think we know the pion exchange, that immediately leads to the information on g', and in particular, g_a' corresponding to this quantity here.

Now let's look at the beta decay. We have very precise beta decay information on single-closed-shell nuclei. Now why do we say that the beta decay has any relevance to the pion condensation? Well, it's very simple. In fact, if you look at the chiral symmetry-based arguments for the pion condensation, you proceed in the following way. You say that you take a σ and the pion. It has a certain structure, which in fact, I skipped without discussion (see graph on Fig. 8.4). The σ and π are chiral partners and the chiral symmetry makes certain statements about what this circle amounts to if you believe in some kind of low energy theorems and so on. Now the pion condensation essentially means that the normal state sitting here is rotated to the state containing not only the pion field (that is, the expectation of pion field being non-zero) but also the expectation value over non-zero, so there is some kind of mixing, which is represented by the angle . So you're actually mixing which is represented by the angle . So you're actually mixing the expectation value over and the pion in this instance, and that gives rise to the pion condensation. Now when you do this rotation, in order to get to the pion condensation you do not do the global rotation but the local rotation. So you take a Lagrangian, which describes the normal state reasonably, and you make a local chiral rotation with $\theta \neq 0$, and that leads to some kind of pion condensed state. And doing this local rotation is nothing but generating currents in the system. In fact, you will have not only the vector current in the system but also an axial current, and the strength of this axial current will be modified by the g' effect. Now this axial current occuring in the pion condensation is approximately the same as the effective coupling constant occuring in the normal beta decay because there were three conditions associated with the pion condensation, the last condition being that the parameters in both phases are the same. Therefore, this parameter, which occurs in the pion condensation, must be reflected in the beta decay.

Let's look at the π-mesic atom. Well, for the π-mesic atom two things are measured. There are the energy shifts associated with x-ray transitions and the width. In particular, the energy shift is relevant to this question and that relevance can be seen in the following way. Again we get the ground state of the pion condensed system as a function of θ. If it's a small θ you can make the expansion in this way. The coefficient that corresponds to θ^2 is precisely the inverse pion propagator in the medium and that is nothing but the self energy of the pion inside the medium. In particular the p-wave part of the self-energy of the pion inside the medium is related more directly to the energy shift in the π-mesic atom transition. If you draw the diagram for this particular thing that is precisely this (Fig. 8.6), and in particular if you look at this graph here on this line (Fig.8.4) that is this one here.

What are the situations obtained from the experimental data? The spectra have been analyzed and that gives you something of the order of 0.7 ± 0.1. It could be 0.7 ± 0.2, it's not so much variation but that's that thing reported by the people who have looked at it. However, what it amounts to is that it is sufficiently larger than the classical Lorentz-Lorenz. Now the second piece of information one gets from the beta decay is the order of 0.7; and just to show what I mean by this kind of thing look at the data and consider what a 0.7 implies in terms of theory. In fact it resolves nicely one long-standing problem in nuclear physics: the systematic quenching of the axial vector strength in light nuclei is explained.

Now this is not the entire story because of the π-mesic data. In fact, the information coming from there seems to be rather contradictory to the previous thing. Therefore, that softens the argument I have been making. I will just briefly mention what that is, without the details, since I don't have much time. As I said, if you analyse the π-mesic data, that gives you information of the diagonal Δ-hole interaction, in particular the local repulsive interaction g_b'. There are a lot of complications, however. The data are beautiful (Fig. 8.8) but the theory is not in such a beautiful state. Much of the complication is due to our present lack of understanding of some of the pion-nuclear interactions, particularly the complications due to the pion absorptions, the off-shell phenomena, etc. Therefore, it does not give us very precise information. However, one particular aspect is interesting, which is that the pion-nuclear s-wave off-shell effect can actually modify — can affect essentially — the optical potential relevant to the p orbit which we would like to use in order to get the g' information. Particularly, if one uses the soft pion theorem, the non-Born isospin symmetric s-wave amplitude (which I have written $A^{(+)}$) — essentially the forward scattering amplitude — and consideration of all the off-shell dependencies of this object lead to a further contribution to the p-wave optical potential of this form. It is not terribly important to understand what those things are; but the point is that if you make this kind of rather reliable soft-pion theorem argument, you find that the comparison with the experiment leads you to $g_b' = 0$. Now we have had the two scenarios. Of course, none of this actually fits in with the scheme and therefore, the question is still quite open — one cannot make a very strong statement, but as it stands the evidence is for rather large g', which is not something you can just shrug off by saying that maybe the experiment is wrong. Because the experiments are rather precise; maybe the theories are wrong, but I cannot see anything wrong with them.

Now we want to know what those constants mean, what to expect. I think the picture is almost self-evident. If you calculate the critical density, you have something like (Fig. 8.9) this (as a function of g') for the critical density of ρ/ρ_0, that is actually ρ_c/ρ_0, and you see that it rapidly increases between 0.6 and 0.7. The precise values are not important because the point is they can be very large; ρ_c could be 3 or 4 times the matter density. The equation of state would have this form; that is, if you have this g' of 0.48, which had given a wonderful reaction in ^{16}O, you would expect this structure here. The equation of state, which gave nothing essentially wonderful, has this particular structure and 0.55 gives you this.

If you go to 0.6 or 0.7 it would be very difficult to disentangle from the uncertainties already abundant in calculating a normal equation of state. Nevertheless, one would like to talk about heavy-ion physics since it's a heavy-ion session. I would just make a brief remark about the consequence of this kind of analysis on the most idealized version of the heavy-ion physics which was not presented here but has been discussed previously. In particular, let me consider the following questions. We know that when you have a heavy-ion collision, you heat the system; whether it's a complete thermalization or not, that is an open question. At this point I will take the most naive view — that it is completely thermalized — and take this idealistic extreme case. What has been studied so far is the discussion of the critical density in the presence of temperature. Actually you might talk about critical density and critical temperature. Now I have written down here for the theorists whether this question has been really understood. It was never clear that in fact one understands very well how to treat those two variables at the same time. But never mind. We take the road people mostly use; that is, in discussing the critical behavior, we usually assume the standard thermalization of ideal fermion and boson gases and see what one can say about the possibilities or impossibilities of various phenomena.

I have taken some things from other people. In particular, those relativistic hydrodynamic shock wave calculations seem to indicate that it will occur along this line of temperature versus the density (Fig. 8.10). Now if somehow the critical temperature and critical density for the pion condensation occurred along this line, then everything would be fine, you would see some spectacular things. If something happened along this line, then it would not be anything interesting. Now the situation is really very delicate because we are right on the marginal line. Either you take the one that corresponds to 0.6 or 0.7, which seems to be the one indicated by the normal. It is not at all clear that we are going to have anything spectacular. Now one caveat for this is, of course, that Migdal does not agree. And in such situations, of course, one would have to think about other fancy experiments. I cannot propose a very definite experiment, but it seems quite clear that what we need to see is a direct signal. Someone mentioned, and I agree, that neutrinos would be very nice to see, because, after all, what happens inside is not going to be transmitted directly by the exploding hadrons that come out. It will require an enormous amount of work.

Now there have been suggestions that maybe one should measure the hard photons. That, of course, is somewhat more direct — it's more a direct snapshot of what's going on inside than the hadrons. It's not clear what the feasibility of such an experiment is. There have been questions of the utilization of the dynamic instability. That is, it's not an equilibrium situation but it's something occurring in dynamic situations. You try to take advantage of dynamic instability, which seems to me to be the only possible way of looking at this question.

We now go to the next problem - the Lee-Wick state (Fig. 8.11). The rather firmly believed* general concept, on the Goldstone realization of a symmetry

* There is no direct evidence so far to indicate, at least in particle or nuclear physics, that such is the case.

that is spontaneously broken, indicates that at some high temperature and density the symmetry broken in the normal phase should be restored at some abnormal phase, and if I associate this symmetry realization in the normal phase with the Goldstone mode, I can associate the symmetry realization in an abnormal phase with the Wigner mode. This is rather general in the sense that these concepts are used everywhere — in solid-state physics, particle physics, and in nuclear physics — but in completely different contexts. Now one example is this Gauge theory. One thinks that the quark confinement is associated with some kind of phase transition, and if you heat the system the quark might be released. That's a conjecture. If you associate normal nuclei with the Goldstone mode, then in high density it might make a phase transition to an abnormal matter, which corresponds to the Wigner mode.

All these problems are essentially a problem of vacuum change. We thought that it was very simple but now it is becoming more and more complex; in fact, I don't think anybody understands the vacuum very well. The possibility exists by various means (heavy ion physics is one mean but there are others) to make the change of vacuum by experimental processes. Now in particular, the experimental area in which to study chiral symmetry is essentially normal nuclei, extended objects, and one could also use the associated density of this extended object to make the phase transition, which is a very exciting possibility. The degrees of freedom associated with this phase transition are the scalar meson 0^+ object and, as I have already asked in connection with the pion, what do we know about these degrees of freedom in nuclei? There have been discussions that maybe this is associated with the intermediate-range attraction in nucleon-nucleon potential. For instance, the one boson exchange essentially describes the attractions felt between the nucleons.

To be more specific, let me just write down these Lagrangians (Fig. 8.12). I think this is the only equation I'm going to write down here — Lagrangians which consist of the scalar field, ϕ, and the spinor ψ — it could be nucleon or quark, but we will be specifically considering only nucleon degrees of freedom in the following. That is, the nucleon coupled to the here and the mass term, and that is the kinetic energy term for the scalar meson field, and then there is a potential. That potential has ϕ^2, ϕ^3, ϕ^4.

Now if you are restricting yourself to a renormalizable theory, then you are supposed to stop here, at least in four dimensions. Of course this is not an entire story for nuclear physics. We know that there is a short range interaction; therefore I have written down that there are additional degrees of freedom one has to take into consideration. (Maybe it is associated with exchanges, and so on.) Now in the quasi-classical approximation or mean field approximation, if you take the coefficients b and c to be positive, then the in general is negative and therefore this term here is attractive, if you consider this as some kind of an energy contribution, and this term here is repulsive. There is a specific model for what I am talking about, which is rather simple: that's the sigma model, which has the σ and π as the ingredients, σ and the three π_1, π_2, π_3, or π^+, π^-, π^0. I'm going to use this variable σ rather frequently so is just related to this field here by some σ_0, which is the constant corresponding to the usual normal vacuum in this diagram. I have already mentioned that pion condensation

is along this way and what we will be considering as a Lee-Wick state is essentially this point. We will just simply ignore in the discussion the pion degrees of freedom so I can talk about the reduced σ-model in which no pion appears explicitly. The potential I have written has the simple structure; you can see that this object is invariant under the discrete symmetry $\sigma \to -\sigma$, which in this language is equivalent to the chiral symmetry. Of course there is also symmetry breaking. Everybody knows that the pion mass is not zero, but for the discussions I think that's not important.

Now the essential issue is the following: b^2, the coefficient corresponding to the cubic term, is larger than 4ac and this is required in order to have more than one minimum in this potential (Fig. 8.13). And for some density larger than nuclear matter density, if you consider the normal nuclei as a particular ground state associated with some particular structure of the vacuum, this vacuum changes its structure. In particular, mathematically stated, it means that the σ variable in the normal phase has σ_0 and effective mass of the nucleon, which is of the order of 1 GeV, and is changed into the $\sigma = 0$, effective mass equal to zero, driven by the density or temperature. Nobody has yet looked at the questions associated with temperature but in particular in connection with Lee-Wick it is the density. This phase we know very well is the normal phase; the other phase is the abnormal phase. Now the major controversy since the original proposal of this theory was the following: Does the theory describe both the normal and abnormal states? In describing the controversies I think it is sometimes useful to know how certain we are about certain conjectures or statements or arguments. I won't be able to give you any numbers from now on but I'll try to specify to what certainty can we make statements concerning this issue. Let me define in the quasi-classical sense this quantity, $\zeta_{3\text{-body}}$, which is just the b term divided by the coupling constant g and mass of the nucleon. And then let me define the 4-body which is c divided by g^2. And the ratio ζ_3 divided by ζ_4. Now I have said that the 3 body term is attractive and the 4-body term is repulsive and therefore the ratio is the attraction to the repulsion. The criticism is the following: b^2 greater than 4ac, which is necessary for generating the Lee-Wick state, for instance, in the sigma model, implies with the coupling constants associated with this, that normal matter is unstable, and therefore you cannot describe the normal matter with the same theory. The reason is interpreted to be due to the too strong three-body attraction, that is to say, the normal matter simply collapses because of the attraction.

I have summarized the general criticisms in a table. (See Fig. 8.14.) There are many others, but these are essentially the samples associated with this. Given the theory, since we know the normal nucleus the best, we would like to recover the normal nuclear matter and we can do various things to the theory to do it. Of course a short range repulsion should be added somehow in some manner but that's not terribly important for the qualitative discussion here. The first possibilities weaken or drop the 3-body and 4-body terms entirely; usually one does this with this particular ratio of the coupling constant and the sigma mass corresponding to the rather small mass four times the pion mass. And if you ask what does that nuclear theory correspond to in that framework with respect to the chiral symmetry, there

is no question about the fact that this is manifestly broken. And with this theory, abnormal states cannot be obtained. The second argument is that you keep the large 3-body attraction but that you increase the repulsion even further in such a way that you have net repulsion. Now compare that to the situation in the σ model where it's the contrary. And furthermore, the analysis to understand the nuclear bulk properties, for instance, nuclear matter energy and other things, and also the surface properties, requires a sigma mass roughly 1.8 times the pion mass.

The last possibility is a rather intricate one. The nonlinear term is suppressed in a chiral symmetric fashion, that is, in terms of the chiral variable I have written here. You drop it in the following way: with combinations of $\sigma^2 + \vec{\pi}^2$, which is chiral-invariant and the whole thing squared equal to 0, if you set the pion field equal to 0, then you have various terms you are actually dropping at the same time. Also, at the same time, you drop this non-linear term. So in the dropping process you keep the manifest chiral symmetry; in the Lagrangian it looks as if it is unbroken. But, however, if you go to the mean field approximation to do the nuclear matter calculations it is also violently broken. (See Fig. 8.12.) That theory also will lead to no abnormal states.

Now all this can be summarized in the following way (Fig. 8.15): These alternative arguments lead to some kind of compromise with what comes afterwards, that is, that you need no many-body attraction in the normal phase, chiral symmetry is somehow broken in the normal phase, and that gives rise to the conclusion that the abnormal state is completely absent. This, as I have argued previously, is inconsistent with the successful description of the axial charge distribution, which is based on chiral symmetry, and there is further information about which I won't go into detail. It is a Σ term, which has to do with the degrees of symmetry breaking in nuclear matter rather than in nucleons, in hadrons, and the indication is that there is no reason to believe that inside the nuclear matter chiral symmetry is manifestly broken.

So the issue is: are we in a position to say anything about the relationship between the effective parameters that occur in the normal phase and the abnormal phase? It is because the effective parameters are rather different in the two phases. That is, to understand the normal you need this kind of relationship, and to understand the abnormal you need that kind of a relationship (bottom of Fig. 8.15).

The crux of the matter is the quantum fluctuation because the mean field does not take into account any of the quantum fluctuations; and this has been studied (see Fig. 8.16). It is a situation in which the coupling constant is strong; therefore, the usual perturbation theory does not have much meaning. However, you can again resort to the arguments based on the chiral symmetry and in particular, near the normal nuclear matter situations, this $\sigma - \sigma_o$ (σ_o is the vacuum value) is rather small. Therefore you hope to expand the quantum corrections in terms of this variable, keeping the chiral symmetry intact in the language of the reduced sigma model. Now we have one free parameter in this theory and that is this λ (Fig. 8.12) or n_σ, and you can arbitrarily

demand that the coefficient of the 3-body force be small because nuclear physicists do not like it. And the Δv then, this quantum correction, is small for other reasons, which I hope to discuss. You can make this demand and you can try to calculate in some scheme along this line. This can be done, whether or not this is good. But an amazing thing that happens is that it is extremely sensitive to one single parameter, m_σ. You can have either one or the other, depending upon less than 10% change in the parameter. And you may have the critical density, which is five or three times the nuclear matter density. The binding energy is unbound by 180 MeV or bound by 100 MeV.

I will not go into the quark matter since there is no time but I will finish the major issues of the sigma model in the following way (see Fig. 8.17). The big issue was raised by the three-body forces and I think this is relevant for any of the attempts to understand the basic issues of the Lee-Wick states. Nuclear physicists usually take the following coupling constants, and this is essentially motivated by the one boson exchange, and so on. If you look at the coupling constants and the masses involved they are rather drastically different from the parameters that appear in the original Lagrangian. Now, you argue, that is nothing but what Gerry Brown calls pionization. In other words, it is some kind of fluctuation effect, e.g., quantum corrections to this. In fact, m_σ, which is seen here to be 500 MeV, (or if you want to have surface effect correctly coming out, 250 MeV) is given by these bubbles for the pion. Or if you believe in this ratio then the coupling constant associated with this is something like 7, compared with the original σ model Lagrangian, which is something like 15. Therefore this also is complicated. It is clear that the effective Lagrangian used for understanding the nuclear matter has no bearing and gives no information as to which Lagrangian or fundamental theory it comes from. Therefore the domain of the applicability has no connection whatsoever. And furthermore, even if you take the point of view that three-body force should not be large, that depends upon which mass you are taking. Here if you have taken the effective coupling constant corresponding to the normal region then of course you are sitting here; therefore, that three body contribution is rather large. But we know that if you have a three-body system then it depends very singularly, essentially very importantly, on the mass that was exchanged, and that is due to the short-range correlations. And in fact if you believe that the numbers associated with the abnormal phase are the relevant ones, then you find that practically no three body contribution disaster occurs here. Therefore, the question then arises that I mentioned previously, namely, is there any connection whatsoever between the two parameters involved, the normal and the abnormal?

Now the answer to this quite strongly hinges on the meaning of the scalar field, σ (Fig. 8.18). I think many of the objections raised to the original idea, interpreting the σ as something that occurs in nuclear physics, the nucleon-nucleon potential, are based on the fact that there is nothing like σ in the free space in the Particle Data Group's Review of Particle Properties. But in order to understand this issue correctly one really would have to follow some of the ideas or the reasonings given recently by Friedberg and T.D. Lee; if you want to look at hadrons in terms of the Soliton model, the same scalar field appears but it is a collective interpolating field,

and you imagine the hadron as a gas bubble in the medium in which the $\langle\sigma\rangle$ becomes zero inside and something large outside of the domain structure, and this has a long-range order if the volume goes to infinity. Since it has long-range order there are now no short range fluctuations, therefore the mean field would be good.

You can argue the same way for the σ field in nuclei. You associate this with a collective field, therefore it's not necessarily associated with the scalar meson in the Review of Particle Properties and you make the similar arguments that the mean field should be accurate for the abnormal state in the limit that the number of nucleons goes to infinity. Now there are very interesting parallels between the two. How is the relation between the σ scalar field that appears here and the scalar field that appears there? This is a question for the theorists.

The major unknowns are that the parameter in this abnormal state is essentially the "m_σ" — what it is, we don't know — and of course there is also a delicate balance between the short range correlations. All these are not calculable with certainty and it is probably necessary to wait until we understand the hadron dynamics before we can make a certain statement on this question.

As a conclusion let me just say the following. The phase transition in nature occurs whenever it is given a chance. We know an enormous number of them, molecules and polymers. We have liquid ^{3}He, ^{4}He, and many, many others, and in fact the confinement and the releasing of the quarks may be associated with a phase transition. And somehow in between these two steps something is missing. And I ask why is it that the nuclear matter should not manifest its phase transition? All the common features of nuclear critical phenomena seem to be that they are very elusive, at least up to now. And also it is very sensitive to parameters of the theory, in particular, g' for the pion condensation, the effective σ mass in the Lee-Wick state, and the mass scale Λ for the quark matter. And of course an interesting question to ask is: do all these manifestations of nearness not indicate that we are very near the instability point? Are we not just reaching it?

I. Wonderful things that COULD happen in Heavy-Ion Collisions :

Low Energy

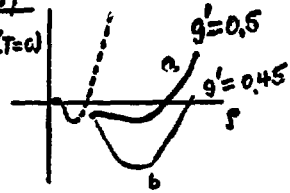

[Bonche, Birner, R., Yazaki]

Scenario (b) : TDHF

$^{16}O + ^{16}O$: 20 MeV/N in C.M.

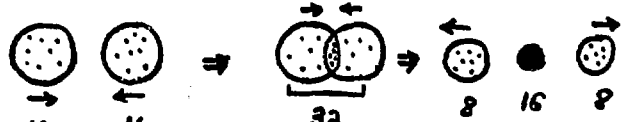

"Abnormal" (!)

Scenario (a) : TDHF

Nothing happens !

Fig. 8.1

Higher Energy

[Stöcker, Greiner & Scheid]

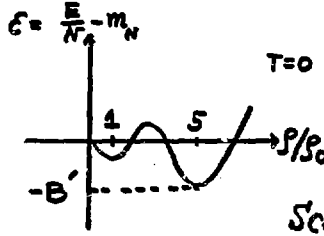

Scenarios :

Relativistic Hydrodynamics (Complete thermalization)

$B' = m_\pi$

$B' = 0$

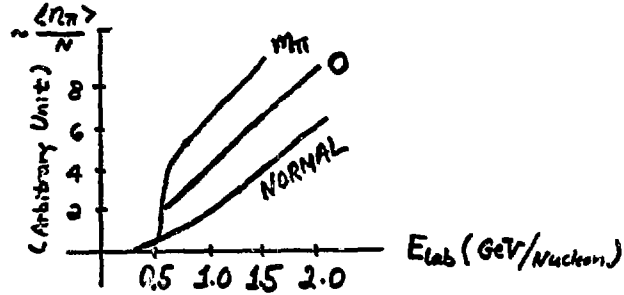

Not valid if Nucleons → Quarks

Phase Transition.

Fig. 8.2

II PION CONDENSATION

π : 0^-]
σ : 0^+] Chiral Partners.

Pion degrees of freedom [Delorme, Kubodera, R./ Guichon, Giffon, Samour]

What do we know and with what degree of certainty ?

Soft Pions [Chiral Symmetry] $\Rightarrow$ Axial Charge density in Nucleus

Vector Charge

Axial Charge

How to see the "Sharing" of the Axial charge ?

Fig. 8.3

Measure : $\langle 0^- | Q_A | 0^+ \rangle$ Gentle Probe

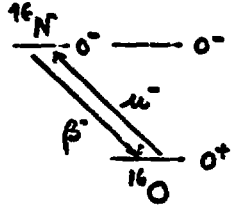

$|2S_{\frac{1}{2}} 1P_{\frac{1}{2}}^{-1}\rangle + \eta\, |1d_{\frac{3}{2}} 2P_{\frac{1}{2}}^{-1}\rangle$

$\mathcal{R} \equiv \Lambda(\mu^-)/\Lambda(\beta^-)$

R : 1. Very Sensitive to Axial Charge distribution

2. Nearly (Nuclear) Model-independent

i.e., $\frac{\partial \mathcal{R}}{\partial \eta} \approx 0$

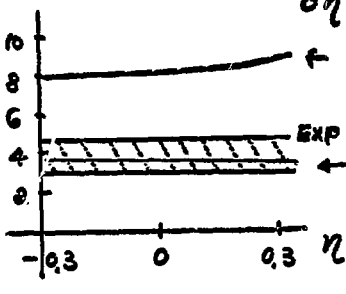

↳ Pion degrees of freedom : ✓
: ✓

Chiral Symmetry

Collective effect (e.g. Pion Condensation) : ?

↳ $\omega \sim 0$, $k \sim 2\text{-}3\, m_\pi$

$\omega \sim 0$, $k \sim 0$] Axial charge

Fig. 8.4

Pion Condensation

[Migdal / Sawyer, Scalapino]

Chiral symmetry ⇒ ∃ "Pion Condensed" State Ψ_c such that

[Baym, Campbell, Dashen, Manassah]

1. $\langle \pi^i \rangle_c \neq 0 \quad [V \to \infty]$
2. $E_c \lesssim E_{Normal}$
3. $(Parameters)_{Cond.} \approx (Parameters)_{Normal}$

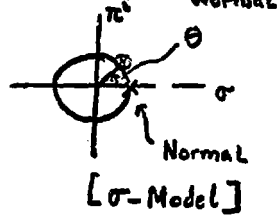

π-N ; S-wave repulsive
P-wave attractive

$$V_{eff} = -\frac{f^2}{m_\pi^2}\tau_1\cdot\tau_2\left[\frac{\vec{\sigma}_1\cdot\vec{k}\;\vec{\sigma}_2\cdot\vec{k}}{k^2-\omega^2+m_\pi^2+\Pi_\Delta} - g'(\sigma_1\cdot\sigma_2)\right]$$

Pion

Local, repulsive

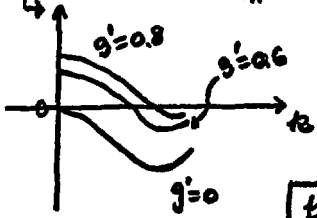

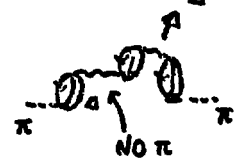

$k \neq 0$

Fig. 8.5

Local interaction g': Repulsive in "Pion" Channel

↓

Fermi Liquid parameter (Landau / Migdal)

or "Lorentz-Lorenz" effect.

└ Classical value $g' = \frac{1}{3}$ Ericson & Ericson

Generalization:

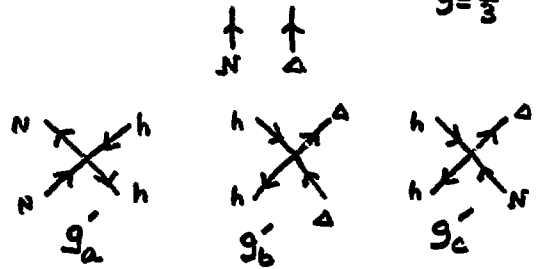

Different Scenarios for Heavy-Ion Physics

1. $g_a' \simeq g_b' \simeq g_c' > \frac{1}{3}$ Others (SUGA)

2. $g_a' > \frac{1}{3}$, $g_b' \approx g_c' \approx 0$ Migdal, Markin & Midurtin

Information on g' from Normal Nuclei

Source	g_a'	g_b'	g_c'
Spectra	0.7±0.1	Insensitive	Insensitive
β-Decay	—	Insensitive	≈ 0.7
π-Mesic Atom	—	?	—

Fig. 8.6

CONSTRAINTS ON g'

Spectra & M1 transition $0^-, 1^+, 2^-, \ldots$	β-Decay	π-mesic Atom
[Meyer-ter-Vehn / Speth Brown & Anastasio / Birner, R., Yazaki]	[Oset & R.]	[Migdal / Barshay, Brown & R.]
E9. $\Delta E = E(0^-) - E(0^+) =$ 12.79 MeV ^{16}O	$^{15}O \xrightarrow{\beta} {}^{15}N$ $^{17}F \longrightarrow {}^{17}O$ $^{39}Ca \rightarrow {}^{39}K$ $^{41}Sc \rightarrow {}^{41}Ca$	Energy shift ΔE_{1p}
V_{eff} : Competing effects π-exchange : attractive g' : repulsive	NORMAL → π-Cond. $\mathcal{L}(\theta=0) \rightarrow \mathcal{L}(\theta)$ Local Chiral Rotation Axial Current (A_μ^α) $g_A(g')$ Same as g_A^{eff} of normal β-decay	$E(\theta) = E(0) + \theta^{-1}\theta^2 + \ldots$ θ^{-1} = (pion propagator in medium)$^{-1}$ $\propto \Pi(q,\omega)$ Pion self-energy P-wave : ΔE_{1p}

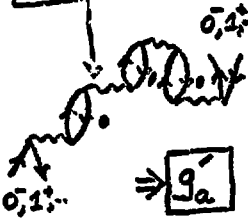

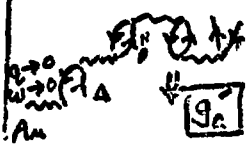

Fig. 8.7

π-Mesic Atom $\longleftrightarrow$ g_b' 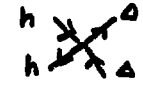

Complications

[Absorption
[Off-Shell

π-N S-wave off-Shell Effect [Migdal]

Soft-pion theorem $\Rightarrow$

$\bar{A}^{(+)}(q,\omega)$: Non-Born Isospin Symmetric S-wave amplitude

$$U_{opt} \approx \frac{\partial \bar{A}^{(+)}/\partial q^2 + \partial \bar{A}^{(+)}/\partial \omega^2}{2\left[1 - \rho\left(\partial \bar{A}^{(+)}/\partial \omega^2\right)\right]} \rho q^2$$

$\downarrow \Delta E_{1p}$

Comparing with experiment

$\Rightarrow g_b' \approx 0$???

No repulsion between N & Δ

Fig. 8.8

- CONSEQUENCES -

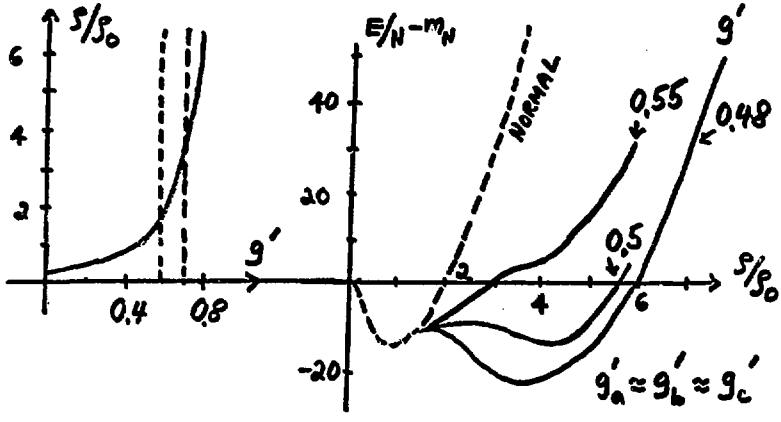

Heavy-Ion Collision [Ruck, Gyulassy, Greiner / Stöcker, Hofmann, Scheid, Greiner / Hecking, Weise, Akhoury / Toki, Futami, Weise]

Thermal excitation
$kT \sim m_\pi/2$

- ρ_c, T_c ;
- Equation of State ;

→ Assume standard thermalization of ideal Fermion and boson gas :

[Phase transition (T, ρ) in field theory ?]

Fig. 8.9

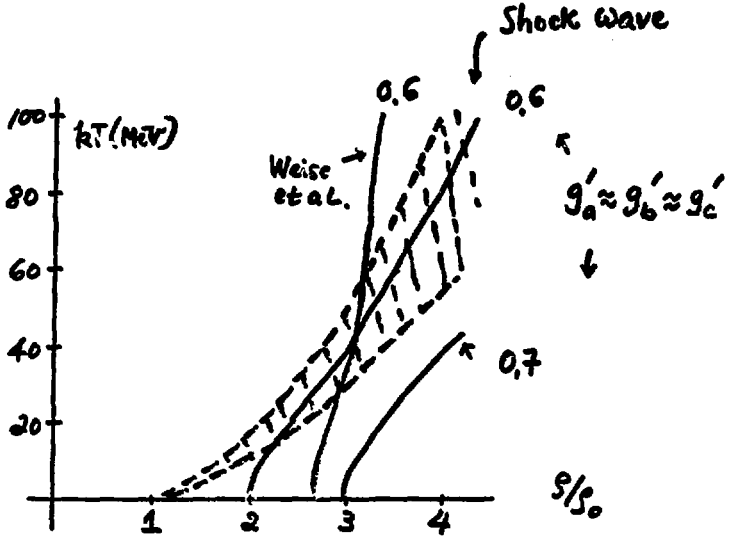

$0.6 \lesssim g' \lesssim 0.7$: "Ideal" H.I.

Touch and Go

Caveat : Migdal

Fancy Experiments :

Measure $2\delta'$ [Barshay, ...]

- Dynamic instability [Gyulassy]
  Critical phenomena
  in scattering etc.

Fig. 8.10

III THE LEE-WICK STATE

General Considerations
[Spontaneous Symmetry Breaking, Goldstone Mode etc.] ⇒ Symmetry Restoration [i.e. Wigner mode] at "high" T, "high" ρ

E.g.

Gauge Symmetry

Quark Confinement $\xrightarrow{T}$ Quark Release?

Chiral Symmetry

Normal Nuclei $\xrightarrow{\rho}$ Abnormal Nuclei?

Problem of Vacuum Change : Lorentz Scalar σ^+ [σ/ϕ]
↳ Complex!

What do we know about scalar mesons in nuclei?

Intermediate-range attraction ?

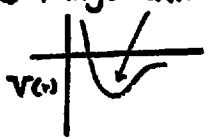

Fig. 8.11

ϕ : Scalar

ψ : Spinor (Nucleon, quark, ...)

$$\mathcal{L} = -\frac{1}{2}[\partial_\mu \phi]^2 - U(\phi) - \bar{\psi}[\gamma_\mu \partial_\mu + (m + g\phi)]\psi$$

$U(\phi) \hookrightarrow \frac{1}{2}m_\phi^2\phi^2 + \frac{1}{3}b\phi^3 + \frac{1}{4}c\phi^4$

$+ \cdots$

S.R. $(\omega, \cdots)$

[Renormalizable]

[Quasi-Classical]; $b, c > 0$, $\phi < 0$ $\Rightarrow$ [Attractive] [Repulsive]

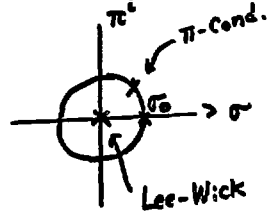

σ-Model : $[\sigma, \vec{\pi}]$

$\sigma = \phi + \sigma_0$

$m_\sigma^2 = 2\lambda^2\sigma_0^2 + m_\pi^2$; $m = g\sigma_0$

$b \to 3\lambda^2\sigma_0$

$c \to \lambda^2$

"Reduced" σ-Model : Invariant $\sigma \to -\sigma$

$$U(\sigma/\phi) = \frac{\lambda^2}{4}(\sigma^2 - \sigma_0^2)^2$$

$+$ S.B.

Fig. 8.12

For $b^2 > 4ac$ [requirement for more than one minimum] and for $\rho = \rho_c > \rho_0$,

"Vacuum" re-structuring! [T.D. Lee, Wick]

$$\langle\sigma\rangle = \sigma_0 \xrightarrow{\rho[T?]} \langle\sigma\rangle \simeq 0$$

$$m_{eff} \simeq m_N \quad \text{[Phase Transition]} \quad m_{eff} \simeq 0$$

NORMAL ABNORMAL

CONTROVERSY

Does the theory describe <u>both</u> the NORMAL & ABNORMAL States??

$$\zeta_{3\text{-Body}} \equiv b/gm_N \; ; \; \zeta_{4\text{-Body}} \equiv c/g^2$$

$$R \equiv \zeta_3/\zeta_4 \; [=3 \text{ in } \sigma\text{-model}]$$

<u>Critics</u>: $b^2 > 4ac$ [e.g. σ-Model] $\Rightarrow$ NORMAL matter unstable [Kerman Miller]

Reason: 3-body attraction <u>TOO STRONG</u>! [Barshay, Brown]

Fig. 8.13

Recovering Normal Nuclear Matter

(in Mean Field)

	Non-linear terms	Chiral Symmetry	Abnormal State
1 Mazkowski & Källman/ Pandharipande & Smith / Walecka ...	Weaken or drop f_3 & f_4 [$\frac{g}{m_\sigma} \approx 18\,GeV^{-1}$, $m_\sigma \approx 4 m_\pi$]	Manifestly BROKEN	No
2 Bodmer & Boguta	Large f_3 but $f_4 \gg f_3$ i.e. Net Repulsive [cf: $\frac{f_3}{f_4} = 3$ σ-Model] [$g/m_\sigma \approx 8\,GeV^{-1}$, $m_\sigma = 1.8 m_\pi$] ↑ Surface!	Manifestly BROKEN	No
What about ^{3}He?			
3 Vautherin & Gyulassy	Suppressed in a "Chirally Symmetric" fashion; i.e., $C'(\sigma^2+\vec{\pi}^2)^2 = 0$	UNBROKEN in Lagrangian, but BROKEN in mean field approximation. $\mathcal{L}_{S.B.} = -\alpha\sigma - \beta\vec{\pi}^2$	No

$\vec{\pi} = 0$

$\rightarrow$ Const. $\left(1 + 4\frac{\phi}{\sigma_0} + 6\left(\frac{\phi}{\sigma_0}\right)^2 + 4\left(\frac{\phi}{\sigma_0}\right)^3 + \phi^4\right)$

$= 0$

Fig. 8.14

1,2,3 $\Rightarrow$ No many-body attraction

Chiral symmetry broken in normal

$\Rightarrow$ Normal O.K.

Abnormal absent

Inconsistent (?) with $0^+ \leftrightarrow 0^-$

Experiments { a. Axial Charge Distribution : $M(p^2)/M(p^2)$

b. Nuclear Σ-term :

$[\Sigma_A \simeq A\Sigma_{Nucleon}]$ [Ericson, R.]

Crucial issue in MEAN FIELD.

NORMAL		ABNORMAL
Effective parameters :	$\neq$	Effective parameters
$b \approx c \approx 0$ or		$b^2 > 4ac$, $b \neq 0$
$R = S_3/S_4 \ll 1$		$R \approx 3$

Are they related in an obvious way?

Fig. 8.15

Quantum Fluctuation

T.D. Lee & Margulies/ Nyman & R.

$g, \lambda \gg 1$ Strong Coupling ; Perturbation theory meaningless (?)

However

Chiral Symmetry $\Rightarrow$ for $\frac{\sigma-\sigma_0}{\sigma_0} \ll 1$ (ie. Normal)

$$\Delta U = \text{Const.}\,(\sigma^2-\sigma_0^2)^3 + \cdots[(\sigma^2-\sigma_0^2)^4]$$

quantum Correction $\uparrow \phi^3, \ldots, \phi^6$ [Reduced σ-Model]

Free parameter : λ (or m_σ)

Demand : (i.e. NO 3-Body Attraction)

a. Coefficient of ϕ^3 in $(U+\Delta U) \approx 0$

b. $\Delta U \approx 0$] $\Rightarrow \lambda$ (or m_σ)

E.g. $\Delta U \sim$ 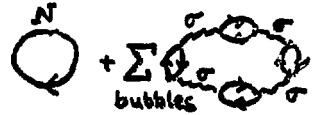

	a. ≈ [Nyman & R.]	b ≈ [Lee & Margulies] R.P.A
m_τ	≈ 1.4 GeV	≈ 1.5 GeV
g_c	≈ $5 g_c$	≈ $3 g_c$
$E/A - m_N$	≈ 180 MeV	≈ −100 MeV

Fig. 8.16

What about 3-Body force ?

[If $\Delta U \approx 0$]

Nuclear Physics Lore :

$\frac{g_{\sigma NN}}{m_\sigma} \approx 15\ \text{GeV}^{-1}$ (OBEP)

$m_\sigma \approx 500\text{MeV}$ [$\approx 250\text{MeV}$; surface] [Bodmer, Baguta]

$g_{\sigma NN} < g_{\pi NN} = g$
$\sim 7.6 \quad \sim 15$

"Pionization"

Effective Lagrangian ← "m_σ" : 

Where from? $g_{\sigma NN}$: 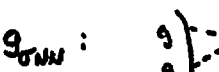

Meaning of MEAN FIELD ?

[Nyman]

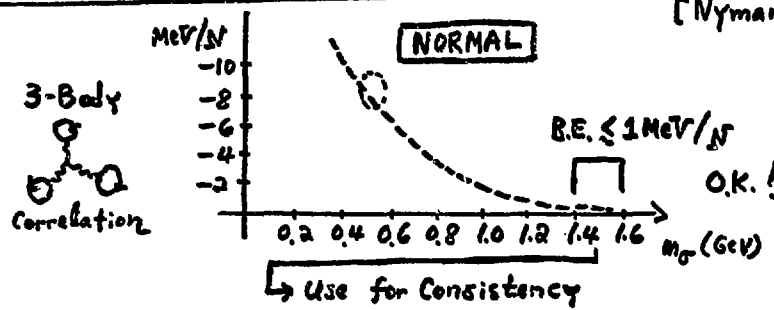

Fig. 8.17

MEANING OF SCALAR FIELD σ

Hadrons (Soliton Model) Friedberg & T.D. Lee	Abnormal Nuclei
σ : Scalar gluon Collective interpolating field : e.g. $V(F_{\mu\nu}F_{\mu\nu})$ gluon	σ : Collective field, Not necessarily associated with a Scalar meson (e.g. Phonons in Solid)
Long-range order as Volume $\to \infty$	
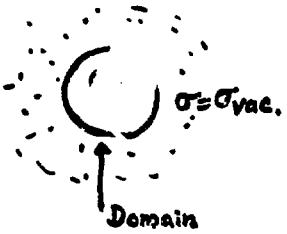	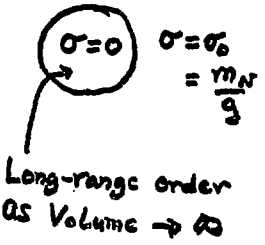
Mean field accurate for Soliton solution (for $g \to \infty$)	Mean field accurate for abnormal state ($N \to \infty$) ?

$$\sigma \quad \overset{?}{\longleftrightarrow} \quad \sigma$$

Fig. 8.18

PARTICLE PRODUCTION IN HADRON-NUCLEUS COLLISIONS ABOVE 10 GeV

Wit Busza

In this talk I will attempt to summarize the facts that are known about the interaction of hadrons with nuclei at incident energies above 10 GeV. I will also discuss why I consider some of the observed phenomena to be interesting. It will not be a comprehensive review[1] of the latest data and theory, and except for very general comments I will say little about the comparison of data with theoretical models.

I apologize, in advance, to the experts. There will be little that I will say that is very new.

This conference has concentrated on a discussion of heavy ion collisions in the few GeV range. The phenomena that I will describe are probably not too relevant at these energies; on the other hand, understanding them will become crucial if one is ever to understand heavy ion collisions at higher energies — in particular if one is to understand which are the most interesting implications of the observed phenomena. After all, I am sure you will all agree that the most important physics that will come out of heavy ion collisions is related to those phenomena that cannot be explained in terms of the superposition of single particle-nucleus collisions.

Starting about a decade ago there was a dramatic increase in the attention paid to hadron-nucleus collisions at high energies. Why this interest? The reason, I believe, is two-fold. Firstly, in several experiments where nuclei were used as targets results were observed that were not at all expected a priori. Secondly, it was finally realized by the community that by studying hadron-nucleus collisions there was a possibility of learning something about the space-time development of particle production, and about some aspects of the nature of hadrons not readily accessible through the study of hadron-nucleon interactions. A factor that helped a great deal in this surge of interest in collisions with nuclei was the general ignorance of the facts that were known to cosmic ray physicists from the late '50's, and more important, the ignorance of theoretical work on questions to do with the time of formation of particles (e.g., work of Landau, Feinberg, etc.). It turns out, as I shall emphasize throughout this talk, that the most general character of data in hadron-nucleus collisions follows simply from the uncertainty principle and special relativity. Clearly if this were immediately fully realized, the experimental and theoretical work would have attracted less attention. Fortunately, this was not the case, and thus I have something to say today.

To start out, let me follow the historic path. What are these unexpected observations that stimulated the study of hadron-nucleus collisions at the highest available energies?

If one looks at the total or absorption cross sections (see Fig. 9.1) at high energies, be it for πA or pA, one sees nothing interesting. The A-dependence, for example, is in accordance with Glauber's model. Naively this means that to at

least the 10% level it is that which one would expect from a classical analysis of the collision of spheres on a collection of other spheres distributed with a Wood-Saxon density distribution. Knowing the elementary cross section between an incident hadron and a nucleon, one can predict the cross section on any nucleus. The surprise is that these arguments fail when applied to the cross section of multiparticle states. Take, for example, the coherent production of the $p\pi^+\pi^-$ system in a pA collision. From the A-dependence of the production of this system, using multiple scattering theory, one can derive the total cross section of $p\pi^+\pi^-$ on a nucleon. The results are shown in Fig. 9.2. As you can see, the apparent cross section of the $p\pi^+\pi^-$ system on a nucleon is very small and mass-dependent. At a 2 GeV mass, for example, it is only 15 μb; this is less than the cross section of one pion on a nucleon, let alone that of a proton plus two pions! These results imply either 1) some kind of a transparency of nuclear matter to newly produced particles or 2) that for the production of particles a simple multiple scattering analysis does not apply.

Another phenomenon in hadron-nucleon collisions, which was not expected a priori, is the low average multiplicity. For example, above about 50 GeV, the multiplicity off a lead target is only 2 1/2 times that off a nucleon. Why is this surprising? Remember a lead nucleus has a size such that a hadron sees about six or seven mean free paths across the center and an average, over all impact parameters, of about three mean free paths. Naively, suppose particles were produced at the collision point in the nucleus. After the first mean free path, a 100-GeV incident proton, for example, would produce about 10 secondary hadrons. These would then further cascade in the nucleus (see Fig. 9.3), leading to a final multiplicity of between 10 and 100 times that observed in a pp collision, not a mere factor of 2 1/2!

Yet another unexpected observation was that the nuclear fragment distributions (number, angle, energy, etc.) are very insensitive to the energy of the incident hadron.

These phenomena aroused the curiosity of many particle physicists. Why is the nucleus apparently so transparent? Why is there so little multiplication of secondaries? Why is the energy deposited in the nuclear fragments so independent of the energy of the incident hadron? In short, what is going on?

It is these phenomena that stimulated interest in this subject, and yet as it turns out, they are not remarkable at all. The opposite would be remarkable. They simply follow from the size of hadrons, quantum mechanics, and relativity.

I will now give you some hand-waving arguments for why this is so. I will then survey in some detail, as much as time will allow, the known facts about particle production in nuclei at high energies. I will also attempt to indicate what these facts may be telling us about the nature of hadrons and their interactions.

Look at Fig. 9.4. It is a bubble chamber photograph of a 200-GeV p-p collision producing 24 charged particles. Imagine that this collision took place in the center of a uranium nucleus. If all the particles were produced

at one point in space, immediately after production we would have at least 24 strongly interacting hadrons, all on top of each other. Does it make any sense to presume that they will all interact independently with subsequent nucleons in the nucleus? Clearly this is nonsense. In fact it is fairly easy to see that a produced particle of energy E GeV cannot be considered to be independent of other produced particles up to very great distances, distances ~E fermi from the point of interaction. Just think, this means a 100-GeV particle is "produced" more than 1Å from the point of interaction. The simplest way to see this is to go through the exercise explained below.

We know that at high energies the rapidity distribution of produced particles is approximately uniform. On the average, particles come out separated by approximately one unit of rapidity. Consider any two neighboring particles that finally come out from the interaction with rapidities y_1 and y_2 ($y_2 - y_1 \approx 1$). Project these particles back in time (N.B.: Gottfried and Low[4] have shown that if one projects back in time the asymptotic final states of produced particles they all meet at the collision point), and ask yourself the question at what distance from the collision point will the two touch for the first time, i.e., be separated by ~1 fermi in the center of mass system of the two. It is a trivial exercise in relativistic transformations from one frame of reference to another to show that the two particles separate from each other at a distance

$$\frac{\sim R_o \sinh \frac{y_1+y_2}{2}}{\sinh \frac{y_2-y_1}{2}} \approx E,$$

i.e., in the laboratory frame, a distance of the order of the energy of the particles. (R_o is the nucleon radius in fermis and E is in GeV.)

If you don't like an argument based on a consideration of the space-time development, you can use one based on the uncertainty principle. Consider a hadron interacting at some point in space with a target. As a result of the interaction suppose a new particle of mass m is produced with transverse momentum p_t and longitudinal momentum $p_{//}$. The uncertainty in energy tells us that you cannot localize this formation time (and therefore position) to within a distance

$$\sim \frac{p_{//}}{\sqrt{m^2+p_t^2}}$$

(A way of looking at this uncertainty in distance is to consider it to be the distance over which the phases of the two particles have not separated significantly, and thus the superposition of the two is equivalent to the incident state.)

Once again we see that a particle of energy E(GeV) is "produced" a distance ~E fermi from the collision point. Although the two arguments appear to be independent, the physics is actually identical. Basically it reflects the fact that hadronic sizes and masses are related.

I hope these arguments are sufficient to convince you that at high energies the particles are not produced instantaneously. They are produced over very long times or distances. The general character of the production of particles in hadron-nucleus collisions follows from this fact and in that sense is uninteresting.

The crucial question is how, knowing this, one can use the details in the data to learn more about the nature of hadronic matter.

Let us go back and once again attempt to visualize what happens immediately following a hadron-nucleon collision. Some state of hadronic matter (maybe equivalent to a collection of almost-free quarks) is produced. It does not immediately develop into the final hadrons. Suppose that the hadron-nucleon collision occurs in a nucleus. This hadronic state is produced inside nuclear matter; it evolves, passes through subsequent nucleons, and interacts with them. A study of what happens in such a process, with luck, should teach us a great deal, not only about the space-time development of particle production, but also about hadronic matter, and further, about aspects of the nature of hadrons that are not directly accessible from a study of elementary hadron-proton collisions. Personally, I am convinced that present-day data are already rich enough to throw a great deal of light on our knowledge of hadrons.

Enough of that, let me now go on to summarize what is known and what it may mean.

In discussing the data, there are a few parameters that I will frequently use. Their definitions are summarized in Fig. 9.5. Let me briefly discuss the meaning of some of them. For technical reasons, in most experiments on multiparticle production in hadron-nucleus collisions the only measured quantities are the number of charged particles and the direction of each particle and whether it is relativistic or not. In this talk the symbol N will refer to the number of charged particles produced with $\beta \gtrsim 0.75$. N_h is the total number of slow charged-particles ($\beta < 0.75$), primarily recoil nucleons and other nuclear fragments. R_A is the ratio of the average number of relativistic particles produced off a nuclear target A to that off a proton target, i.e.,

$$R_A = \frac{\langle N \rangle_A}{\langle N \rangle_p} .$$

For a particle produced with a polar angle θ in the laboratory frame of reference, a pseudo-rapidity η is defined as $\eta = -\ell n \tan \theta/2$. is approximately equal to the laboratory longitudinal rapidity

$$y = \frac{1}{2} \ell n \frac{E+p_{//}}{E-p_{//}} .$$

The approximation is good provided that the mass of the particle is less than its transverse momentum. In other words, it is excellent for pions and terrible for protons. Throughout this talk I will rarely differentiate between rapidity and pseudo-rapidity.

It has become common practice to measure the average thickness of the nucleus in units of the absorption mean-free path of the incident particle. For a given nucleus A, the average thickness, ν, is defined by the average number of inelastic collisions that the incident particle would make assuming that it remained intact after each collision. $\bar{\nu}$ can be measured experimentally. It is given by

$$\bar{\nu} = \frac{A\sigma_{inel}(hp)}{\sigma_{inel}(hA)} \quad .$$

This formula is exact and is independent of nuclear shape or density.

At this point, a word of caution is in order. Although $\bar{\nu}$ gives the average thickness of a nucleus it does not mean that the nucleus is equivalent to a slab of nuclear matter of thickness $\bar{\nu}$. This should be remembered when comparing theoretical predictions with data obtained with real nuclei.

Finally, it is often convenient to parameterize various cross sections as a power of A. The symbol α refers to the power of A in such a parameterization.

Figure 9.6 illustrates the most important features of hadron-nucleus multiparticle production. It is a comparison of the rapidity distribution for a lead and proton target at 200 GeV. The lack of intranuclear cascading is apparent; for a lead target the number of charged particles produced is only about a factor 2.5 greater than for a proton target. The increase of particles occurs primarily in the target fragmentation region. There is very little change in multiplicity in the forward direction, i.e., there is at large rapidity. Figure 9.7 shows that the multiplication process does depend on the nature of the incident particle, the larger the cross section of the incident particle on a nucleon, the more multiplication for a given target nucleus. For all particles the multiplication is approximately linear in nuclear thickness, $A^{1/3}$. Notice for lead the large excess of particles in the very backward direction. I believe that there are two possible explanations for this excess and that at present there are insufficient data to differentiate between them.

One possibility is that the time scales are so long that the whole nucleus, or part of it, in some way acts coherently as a single massive target. The more massive the target is, the farther back the center of mass moves, and the more particles are produced backward. Also the effective center-of-mass energy increases giving rise to the larger observed multiplicity. Several authors[7] have attempted to interpret all of hadron-nucleus collisions in terms of such a coherent mechanism. They all find that without further assumptions such a model is inadequate to account for the data. However, it is interesting to note that with the addition of relatively few and plausible assumptions they can fit a large fraction of the data.

An alternative explanation of the large excess of particles in the very backward direction is that it comes from the cascading of the very slow particles which are produced within the nucleus. The overall linear increase in the target fragmentation region is attributed to the repeated collisions of the hadronic state that exists immediately following a hadron-nucleon collision. The forward region is populated by particles produced well outside of the nucleus and thus is only weakly A-dependent.

Figure 9.7 showed that the multiplication process depends on both the nature

of the incident particle and the size of the target nucleus. A replotting of the data as a function of $\bar{\nu}$ (Fig. 9.8) indicates that the A- and incident-particle dependencies can be reduced to a dependence on a single variable, $\bar{\nu}$. The most natural interpretation of Fig. 9.8 is that following a collision between an incident hadron and a nucleon, the produced state has an interaction with subsequent nucleons that is very similar to that of the incident hadron. Although I believe that this interpretation is correct, I wish to emphasize that it is not unique. Data and models are still too crude to eliminate other possibilities, such as the one I mentioned earlier, the possibility that part of the nucleus (size depends on incident particle) acts coherently.

One unsurprising feature of multiparticle production in hadron-nucleus collisions is that many nucleons participate in the process and that the number of relativistic particles produced is related to the number of nucleons participating. This is evident, for example, from the correlation between the number of relativisitic and non-relativistic particles produced in a collision (see Fig. 9.9). A fact that is perhaps more intriguing is that the number and momentum distribution of the visible nuclear fragments at high energies seem to be independent of incident energy. The probability of obtaining a certain number of nuclear recoils is the same for 6-GeV proton as it is for 400-GeV incident proton. Furthermore, it is only very weakly dependent on the type of the incident particle, even for particles as different as neutrinos and pions. (See Figs. 9.10 and 9.11.)

All these properties of the nuclear fragments indicate that a) many nucleons participate in the production process and b) the energy deposited in the nucleus and its distribution as a function of position in the nucleus is, to a good approximation, independent of the energy and type of the incident particle. A result consistent with the assumption that the immediate product of a hadron-nucleon collision is not too different from the incident hadron.

The lack of variety observed in the nuclear fragment distribution suggests that, other than the above general conclusions, the nuclear fragments contain little information about the produced state. However, there are indications in recent data of some very puzzling and perhaps fascinating nuclear phenomena occurring as a result of the passage of a relativistic particle through the nucleus. For example, Porile et al.[13] have observed the remarkable phenomenon that in p-Uranium collision, as the incident energy of the proton is increased from 0.8 GeV to 400 GeV, the angular distribution of ^{48}Sc fragments peaks at larger and larger angles. In fact at 400 GeV the number of ^{48}Sc fragments in the backward hemisphere exceeds that in the forward hemisphere by about 5%. From the point of view of this conference, this result could well prove to be the most interesting.

So far I have only discussed the number distribution of the target fragments; how about that of the relativistic particles? As you know, in pp collisions the average number of relativistic particles increases logarithmically with energy and the number distribution obeys the so-called KNO scaling (an empirical universal curve fits all the data over the entire 4 to 500-GeV range provided that at each energy the distribution is plotted as a function of the scaled number, $N/\langle N \rangle$).

A surprising feature of the hadron-nucleus data is that they seem also to satisfy KNO scaling, (see Fig. 9.12). If independent multiple collisions of any kind occur in a nucleus, one expects from Poisson statistics alone that the dispersion would decrease as a fraction of the average multiplicity. KNO scaling, of course, implies that the dispersion is proportional to the average. One possible interpretation of this is that it is an accident, simply a consequence of the fact that the nucleus does not have a uniform thickness, which leads to a number distribution that is an average over distributions with different means. The data are neither extensive nor precise enough to confirm or disprove this hypothesis.

I have already discussed the general character of the rapidity distributions. Let me now concentrate on some of the details of the distributions. The rapidity distributions for thicker and thicker targets are shown in Fig. 9.13 . These are the distributions averaged over all the produced charged particles. However, it is found that the general features seen in these distributions (i.e., the almost A-independent forward region, the linear increase with ν of the target fragmentation region, and the backward shift with increasing A of the distribution) are reflected in all specific channels. It seems to be irrelevant what particular particle comes in or what particle comes out. See, for example, the comparisons in Fig. 9.14. of $K^+A \to K^0x$ with $K^+p \to K^0x$ or $\pi^-Ne \to \pi^-x$ with $\pi^-p \to \pi^-x$ or $\pi^+Ne \to \pi^-x$ with $\pi^+p \to \pi^-x$, or even $\nu Ne \to \pi^\pm x$ with $\pi^\pm Ne \to \pi^\pm x$.

From the point of view of a comparison of the production of specific particles, I consider the forward region of rapidity to be particularly interesting. It should contain most of the information about how the state of hadronic matter produced immediately following a hadron-nucleon collision interacts and is influenced by subsequent nucleons. After all, thickest nuclei correspond on the average to targets of three or four mean free paths for some kind of hadronic interaction. If these interactions significantly influence the state, particularly its fast components, one would expect large differences in the A-dependence of fast particles that have or have not the same quantum numbers as the incident hadron. For example, in π^-A one would expect in the forward direction a depletion as a function of A of the production of π^-, while perhaps even an increase of the production of π^+. Furthermore, for both one would expect an increase with A of the average $p_\perp$. On the other hand, if for some reason nuclear matter is transparent to the fast components, very little A-dependence should be seen in the very forward direction, in particular in the case of particles produced that have the same quantum numbers as the incident hadron. To be more specific, consider the most naive parton model. An incident hadron is considered as a superposition of parton states. Any one state can be represented as a chain of partons of higher and higher rapidity (see Fig. 9.15a). The usual assumption is that only 'wee partons' interact strongly. Furthermore, for reasons discussed earlier, the higher the momentum of a parton the later it decays into a real hadron. All this leads to a picture of hadron-nucleon and hadron-nucleus multiparticle production as illustrated in Figs. 9.15b and 9.15c respectively. The rapidity distribution would then be as shown in Fig. 9.15d. The depletion of particles near the center is a consequence of energy conservation.

So much for hand-waving, what are the facts? Until recently, there was great confusion about what happens in the forward direction. A few experiments showed some absorption of all produced particles; others showed, if anything, a slight increase with A. This problem I believe, is now resolved. Everybody is right. The problem is that at very small angles, even for pions, η and y are not identical. Results plotted as a function of y show depletion, while the same results, when plotted as a function of η, show an increase (see Fig. 9.16). Clearly the very forward direction is a region of phase space where η is not a suitable approximation for y. Thus, when considering the significance of data in this region, one should only look at experimental results where the true rapidity of the particle is measured. A summary of all the data on this subject familiar to me is given in Fig. 9.17. From these data it is apparent that, at least qualitatively, the A-dependence of the forward region is independent of the incident or outgoing particle; with increasing A there is a decreasing number of all particles in the two units of rapidity that are most forward. There may be slight differences for produced particles with different quantum numbers, and there may be a slight rise near the edge of phase-space, but the data are inadequate so far for a meaningful statement to be made. As to the $p_\perp$ distribution of leading particles, there is some evidence from Λ^0 data[21] that, as expected, the average $p_\perp$ increases with A.

The last aspect of multiparticle production I wish to discuss is its energy dependence. It is interesting for similar reasons that the characteristics of the leading particles are interesting. It can probably best be explained by considering once again what a model, like the simplest version of the parton model mentioned earlier, predicts. In Fig. 9.15 consider what would happen if the energy of the incident hadron increases. The low rapidity partons and their interactions with a nucleon or nucleus will be unaltered. If the energy is increased, all that happens is that in the incident state there will be partons of larger rapidity. The net result would be that the rapidity distribution would expand as shown in Fig. 9.18 and $R_A \to 1$ as $E \to \infty$. In Figs. 9.19 and 9.20 I have attempted to summarize what is known about the energy dependence of the rapidity distributions. The data are primarily from emulsion experiments because they cover the largest range in energy.

Clearly R_A does not decrease with E. If anything, it slowly rises throughout the energy range accessible to accelerators. Cosmic ray data at larger energies are not precise enough to throw any light on this question. A closer study of the energy variation of the total rapidity distribution (see Fig. 9.20) shows the following: as the energy is increased, both the target and projectile fragmentation regions remain constant. All that happens is that the central region expands, and this expansion occurs both for a nucleon and nuclear target. In fact, Otterlund[24] has shown that the data are consistent with the assumption that the A-dependence of the central region is energy-independent. From the above one can immediately conclude that any model (e.g., the naive version of the parton model I described) in which the interactions have only short-range order is inconsistent with the nuclear data. Here is a clear-cut example of a hadron-nucleus collision giving direct information about hadron-hadron interactions. From a theoretical point of view the observed energy dependence can be interpreted in many ways. I do not want to go into details

because to date there is no consensus on what is the correct interpretation of these data. Let me just, in the way of an example, give one plausible interpretation of what the data may be telling us about the nature of hadrons.

The picture that an incident hadron is simply a collection of partons of increasing rapidity with only the slowest partons participating in an interaction is probably too naive. More likely a hadron can be represented as a superposition of many independent sets of such partons, some containing one "chain", some two "chains" etc. (See Fig. 9.21.) The collision of such a hadron with a target will automatically exhibit some long-range order, and the model can be made consistent with nuclear data.[25]

I have taken much more time than I hoped in discussing multiparticle production in hadron-nucleus collisions. In the last few minutes it is impossible to do justice to experiments that have looked at the A-dependence of very specific production processes. All that I can do is to survey briefly some of the other data that exist:

1) Coherent production of hadronic states[26] — I have already briefly discussed some of the interesting phenomena observed and will therefore now bypass this topic.

2) A-dependence of the production of particles with large transverse momenta[27] — a wealth of data exists on this subject. The most surprising, and so far not understood, feature of these data is the strong (and increasing with P_t) A-dependence at large values of the transverse momentum. See, for example, Fig. 9.22. Parameterizing the differential cross section as A^{α}, one finds α in excess of 1 for $P_t > 1$ GeV. This means that although the production of a particle at high P_t is highly improbable, in a collision with a nucleus more particles are produced at high P_t per nucleon than from a proton target. In principle, since particles with large P_t can be produced inside the nucleus, an uninteresting mechanism such as multiple scattering could give rise to this phenomenon. However, all estimates to date indicate that multiple scattering cannot give rise to such a strong A-dependence. It has been suggested that even at large P_t, real particles are produced in distances large compared to nuclear diameters, and that the data are evidence of multiple scattering of partons inside the nucleus.[28] A fascinating idea. Similar large A-dependences have been observed in the study of jets[29] and in the production of various pairs of particles.[30]

3) Deep-inelastic electron-nucleon collisions[31] — the observed features are quite similar to hadron-nucleus collisions, consistent with their idea that one is looking at the interaction of a virtual qq pair.

4) A-dependence of di-muon production[32] — there the results (Fig. 9.23) are interesting in that for $m_{\mu\mu} > 2$GeV, α appears to saturate at a value of one, very suggestive that a Drell-Yan — type of mechanism is responsible for the production process.

To conclude, I have tried to point out to you the many fascinating features

of high energy hadron-nucleus collisions. Although many of them contradicted a priori expectations, I have attempted to show that, at least qualitatively, most phenomena follow from the simple fact that the formation time of particles is very long. This does not make the data uninteresting. On the contrary, it opens up the possibility of learning something about hadronic matter that is not accessible through a study of hadron-nucleon collisions. From the point of view of heavy ion collisions, the physics I have discussed must play a crucial role in interactions of ions at energies greater than about 5 GeV/nucleon.

Finally I wish to emphasize that most of the ideas presented in this talk are neither new nor my own. They are the outcome of the work of a large number of people.

References

1. For reviews of the experimental data see, for example: W. Busza, Acta Physica Polonica B8, 333 (1977), C. Halliwell, Proceedings of the Seventh International Colloquium on Multiparticle Reactions, Kaysersberg, June 1977; T. Ferbel, Proceedings of the XIX International Conference on High Energy Physics, Tokyo, 1978.

   For reviews of some of the theoretical models see, for example: talks by G. Winbow (reggeon theory), N.N. Nikolaev (multiperipheral parton model), Meng Ta-Chung (hydrodynamical model), Y. Afek et al., (collective tube model), in Multiparticle Production at Very High Energies, IAEA-SMR-21, ICTP, Trieste, 1977.

2. Data of Denisov et al., Nucl. Phys. B61, 62 (1973).

3. J.L. Rosen et al., Proceedings of the VIth International Conference on High Energy Physics and Nuclear Structure, Santa Fe and Los Alamos, 1975.

4. F. Low and K. Gottfried, Phys. Rev. D17, 2487 (1978).

5. C. Halliwell et al., Phys. Rev. Lett. 39, 1499 (1977).

6. J.E. Elias et al., Phys. Rev. Lett. 41, 285 (1978).

7. See Y. Afek et al., op. cit. Ref. 1, and references quoted there.

8. Compilation by A. Gurtu et al., Phys. Lett. 50B, 391 (1974).

9. Compilation by I. Otterlund et al., Lund reprint LUIP-7804 (1978).

10. Z.V. Anzon et al., submitted to the XVIII International Conference on High Energy Physics, Tbilisi (1976).

11. S. Azimov et al., Nucl. Phys. B107, 45 (1976).

12. T.H. Burnett et al., University of Washington reprint VTL-PUB-50 (1978).

13. N.T. Porile, private communication. See also D.R. Fortney and N.T. Porile, Phys. Lett. 76B, 553 (1978).

14. J.R. Elliott et al., Phys. Rev. Lett. 34, 607 (1975).

15. W. Busza, VI International Conference on High Energy Physics and Nuclear Structure, Santa Fe and Los Alamos, 1975.

16. D.L. Burke et al., University of Michigan reprint UM-HE-78-6 (1978).

17. O. Concepcion et al., CRN/HE 77-10 (1977).

18. W.M. Yeager et al., Phys. Rev. D16, 1294 (1977).

19. H. Rudnicka et al., University of Washington preprint VTL-PUB-53 (1978).

20. D. Chaney, private communication; also see D. Chaney et al., Phys. Rev. Lett. 40, 71 (1978).

21. K. Heller et al., Phys. Rev. D16, 2737 (1977).

22. F.K. Aliev et al., CERN reprint TH.2551-CERN (1978).

23. Compilation by C. Halliwell op. cit. Ref. 1.

24. I. Otterlund, Lund preprint LUIP-7804 (1978).

25. A. Capella and A Krzywicki, Phys. Lett. B67, 84 (1977).

26. See for example, G. Feldt, Proceedings of the Topical Meeting on High Energy Collisions Involving Nuclei, ICTP. Trieste (1976).

27. J.W. Cronin et al., Phys. Rev. D11, 3105 (1975); and L. Kluberg et al., Phys. Rev. Lett. 38, 670 (1977).

28. G. Farrar, private communication.

29. C. Bromberg et al., Fermilab reprint FNAL-CONF-77/62.

30. R. McCarthy et al., Phys. Rev. Lett. 40, 213 (1978).

31. L.S. Osborne et al., Phys. Rev. Lett. 40, 1624 (1978).

32. M. Binkley et al., Phys. Rev. Lett. 37, 571 (1976);
D.C. Hom et al., Phys. Rev. Lett. 37, 1374 (1976);
J. Cronin et al., private communication.

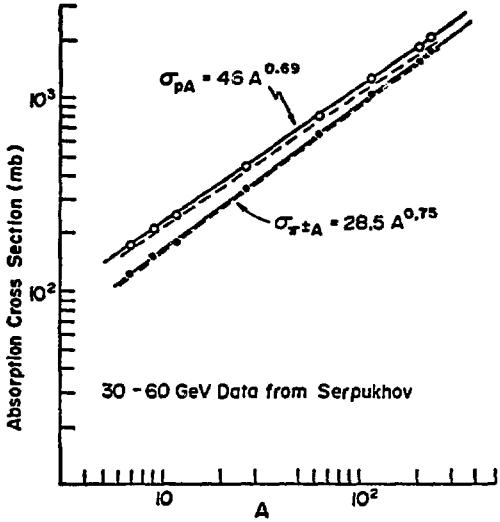

Absorption cross section as a function of the atomic number A. From Ref. 2.

Fig. 9.1

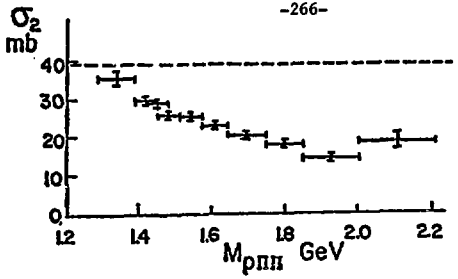

Fig. 9.2 Apparent cross section of a $p\pi\pi$ system on a nucleon, derived from an analysis of $p+A \to p\pi^+\pi^-+A$ at 22.5 GeV (Ref. 3).

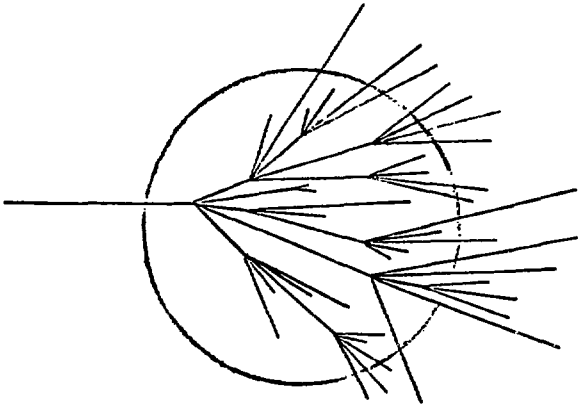

Fig. 9.3

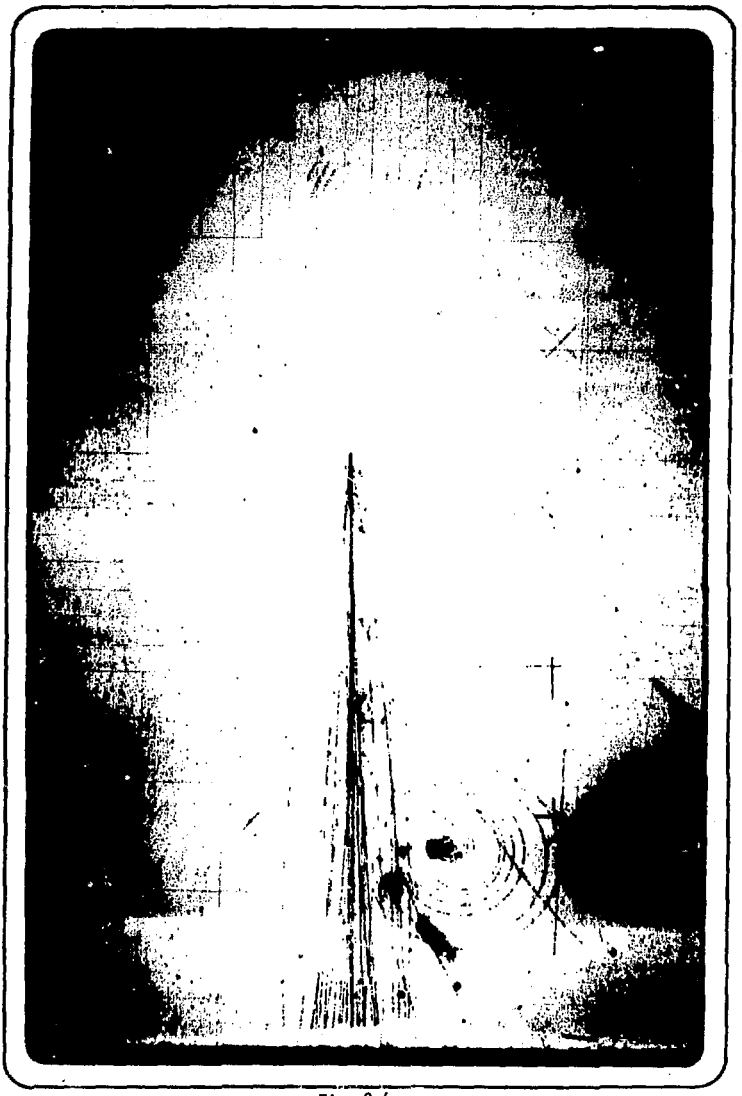

Fig. 9.4

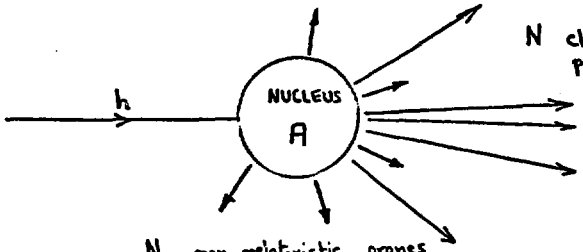

$$R_A \equiv \frac{\langle N \rangle_A}{\langle N \rangle_p}$$

$$y \equiv \frac{1}{2} \ln \frac{E + P_{//}}{E - P_{//}} \approx \eta \equiv -\ln \tan \frac{\theta_{lab}}{2}$$

Common parametrization : $\left[\frac{d^3\sigma}{dp^3}\right] = \text{constant } A^{\alpha}$

$$\nu \equiv \frac{A\,\sigma_{hp}(\text{inel})}{\sigma_{hA}(\text{inel})} = \text{Average number of of mean free paths nucleus presents to incident particle, h.}$$

Fig. 9.5 Definitions of kinematical variables used throughout this talk.

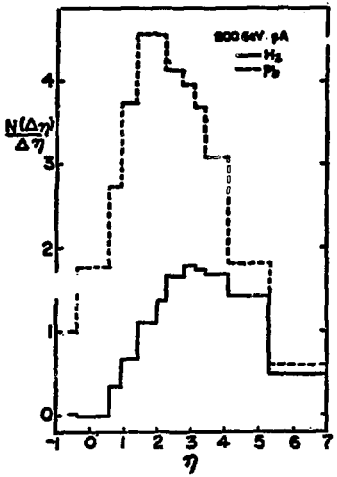

Fig. 9.6 Pseudorapidity distribution of relativistic charged particle at 200 GeV in pA collisions. (Ref. 5.)

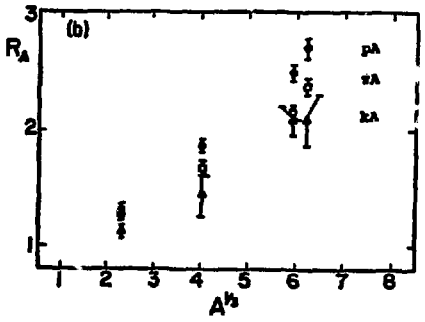

Fig. 9.7 Ratio of average multiplicity off nucleus A to that off a proton target. 100 GeV data from Ref. 6.

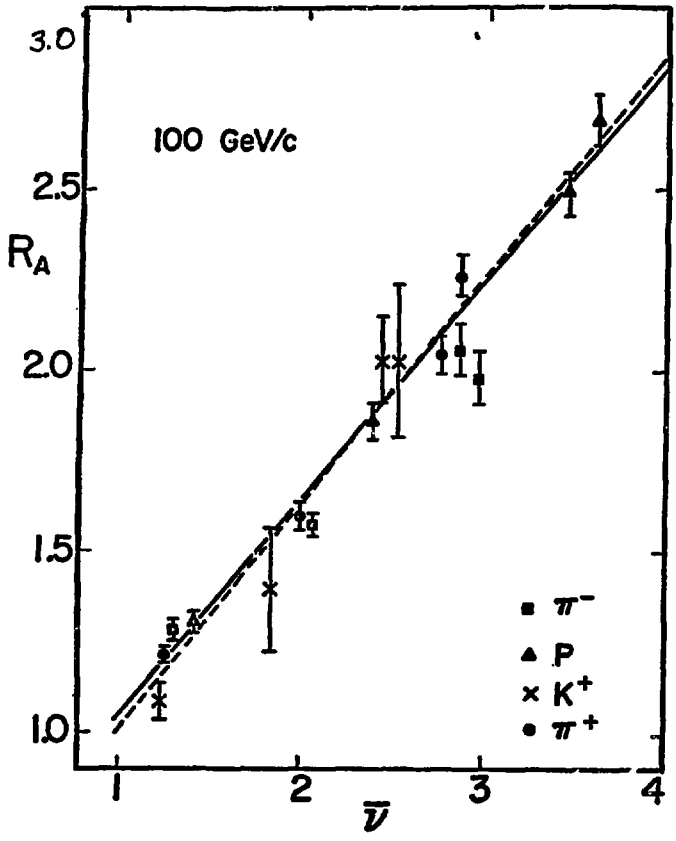

Fig. 9.8 $R_A = \frac{\langle N \rangle_A}{\langle N \rangle_p}$ as a function of $\bar{\nu}$. From Ref. 6.

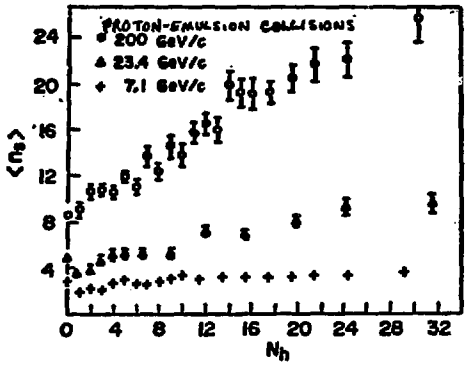

Fig. 9.9 Correlation between the number of relativistic particles produced and the number of nuclear fragments. From Ref. 8.

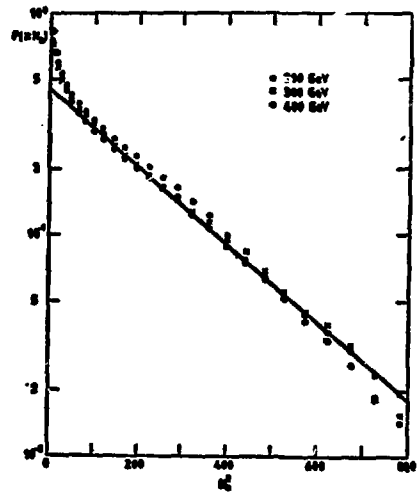

Fig. 9.10a Energy dependence of N_h. From Ref. 9.

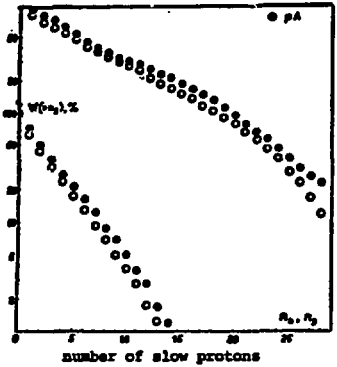

Fig. 9.10b Comparison of number of nuclear fragments produced with incident pions and protons. From Ref. 10.

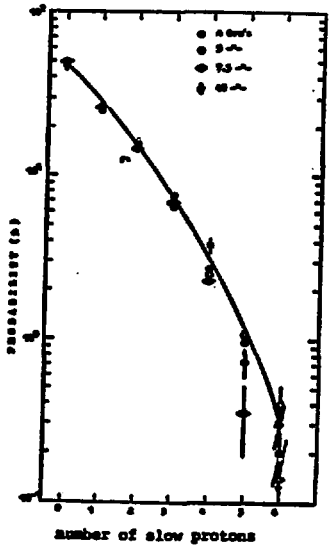

Fig. 9.11a The distributions of the number of visible protons in $\pi^{-12}C$ interactions at momenta of 4 to 40 GeV/c. From Ref. 11.

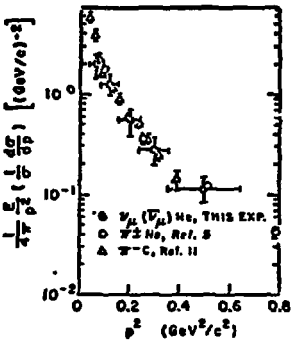

Fig. 9.11b Inclusive cross section of identified protons in ν_μ(0)Ne, π^2Ne, and π^-C interactions. (Ref. 12)

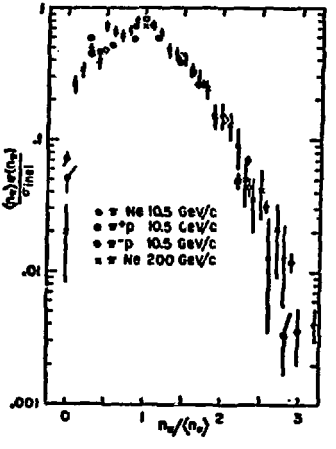

Fig. 9.12a Number distribution of relativistic particles. From Ref. 14.

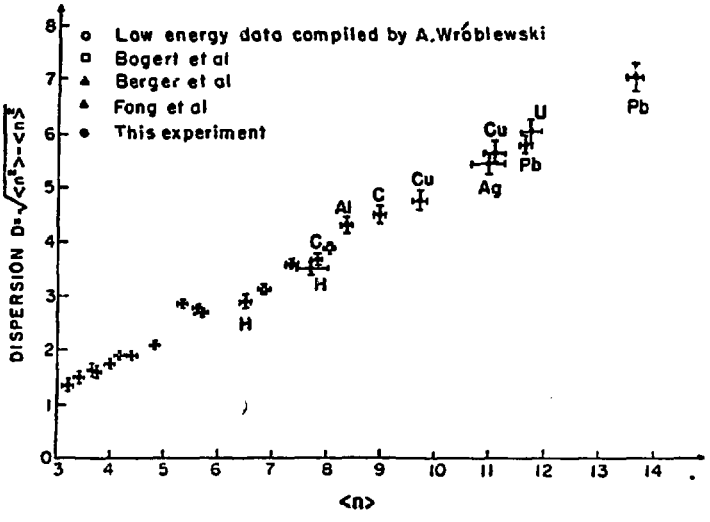

Fig. 9.12b **Dispersion as a function of average number of relativistic particles. From Ref. 15.**

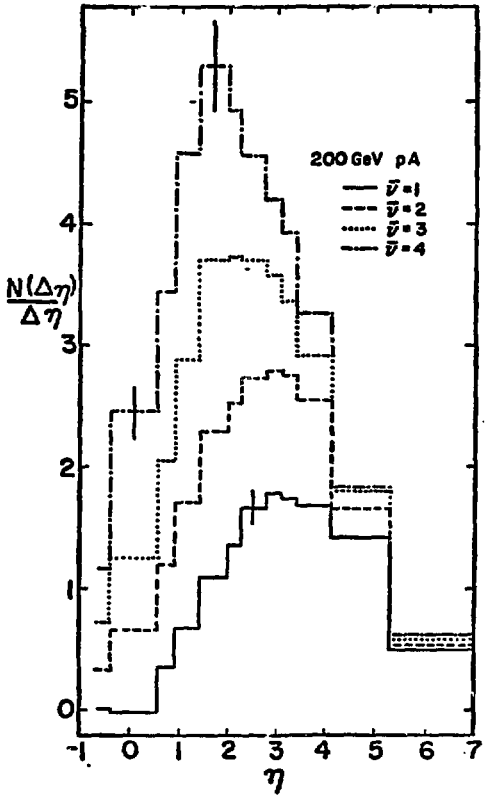

Fig. 9.13a Pseudorapidity distribution for nuclei of various average thickness. From Ref. 5.

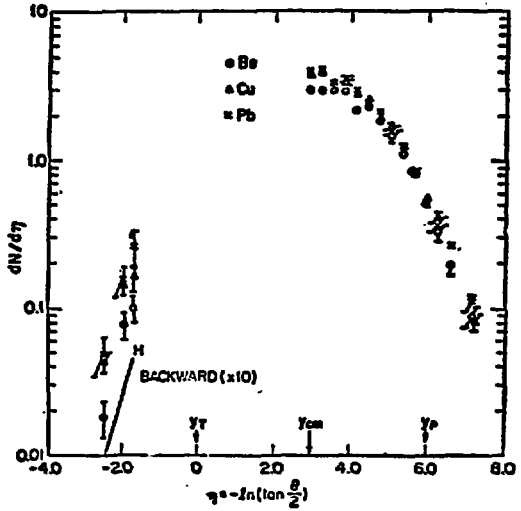

Fig. 9.13b **Pseudorapidity distributions in very backward direction. From Ref. 16.**

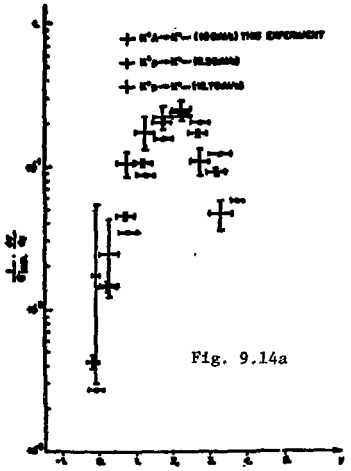

Fig. 9.14a

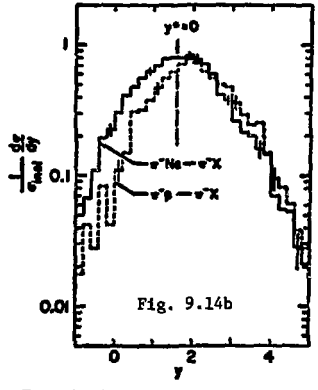

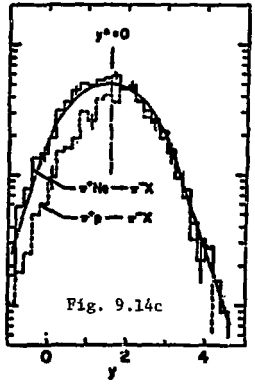

Fig. 9.14 Pseudorapidity distributions of various specific channels. K Data from Ref. 17, Ne data from Ref. 18.

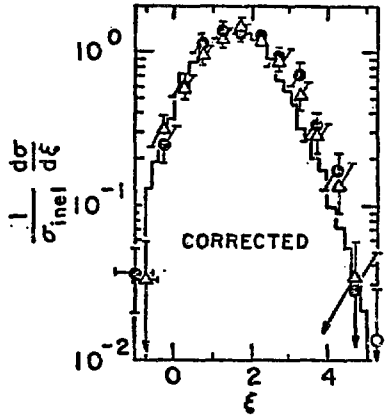

Fig. 9.14d Comparison of the laboratory rapidity distributions for $\pi^{\pm}Ne \to \pi^{\pm}X$ at $\sqrt{s} = 4.4$ GeV (solid line) with $\nu Ne \to \pi^{\pm}X$ (o) and $\bar{\nu}Ne \to \pi^{\pm}X$ (Δ) for ($3 < W < 6$). From Ref. 19.

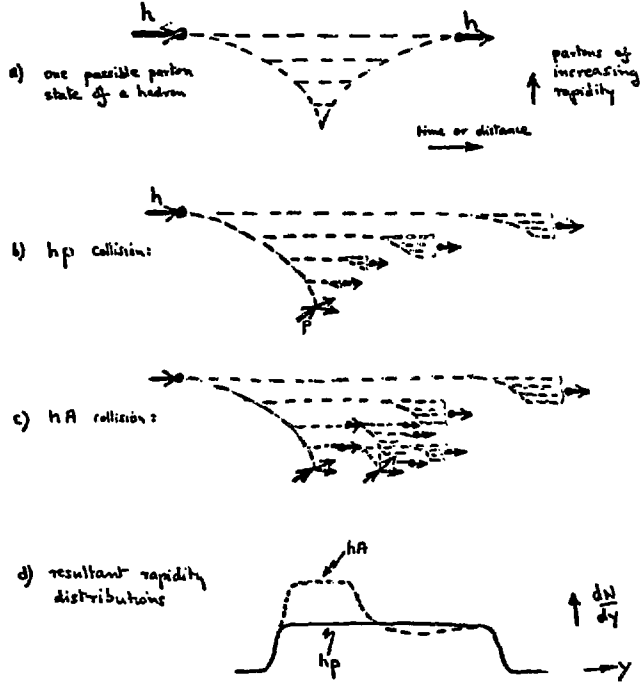

Fig. 9.15 Particle production in the most naive version of the parton-multiperipheral model.

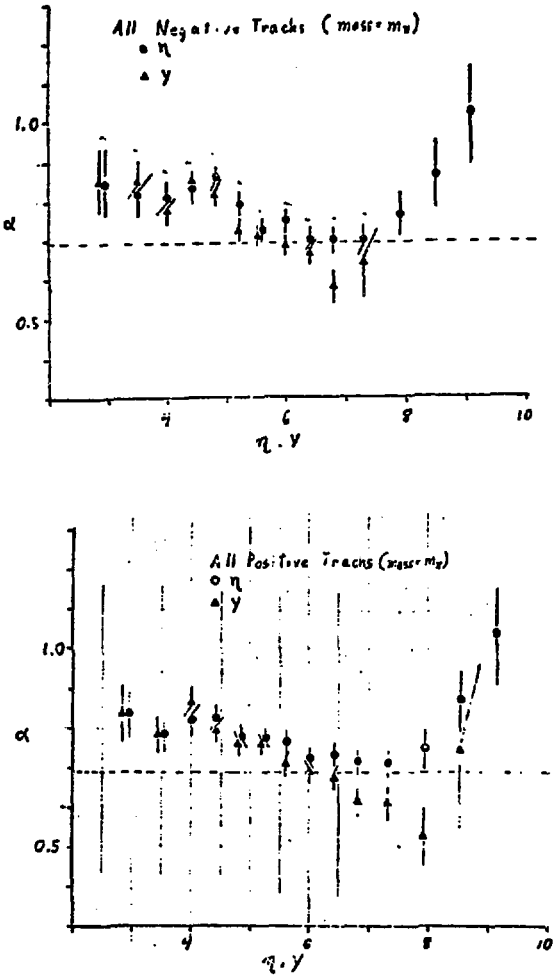

Fig. 9.16 Comparison of rapidity and pseudorapidity distributions in n-A collisions. From Ref. 20.

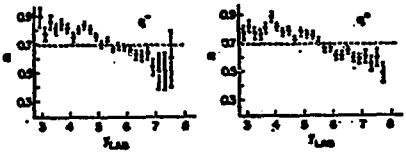

a) nA data from Ref. 20.

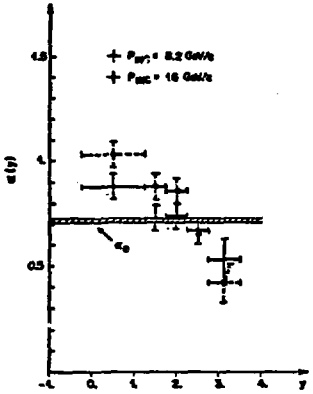

b) $K^+A \to K^0x$ data from Ref. 17.

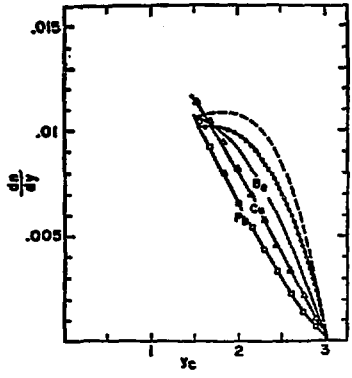

c) 300 GeV $pA \to \Lambda^0 x$ from Ref. 21.

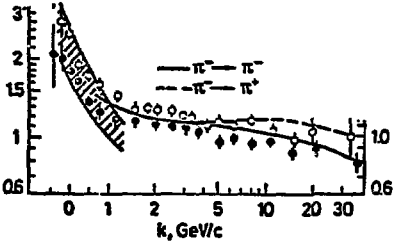

d) 40 GeV Carbon data from Ref. 22.

Fig. 9.17 A-dependence of particles in the very forward direction.

hp collisions at two energies:

resultant rapidity distributions:

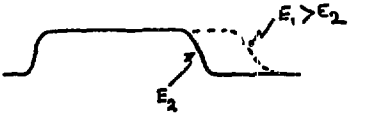

Fig. 9.18

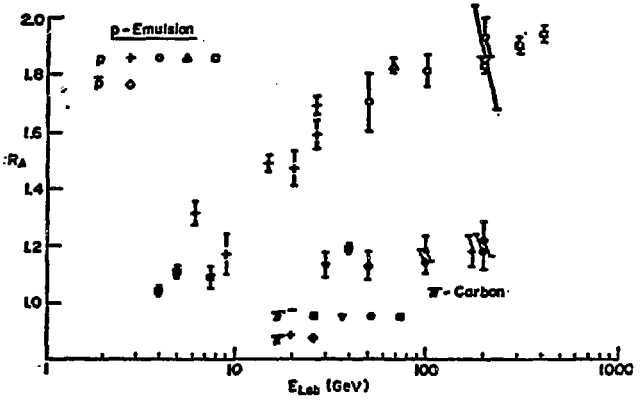

Fig. 9.19 Energy dependence of $R_A = \frac{\langle N \rangle_A}{\langle N \rangle_p}$. From Ref. 23.

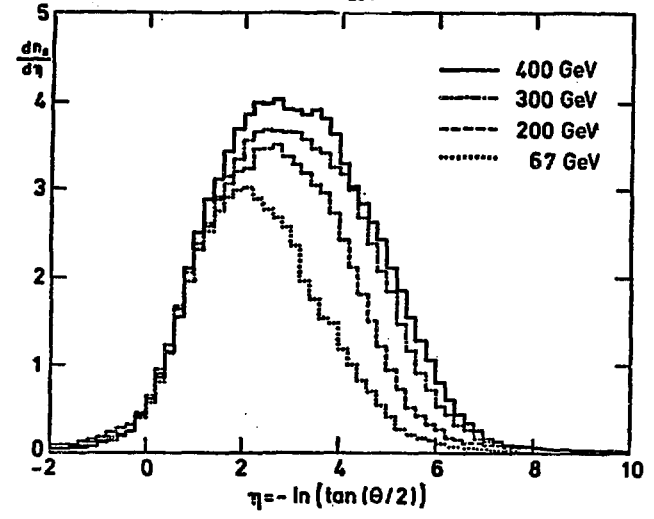

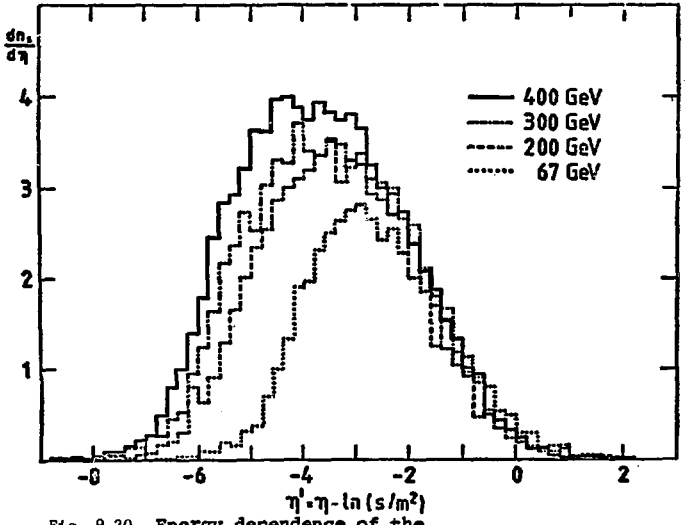

Fig. 9.20 Energy dependence of the pseudorapidity distribution in p-Emulsion collisions. η , η' are approximately the rapidities in the target and projectile rest frames respectively. From Ref. 24

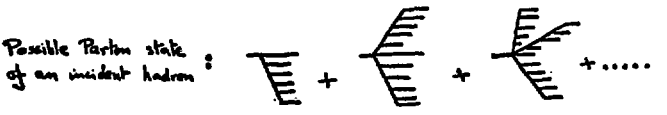

Fig. 9.21

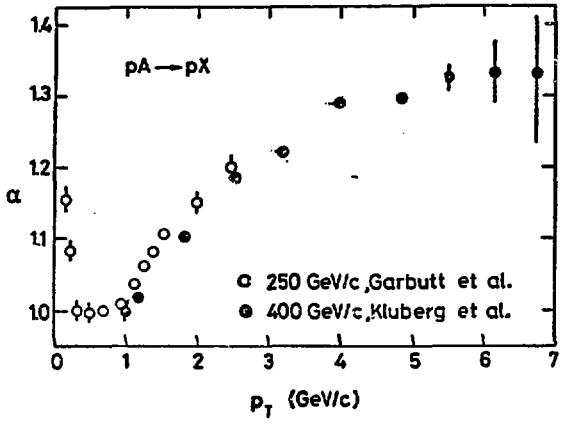

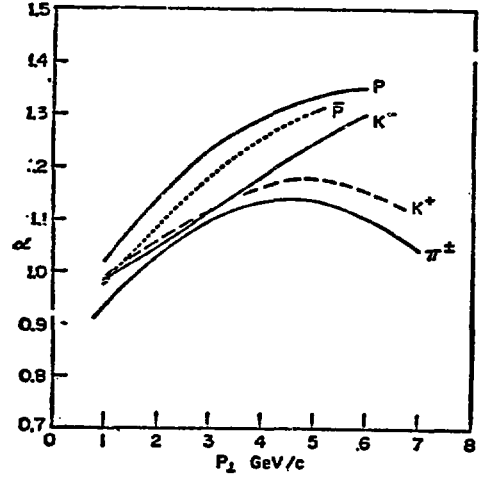

Fig. 9.22 A-dependence of the production of particles at large p_t. Data from Ref. 27.

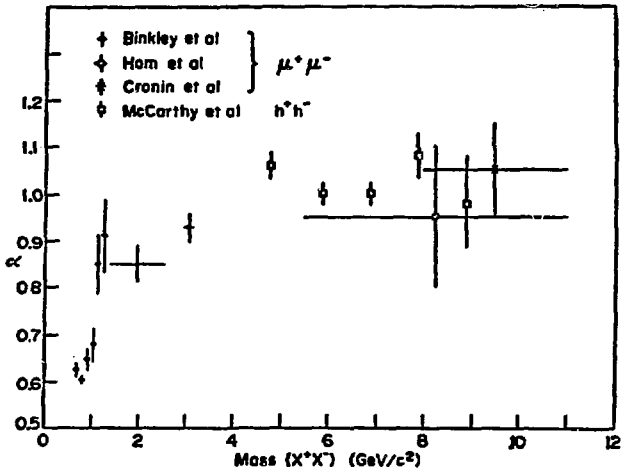

Fig. 9.23 A-dependence of the production of hadron pairs (from Ref. 30) and μ pairs (from Ref. 32).

CENTRAL HEAVY ION REACTIONS AT 1-1000 GeV/NUCLEON

I. Otterlund

INTRODUCTION

Heavy ion reactions can be preferencially disentangled into three different types of collisions: peripheral, quasi-central and central reactions. From a geometrical point of view, the type of collision is determined by the size of the impact parameter. Fig. 10.1 shows that the characteristic features of heavy ion reactions at relativistic energies depend sensitively on the impact parameter of the collisions.

When the impact parameter, b, is $\approx R_1 + R_2$, where R_1 and R_2 are the radii of the projectile and target nuclei, respectively, only a small momentum is transferred between the nuclei. In these so-called peripheral reactions, one or both of the nuclei disintegrate through a fragmentation process where the characteristics are detemined by the intrinsic Fermi-momentum distribution of the nucleons within the fragmenting nucleus.[1] We observe then pure projectile-nucleus and/or target-nucleus fragmentation. These processes are illustrated in Fig. 10.1a by the pseudo-rapidity distribution of the projectile-nucleus fragments (PF) and the target-nucleus fragments (TF). (Rapidity and pseudo-rapidity will be discussed in the next section.) The fragments of the projectile are emitted in a narrow forward cone while the fragments of the target are nearly isotopically distributed in the lab system.

In general when a nucleon no longer is a spectator but participates in the reaction, it is scattered into the rapidity space between the two fragmentation regions PF and TF. Therefore in quasi-central reactions, where $|R_1 + R_2| > b > |R_1 - R_2|$, the whole kinetmatically-allowed rapidity space is available for produced particles (Fig. 10.1b).

The simplest definition of central collisions is $0 \leq b < |R_1 - R_2| = b_0$, i.e., both nuclei overlap. When $R_1 < R_2$, every projectile-nucleus fragmentation process is highly forbidden, i.e., the rapidity space available for the particles is almost limited to the region between PF and TF (Fig. 10.1c).

When the sizes of the interacting nuclei are comparable, the cross section for total overlapping (i.e., $b < b_0$) is very small. If we define, for example, central collisions when $b < b_0$, only $\sim 0.7\%$ of Fe + AgBr reactions are central. If the interacting nuclei are of the same size (i.e., $R_1 = R_2$) the probability for central reactions is, of course, zero. This shows that a strict geometrical definition of central collisions is not very appropriate. To this we can add that interesting phenomena associated with central reactions, like high nuclear densities and high pion multiplicities, are not necessarily connected with reactions having $b < b_0$.[2-4] Therefore, slightly larger impact parameters are accepted when studying central collisions. Consequently, we do not have any strict definition of what we mean by a central collision. Instead the detection criteria used in the experiments to avoid peripheral reactions determine the centrality.

In this talk I will discuss central collisions, but will limit myself to observations made in nuclear emulsion experiments. Nuclear emulsions are very suitable for studies of central reactions because of their wide range of sensitivity, the possibilities of event-by-event studies in a 4π geometry, and because of high angular resolution. Average emulsion targets will be denoted hereafter as Em. Em targets are H, CNO and AgBr. The composition of reactions with H, CNO and AgBr in emulsion depends on the mass of the beam particles (see Fig. 10.2). Therefore, comparisons between Em-data obtained for different projectiles must be done with caution.

Fig. 10.1 reveals one possibility for us in our efforts to select central collisions. A participating projectile fragment has most often a pseudo-rapidity value $\eta < \eta_p - \sigma$, where η_p is the pseudo-rapidity of the excited residual projectile nucleus and σ is the dispersion of the distribution PF. $\eta_p - \sigma$ corresponds to an emission angle θ_0 in the lab system. If n_i is the number of charged fragments with $\theta < \theta_0$, then a central collision is defined by Eq. (1).

$$\begin{cases} n_i = 0 \\ N_F = 0 \end{cases} \quad \begin{array}{l} \text{(central collision when the} \\ \text{observables are projectile fragments)} \end{array} \qquad (1)$$

N_F = the number of projectile fragments with $Z > 2$.

This criterion has been used by Adamovich et al.[5] and Chernov et al.[6] to select central ^{12}C + Em and ^{14}N + Em reactions at 3.3 GeV/nucleon and 2.1 GeV/nucleon, respectively. To select central reactions Heckman et al.[1] use a θ_0-value corresponding to θ-1.5σ for protons. They allow one or two singly-charged particles with $\theta < \theta_0$ in ^{16}O + Em and ^{40}Ar + Em reactions.

A useful quantity Q is defined by Eq. (2).

$$Q = \Sigma\, n_i\, Z_i \ . \qquad (2)$$

Z_i is the charge of the fragments with $\theta < \theta_0$. Q is the total charge of the noninteracting projectile fragments and is a reasonable measure of the impact parameter. A measure of the number of participating projectile nucleons is then, n_{int}, given by Eq. (3).

$$n_{int} = A - 2Q \qquad (3)$$

A is the mass of the incident nucleus.

Central reactions are by definition, Eq. (1), observed when no charged projectile fragments have $\theta < \theta_0$, i.e., a total disintegration of the projectile nucleus. However, observations of the degree of destruction of the target nucleus also can be used for defining central collisions. Charged particles emitted from the target are observed in emulsion as heavy track particles (h-particles). The number of h-particles is denoted N_h and includes all charged target fragments except singly-charged particles having $\beta > 0.7$. Reactions with $> 2\bar{8}$ h-particles are often classified as central reactions with AgBr targets.[7] The h-particles are disentangled into two components. One component is b-particles (black track particles, N_b = the number of b-particles, which

are low energy fragments), which are mainly emitted from the residual excited target nucleus (spectators). The other component is g-particles (grey track particles, N_g = the number of g-particles, which are mainly protons with $30 < E < 400$ MeV), which are participants in the reaction. The g-particles exceed the b-particles when $n_{int} > 0.5$ A (Fig. 10.3). An additional criterion of $N_h > 28$ is that the number of g-particles should be larger than the number of b-particles and that the charged particles should be emitted symmetricallly in the azimuthal plane. In other words:

$$N_h > 28,\ N_g > N_b \quad \text{(Central collisions when the observables are target fragments).} \tag{4}$$

In studies of ^{56}Fe + Em reactions at 1.7 GeV it has recently been observed that central collisions with the light nuclei CNO may be obtained by using the criterion $N_s > 26$ and $N_h \leq 5$.[8] N_s is the number of shower particles (s-particles), i.e. protons with $E > 400$ MeV, and pions with $E_\pi > 60$ MeV (they have $\beta > 0.7$). The 10% of the reactions with CNO that fulfill this criterion also have comparatively small Q-values. One important observation in central Fe + CNO reactions is that protons often are emitted from the target with momenta > 1 GeV/c, i.e.[8,9], they are shower particles.[8] This is illustrated in Fig. 10.4a and b.

RAPIDITY AND PSEUDO-RAPIDITY

In the following, the pseudo-rapidity variable

$$\eta = \ln \operatorname{tg} \frac{\theta}{2} \tag{5}$$

will be used. At high energies η is a reasonably good approximation for the rapidity y,

$$y = -\ln \frac{E-P_\parallel}{E+P_\parallel} \tag{6}$$

at least for pions ($p_\perp >> m_\pi$, $p_\parallel >> m_\pi$). A few distributions will be given in the cosmic ray variable

$$u = -\log \operatorname{tg} \theta \ . \tag{7}$$

When using the variable η for protons, one must proceed cautiously because $\langle p_\perp \rangle << m$, i.e., η is most often a bad approximation for y. This is exemplified in Fig. 10.5, where η and y are exhibited for different values of $p_\parallel$ and $p_\perp$. If the transverse mass, μ, is much smaller than $p_\parallel$, i.e.,

$$p_\parallel >> \mu = \sqrt{p_\perp^2 + m^2} \ , \tag{8}$$

the difference between η and y is

$$\eta - y \approx 1/2 \ln\left(1 + \frac{m^2}{p_\perp^2}\right) . \tag{9}$$

When $m >> p_\perp$, we obtain

$$\eta - y \approx - \ln \frac{m}{p_\perp} \quad . \tag{10}$$

For example, let us look at the projectile fragmentation protons. From experiments we know that $\langle p_\perp \rangle \approx 100$ MeV/c,[1,10] which is much smaller than the proton mass. The difference between the center of the η-distribution and the center of the y-distribution for pure projectile fragmentation protons is then[11]

$$\eta - y \approx \ln 10 = 2.303 \quad . \tag{11}$$

However, even in those cases where η deviates from the rapidity y, I shall use the variable $\eta = -\ln \text{tg } \theta/2$. The reason for this is that η is one observable in emulsion experiments (usually it is not possible to measure y in this kind of experiment) and that the η-variable extends the small-angle part of the distribution.

GENERAL FEATURES OF RHI REACTIONS

Multiplicity, Energy and Angular Distributions

Figs. 10.3 and 10.6 to 12 show some general features of relativistic heavy ion reactions (RHI). Fig 10.6 shows that the angular distribution of s'-particles are similar to the shower distribution in pA reactions of the same energy[6] (s'-particles are the shower particles without noninteracting singly-charged projectile fragments, see Eq. (1)). Fig. 10.7 shows that the mean multiplicity of s'-particles increases monotonically with n_{int} and that $\frac{\langle n_s' \rangle}{n_{int}}$ is close to the shower-particle multiplicity in pEm reactions at the same energy per nucleon ($\langle n_s \rangle_{pA} = 0.95 \pm 0.05$ at 2.23 GeV).[6]

Fig. 10.3 shows the ratio between the number of g-particles (partipant particles) and the number of b-particles (spectator particles) in ^{12}C + Em reactions at 4.2 GeV/c per nucleon.[5] This ratio increases with n_{int}. For small values of n_{int}, the number of spectator particles (b-particles) exceeds the number of participant particles (g-particles). Where n_{int} is equal to A_p, i.e., the impact parameter is small, the number of participant particles is about twice the number of spectator particles. In the fireball model with clean geometrical cuts, the ratio between the number of participating target nucleons and the number of spectator nucleons in central ^{12}C + Ag reactions is only ≈ 0.48. The much higher experimentally observed value of $\frac{\langle N_g \rangle}{\langle N_b \rangle}$ can be explained if

1) there are many more participant nucleons than given by the clean cut fireball model, and

2) the target nucleus is not totally disintegrated into nucleus, i.e.,

many of the b-particles are multiply charged fragments.

The angular distribution of g-particles (protons with energies in the range 30-400 MeV) in p-Em reactions follows the form (see Fig. 10.8).[12]

$$\frac{1}{\sigma}\ \frac{d\sigma}{d(\cos\theta)} \sim \exp(1.0\cos\theta) \qquad (12)$$

and stays constant in the energy range 2-400 GeV.[12] This distribution is also very close to that observed in d-Em reactions at 9.4 GeV.[13] In Fig. 10.9 angular distributions of g-particles in pA and dA reactions are compared with corresponding distributions in ^{12}C + Em reactions for three different values of Q. The dependence on E_p, A_p, and Q is very weak. In Fig. 10.10a and b, angular distributions of b- and g-particles in p + Em reactions at 2.23 GeV are compared with corresponding distributions in ^{14}N + Em reactions at 2.1 GeV/nucleon and we observe that there is no dependence of these distributions on the atomic number of the projectile.[6]

Fig. 10.11a and b show that the angular distribution of g- and b-particles in ^{14}N + Em reactions are in good agreement with predictions from cascade-evaporation calculations performed by Gudima and Toneev.[14] Their calculations are also in quite good agreement with energy distributions of h-particles measured in ^{16}O-CNO and ^{16}O-AgBr reactions at 2.1 GeV/nucleon (Fig. 10.12). We shall observe that the cascade-evaporation calculation gives the absolute yield of particles both from light (C,N,O) and heavy (AG,Br) targets. The worth of the cascade-evaporation calculations is to subtract the background of kinematical effects[14] but in neither the angular nor in the energy distributions do we observe any significant deviations. Therefore, we must conclude that the observations of inclusive multiplicity, angular, and energy distributions in emulsion experiments do not seem to differ very much from pA reactions if we take into consideration the increase in the cross section, i.e, simple geometrical effects explain the observables. To observe signals characteristic for RHI-reactions we must select unique samples of collisions and study correlations. One possibility is to investigate central RHI-reactions. Correlation properties of s-, g- and b-particles are quite different in proton-nucleus and nucleus-nucleus collisions.

Azimuthal Correlations

The Tashkent group has recently studied azimuthal correlations in ^{14}N + Em reactions at 2.1 GeV/nucleon.[15] The projected tracks of emitted charged particles are described by unit vectors in the azimuthal plane $\vec{s}_i$ for s-particles, $\vec{g}_i$ for g-particles and $\vec{b}_i$ for b-particles. Figs. 10.13 and 10.14 show distributions of ϕ_{sg} and ϕ_{sb} in dA, αA and ^{14}NA reactions.

$$\phi_{sg} = \arccos\ [(\Sigma\vec{s}_i)\cdot(\Sigma\vec{g}_i)] \qquad (13)$$

$$\phi_{sb} = \arccos\ [(\Sigma\vec{s}_i)\cdot(\Sigma\vec{b}_i)] \qquad (14)$$

The azimuthal correlations are weak in dA and αA reactions. However, with

increasing mass of the incident nucleus, an increased correlation is observed. In ^{14}NA reactions the correlations are quite strong. For g-particles, such a correlation is expected if they are participants in the pion production process. However, the strong correlation between s- and b-particles is quite astonishing if all the b-particles are spectators. When $\phi_{sb} < \pi/2$, the distribution is quite isotropic (the isotropic distribution is dotted in Fig. 10.14). An extrapolation of the isotropic distribution to the range $\phi > \pi/2$ shows that ~ 15% of the b-particles are correlated to the s-particles.

CENTRAL HEAVY ION REACTIONS AT 1-2 GeV/NUCLEON

Studies of the emission of target fragments in central RHI-reactions have been performed in a series of investigations in emulsion and AgCl detectors.[1,5,6,16-18] Here I would like to mention the investigation by Heckman et al.[1] I showed in Chapter 3 that the angular distribution of g-particles ($30 \leq E \leq 400$ MeV) is independent of E_p, A_p, and Q. Heckman et al.[1] have shown that this is also the case for central reactions at least where $A_p < 16$. (See Fig. 10.15) However, a mass dependence is observed for heavy projectiles. In central ^{40}Ar + AgBr reactions the angular distribution is much more forward-peaked than in reactions induced by light (^{4}He) and medium (^{16}O) projectiles. Low energy fragments ($E \leq 31$ MeV/A) have angular and energy distributions that do not depend on the mass of the projectile or on the centrality of the collision.

Central ^{56}Fe + CNO and ^{56}Fe + AgBr reactions at 1.7 GeV/nucleon have recently been studied by the Lund University group.[19] The central reactions were selected by the following criteria. Ten percent of the Fe + AgBr reactions with the highest multiplicity of charged particles were chosen as a representative sample of central Fe + AgBr reactions. Reactions with $N_s > 26$ and $N_h \leq 5$ were chosen for central CNO collisions. Fe + H reactions can be neglected since there is a very small probability that such collisions have multiplicities > 26 at 1.7 GeV.

The number of nucleons in the overlapping and non-overlapping parts of the interacting nuclei are given in Fig. 10.16 as a function of the impact parameter (b) for Fe + CNO ($b < 2.5$ fm) and Fe + AgBr ($b < 3.5$ fm) reactions. The range of impact parameters shown in Fig. 10.16 are assumed to be representative for the selected samples of collisions.

Central Fe + CNO and Fe + AgBr reactions are quite different from a fireball-model point of view. In Fe + CNO reactions the number of projectile spectator nucleons are ~ 75% of the number of nucleons in the fireball. In Fe + AgBr reactions this percentage is much smaller (~ 8%). For the target spectator the situation is reversed (~ 0% respectively ~ 20%).

The η-distributions of charged particles emitted in central Fe + CNO and Fe + AgBr reactions is shown in Figs. 10.17a and b (histograms). The two distributions are very similar in spite of the targets, which are quite different. Only a comparatively small number of the 26 projectile protons are observed in the η-space where we expect spectator particles. In central

Fe + AgBr reactions this is expected since the projectile is almost totally overlapped, and consequently, most of the projectile nucleons participate in the reaction. It is quite astonishing that a similar suppresion is also observed in Fe + CNO reactions. The widths of the distributions are almost the same, but the center of the distributions are shifted $\Delta\eta = 0.51$.

The curves in Fig. 10.17 show predictions from the clean-cut fireball break up and spectator evaporation model.[19] It is obvious that the fireball model contradicts the experimental observations. Also, cascade-evaporation calculations, using the same criteria as in the experiment, disagree with the results.[20] To explain the experimental findings, we must assume that the participant volume is extended in the transverse direction. The firestreak broadening of the temperature and velocities must have a position effect in this direction.

The transverse expansion of the participating volume is illustrated in Fig. 10.18. Two characteristic times, the passage time = t_{pass} and the communication time = t_{co}, are of interest here.[21] If $t_{pass} > t_{co}$, the transverse communication is propogated over the whole volume of nuclear matter. If, for example, b = 0 fm this is the case when[2]

$$A_2/A_1 < \left(\frac{v_\ell}{v_t} + 2\right)^3 \left(\frac{v_\ell}{v_t} - 2\right)^{-3} (A_2 \geq A_1) \quad . \tag{15}$$

v_ℓ and v_t are the longitudinal and transverse velocities, respectively. In high energy hadron reactions, the average transverse momentum of emitted singly-charged particles is 0.35 GeV/c, and this has been found to be independent of the incident energy. If this value determines the transverse propagation, i.e., $v_t = 0.35$ c, the passage time is larger than the communication time in central Fe + CNO and Fe + AgBr reactions. We can then expect a large friction between overlapping and non-overlapping parts of the nuclei. This may give rise to a process close to an explosion of nuclear matter.

CENTRAL HEAVY ION REACTIONS AT 2-20 GeV/NUCLEON

When we now step further in energy we have to rely on emulsion experiments using cosmic ray particles. Baranov et al.[22] have recently presented $x = \log \mathrm{tg}\theta$ distributions of s-particles in relativistic nucleus-nucleus interactions of Fe-group primaries ($26 \geq Z \geq 20$) with AgBr nuclei at a complete or nearly complete overlap of the geometrical cross sections of the colliding nuclei. Examples of distributions at different energies are shown in Fig. 10.19.

Kalinkin et al.[23] have suggested a nuclear pionization model involving a collective interaction mechanism (Fig. 10.20). They point out that the time of interactions of an incident nucleus and one of the nucleons of the target nucleus is

$$\Delta\tau_{int} \approx 4/3 \; \frac{R}{\sqrt{\gamma^2 - 1}} \tag{16}$$

where R is the radius and γ the Lorenz-factor of an incident nucleus. The characteristic time of inelastic interactions between the two nucleons is

$$\tau_0 \sim 10^{-23} \text{ sec.} \tag{17}$$

All the nucleons of the incident nucleus will overlap with a given nucleon of the target nucleons when $\Delta\tau_{int} \leq \tau_0$. Such a situation takes place for a Ca + A reaction when E > 21 GeV/nucleon. They suggest that the Lorentz-compressed incident nucleus interacts consequently with layers of the target nucleus, resulting in formation and decay of three independent-excited systems, i.e., the incident nucleus, a part of the target-nucleus overlapped by the incident nucleus, and a pionization cluster (Fig. 10.20). The number of s-particles emitted is defined by the expression

$$n_s = \frac{2}{3}\frac{M}{\bar{\epsilon}_{\pi^-}} + Z_p \tag{18}$$

where M is the mass of the cluster and $\bar{\epsilon}_\pi$ is the mean energy of the pions in the center of mass of the cluster at a decay temperature of T = 0.14 GeV. Z_p is the charge of the incident nucleus (fragmentizes into nucleons). Figs. 10.19 and 10.21 show comparisons between predictions from the pionization model and results from the experiment by Baranov et al.[22] Fig. 10.22 shows that the median angle of s-particles, $\theta_{s_{1/2}}$, approaches the $\theta^{NN}_{s_{1/2}}$-angle of nucleon-nucleon reactions with increasing mass of the projectile.

The following observations from cosmic ray experiments may be of special importance for the interpretation of the reaction mechanisms in high energy central collisions.

1) Events occur with high multiplicities of fast (E_{He} > 40 MeV) helium nuclei from the target nucleus.[24]

2) There exist reactions with small impact parameters where no protons emitted from the incident nucleus can be observed within a narrow forward cone in the lab system.[24] This is clearly seen in Fig. 10.23, where the excess (= the difference between the histogram and the curve) is in the range of 5° to 35°.

3) The η-distribution of relativistic singly-charged particles has a surprisingly small dispersion in interactions where both the interacting nuclei are almost totally disintegrated.[24] In central RHI reactions σ is smaller than the dispersion in pp reactions at the same energy per nucleon.

CENTRAL HEAVY ION REACTIONS AT 50-1000 GeV/NUCLEON

As an introduction to the discussion of heavy ion reactions at very high energies, I shall summarize reactions having a hadron as the incident particle (Fig. 10.24).[25] A well-known observation is that the s-particle production is

low and does not depend very much on the amount of nuclear matter passed by the incident hadron. For medium nuclei ($A \lesssim 100$) one observes that the ratio R between the s-particle multiplicities in hadron-proton (hp) and hadron-nucleus (hA) reactions is $\lesssim 2$. This is a consequence of the limited space-time development of hadronic reactions inside the hit nucleus. The experimentally observed particle multiplicities follow the formula

$$\langle n_s \rangle_{hA} = \alpha \langle n_s \rangle_{hN} + \beta \langle n_s \rangle_{hN} \bar{\nu} \qquad (19)$$

where $\langle n_s \rangle_{hA}$ is the average number of s-particles in hA-reactions and $\langle n_s \rangle_{hN}$ is the average number of s-particles in hN-reactions. $\bar{\nu}$ is the average "thickness" of the target and is given by

$$\bar{\nu} = \frac{A\, \sigma_{hN}}{\sigma_{hA}} \qquad (20)$$

where σ_{hN} and σ_{hA} are the inelastic cross sections and A is the target mass. Every scattering of the leading hadron inside the hit nucleus produces $\approx \beta \langle n_s \rangle_{hN}$ s-particles. Associated with the leading hadron is a contribution of $\alpha \langle n_s \rangle_{hN}$, which is not developed inside the nucleus (Fig. 10.24).

We rewrite Eq. (19) in a more general form:

$$\langle n_s \rangle = N_p \cdot \alpha \langle n_s \rangle_{hN} + N_T \cdot \beta \langle n_s \rangle_{hN} \qquad (21)$$

where N_p and N_T are the number of participating hadrons in the projectile and in the target, respectively. In hA-reactions we have $N_p = 1$ (one hadron) and $N_T = \bar{\nu}$ (the number of scattering of the leading hadron or the average "thickness" of the target).

The s-particle multiplicities can be divided into three different parts[26] (see Fig. 10.25a and b).

$$n_s(A,E) = n_s^T \text{ (target fragmentation)} + n_s^C \text{ (central region)} +$$

$$n_s^P \text{ (projectile fragmentation)} = n_s^T(A) + n_s^C(A,E) + n_s^P \,. \qquad (22)$$

The multiplicity in the central region depends on energy, while the target and projectile fragmentation multiplicities are energy independent. The multiplicities in the central region an in the target fragmentation region are further more mass dependent.

From experiments we obtain the following relations for the pseudo-rapidity ($\eta = -\ln \tan \theta/2$) distribution on pA reactions (Fig. 10.24b)

$$n_s^P(\eta) \approx n_s^{NN}(\eta) \qquad \text{projectile fragmentation} \qquad (23)$$

$$n_s^T(\eta) \approx n_s^{NN}(\eta)\, \bar{\nu} \qquad \text{target fragmentation} \qquad (24)$$

where n_s^{NN} is the corresponding pseudo-rapidity distribution in nucleon-nucleon

collisions. Eq. (23) is only approximately correct and is known to be slightly violated in hadron-nucleus collisions. A decrease with increasing amount of transversed nuclear matter is observed in the very forward direction but this extinction of the leading particle has been taken into consideration in the following discussion.

An Independent Particle Model for Very High Energy Heavy Ion Reactions [25]

Let us now consider heavy ion (AA) reactions illustrated in Fig. 10.24. All nucleons in the overlapping parts of the two interacting nuclei participate in the production of s-particles. We assume that when a nucleon has collided once, the repeated scatterings do not, on an average, change the number of s-particles associated with this nucleon. This statement is verified from hA-experiments where the multiplicity of s-particles in the projectile fragmentation region depends weakly on the amount of nuclear matter transversed by the incident hadron. Depending on the limited space-time development of hadronic reactions inside the hit nuclei, the pions are emitted first when the two nuclei are separated. We consequently assume that each participating nucleon from the projectile contributes, on an average, with a multiplicity of $\alpha \langle n_s \rangle_{NN}$ and that each participating nucleon from the target contributes with $\beta \langle n_s \rangle_{NN}$. The multiplicity can thus be written [compare Eq. (21)]

$$\langle n_s \rangle = N_p \alpha \langle n_s \rangle_{NN} + N_T \beta \langle n_s \rangle_{NN} + \delta_p \qquad (25)$$

where N_p and N_T denote the number of participating nucleons in the projectile and in the target, respectively. $\delta_p \approx \frac{Z_p (A_p - N_p)}{A_p} - Z_F$ denotes the number of s-particles associated with the nucleons from the projectile that do not participate. N_p, N_T, and δ_p are dependent on the impact parameter, b. For reactions where $A_T > A_p$ and $b < |R_T - R_p|$, all nucleons in the projectile participate, and consequently $\delta_p = 0$.

Very high energy heavy ion reactions are reported in references 27 and 28 and here we compare predictions from the independent particle model with multiplicities and pseudo-rapidity distributions presented in these articles.

Table I compares multiplicities in central heavy ion reactions with predictions from Eq. (25). We have chosen $\alpha = \beta = 1/2$ because these values give approximately the s-particle multiplicites in h-A reactions. The upper and lower limits of N_T correspond to $b = 0$ and $b = |R_T - R_p|$, respectively.

In Fig. 10.26 we compare the η-distribution of s-particles from a Ca + Pb reaction at 300 GeV/nucleon with the distribution expected for protons emitted in a pure projectile nucleus fragmentation process (dotted curve in Fig. 10.26). To simulate projectile nucleus fragmentation we have used a Gaussian distribution with $\sigma = 71$ MeV/c for longitudinal and transverse momentum components.[1,10] It is evident that all protons have disappeared ($\delta_p = 0$) from the projectile nucleus fragmentation region of rapidity space, i.e., we observe a central reaction.

The simple model discussed above also predicts pseudo-rapidity distributions in the projectile and target nucleon fragmentation regions (Fig. 10.24). According to Eq. (23) and Eq. (24), we obtain for AA reactions

$$n_s^P(\eta, A_p) \approx n_s^{NN}(\eta) \cdot N_p \,, \tag{26}$$

$$n_s^T(\eta, A_T) \approx n_s^{NN}(\eta) \cdot N_T \,. \tag{27}$$

Fig. 10.26 shows that the predictions from Eq. (26) and (27) are in surprisingly good agreement with experimental findings. The upper and lower curves in the figure correspond to $N_T(b=0)$ and $N_T(b=|R_T-R_p|)$, respectively. The pseudo-rapidity distributions of another three events, analyzed in the same way, are shown in Fig. 10.27.

We know from pA reactions that $n_s^T(A)$, i.e., the s-particle production in the target nucleon fragmentation region does not depend on the incident energy but only on the target mass.[12] If this also is a truthful statement for AA reactions, we should expect good agreement in the target fragmentation region. However, in all reactions we observe a suppression in the target region, which could be an evidence for shadow effects, i.e., not all N_T nucleons are effective collision centers.

The Coherent Tube Model for Very High Energy Heavy Ion Collisions.[29]

Finally I shall also compare with the Coherent Tube Model (CTM), whose applications to very high energy heavy ion reactions have been discussed by A. Dar and by L. Bergström and S. Fredriksson. Here I will limit myself to the CTM predictions given by A. Dar.[29]

In the CTM a high energy nucleus-nucleus collision is a sum of the incoherent tube-tube collisions that take place in the overlapping region of the colliding nuclei. A tube-tube collision is assumed to produce the same number of pions as a pp-collision at the same cm energy (universality assumption). The s-particles are pions produced in the tube-tube collisions, protons emitted from the target tubes and protons emitted from the projectile tubes. The s-particles are then disentangled into a proton component $(n_p)_s$ and a pion component n_c:

$$\langle n_s \rangle = \langle n_p \rangle_s + \langle n_c \rangle \,. \tag{28}$$

For central heavy ion collisions ($b < b_0$, $A_1 < A_2$) the mean number of protons and pions is:

$$\langle n_p \rangle_s \cong Z_1 + \left(\frac{A_1}{A_2}\right)^{2/3} Z_2 \tag{29}$$

$$\langle n_c \rangle_{A_1 A_2} \cong A_1^{2/3} \langle n_c(Q) \rangle_{pp} \tag{30}$$

Q is the available energy in the tube-tube cm system and $\langle n_c(Q) \rangle_{pp}$ is the pion multiplicity in pp reactions. Fig. 10.28 exhibits the multiplicity

distribution predicted from the CTM in central Ca + Pb reactions at 300 GeV/nucleon. The distribution is narrow and shows that the probability of finding an individual central event with an s-particle multiplicity that deviates (e.g., with a factor of 2 from the average multiplicity in central collisions) is very small. It is then evident that the high multiplicity events observed (i.e. $n_s \sim 500$) cannot possibly be predicted by this approach of the CTM. In order to explain the high multiplicity events Dar therefore assumes that only violent tube-tube collisions are at work in central heavy ion reactions. The violent collisions mainly populate the central rapidity region. They are "universal" and have multiplicities that increase faster with the incident energy than the average multiplicities in pp collisions. Also pA reactions are mainly built up of central (violent) p-tube collisions.

The pp data are not easily disentangled into the peripheral and central components. To overcome this difficulty pA data are used as input in the modified CTM model. Multiplicities and pseudo-rapidity distributions in the modified CTM are then given by Eqs. (31) and (32):

$$\langle n_s \rangle_{A_1 A_2} = Z_1 + (\sigma_{in}^{A_1}/\sigma_{in}^{A_2}) Z_2 + \langle n_c(Q) \rangle_{\text{central pp}} \approx \frac{\sigma_{in}^{A_1}}{\sigma_{in}^{p}} \; R_{A_1} R_{A_2} \langle n_{pp} \rangle \qquad (31)$$

$$R_A = \frac{\langle n_s \rangle_{pA}}{\langle n_s \rangle_{pp}} \,,$$

$$\left(\frac{dn_s}{d\eta}\right)_{A_1+A_2, E_0} = \frac{\sigma_{in}^{A_1}}{\sigma_{in}^{p}} \left(\frac{dn_s}{d\eta}\right)_{p + A_2;\; E} \qquad (32)$$

E_0 = the incident energy per nucleon

$E = \bar{\nu} \cdot E_0$.

This modified CTM can satisfactorily explain the observed multiplicities and pseudo-rapidity distributions (cf. Figs. 10.28 and 10.29).

The improvement of the CTM, caused by observations in very high energy heavy ion reactions, illustrates beautifully how heavy ion studies can contribute also to our understanding of more elementary reactions, e.g. nucleon-nucleon and nucleon-nucleus collisions.

I have here only given a few characteristics of very high energy heavy ion reactions observed in cosmic ray reactions. Besides the high multiplicity events discussed here, there are events which seem to be central but they show up very small s-particle multiplicities. They cannot be accounted for by the two models outlined here.

Even if the cosmic ray experiments suffer from low statistics and limited control over the experimental conditions they certainly show that very high energy heavy ion accelerators will open a window to a very exciting field of physics.

Acknowledgments

I would like to acknowledge the collaboration in part of this work to my colleagues in Lund, S. Herzman, B. Jakobsson, A. Oskarsson and E. Stenlund. I am grateful to A. Dar and S. Fredriksson for stimulating correspondence concerning the application of the 3TM to very high energy heavy ion reactions. The author also has profited from many discussions with G.M. Chernov, K.G. Gulamov, U.G. Gulyamov, H. Heckman, B.N. Kalinkin, K.D. Tolstov and V.D. Toneev.

REFERENCES

1. H.H. Heckman, H.J. Crawford, D.E. Greiner, P.J. Lindstrom and Lance W. Wilson, Lawrence Berkeley Laboratory Report LBL-6501 (1977).

2. B. Jakobsson, Invited talk at the Vth Int. Seminar on High Energy Physics Problems, Dubna USSR, June 1978.

3. J.I. Kapusta, Phys. Rev. C16, 1493 (1977).

4. J. Gosset, J.I. Kapusta and G.D. Westfall, Lawrence Berkeley Laboratory Report LBL-7139 (1978).

5. M.I. Adamovich, et al., JINR, E1-10838, Dubna (1977).

6. G.M. Chernov et al., Nucl. Phys. A280, 478 (1977).

7. K.D. Tolstov, Z. Physik A284, 283 (1978) and private communication.

8. K.B. Bhalla, S. Herzman, B. Jakobsson, A. Oskarsson and I. Otterlund, Lund University Preprint LUIP-7805 (1978).

9. H.H. Heckman, D.E. Greiner, P.J. Lindstrom, and D.D. Tuttle, An Atlas of Heavy Ion Fragmentation Topology, Lawrence Berkeley Laboratory Rept. 8132, to be published.

10. D.E. Greiner, P.J. Lindstrom, H.H. Heckman, Bruce Cork, and F.S. Bieser, Phys. Rev. Lett. 35, 152 (1975).

11. I. Otterlund and E. Stenlund, to be published.

12. I. Otterlund et al., Lund University Preprint LUIP-7804 (1978), to be published in Nucl. Phys.

13. J.A. Galstyan et al., Nucl. Phys. A208, 626 (1973).

14. K.K. Gudima and V.D. Toneev, Yad Fyz. 27, 658 (1978). Phys. Lett. B73, 297 (1977).

15. G.M. Chernov and K.D. Gulamov, private communication.

16. B. Jakobsson and R. Kullberg, Physica Scripta 13, 327 (1976).

17. E. Schopper, H.G. Baumgardt, and E. Obst, Proceedings of the Meeting on Heavy Ion Collisions, Fall Creek Falls, Tennessee, Oak Ridge National Laboratory Report Conf.-770602, 398 (1977).

18. B. Jakobsson, R. Kullberg, and I. Otterlund, Nucl. Phys. A276, 523 (1977).

19. K.B. Bhalla, S. Herzman, B. Jakobsson, A. Oskarsson and I. Otterlund, to be published.

20. V.D. Toneev, private communication.

21. J.P. Bondorf, Invited talk at the Workshop on "High Resolution Heavy Ion Physics at 20-100 MeV/A," Saclay 1978.

22. Baranov et al. Leningrad preprint 562 (1977).

23. B.N. Kalinkin, S.N. Koltochnich and V.L. Shmonin, Alma-Ata preprint HEPI 61-78 (1978).

24. B. Jakobsson, R. Kullberg and I. Otterlund, Z. Phys. 268, 1 (1974), A272, 159 (1975).

25. I. Otterlund and E. Stenlund, Lund University Report LUIP-7806 (1978) to be published.

26. B. Andersson, G. Nilsson and I. Otterlund, Lund University Preprint LUTP-77-16 (1977), to be published.

27. K. Rybicki, Nuovo Cimento 28, 1437 (1963).

28. D. Abraham et al., Phys. Rev. 159, 1110 (1967).

29. A. Dar, private communication.

Figure Captions

Fig. 10.1 A schematic outline of pseudo-rapidity distributions in heavy ion reactions at high energy.

Fig. 10.2 The percentage of reactions with H, CNO and AgBr as a function of the charge of the beam particle.

Fig. 10.3 $\langle N_g \rangle / \langle N_b \rangle$ as a function of the number of interacting nucleons, n_{int}. Data points from ref. 5.

Fig. 10.4 Examples of central reactions with C, N and O targets
a) N + CNO at 2.1 A GeV
b) Fe + CNO at 1.7 A GeV.

Fig. 10.5 Rapidity, y, and pseudo-rapidity, η, for different values of $p_{\parallel}$ and $p_{\perp}$.

Fig. 10.6 Angular distribution of s'-particles. s'-particles are shower-particles without non-interacting singly charged fragments (Chernov et al.).[6]

Fig. 10.7 Mean multiplicities per interacting nucleon as a function of the number of interacting nucleons (Chernov et al.).[6]

Fig. 10.8 The angular distributions of protons with energies in the range 30-400 MeV observed in pA reactions.

Fig. 10.9 The angular distributions of protons with energies in the range 30-400 MeV observed in pEm, dEm and ^{12}C + Em reactions.

Fig. 10.10 Angular distribuutions of b-particles (a) and g-particles (b).[6]

Fig. 10.11 Angular distributions of g-particles (a) and b-particles (b) compared with cascade-evaporation model predictions (histograms).[14] The points are from experiment.[16]

Fig. 10.12 Energy distributions of protons compared with cascade-evaporation model predictions (histograms).[14] The points are from experiment.[16]

Fig. 10.13 ϕ_{sg} and ϕ_{sb} in dEm and αEm reactions.

Fig. 10.14 ϕ_{sg} and ϕ_{sb} in ^{14}N + Em reactions.

Fig. 10.15 Angular distributions for fragments with E < 250 MeV emitted from central collisions observed in nuclear emulsion.[1]

Fig. 10.16 The number of nucleons in the fireball and the spectators for different impact parameters in Fe + CNO and Fe + AgBr reactions.[19]

Fig. 10.17 $\eta = -\log \operatorname{tg} \theta/2$ distributions of charged particles
a) in central Fe + AgBr reactions
b) in central Fe + CNO reactions
The curves show predictions from the fireball model + spectator evaporation.

Fig. 10.18 A schematic illustration of the expansion of the participating volume.

Fig. 10.19 $X = \log \operatorname{tg}\theta$ distributions at different energies.[22]

Fig. 10.20 Illustration to the nuclear pionization model.[23]

Fig. 10.21 $u = -\log \operatorname{tg}\theta$ distribution of s-particles at 3-7 GeV/nucleon (histogram) compared with predictions from the pionization model (curves).[23]

Fig. 10.22 The median angle $\theta_{1/2}$ of s-particles as a function of incident energy.[23]

Fig. 10.23 $x = \log \operatorname{tg}\theta$ distributions of shower particles in central Si + Em and Fe + Em reactions at ~ 10 GeV/nucleon.[24] The curves are pion distributions in 10 GeV pp interactions.

Fig. 10.24 A sketch of pseudo-rapidity distributions in high energy nucleon-nucleon (N-N), nucleon-nucleus (N-A) and nucleus-nucleus (A-A) reactions, predicted from the independent particle model.

Fig. 10.25 The total inclusive shower-particle pseudo-rapidity distribution,
a) in the target nucleus rest frame, and
b) in the projectile rest frame.

Fig. 10.26 Pseudo-rapidity distribution of s-particles in a central Ca + Pb reaction at 300 GeV/nucleon. The dotted curve shows the distribution expected for the projectile nucleus fragmentation protons. The dashed curves show the distributions predicted from the independent particle model discussed.

Fig. 10.27 Pseudo-rapidity distributions of central B + AgBr, N + AgBr and Mg + AgBr reactions at 300 GeV/n, 70 GeV/n and 70 GeV/n respectively.

Fig. 10.28 Multiplicity distributions from the CTM and the modified CTM.[29]

Fig. 10.29 Pseudo-rapidity distribution predicted from the modified CTM compared with the distribution obtained in a Mg + Ag + Br cosmic ray event at ~ 70 A GeV.

Table I

P	T	E_{inc} (GeV/N)	n_s	N_h	$\langle n_s \rangle_{pN}$	N_T	N_p	n_s Eq. (25)
Ca	Pb	~300	518	>10	8.4	~81-94	~40	508-563
B	Ag(Br)	~300	204	30	8.4	~25-33	~11	151-185
N	Ag(Br)	~70	142	42	5.9	~29-33	~14	127-153
Mg	Ag(Br)	~70	182	32	5.9	~42-53	~24	195-227
Al	Ag(Br)	~500	242	32	~9.3	~46-57	~27	339-391
B	Ag(Br)	~500	190	18	~9.3	~25-33	~11	167-205
C	Ag(Br)	~3000	215	13	~12.5	~26-35	~12	238-294
He	Ag(Br)	~4300	95	23	~13.1	~11-17	~4	98-138
B	Ag(Br)	~14000	179	24	~15.2	~25-33	~11	274-334
Si	Ag(Br)	~300	517	17	8.4	~47-58	~28	315-361
Li	Ag(Br)	~400	120	17	9.0	~17-25	~7	108-144
Si	Ag(Br)	~500	515	17	~9.3	~47-58	~28	349-400
C	Ag(Br)	~1200	289	26	~10.8	~26-35	~12	205-263
LiBeB	Ag(Br)	~1500	174	26	~11.2	~17-33	~7-11	134-246
B	Ag(Br)	~1700	193	20	~11.4	~25-33	~11	205-251

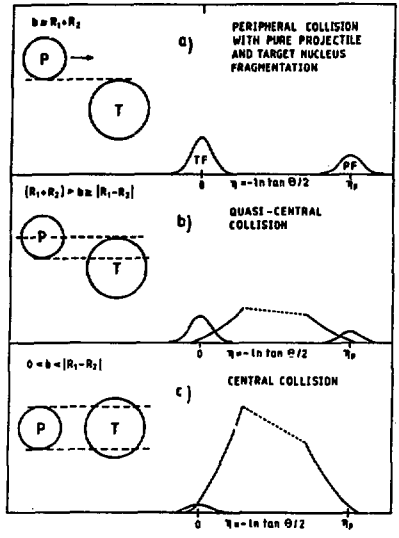

Fig. 10.1

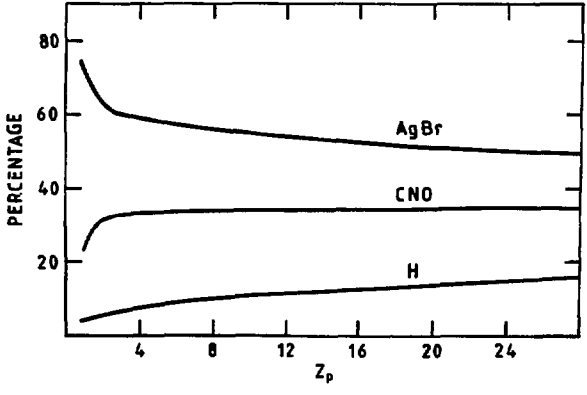

Fig. 10.2

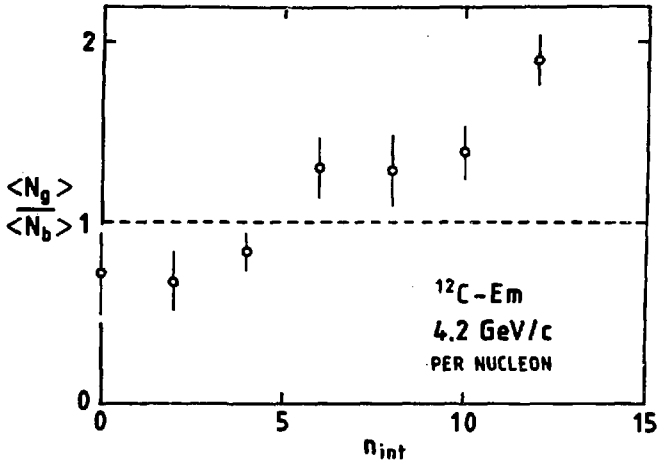
2
1
0
$\frac{\langle N_g \rangle}{\langle N_b \rangle}$
^{12}C-Em
4.2 GeV/c
PER NUCLEON
0
5
10
15
n_{int}

Fig. 10.3

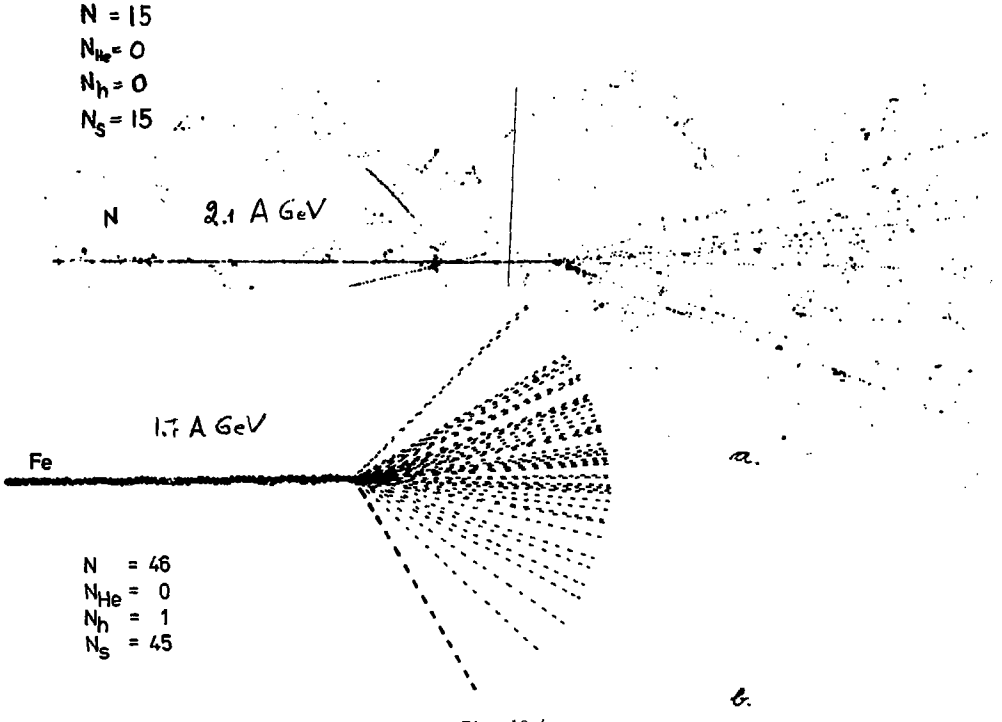

Fig. 10.4

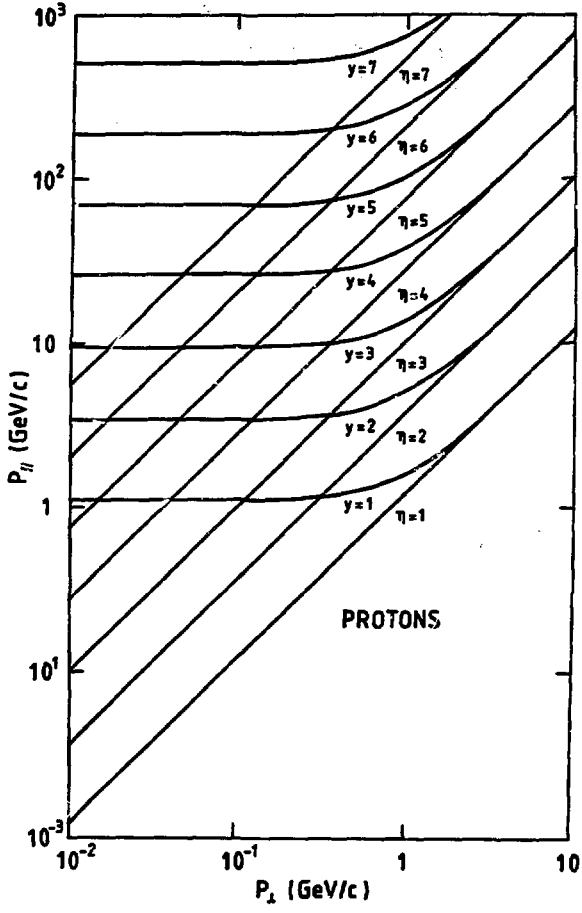
10^3
10^2
10
1
10^1
10^{-3}
10^{-2}
10^{-1}
1
10
$P_{//}$ (GeV/c)
$P_\perp$ (GeV/c)
y=7
η=7
y=6
η=6
y=5
η=5
y=4
η=4
y=3
η=3
y=2
η=2
y=1
η=1
PROTONS

Fig. 10.5

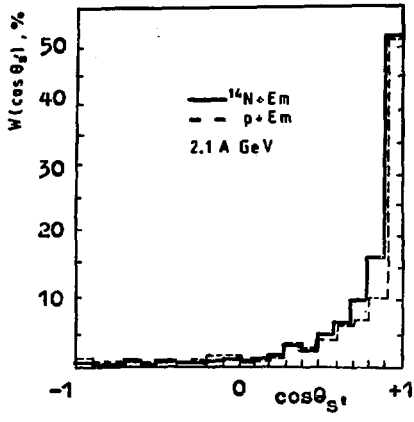

Fig. 10.6

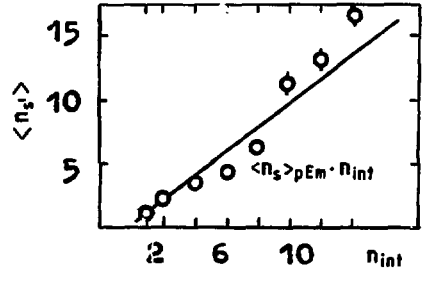

Fig. 10.7

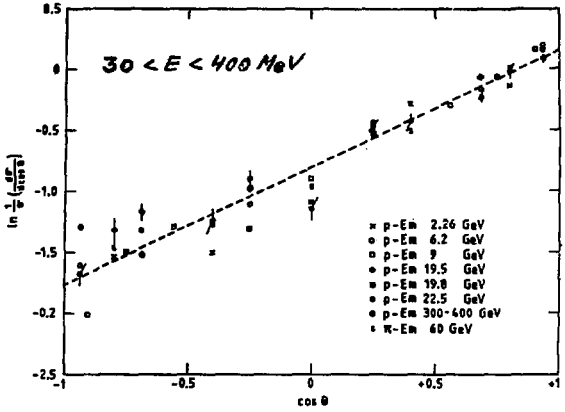

Fig. 10.8

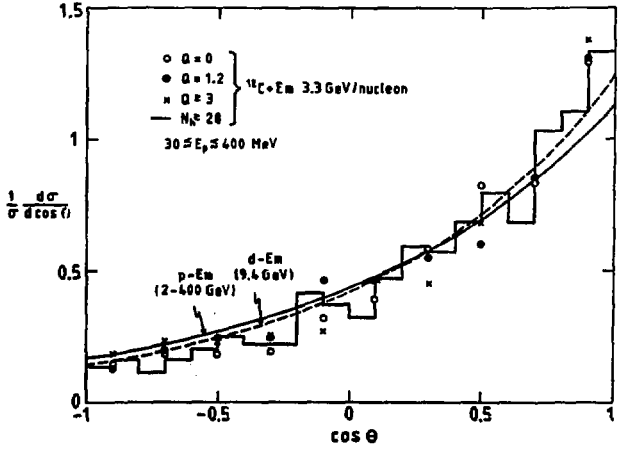

Fig. 10.9

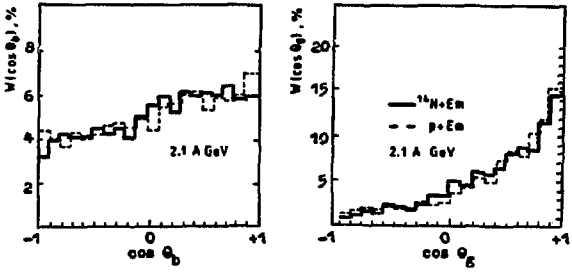

Fig. 10.10

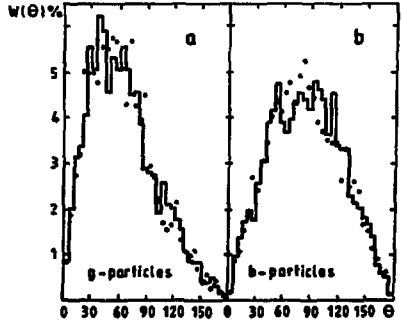

Fig. 10.11

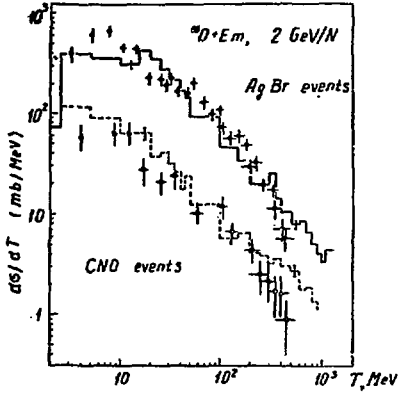
^{40}D+Em, 2 GeV/N
Ag Br events
CNO events
dσ/dT (mb/MeV)
T, MeV
10³
10²
10
1
10
10²
10³

Fig. 10.12

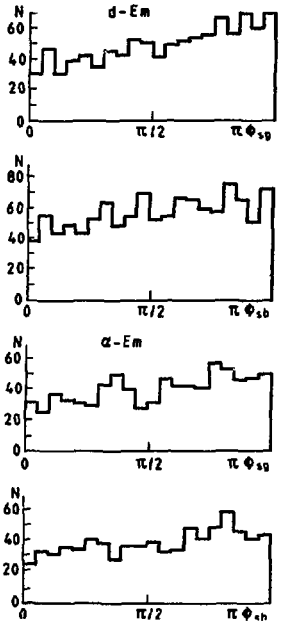

Fig. 10.13

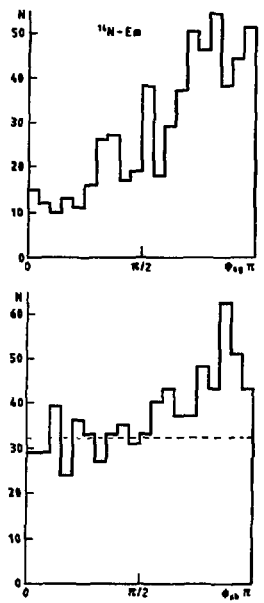

Fig. 10.14

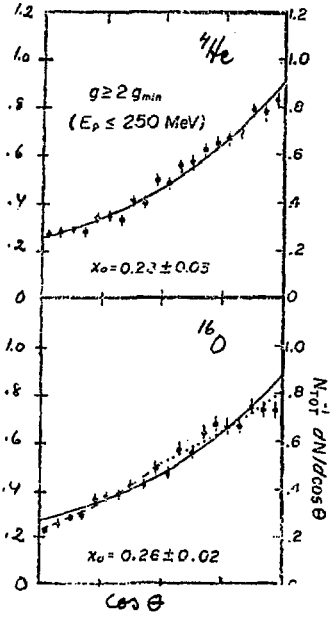

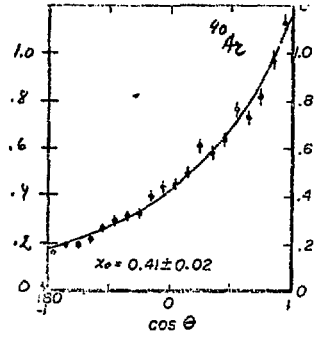

Fig. 10.15

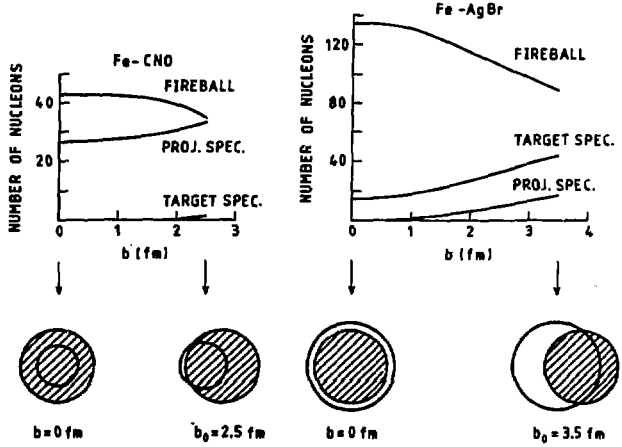

Fig. 10.16

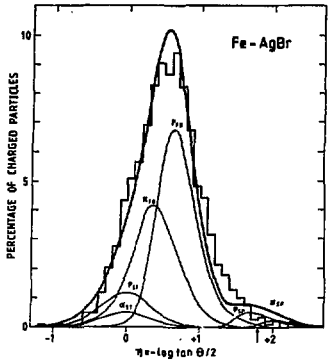

Fig. 10.17a

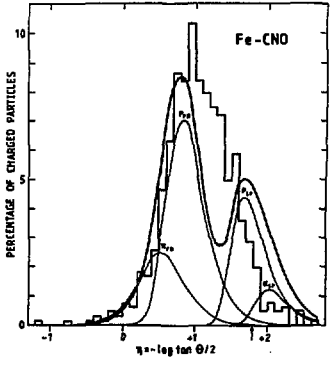

Fig. 10.17b

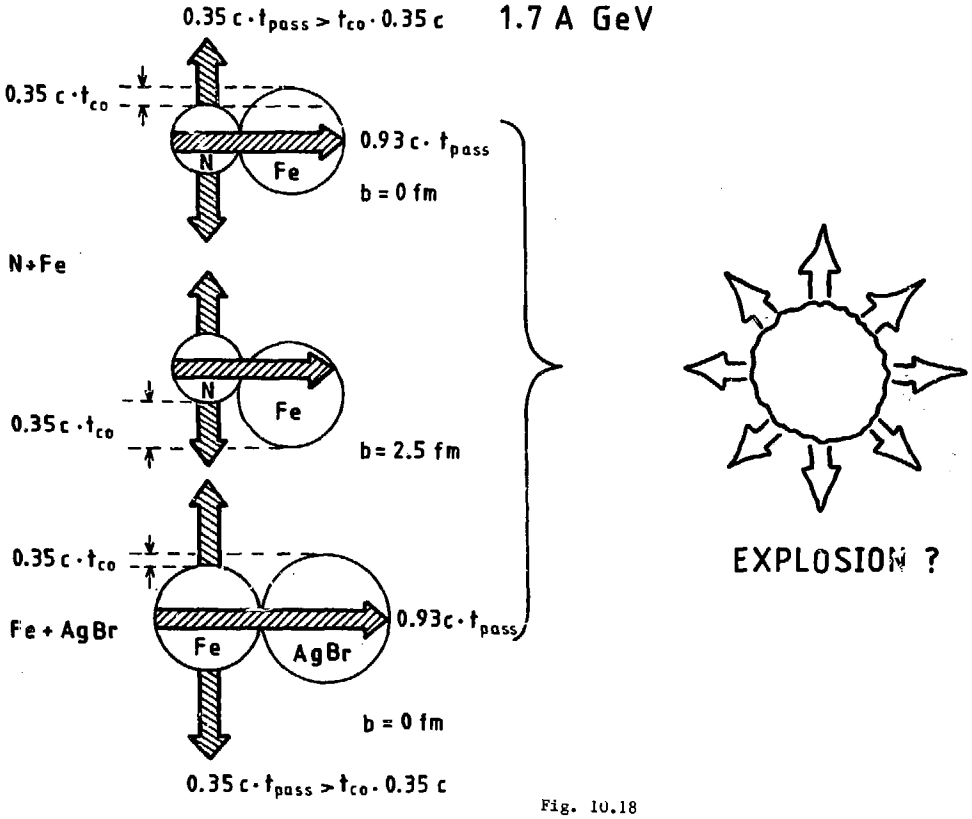
0.35 c · t_pass > t_co · 0.35 c
1.7 A GeV
0.35 c · t_co
N
Fe
0.93 c · t_pass
b = 0 fm
N+Fe
N
Fe
0.35 c · t_co
b = 2.5 fm
0.35 c · t_co
Fe + AgBr
Fe
AgBr
0.93c · t_pass
b = 0 fm
0.35 c · t_pass > t_co · 0.35 c
EXPLOSION ?

Fig. 10.18

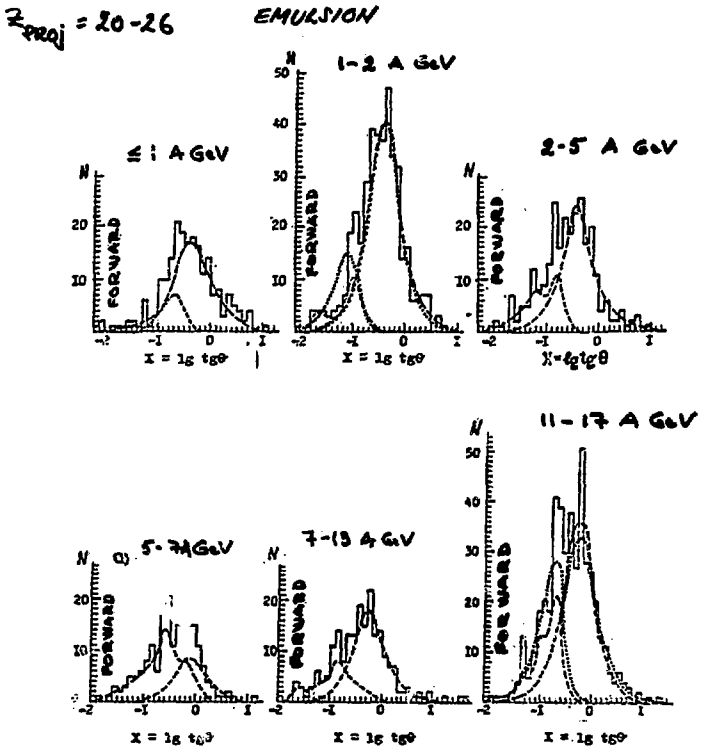
Z_{proj} = 20-26
EMULSION
≤ 1 A GeV
1-2 A GeV
2-5 A GeV
5-7 A GeV
7-11 A GeV
11-17 A GeV
N
FORWARD
X = lg tgθ
HISTOGRAMS EXP. GAGARIN ET AL. (LENINGRAD)
CURVES THEORY KALINKIN ET AL. (DUBNA)

Fig. 10.19

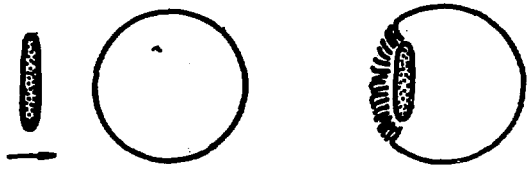

NUCLEAR PIONIZATION MODEL
KALINKIN ET AL. (DUBNA)

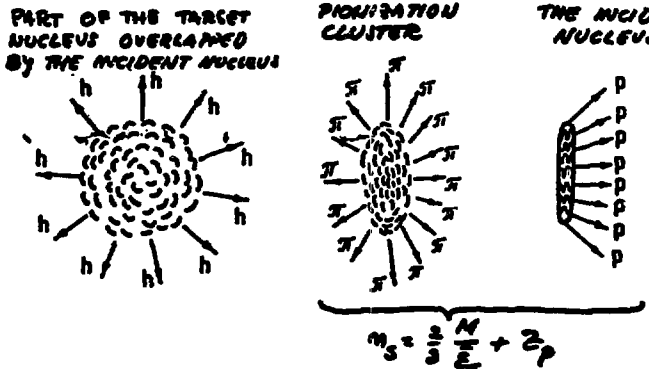

THE LORENTZ COMPRESSED INCIDENT NUCLEUS INTERACTS CONSECUENTLY WITH LAYERS OF THE TARGET NUCLEUS RESULTING IN THE FORMATION AND DECAY OF THREE INDEPENDENT EXCITED SYSTEMS.

Fig. 10.20

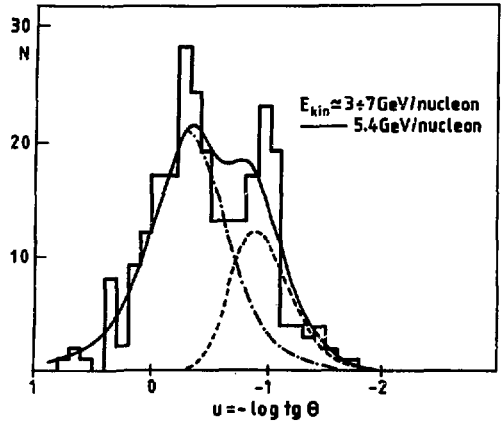

Fig. 10.21

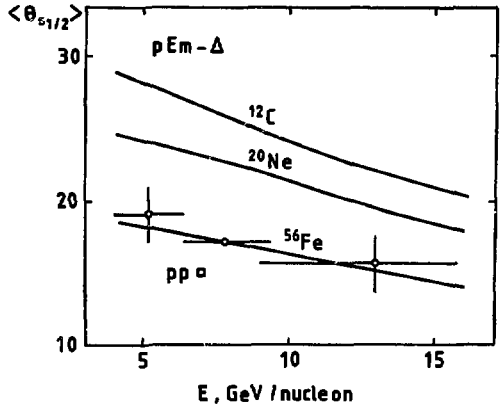

Fig. 10.22

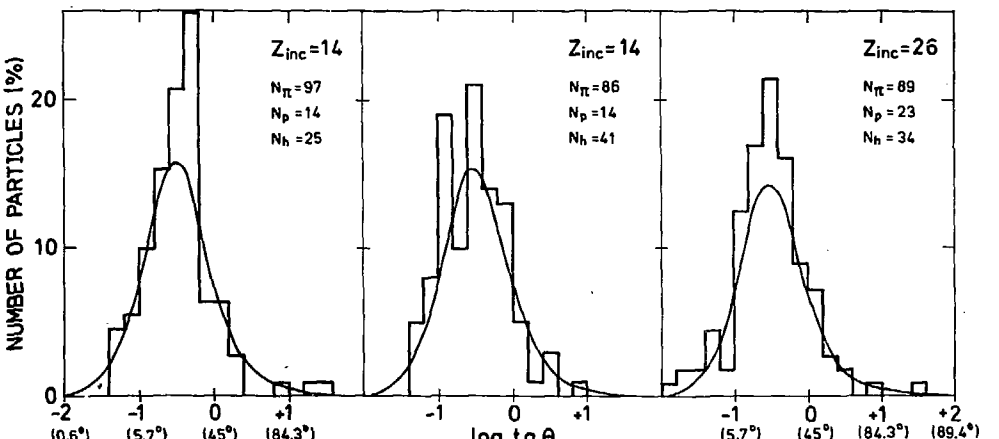
NUMBER OF PARTICLES (%)
20
10
0
Zinc=14
Nπ=97
Np=14
Nh=25
Zinc=14
Nπ=86
Np=14
Nh=41
Zinc=26
Nπ=89
Np=23
Nh=34
-2
(0.6°)
-1
(5.7°)
0
(45°)
+1
(84.3°)
-1
0
+1
log tg θ
-1
(5.7°)
0
(45°)
+1
(84.3°)
+2
(89.4°)

Fig. 10.23

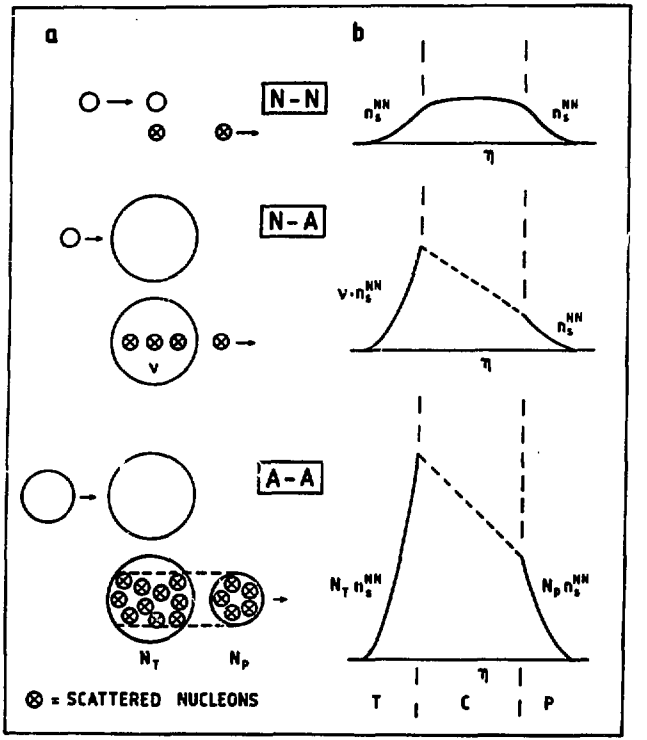
a
b
N-N
N-A
A-A
n_s^{NN}
n_s^{NN}
η
$\nu \cdot n_s^{NN}$
n_s^{NN}
η
$N_T n_s^{NN}$
$N_p n_s^{NN}$
η
N_T
N_p
⊗ = SCATTERED NUCLEONS
T
C
P

Fig. 10.24

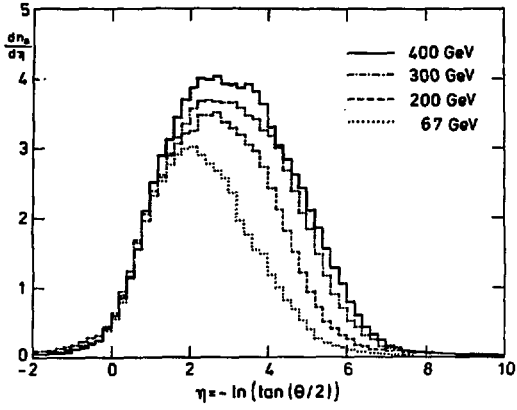

Fig. 10.25a

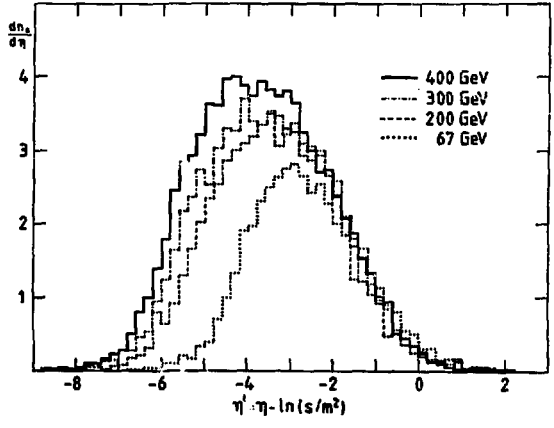

Fig. 10.25b

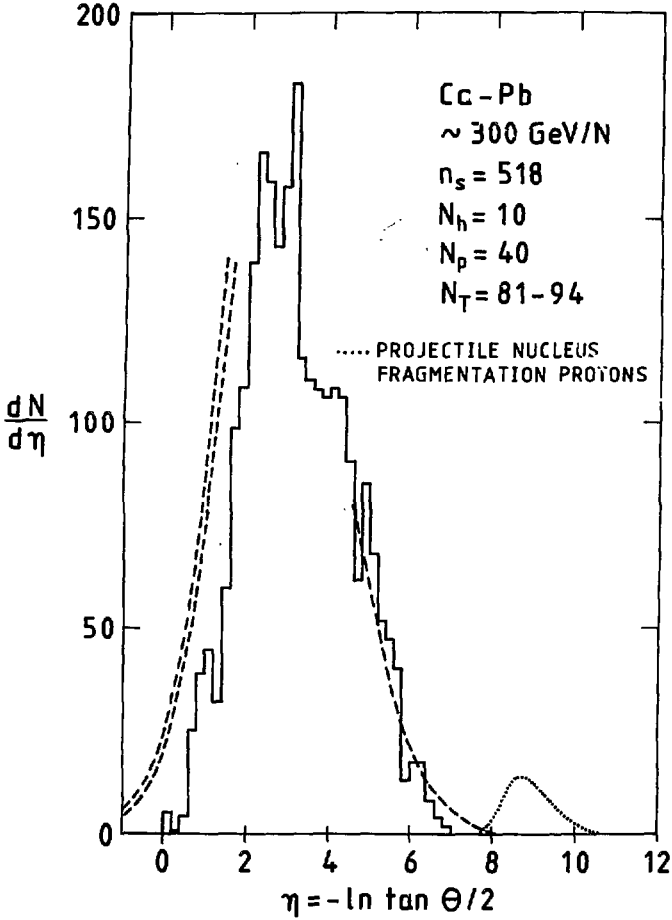
Cc-Pb
~ 300 GeV/N
n_s = 518
N_h = 10
N_p = 40
N_T = 81-94
..... PROJECTILE NUCLEUS FRAGMENTATION PROTONS
$\frac{dN}{d\eta}$
200
150
100
50
0
0
2
4
6
8
10
12
$\eta = -\ln \tan \Theta/2$

Fig. 10.26

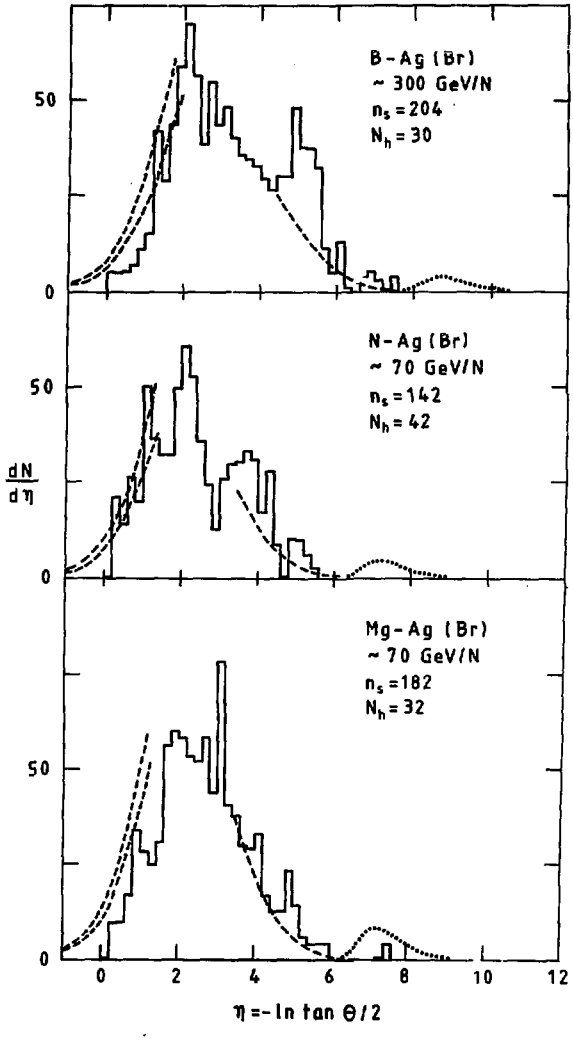
B-Ag (Br)
~ 300 GeV/N
$n_s = 204$
$N_h = 30$
N-Ag (Br)
~ 70 GeV/N
$n_s = 142$
$N_h = 42$
Mg-Ag (Br)
~ 70 GeV/N
$n_s = 182$
$N_h = 32$
50
0
$\frac{dN}{d\eta}$
0
2
4
6
8
10
12
$\eta = -\ln \tan \Theta/2$

Fig. 10.27

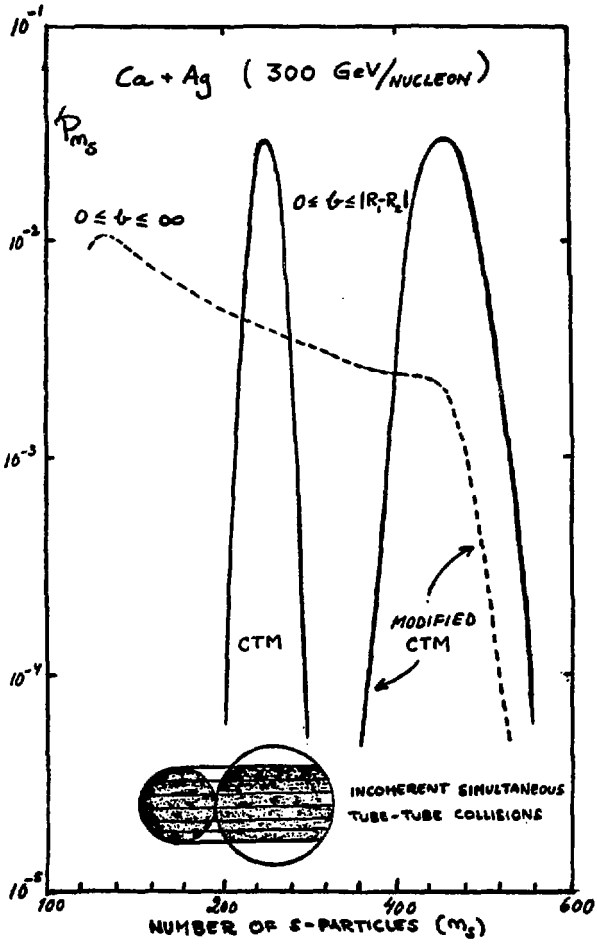
Ca + Ag (300 GeV/NUCLEON)
P_{m_s}
$0 \le b \le \infty$
$0 \le b \le |R_1 - R_2|$
CTM
MODIFIED CTM
INCOHERENT SIMULTANEOUS TUBE-TUBE COLLISIONS
10^{-1}
10^{-2}
10^{-3}
10^{-4}
10^{-5}
100
200
400
600
NUMBER OF S-PARTICLES (m_s)

Fig. 10.28

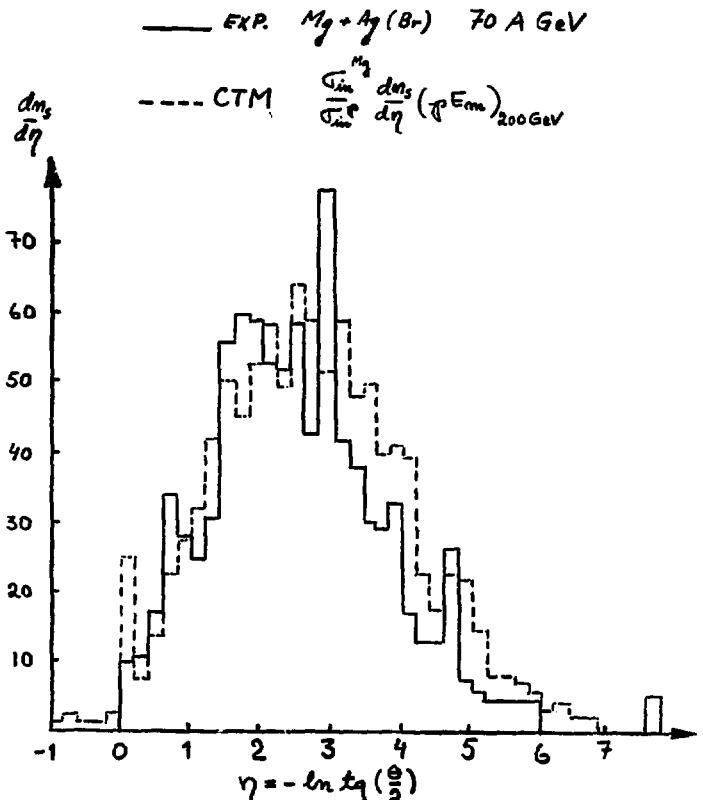
EXP. Mg + Ag (Br) 70 A GeV
CTM
$\frac{\sigma_{in}^{Mg}}{\sigma_{in}^{p}} \frac{dn_s}{d\eta}(p^p E_{cm})_{200\,GeV}$
$\frac{dn_s}{d\eta}$
70
60
50
40
30
20
10
-1
0
1
2
3
4
5
6
7
$\eta = -\ln tg(\frac{\theta}{2})$

Fig. 10.29

INTERMEDIATE ENERGY HEAVY IONS -- FROM THE LOW ENERGY PERSPECTIVE

C. Konrad Gelbke

Let me first acknowledge all the people who either collaborated on the various experiments I would like to discuss or who made available their data prior to publication (Fig. 11.1). I have to apologize to everybody whom I did not mention and I'm pretty sure I forgot some of the people who gave me their data prior to publication or after publication.

As I was coming to Berkeley by airplane I remembered that two years ago at the summer study we talked a lot about flowers and weeds. Looking out of the airplane I tried to see some flowers on the ground, but I couldn't see any (Fig. 11.2). I wondered why. Finally when I walked up the hill this morning I took the path by foot and looked at all the stones and once in a while I saw a flower. So today I will take a rather pedestrian-type approach. I will remind you of all our everyday hardships and all the small niceties that we have encountered in low energy physics. I'm pretty sure that you know most of the facts, but as David Scott said, physicists like to hear what they already know, so I'll follow the tradition.

In order to organize my talk I'll follow the convention that one breaks up the reaction cross section into central collisions and into peripheral collisions (Fig. 11.3). At low energies, peripheral collisions are defined as elastic scattering, quasi-elastic scattering, and deeply-inelastic scattering (the latter class of reactions being a very interesting field of research in the last few years). At relativistic energies we talk about peripheral fragmentation reactions. At low energy, central collisions are generally fusion type reactions (at least for projectiles which are lighter than, let's say, mass 50), i.e., compound nucleus formation and some subsequent particle evaporation reactions or, for heavier target nuclei, de-excitation by fission. At relativistic energies a completely different picture has emerged. Here we are talking about nuclear fireballs, shock waves, pion condensates, and density isomers. You see I put two question marks to the right and to the left hand side of Fig. 11.3 because I'm pretty sure that this is not going to be the final word.

Now let me start very gently — with the most gentle process we know for heavy ion scattering, that is, the elastic process. Let me just remind you of what we have learned in the last few years about heavy ion elastic scattering (Fig. 11.4). (And actually it's not very much.) We know that we are only sensitive to the extreme tail region of the nuclear potential. The region where we can determine the optical potential reasonably well corresponds to a density overlap of the two nuclei of less than 10%. So if one plots a typical potential that is used in optical model calculations all the hatched region (marked by the question mark in Fig. 11.4) is not determined experimentally and hence is unknown. There is some evidence that we are getting more sensitive to slightly smaller radii if we increase the beam energy. There has been a very nice systematic study by Cramer and collaborators of the elastic

scattering of ^{16}O from ^{28}Si for energies very close to the Coulomb barrier up to something like 200 MeV (Fig. 11.5 top only). (You can see that what I understand as intermediate energies is everything that we cannot access right now with existing tandem accelerators. So I will take the liberty of redefining this intermediate energy domain.) The result is that one can determine a class of potentials, although one can still not remove all the ambiguities existing in these potentials. But you see, however, that one gets a very good overall description of the data even with an energy-independent potential for these elastic scattering data.

I would like to convey to you the excitement which came about in the low energy physics community when people decided to look at back-angle elastic scattering. I'll show you back angle elastic scattering data from Braun-Munzinger and Jean Barrette and collaborators (Fig. 11.5, bottom) taken at Brookhaven. We see that the optical potential, which has been derived by such a very careful and extensive study of forward-angle elastic scattering, fails to reproduce the back angle elastic scattering cross sections by several orders of magnitude. I think the lesson we can learn from such experiments is that whenever you do an extraordinary experiment that is difficult, you find something exciting. And at present, back-angle elastic scattering is a very rapidly expanding field and causes a lot of excitement in low energy nuclear physics. Actually I'm so excited about this field myself that I cannot refrain from showing you another set of data that was obtained recently at Brookhaven National Laboratory. Here (Fig. 11.6) one sees that different channels corresponding to the same compound nucleus exhibit this anomalous back angle rise. And we even have indications, as shown here by large dots, that transfer reactions also show a back angle rise of one to two orders of magnitude. At the present time we don't understand those phenomena. The highest accessible energies at tandem accelerators show that this process does not dwindle away. So we should do similar experiments at high energy, and I'm pretty sure we are going to have a lot of exciting phenomena, although I don't know whether this will persist up to 100 MeV/nucleon. It's a very worthwhile phenomenon, however, to study over a large dynamic energy range.

Getting a little bit more violent and letting the nuclei overlap a little bit more, I would like to show you at least one example of transfer reactions studied over larger dynamic range, that is, over a dynamic range which is accessible, let's say, by the 88-inch cyclotron (see Fig. 11.7). These data were taken by Cathy Olmer et al. The experimental cross sections are shown here as the solid lines. If one compares these cross sections with the standard model with which we analyze single-nucleon transfer reactions, we see that the energy dependences of those cross sections are not reproduced at all. Now if one divides the cross section predicted by the distorted-wave-born-approximation by the cross section which is measured experimentally, we get a rather general trend. That means that all the relative strengths of the various transitions are rather well reproduced. However, we don't understand the energy dependence of the cross sections for transfer reactions at all. And this is a discrepancy over a range from the Coulomb barrier, let's say, to only 15 MeV/nucleon above the Coulomb barrier, where the distorted-wave-born-approximation fails by about a factor of 5 or even more.

Now let me come to another phenomenon that we have encountered at low energies (which has perhaps caused the largest excitement during the last few years), i.e., deeply-inelastic reactions (Fig. 11.8). I've chosen here one recent experiment (according to my own prejudices, of course) where you see the typical phenomenon. In this experiment, we have charge (see left of Fig. 11.8) and mass identification (see right of Fig. 11.8) of all outgoing reaction products and a band of particles at rather low energies. Note that the elastic scattering peaks are clearly visible. These reactions are characterized by large amounts of energy, mass, angular momentum, and charge transfer. They have attracted alot of interest; rather detailed and careful experiments have been done to disentangle the various phenomena and to answer questions, such as, how strongly are these nuclei excited that are produced with very negative Q values? In a very nice neutron-coincidence experiment that was performed by Eyal et al. (Fig. 11.9) it has been shown that the ratio of the number of neutrons emitted from the heavy fragment to the number of neutrons emitted from the light fragment in such a deeply-inelastic collision is like the mass ratio of the fragments observed. This finding is consistent with the fact that the excitation energy is shared in proportion to the mass which means that it is also consistent with the assumption that the two fragments are in thermal equilibrium and have the same temperature just before they separate. We also understand rather well the isotope cross sections which are produced in these reactions. Here I show some data of argon-induced reactions on ^{42}Ca, ^{48}Ca, ^{50}Ti and a variety of other targets (Fig. 11.10). We can understand the isotope-production cross sections making a couple of rather simple assumptions. One assumption is that the mass-to-charge ratio of these two nuclei just before separation is in equilibrium. If we take this assumption by itself we obtain curves like the dashed curve shown in the figure which does not really correspond to the observations. However, we have also seen in these neutron coincidence experiments that the excitation energy is shared proportionately to the mass between those two nucleons. Therefore, what one has to do in order to understand those isotope production cross sections is to calculate the de-excitation of these primary fragments and fold this in with the primary distribution. The results are shown by the histograms in Fig. 11.10. We see that one can predict the isotope production cross sections rather well, at least at low energies, by the two assumptions of charge equilibration and secondary decay of the isotopes.

I don't want to go into more detail for peripheral collisions, but I do want to show you what we know about low energy central collisions. These processes are rather well understood, as you all know. In Fig. 11.11 we see a typical example of a fusion-type reaction. This is sulfur on aluminum and several magnesium isotopes. I have marked the compound nucleus we are populating at rather high excitation energies which then decays by the evaporation of nucleons and alpha particles. The evaporation codes now existing are rather precise and can describe the observed isotope production cross section to a rather surprising degree of accuracy. Fig. 11.12 compares calculations and data of Pühlhafer et al. The experimental isotope production cross sections are shown by the histograms and the theoretical isotope production cross sections by the solid bars. The overall agreement between the data and the theory is remarkably good. And again the assumption is that we are

forming a compound nucleus which goes into complete equilibrium and then simply decays according to the statistical model.

Now this looks rather simple, but I would like to remind you that we don't know anything about the energy dependence of these processes. I find it challenging to investigate the energy dependence of quasi-elastic, deeply-inelastic reactions and also fusion-type reactions. There are some data available for lighter systems over a larger energy range and of course, as everybody expects, the fusion cross section goes down as a function of energy (see Fig. 11.13). But I think there are a couple of questions that are absolutely open and I will be very excited to see the solutions during the next few years. One such question is, up to which energies is the equilibrium hypothesis valid? By equilibrium hypothesis I mean the hypotheses of the independence of formation of decay, and that the compound nucleus decays just according to the equilibrium statistical model. Also it is not clear, even for the gross cross sections, how they develop with energy. Nobody can answer at present the question of what happens to a 50-MeV/nucleon argon nucleus if it strikes a thorium target. Do we still observe the phenomenon of deeply-inelastic scattering, and at which energies does it vanish? Also, we don't expect that the charge equilibration hypothesis, just to mention one, holds at higher energies. Departing from this equilibrium situation will give us a richness of information about the various theoretical approaches.

Now let me give you a simplified perspective of relativistic reactions. At relativistic energies there are two main concepts that emerge regardless of the details of the theory (Fig. 11.14). (I don't want to defend any theory here.) It appears that at relativistic energies the geometry dominates and that one can split the interaction region into two parts. One part would be the overlapping region of projectile and target nucleus, and for that overlapping region it is assumed, at least in some models, that you have a full momentum transfer. In addition, we can assume that we have complete equilibrium in this overlapping part of nuclear matter, since the data are consistent with this assumption. That was the origin of the nuclear fireball model. The other assumption is that the other parts of the nuclei, the target and the projectile nuclei, which do not belong to the overlap region, don't feel very much momentum transfer; they play the role of spectators. They are excited and they decay, of course, but nothing very special happens to the remnants of those nuclei. I would say that the pictures which have emerged from inclusive experiments are not at all established, and I am really looking forward to experiments that are more sensitive to the details of assumptions and that test various correlations. I'm pretty sure that Steve Koonin will have a couple of words to say about that.

I would like to talk about some observations which have been made at the 88-inch cyclotron about the energy dependence of oxygen-induced reactions. We are starting a program right now with argon-induced reactions, but I think with the existing accelerators it will take quite a while before we have a set of data over a comparable range of energies. Of course, argon is a truly heavy ion, whereas oxygen is mainly surface. I therefore ask you to take the results we obtained with oxygen with a grain of salt. It might be an idea that we can follow in future research, but I don't think it's the final word either.

Let me just remind you of the observations we made about two years ago about the similarity of elemental cross sections at 2 GeV/nucleon and at 20 MeV/nucleon. Fig. 11.15 shows the ratio of cross sections at 315 MeV to 33.6 GeV (these are the elemental cross sections without isotope production). And those ratios are nearly energy independent. Now I still claim that the complete interpretation of this phenomenon has not been given yet. We know a couple of approaches which are very fruitful. The work of Jörg Hüfner and collaborators, I think, is really leading us down the correct path, but the question of why we have this constant production of lithium, beryllium and boron isotopes is still not resolved. On the other and, and this is sometimes misunderstood, the isotope production cross sections are not at all energy independent. There is a very strong energy dependence, and that is very often disregarded. At low energies we tend to produce many more neutron-rich nuclei than at high energies. Of course, what comes into one's mind, immediately, is the question of whether at lower energies we still observe this mass-to-charge-ratio equilibration. I do believe that this is actually important at low energies. (Jörg Hüfner et al. actually introduced the charge exchange process as an important process.) At high energies, of course, you don't believe that you still have this mass-to-charge-ratio equilibration. There's another fact, just to remind you, namely that if we go below 20 MeV/nucleon we have a very strong energy dependence of the various element production cross sections.

Some recent experiments performed at the Bevalac compared with low energy experiments, seem to support the idea that at lower energies we are dealing with a mass-to-charge-ratio equilibration, but at high energies we are not. Fig. 11.16 shows lighter fragments produced in argon-induced reactions at 213 MeV/nucleon. These are shown with dark circles and compared to argon-induced reactions on ^{48}Ca at 6 MeV/nucleon (shown with open squares). We see, indeed, that at 6 MeV/nucleon we are producing rather neutron-rich isotopes, whereas at 213 MeV/nucleon we are producing more neutron-poor isotopes. An important question which we have to answer in the future will be how to understand these isotope production cross sections at relativistic energies. (This could, in fact, open a wide field of nuclear spectroscopy far from the valley of stability.) We generally imagine that we make sort of a sharp cut into the nucleus but do not yet understand how much excitation energy we deposit into the nucleus at relativistic energies or how it decays. I have another rather nice picture that shows the average neutron over proton number for the various elements we are observing. Fig. 11.17 shows data of ^{40}Ar on Th at 7 MeV/nucleon, ^{40}Ar on ^{48}Ca at 6 MeV/nucleon, and ^{40}Ar on Th at 213 MeV/nucleon. And, again, we see that we are producing a lot of neutron-rich isotopes at low energies. At high energies, the neutron to proton number decreases.

It has been proposed that the question that must be answered in order to understand isotope production cross section at relativistic energies is whether or not we can observe the effects of ground state correlations at relativistic energies. In order to answer that question we first have to understand the influence of the deexcitation of the primary fragments on the final observation, and I would suggest that we do such experiments as comparing isotope cross sections produced with ^{48}Ca and ^{40}Ca. Here we can

vary the neutron number, and we would probably get a very good feeling of the influence of these de-excitation chains. I believe that both at low energies and high energies and at all the intermediate energies (which will be accessible pretty soon) there will be a large number of isotopes that can be produced far from stability and even at the limits of stability once we understand how these mechanisms work. And a lot of work remains to be done in this field.

Now let me go on to another thing that you all know. Fig. 11.18 shows a typical momentum spectrum that was taken in one of the pioneering experiments of the Heckman/Greiner group. The momentum spectra are plotted in the projectile rest frame and the general observation one had for the energy or momentum spectra of the particles produced in the peripheral reaction is that the particles emerged with approximately the velocity of the projectile. The velocity of the projectile would be at zero and is marked with a line. There is a small downshift, i.e., the particles emerge with a slightly lower velocity than the projectile and the momentum spectra can be fit rather well with the Gaussian shape. That means we are observing a sort of Maxwellian distribution. Now the width of those spectra follows the simple parabolic formula shown in Fig. 11.18, which you are probably all familiar with from previous summer studies. There is one parameter which enters into the expression for the width and there are two approaches that one can use to explain this parameter. One has assumed that we excite the fragment and interpret the whole phenomenon in terms of a temperature. In this case we get an expression like the first one shown below Fig. 11.18. But we also can explain the same findings by assuming a very fast statistical fragmentation process. (It is basically momentum conservation which generates this parabolic dependence.) If this is done, the width parameter σ_0 can be connected to the Fermi momentum of the nuclei.

At low energies we see something that is rather similar. Fig. 11.19 shows reactions of oxygen on lead and gold at various energies. The energies, marked as E_p, are energies corresponding to the velocity of the projectile. We observe energy spectra that are peaked at velocities slightly below the energy of the projectile, and the dashed lines are Maxwellian distributions which would be observed in the frame moving with some velocity. Now an interesting thing to compare is the width of those energy spectra as a function of energy (Fig. 11.20). Unfortunately I've translated these widths of energy spectra into temperatures, although I still think the temperature model needs more confirmation. I want to remind you, however, that there's a simple relation between the temperature and the widths of those spectra. Therefore you could also imagine that I'm plotting the width of the energy spectra as a function of energy. These are shown as open circles in the graph, and I would like to draw your attention to them. There seems to be a very rapid evolution of the widths of the energy spectra. Very rapidly the energy spectra become rather wide as a function of beam energy, at least up to 20 MeV/nucleon. Rather interestingly they have about the same widths at 20 MeV/nucleon and above 500 MeV/nucleon. The temperatures, extracted by particle cross section models developed by Volkov and Lukyanov, have been included as open squares and solid circles in this diagram. It seems that we have a kind of limiting temperature at relativistic energies that would be about 8 MeV/nucleon, and it teases one to wonder whether this represents a boiling point of nuclear matter.

It is like observing water. If we are boiling water and still have some water left in our pot, its temperature will not be above 100°. In analogy, we are observing nuclei which are still bound, and therefore you could say that they should not be hotter than 8 MeV, which is about the binding energy of nuclear matter. Again I would say that these are ideas that one can perhaps flash up, but I would caution you about making interpretations until we have more complete information about them.

I have some new data for argon-induced reactions at 213 MeV/A that I can show (Fig. 11.21). The observations are rather similar to those for oxygen-induced reactions. The statistics are not very good, so I wouldn't insist too much on the data. But you do observe again the Gaussian- or Maxwellian-type energy spectra. Let me show you the whole compilation of energy spectrum widths we have observed in this experiment (Fig. 11.22). Again we observe an average temperature of about 8 or 9 MeV which is rather consistent with a limiting temperature of nuclear matter. However, Karl van Bibber has shown that if we go up to 90 MeV/nucleon we see energy spectra that are much wider than any energy spectra we have observed so far, be it at low or be it at high energies. (This is now the big question mark, and I think it should be checked very carefully before we make any conclusions.) In Fig. 11.23 the solid curve represents the widths of energy spectra which are predicted by the conventional model of Fred Goldhaber, and the points are the widths which have been extracted in those experiments. These observations could be a warning that we have not reached asymptotia and at the same time present a puzzle and challenge for future investigations in the energy range around 100 MeV. I think the situation is rather unclear at present.

Now let me come to proton inclusive data (Fig. 11.24). I want to remind you of all the excitement two years ago when we discovered that we could explain the qualitative features of single-particle inclusive experiments at high energies in terms of the rather simple model, the fireball model. Now I want to call your attention to the fact that we observe rather similar proton spectra at 20 MeV/nucleon. This is in spite of the commonly accepted idea that the mechanisms are rather different at the low and the high energies. We see proton energies up to 100 MeV for impinging oxygen ions of 300 MeV. The lines are fit to the data by assuming that we have a source of nucleons that moves with an intermediate velocity and has a temperature of the order of 6.9 MeV. Somebody told me I should not show such a picture but rather a rapidity diagram. Because of this remark, James Symons has quickly rushed down to the cyclotron and has produced a very nice rapidity diagram. Here (Fig. 11.25) are the invariant cross sections plotted in a $p_\perp$ versus rapidity plot (at low energies the rapidity is nothing but $p_\parallel$). The dotted lines form circles that are centered around a rapidity half that of the beam. As you see, the data are rather consistent with the assumption that those protons are produced by a source moving with approximately half the velocity of the beam. At low energies, however, there is a large variety of theories that can explain high energy light particles emitted in nuclear reactions. For example, one model is the pre-equilibrium model developed by Griffin which allows for a test of the number of excitons produced in such a reaction. Now if we integrate our proton spectra over angle (Fig. 11.26), then plot the expression $\ln(1/E^2 d\sigma/dU)$ versus $\ln U$ we obtain a straight line and from the

slope of this line one can extract the number of excitons within such a model that are responsible for this preequilibrium emission. (U is the excitation energy of the residual nucleus: $U = E^{*}_{ex}-E-B$.) The number of excitons, remarkably, is 27, which is much smaller than the number of nucleons in the composite system. Apparently we're dealing here with a pre-equilbrium phenomenon that appears to be in a localized region in the nucleus, which also travels with an intermediate velocity. Rather similar, qualitatively, is the fireball model. Of course, you don't expect the geometry arguments which are a main ingredient of the fireball model at high energies to hold at low energies because we have the Coulomb deflections, and in addition, the nuclear forces are still important to deal with. Another possibility would be to try to explain the energy spectra with a hybrid model of Marshall Blann (see Fig. 11.27). The circles show the experimental data integrated over angles. Unfortunately, the theory has not yet been developed to a stage where we can predict angular distributions. Two curves are shown assuming 16 excitons and 25 excitons for the excitation, respectively. Again the main point I want to convey here is that these models can (at least crudely) account for the inclusive observations. Also, again one comes out with a number of excitons, or excited particles, that is much smaller than the number of nucleons in the projectile-target complex.

Now let me mention a couple of other models which have been proposed to account for light particle emission. At low energies we have the precompound models for which I showed some calculations. For the cascade models, unfortunately, we don't have calculations, but I'm pretty sure that they will also give the appropriate results at low energies. I would be willing to make a small check here to show that this theory is expected to work. We also have models that say we have projectile excitation and decay in flight. These are not favored too much right now, but we also have evidence that these processes do occur from the experiments that I'll show you in a moment. Also, a piston model has been proposed, which I will come to in a moment. There were also models that provoked the internal fermi motion of the nucleons inside nuclei, and one talks about fermi jets. I'm not really sure at what stage those models are. They are in a rather qualitative stage, I guess. In addition, we also talk about hot spots on the nuclear surface; that is, we have nucleon emission from a small localized region on the nuclear surface.

None of these models is at a stage where one could exclude or include them into any further discussions, since they predict qualitatively correct features. At high energies, just to remind you (if you have not been too much aware of these theories), we have hydrodynamic theories, cascade models, and fireball, firestreak models. Again all these models worked rather well, in fact, and Jörg Hüfner has explained to you why they work so well at high energies. There are two things, namely, geometry and a sort of thermalization in the overlap region. And that's all one really needs. Now if you want to make any progress, and I think this applies as well to high energies as to low energies, we have to go to different experiments and to different theories. What we need, to make progress in the future, are experiments that are "crucial experiments," so to speak. That is, experiments that can verify, or much more importantly, that can <u>falsify</u> a theory. We need predictions that can really exclude or include a certain model for further considerations once we do the

appropriate observations. And the number of those experiments, as well as the number of those theories capable of accomplishing this is rather limited. I am personally rather unhappy about that situation. But at least at low energies we have tried to get some qualitative pictures of what is going on, although they are rather incoherent. I would like to spend the last fifteen minutes just showing you some of the results which we have obtained at lower energies.

Taken that one has to go away from single-particle inclusive experiments, there are of course two approaches. One would be to go to single-particle or two-particle inclusive experiments trying to measure two quantities rather precisely and ignore the rest. I personally am prejudiced and think this is, perhaps, the appropriate way to go. The alternate way would be to try to measure one particle rather precisely, and for the other particles make a counting experiment, that is, to count how many particles are emitted in certain regions. But from our two-particle inclusive experiments we have already learned that it is very difficult to understand the phase space. If we merely count in phase space, i.e., if we don't know whether we have a proton of 5 MeV or 100 MeV energy, it will be very difficult to make conclusive decisions. Probably, in the long run, we will need detectors that detect as many particles as possible with rather high precision and, of course, theories that can explain it. This is a real challenge, and it's not going to be easy. But I do think we have to go that way if we want to make any progress.

Now I would like to show you at least one example of a theory that could be verified or falsified by a rather simple coincidence experiment. This is the piston model which has been proposed by Gross and Wilczynski. This model addresses itself to the early observations that were made about how high energy alpha particles are emitted in low energy nuclear reactions (see Fig. 11.28). That is, for example, high energy particles up to 100 MeV observed in oxygen-induced reactions, let's say, at 300 MeV. The suggestion was that once we have, let's say, a more violent interaction we're propagating the momentum through the target nucleus. In other words, the projectile nucleus is imagined as a piston moving against the nuclear wall that shoots out an alpha particle on the opposite side of the nucleus. Now this particular model predicts a correlation between heavy ions and light particles emitted in such a reaction. If we confine ourselves to the so-called quasi-elastic region where particles move on a more or less perturbed Coulomb trajectory, we would be led to the conclusion that alpha particles and heavy ions are emitted primarily on opposite sides with respect to the beam axis. Of course, you can think of hundreds of other qualitative models which predict different angular correlations, and I would like to show you one, at least qualitatively, which says that the alpha particles are produced, let's say, in a sequential-decay-type of reaction. In that case the alpha particles and the heavy ions are expected to emerge on the same side of the beam rather close together. Also, you can speak of this in the low energy language in terms of tangential friction being responsible for the emission of alpha particles rather than radial friction being responsible for the emission of alpha particles whch would be the previous alternative picture. We performed the coincidence experiment quite a while ago at the 88-inch cyclotron. Fig. 11.29 shows what we observed. The thick vertical line corresponds to the beam axis. Negative angles for

the detected alpha particles are angles where the alpha particle is detected on the opposite side with respect to the beam axis. The heavy ion detector has been set here at the position of the arrows. And all the observations we have at low energies (the data are shown here for both 310 MeV and 140 MeV) show rather clearly that the alpha particles like to be emitted in the same direction as the heavy ions with respect to the beam axis and not on opposite sides. So this is a nice example at least; we had a theory that could be falsified. I think it is very important that theories can be falsified. If you don't have theories that you can disprove they are pretty worthless, I would say. Another interesting observation with regard to the process of simple projectile break up is the large cross section for $^{13}C+\alpha$-particle coincidences. These are shown as open circles in Fig. 11.29. The ^{13}C-alpha coincidence cross section is nearly as large as the ^{12}C-alpha coincidence cross section, a finding which has not been explained until now. If one goes down in energies the trend is more pronounced. Here the open squares are the ^{14}C-alpha coincidence cross section which is, indeed, very large. I think a lot remains to be done before we can understand those processes even at low energies, but what I would like to see is similar experiments done at relativistic energies because I think we can gain more information by doing them.

Now let me show you that we don't have to limit ourselves to carbon isotopes in order to do these experiments. In fact, the trend of the particles being emitted on the same side of the beam axis (or rather close together) holds also for C-α coincidences, B-α coincidences and Be-α coincidences (Fig. 11.30). The alpha cross section seems to peak in a direction between the beam axis and the detection angle for the heavy ion, and the cross sections are fairly large for all those processes. Let me show you a typical spectrum of Q-values (Fig. 11.31). It's an inclusive experiment again; we are measuring two particles but don't know what's happening to the rest. We also can see the Q-value which we are observing for alpha particles emitted at 9°. So, by summing up all the known energies (i.e., the recoil energy of the target nucleus and the alpha particle energy and the carbon energy, which are known in this particular case), we can deduce a sort of Q-value which also includes the kinetic energies, of course, of the unknown particles. Therefore at 9°, that is, at the position of a maximum coincidence cross section, we have a rather wide distribution of Q-values. There is as much as an average of 30-MeV excitation energy which is still not accounted for by the emission of the fast alpha particles. (I don't know whether you would like to call this quasi- or deeply-inelastic reactions; there are different schools in this matter.) Another interesting phenomenon is that the relative energy of the other particles and the emitted carbon ions is rather low. These particles are emitted at about the same velocities (actually I did not prepare such a plot) but if one compares, at least for the case of ^{12}C-alpha coincidences, the excitation energy spectrum which has been calculated by Georg Wolschin and Jörg Hüfner, one sees rather good agreement. Another interesting feature is that if one changes the alpha detection angle one gets a qualitatively completely different Q-value spectrum. At $\theta_\alpha = 30°$ one observes a very sharp peak for the 3-body Q-value which corresponds to a pure break-up reaction. Apparently we observe a variety of reactions. Depending how we kinematically select our coincidence conditions, we are able to sort out pure break-up

reactions from the more violent processes where we still have a lot of excitation energy deposited in the nucleus. Another rather interesting feature is the alpha particle spectra observed in coincidence with projectile-like fragments (Fig. 11.32). (I really cannot go into all the details of these coincidence experiments because we still have not digested everything we have observed.) Again, this is the selection angle for the maximum cross section of the alpha particles, that is, between the beam axis and the heavy ion axis. And you see that the coincidence alphaparticle spectra are not caused by evaporation from the target residue. More important, they have rather a double hump shoulder, which persists for boronalpha reactions and beryllium-alpha reactions. One would observe such an alpha particle spectrum if one assumes a source which moves with a rather high velocity, in this case it is about 15 MeV/nucleon, and emits particles in forward and backward directions. The high energy group would be alpha particles emitted in forward direction, the low energy group alpha particles emitted in backward direction. One would expect a rather similar observation in the angular distributions (see Fig. 11.30). If alpha particles are emitted sidewise the Jacobian gets rather singular and one would expect sort of an enhancement at the maximum particle-emission angle depending on the relative energy of the alpha particle and the emitting source. This is observed most clearly at 140 MeV for the ^{12}C-alpha reaction which is a break-up type of process. So that is rather well understood, we still have indications of those shoulders for ^{12}C-alpha coincidences at 315 MeV. How these things finally show up really depends on the angular distribution of the primary source. We don't observe those shoulders at all, however, even for ^{13}C-alpha coincidences and ^{14}C-alpha coincidences, a fact we don't understand at present.

Now I would like to talk about one more coincidence experiment which addresses itself to another rather qualitative question concerning the role of the target as a spectator (Fig. 11.33). We have seen that the fireball model, at least in its crude over-simplified way, assumes that we're not making a complete momentum transfer to the target nucleus. The target nucleus just sits there more or less like a spectator. We have decided to look into this, at least at lower energies. In the experiment we look for coincidences between projectile-like particles or projectile fragments and fission fragments. On a triple telescope we measure the particles which are emitted from the projectile, everything from lithium nuclei up to oxygen nuclei. In coincidence with these particles we detect two fission fragments. Of course, we do the experiment on an easily fissionable nucleus, that is, oxygen on uranium at 315 MeV. For the two fission fragments, we measure two quantities each, the energy with which they are emitted in the laboratory system and the position along a position-sensitive surface barrier detector. Thereby we measure the emission angles of those two coincidence fragments. Now we needed one assumption to tell us the direction in which the target nucleus would recoil. Therefore I plotted the recoil momentum of the target nucleus and I hope we have found an assumption that gives us an appropriate description for the average recoil momentum. This is one assumption we have to put in, but once we have this recoil angle for the recoil momentum we can determine the mass ratio from momentum conservation. That is rather easy, because all those quantities are known, i.e., the energy, the recoil angle, and also the detection angles of those fission fragments. Now the other assumption made, which I think is fair enough and only introduces a rather

small error, is that we are to calculate the absolute masses of those fragments. This means we assume that these masses add up to the target mass (if we talk about transfer reaction, it's the target mass plus the transferred mass). So those two assumptions are everything we need for a kinematics calculation. Knowing the masses and energies of the particles we can shift into any frame that we wish. Now there's one parameter that was not taken care of, and that is the magnitude of the recoil momentum. Using this magnitude, corresponding to a certain prescription (which I'll talk about shortly), we can transform these two fission fragments into the recoiling system of the target nucleus. If everything was done correctly, what we should observe is that those two fission fragments are emitted with respect to each other at 180°. To check we need to calculate those emission angles in the moving system, see whether they align, and see whether the sum of those two fission angles is 180°. We can do that for various assumptions and we get various curves on which our experimental points lie. We have done this for these particular cases (Fig. 11.34). Along the horizontal axis the various elements we observed in our reaction are plotted. (I really want to warn you these are preliminary results, and we have to go through analysis once again.) I did not break down isotopes here, for example, because of statistics and also because of the argument of speed in producing these plots. The main trends are rather apparent. If we assume that we are talking about a transfer reaction, that is, when we observe a lithium nucleus we have the mass oxygen minus lithium, the mass-10 nucleus, for example, transferred to the target nucleus, which then sticks. At low energies that's a normal transfer reaction. Therefore if we make this assumption, the recoil momentum is frozen, everything is fixed, and we can crank through our data, event by event, and make the calculation. We then can calculate the average emission angle in the recoiling system. What we get here is the upper points, which you see are not aligned at 180° at all. (Actually a nice check that we are doing reasonably well is to look at whether we are aligned for oxygen. That works.) But the interesting thing is that we are not dealing with a transfer reaction. I think it's the first time that one really has had the feeling of the global features. We know that some of those reactions are transfer reactions, but now we have a global picture where we can say most of those reactions are not transfer reactions. A different approach would be to measure the associated light particle cross sections over 4π, which is a hard job (especially if neutron emission is important). This is another attack on a similar problem. One could also take the other extreme case and assume that the missing mass that is not detected, that is, the difference between projectile mass and the mass of the nucleus we are detecting, travels with the same velocity as the detected particle, i.e., the same velocity as the projectile residue. It doesn't really matter whether it is emitted parallel to it or into the beam direction. The important assumption would be that it has the same energy. That would be a typical de-excitation in a flight or projectile break-up type of reaction. This assumption is represented by the lower points. And again we see that we're not dealing with a pure fragmentation-type reaction. The momentum we are transferring to the target nucleus is not the one we would calculate by assuming that we are making a projectile break-up reaction. We are in an intermediate situation, and of course I could probably give you a couple of recipes to produce some result that on the average aligns with

the observations. You know we are averaging over quite a few angles, and all the fission fragments have the bad characteristic of emitting neutrons in flight, so that the angles are jiggled around. Therefore one really can only speak here of average angles, at least with the statistics presently available. One assumption that at least gives us a feeling for the amount of momentum transfer we are missing is that the mass difference between projectile and light particle moves in the beam direction (which is the easiest assumption) with a velocity that is half the velocity of the projectile. With this recipe everything is frozen. Now we can calculate the momentum transfer to the target nucleus and crank through our kinetmatic calculations, now giving the intermediate points that are aligned at 180°. That would be a prescription that on the average produces the observed results. Now I want to issue a warning here because very often we are misunderstood when we are averaging over individual events. Although we have a recipe that calculates the average momentum transfer, each individual case could behave completely differently. It could be that part of the reactions are really normal transfer reactions. That is, half the reactions would give us such a line as is shown here. The other half of the reactions would be normal break-up-type reactions. If we then sum over everything agin, we come up with something like this. (And I'm pretty sure that very similar things happen with the fireball model.) We are averaging over so many things that finally a rather trivial recipe can reproduce the observations. But at least it's one step forward. We have a feeling for what the global trends are on the average, although no more than that as yet. I don't think the whole picture lines up into one consistent set yet, but I think you can produce other assumptions as well. I don't think this is unique; unfortunately, any inclusive experiment is not unique. I think that is one lesson we have learned. We will have to study higher moments of the momentum transfer distribution to make progress. I hope that in future experiments we can break these things down into more qualitative and perhaps even more quantitative statements than that.

Now, let me show you one more thing, which unfortunately we have not worked out completely. We have to repeat the experiment because of efficiency problems in our detection system (Fig. 11.35). Let us look at fission-fission coincidences and not require a coincidence with the projectile residue. By doing this we are taking one step back by going to a more inclusive experiment than the one I just talked about. For simplicity I just summed up the angles for the fission fragments which are emitted in the laboratory system. The observation that one then has is shown here by the black points. There is a sort of a double humped curve, one small peak at an angle slightly smaller than 180° and then we have one peak around 140°. I really cannot tell you where it bends over because we had to fold in efficiencies and that was getting marginal in our data. At least one thing is rather interesting. Emission at 180° implies that the fissioning nucleus sits at rest in the laboratory. That would mean that we have no momentum transferred to the target nucleus. If we go to smaller opening angles we have more and more momentum transfer to the fissioning nucleus. Actually, the opening angle corresponding to full momentum transfer, that is, a full compound nucleus reaction, would be about 140°. Therefore we do have quite sizeable fusion reactions which answers a question that George Bertsch had asked me. Now I cannot tell you right now whether those fusion reactions involved 100%

momentum transfer of the target nucleus or 90%, but it's in this order of magnitude. We are not talking on the average of 50% momentum transfer. So these nuclei still stick at 20 MeV/nucleon. It's interesting to see how this develops with energy towards high energies because at some stage we do believe that they don't stick anymore and the momentum transfer to the target nucleus will be incomplete. The small hump centered about 170° corresponds to a low momentum transfer. If we now look for particles that we detect in coincidence with the fission fragments in our triple coincidence experiment and, first of all, sum over everything from low energy alpha particles up to oxygen, we get a correlation curve which would correspond to the solid line. So those particles, especially the hump, correspond mainly to fission induced by peripheral reactions. One can break this down even more precisely if one looks at particles in coincidence with oxygen nuclei, shown here by the dashed curve. You see we are only making a very small momentum transfer. In coincidences with boron nuclei (triangles), we have a rather broad curve but it peaks at a larger momentum transfer.

Now one thing which I find rather interesting at this stage (and I just want to point out our future intentions perhaps) is to look at light particle emission in coincidence with these fission fragments. You see, now we have a tool to determine, at least on a crude basis, whether we are talking about the peripheral-type reactions or about a central-type collision. This is one of the impact-parameter measuring devices we are dreaming of finding at relativistic energies. At lower energies the situation is rather simple because these nuclei stick if they hit head-on. If we look at the high energy protons we observed in the inclusive experiments up to energies of 100 MeV/nucleon in coincidence with fission fragments, however, we should at least be able to tell whether they are excusively produced in peripheral-type reactions (that would then favor pictures like tangential friction or decay in flight) or whether they are indeed also produced in central-type collisions. This would be a rather interesting feature if we make a compound nucleus reaction and eject a proton with 100-MeV energy. That is something that I cannot talk about now, and I think I should stop when I don't know the experimental answers anymore.

Let me perhaps just for the fun of it remind you of a picture Bromley used to show at conferences years ago (Fig. 11.36). I have taken the liberty to block out the underlining original text and quote a phrase from Masefield that we found on some advertisement during a Bevalac run. It said "All I ask for is a tall ship and a star to steer her by." Now, we do have a tall ship, the Bevalac, which is pretty tall, at least, and I hope that in future we can find the star to steer her by.

ACKNOWLEDGEMENTS:

T. AWES, B. BACK, J. BARRETTE, U. BERG, K. VAN BIBBER, F. BIESER, P. BRAUN-MUNZINGER, H. BREUER, S.A. CHESSIN, H. CRAWFORD, P. DOLL, P. DYER, H. FARAGGI, J. GEAGA, D. GREINER, J.Y. GROSSIORD, H. HECKMAN, D.L. HENDRIE, J.L. LAVILLE, M.J. LEVINE, P. LINDSTROM, J. MAHONEY, A. MENCHACA-ROCHA, M.C. MERMAZ, W.G. MEYER, A. MIGNEREY, C. Mc PARLAND, C. OLMER, L.S. SCHROEDER, D.K. SCOTT, J.T.H. SYMONS, V.E. VIOLA, Y.P. VIYOGI, G.D. WESTFALL, H. WIEMAN, K.L. WOLF

Fig. 11.1

Intermediate Energy Heavy Ions - from the Low Energy Perspective

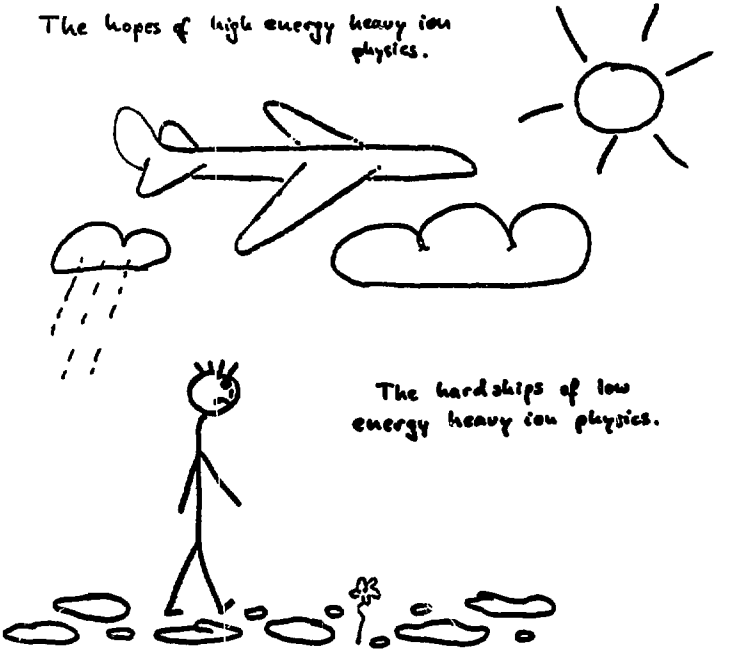

Fig. 11.2

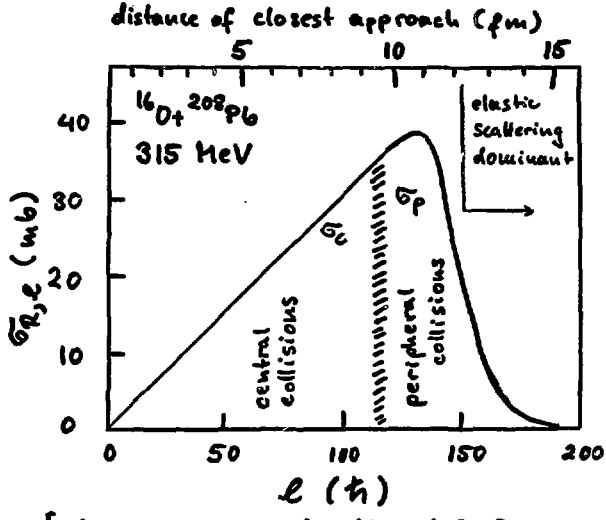

[$A_p \lesssim 50$ amu for this talk]

peripheral collisions : elastic, quasi-elastic, deeply inelastic
↓
fragmentation

central collisions : fusion, fusion-fission
↓
? nuclear fireball, shock waves, pion condensates, density isomers ?

Fig. 11.3

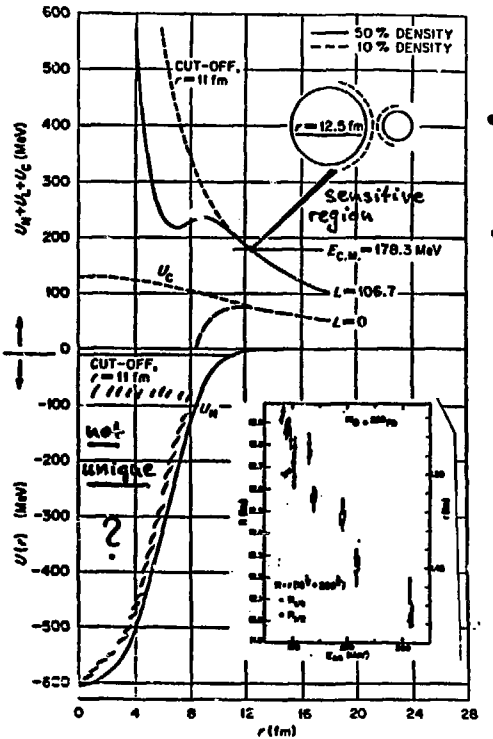

Fig. 11.4

Elastic scattering

- Sensitive only to extreme tail region of optical potential
- sensitive to slightly smaller distances at higher energy; resolve some ambiguities (?) [energy dependence of optical potential.]

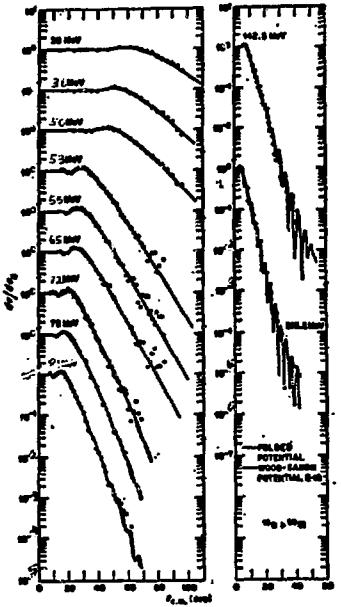

$^{16}O + {}^{28}Si$

energy dependence at forward angles (Cramer, et al.)

elastic scattering

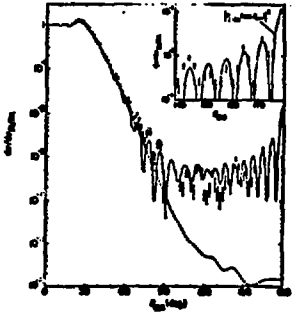

Surprise at backward angles!

(Braun-Munzinger et al.)

Fig. 11.5

$$S_\ell = S_\ell^\circ \cdot \left[1 + i \frac{\mathcal{D}_\ell \cdot e^{2i\phi}}{\ell - \ell_0 - i\Gamma/2}\right]$$

growing excitement in low energy heavy-ion community: resonant structures observed in excitation functions; also for transfer!

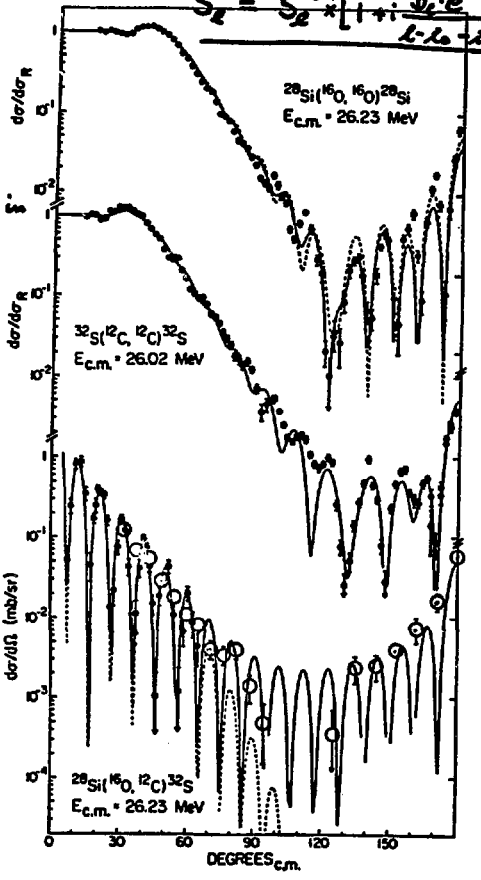

Fig. 11.6

Energy dependence of transfer reactions

$^{208}Pb\,(^{16}O, ^{15}N)\,^{209}Bi$

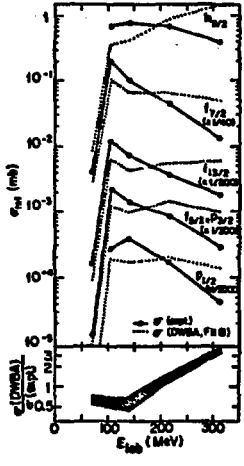

(Olmer, et al)

DWBA fails to predict energy dependence of transfer cross sections by ~ factor 5.
(About same problem for all states — relative strengths "correct" at any energy.)

Fig. 11.7

Deeply inelastic collisions.

low energy peripheral collisions

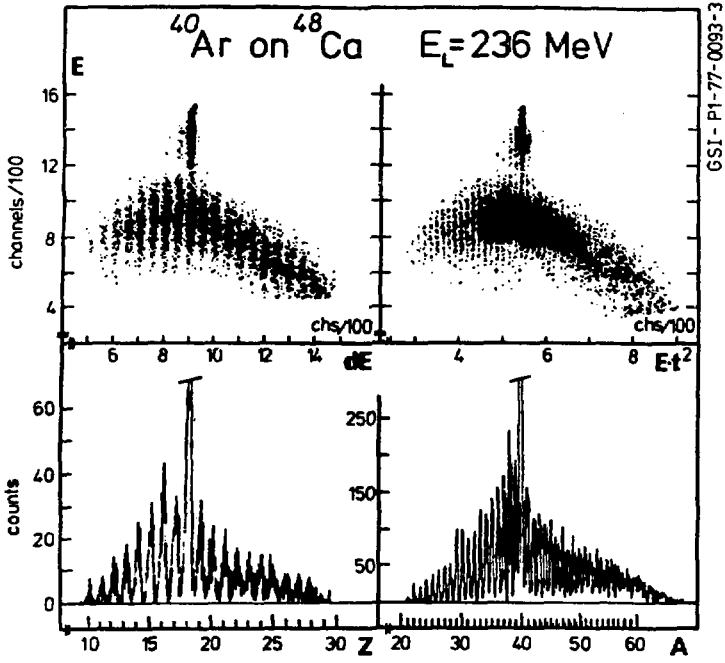

$(E - V_c)/A \approx 3.5$ MeV/A, $E_\ell \approx V_c$ ●

large amounts of energy, mass, angular momentum, charge transferred.

Fig. 11.8

Sharing of excitation energies

$^{86}Kr + ^{166}Er$ at 602 MeV (Eyal, et al.)

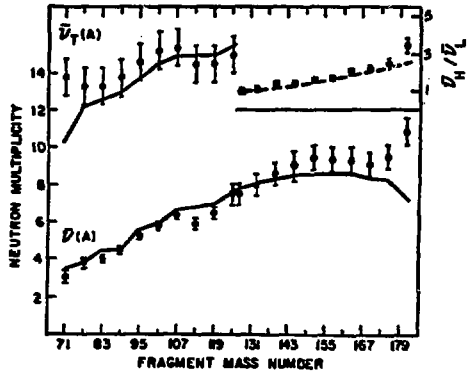

- $\nu_H / \nu_L \sim M_H / M_L$

  ⇝ excitation energy is shared in proportion of the mass.

  Consistent with thermal equilibrium:

  $$E^* \sim \frac{A}{a} T^2 \sim A T^2$$

  T = const:

  $$E_1^*/E_2^* = A_1/A_2$$

Fig. 11.9

Isotope distributions

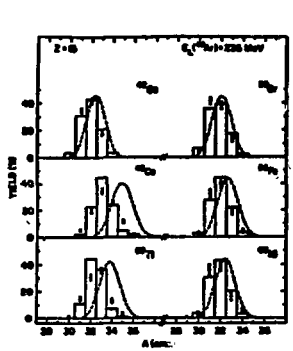

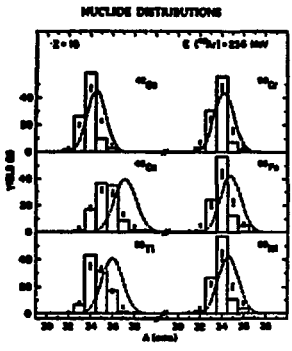

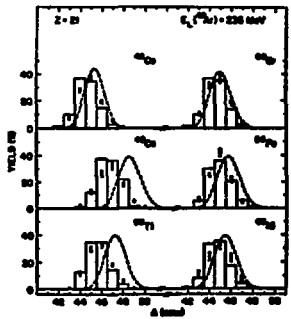

..... primary distribution (charge equilibrium)

experimental isotope distribution

secondary distribution (modified by sequential decay)

Barrette, et al.

Fig. 11.10

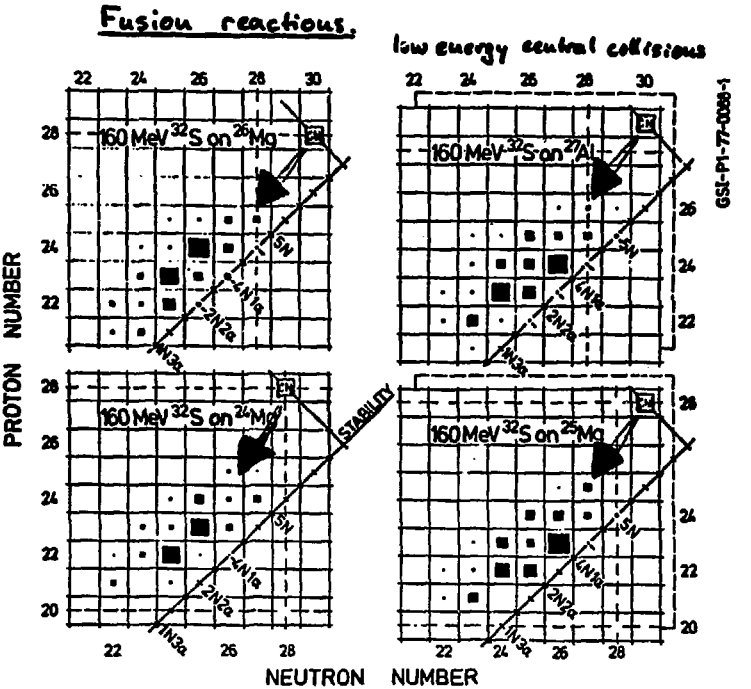
Fusion reactions.
low energy central collisions
160 MeV 32S on 26Mg
160 MeV 32S on 27Al
160 MeV 32S on 24Mg
160 MeV 32S on 25Mg
EN
SN
1N2α
2N2α
1N3α
STABILITY
PROTON NUMBER
NEUTRON NUMBER
GSI-P1-77-0088-1

Fig. 11.11

Isotope cross sections for heavy-ion fusion reactions. (Pühlhofer et al.)

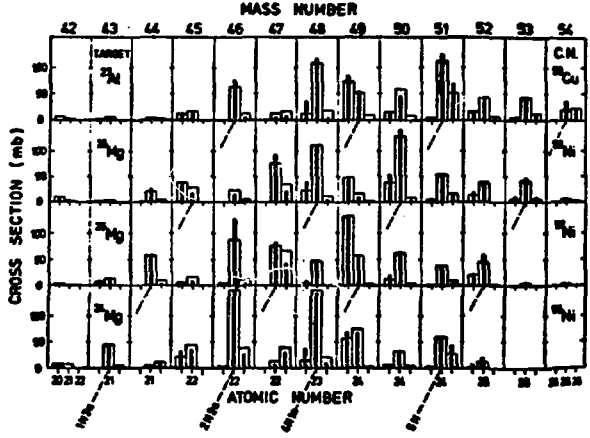

Fig. 11.12

low energies: entrance channel limitations:
↝ fusion barriers, critical radii.

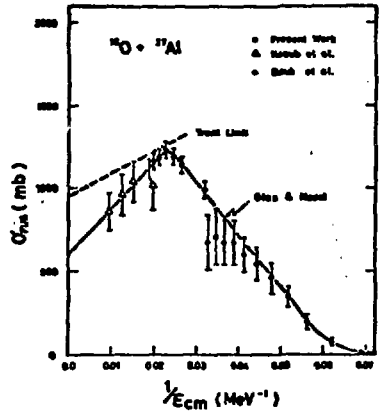

Energy dependence of fusion and deeply inelastic reactions?
At high energies still equilibrium?
Complete or incomplete momentum transfer to target nucleus? (spectator?)

Fig. 11.13

Relativistic energies

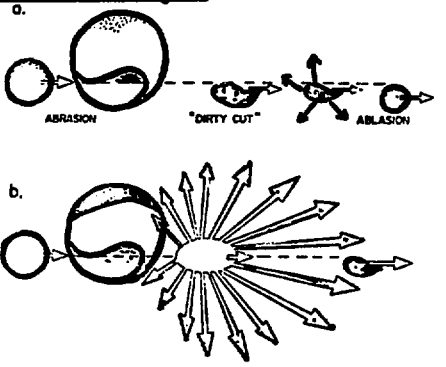

XBL 777-9683

- Small momentum transfer to target and projectile residues.
- full momentum transfer in overlap region: nuclear fireball

(models are based on inclusive experiments; correlations ?)

Fig. 11.14

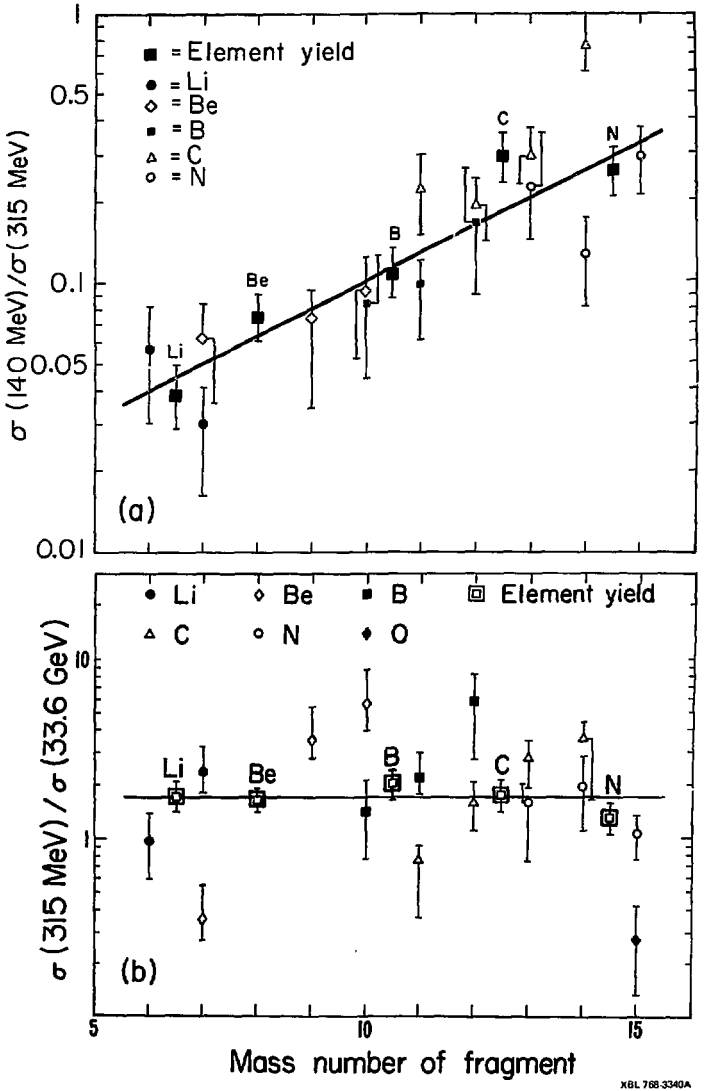
■ = Element yield
● = Li
◇ = Be
▪ = B
△ = C
○ = N
σ (140 MeV)/σ (315 MeV)
1
0.5
0.1
0.05
0.01
Li
Be
B
C
N
(a)
● Li
◇ Be
▪ B
▣ Element yield
△ C
○ N
♦ O
σ (315 MeV) / σ (33.6 GeV)
10
1
(b)
5
10
15
Mass number of fragment
XBL 768-3340A

Fig. 11.15

no charge equilibration at relativistic energies

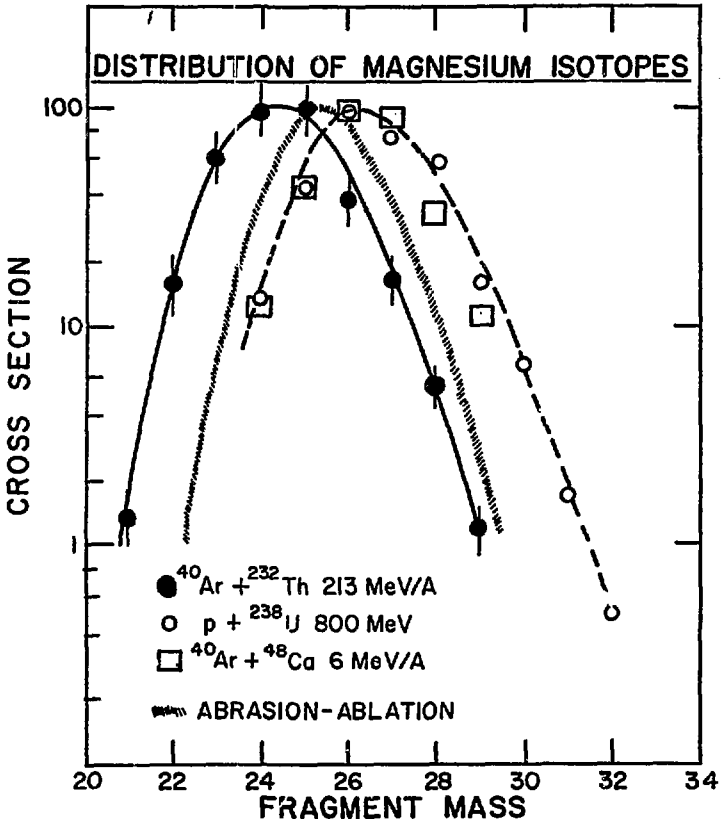

XBL 786-9165

N/Z (^{48}Ca) : 1.40

N/Z (^{40}Ar) = 1.22

N/Z (^{232}Th): 1.58

Fig. 11.16

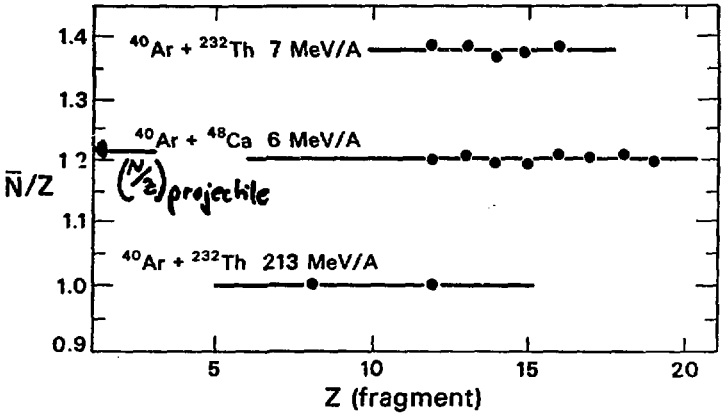

XBL 786-1053

Questions:

- Correlations at relativistic energies?
- Influence of de-excitation on primary fragments?

Fig. 11.17

Projectile fragmentation at relativistic energies:

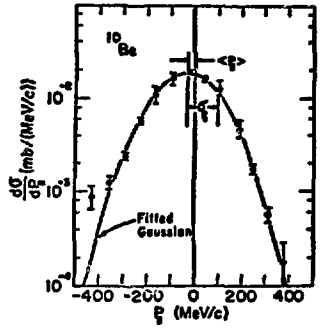

Greiner, et al.

- Gaussian momentum distributions in frame moving with velocity only slightly less than projectile velocity. In projectile frame:
  $d^3\sigma/dp^3 \sim \exp[-(\vec{p}-\vec{p}_0)^2/2\sigma^2]$. $p_0 < \sigma$
  - $\sigma^2 = \sigma_0^2 m_f (m_p - m_f)/(m_p - 1)$
- Thermal equilibrium of excited projectile:
  $\sigma_0^2 = m_N \cdot T \cdot (m_p - 1)/m_p$
- Fast statistical fragmentation process:
  $\sigma_0 = p_F/\sqrt{5}$

Fig. 11.18

Energy spectra observed at grazing angle at low energies.

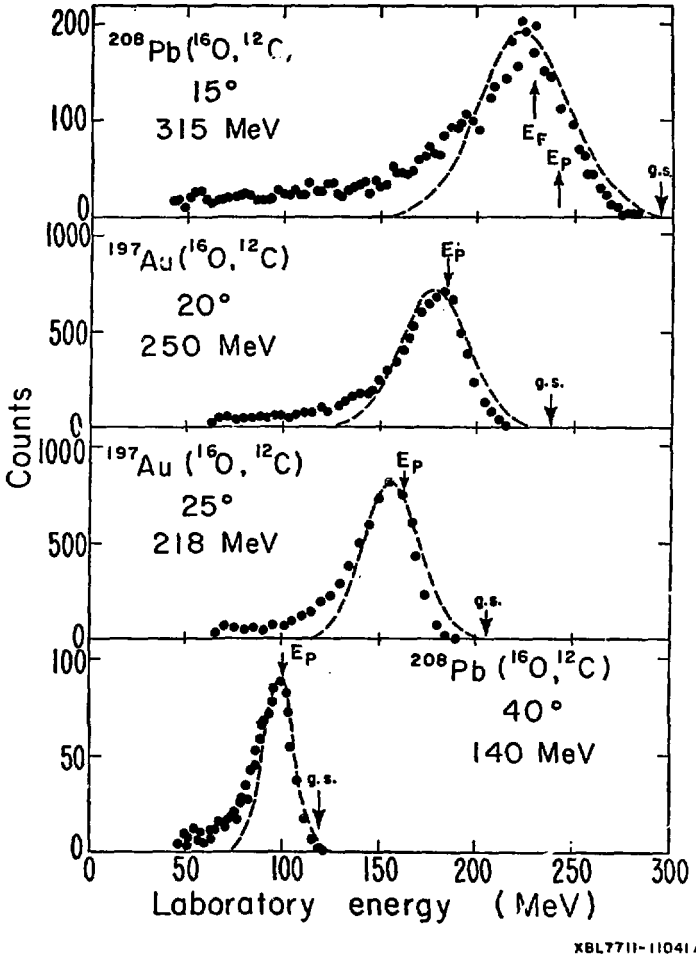

Fig. 11.19

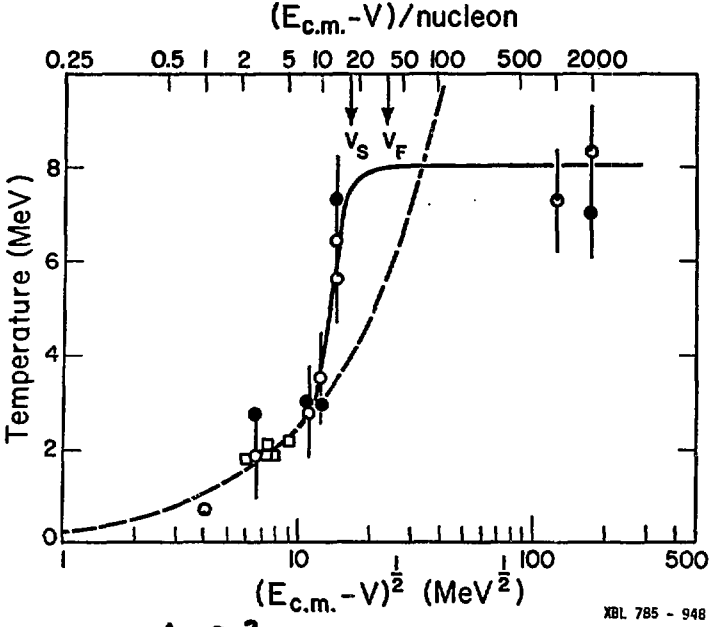

- $T = \dfrac{A_p \sigma^2}{m_N A_f (A_p - A_f)}$

- ▫ ● Temperature from isotope cross sections (Volkov, Lukyanov)

- ▫ data from Volkov, et al.

Fig. 11.20

Projectile fragmentation: ^{40}Ar, 213 MeV/A

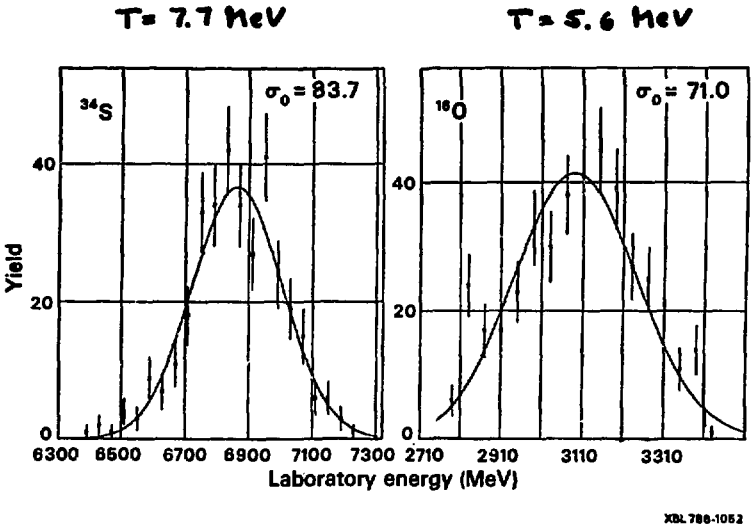

[Is the use of a temperature a meaningful concept ?]

Fig. 11.21

Projectile fragmentation : ^{40}Ar , 213 MeV/A

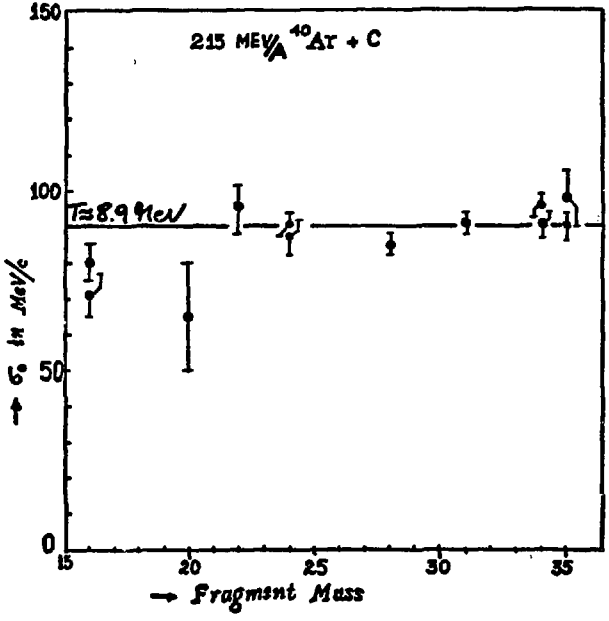

Fig. 11.22

van Bibber, et al.

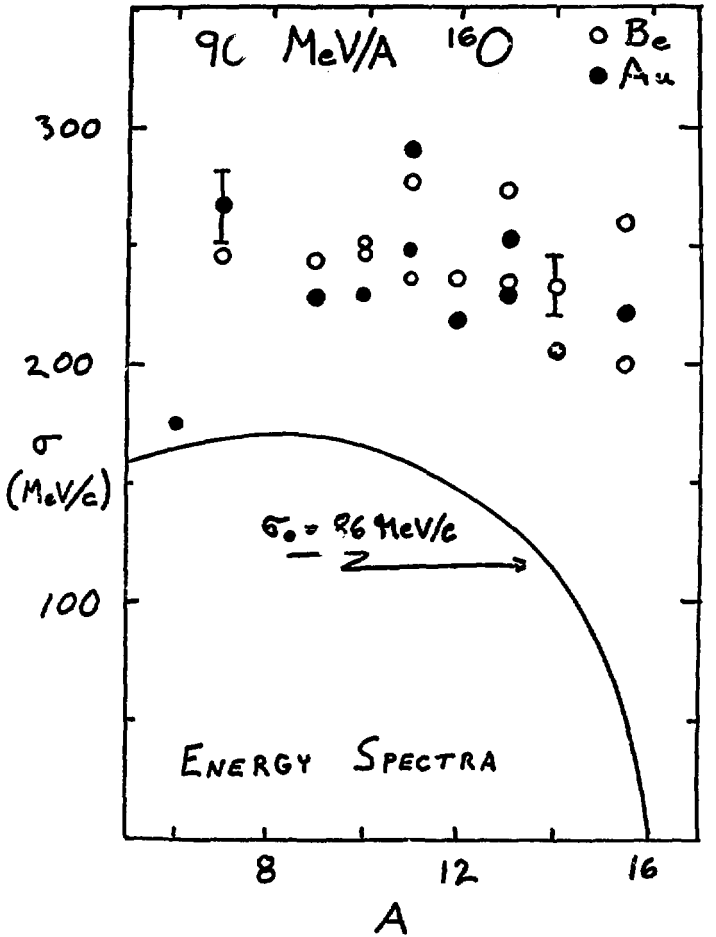

20 MeV/A is not asymptotic !

XBL 786-9141

Fig. 11.23

Inclusive proton spectra:

Fireball model
(Westfall et al.)

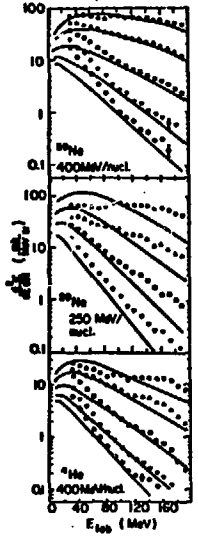

Emission from a moving source: ($v_s \approx 0.5\ v_p$)

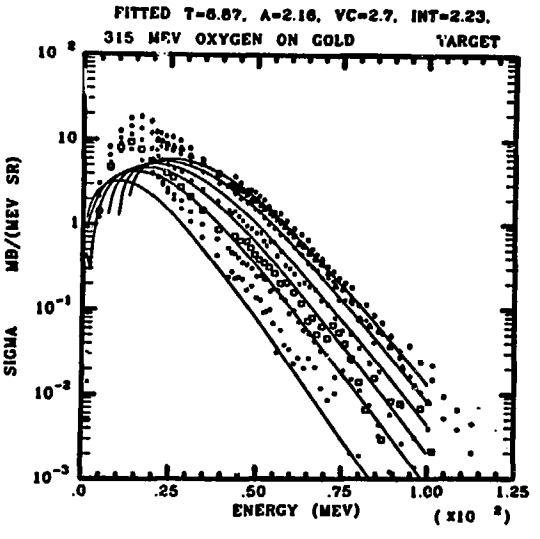

Fig. 11.24

Rapidity vs. p_T diagram for

$^{16}O + Au \rightarrow p + X$ at 315 MeV

(J. Symons, et al.)

• • Contours of $\frac{1}{p}\frac{d^2\sigma}{dE\,d\Omega}$

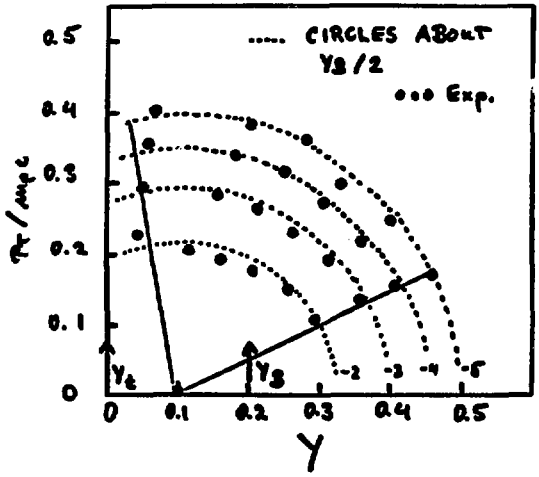

Fig. 11.25

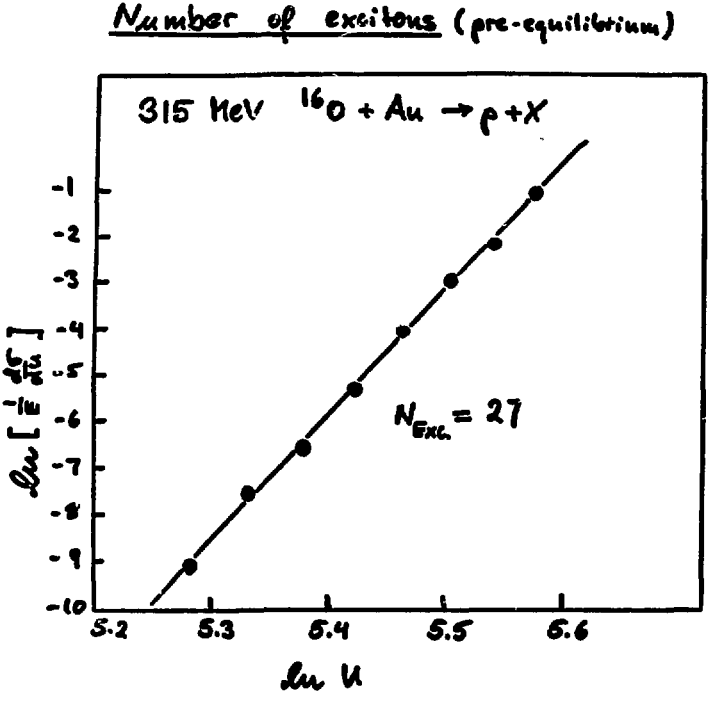
Number of excitons (pre-equilibrium)
315 MeV $^{16}O + Au \rightarrow p + X$
$N_{Exc.} = 27$
$\ln\left[\frac{1}{E}\frac{d\sigma}{dU}\right]$
-1
-2
-3
-4
-5
-6
-7
-8
-9
-10
5.2
5.3
5.4
5.5
5.6
ln U

Fig. 11.26

Hybrid model predictions

315 MeV $^{16}O + Au \rightarrow p + X$

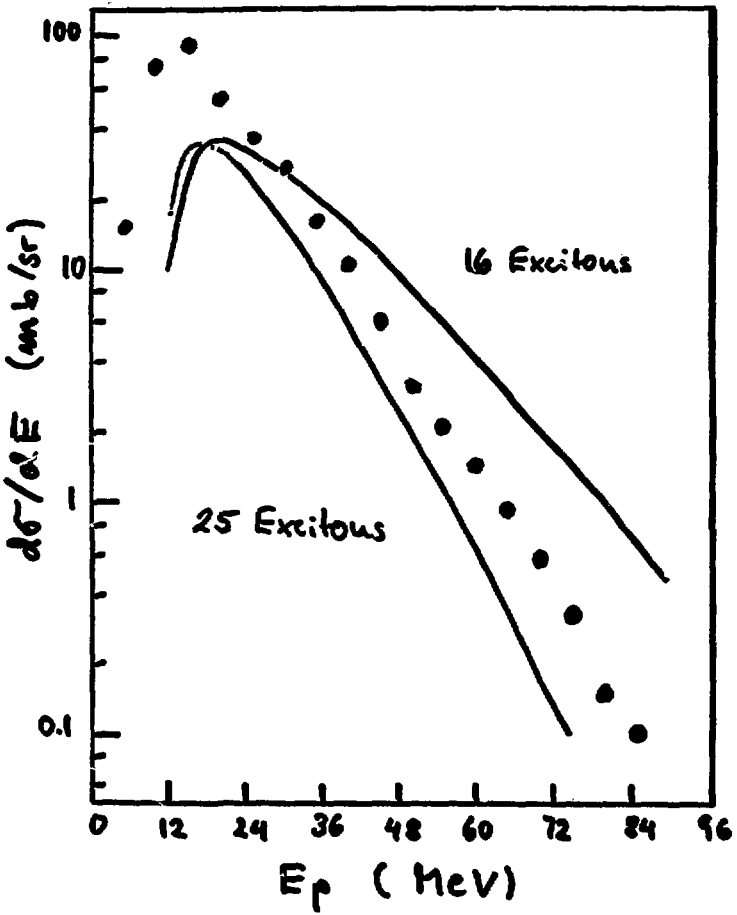

Fig. 11.27

Production of fast α-particles

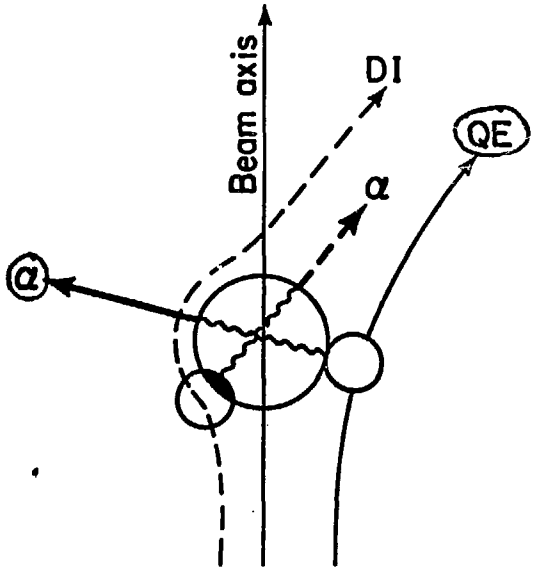

(a)

piston model (Gross, et al):
correlations on opposite sides of beam axis

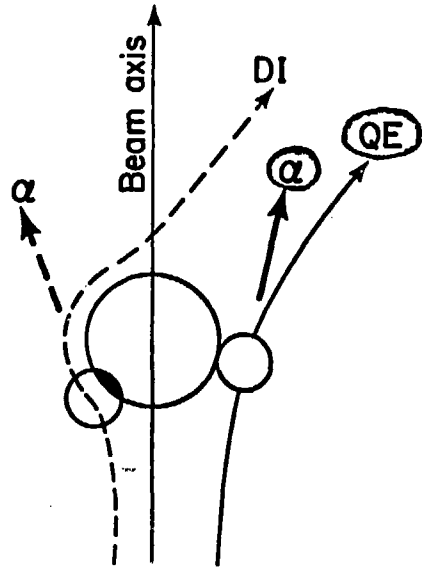

(b)

XBL 774-695

as opposed to, e.g., tangential friction or sequential decay

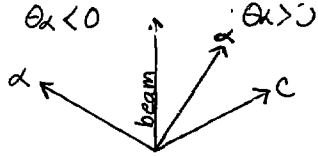
θα<0
θα>0
α
beam
α
c

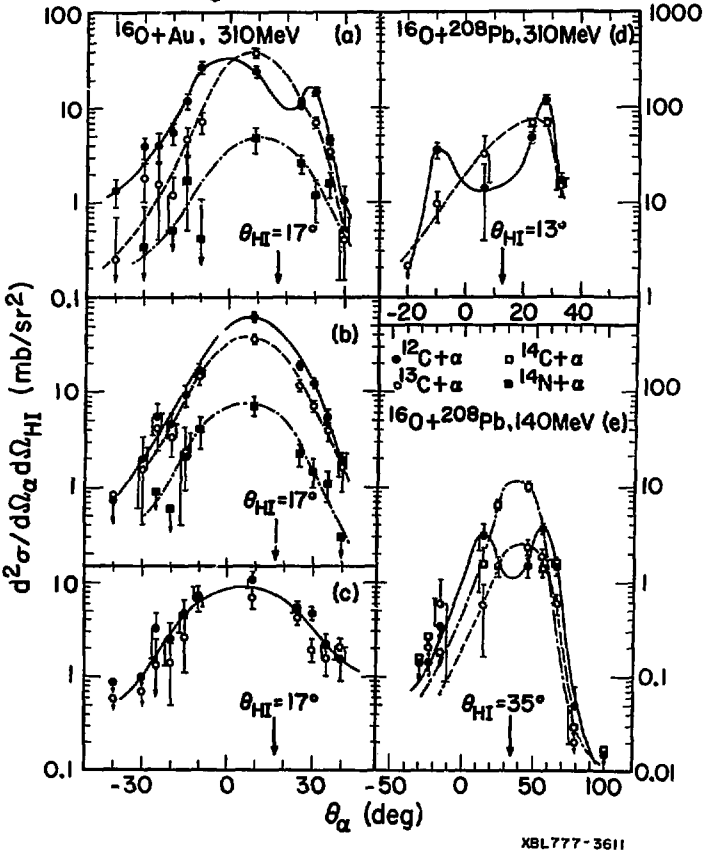
16O+Au, 310MeV (a)
16O+208Pb,310MeV (d)
θHI=17°
θHI=13°
(b)
12C+α
14C+α
13C+α
14N+α
16O+208Pb,140MeV (e)
(c)
θHI=17°
θHI=35°
d2σ/dΩαdΩHI (mb/sr2)
θα (deg)
XBL777-3611

Fig. 11.29

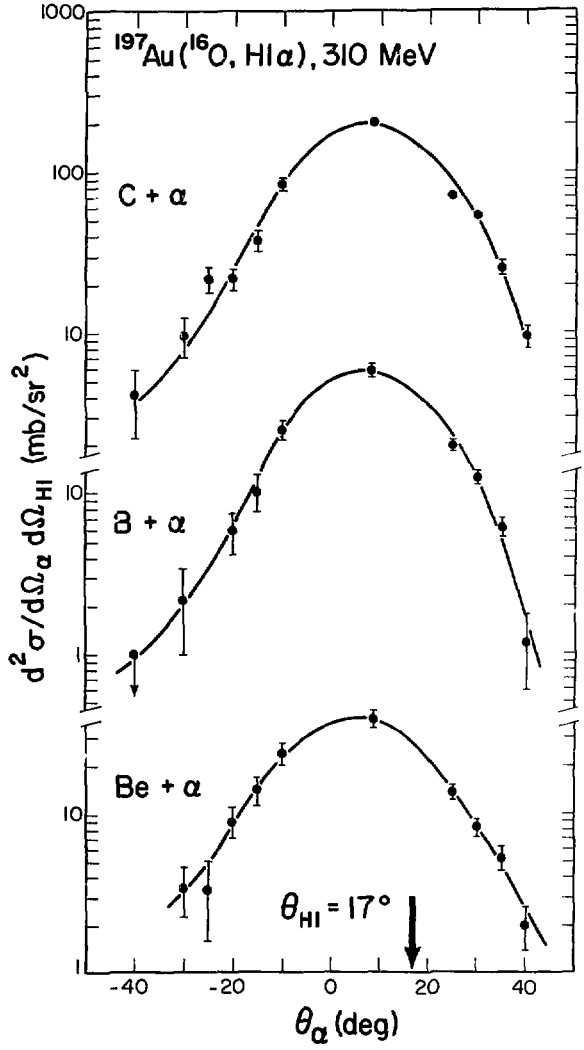

XBL 778-1579 A

Fig. 11.30

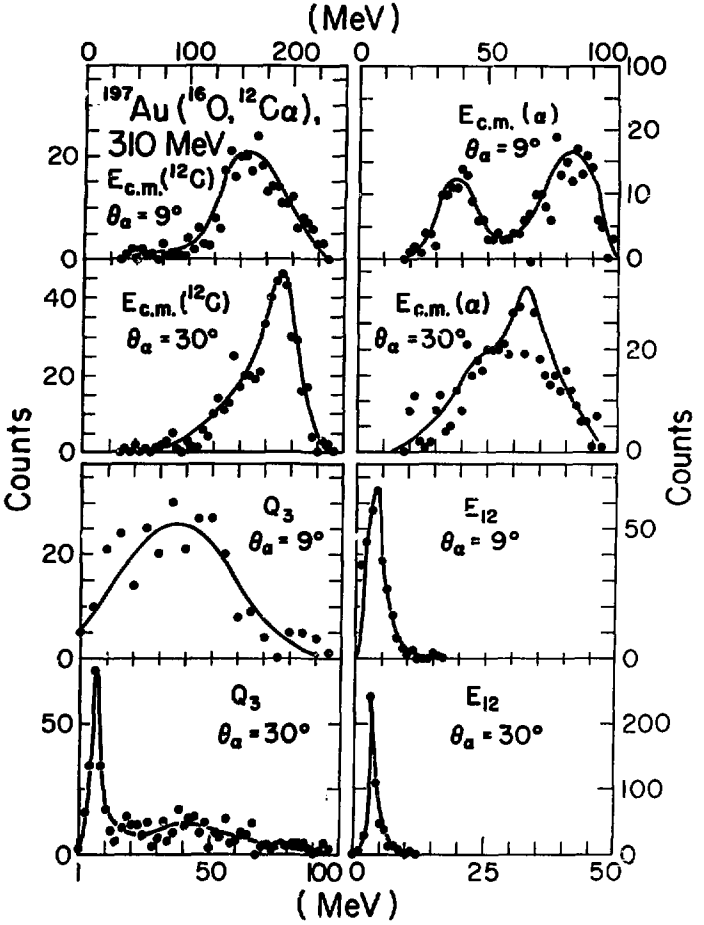
(MeV)
0
100
200
0
50
100
^{197}Au (^{16}O, ^{12}Cα),
310 MeV
$E_{c.m.}(^{12}C)$
$\theta_\alpha = 9°$
$E_{c.m.}$ (α)
$\theta_\alpha = 9°$
$E_{c.m.}(^{12}C)$
$\theta_\alpha = 30°$
$E_{c.m.}$ (α)
$\theta_\alpha = 30°$
Counts
Counts
Q_3
$\theta_\alpha = 9°$
E_{12}
$\theta_\alpha = 9°$
Q_3
$\theta_\alpha = 30°$
E_{12}
$\theta_\alpha = 30°$
1
50
100
0
25
50
(MeV)
XBL 778-1582

Fig. 11.31

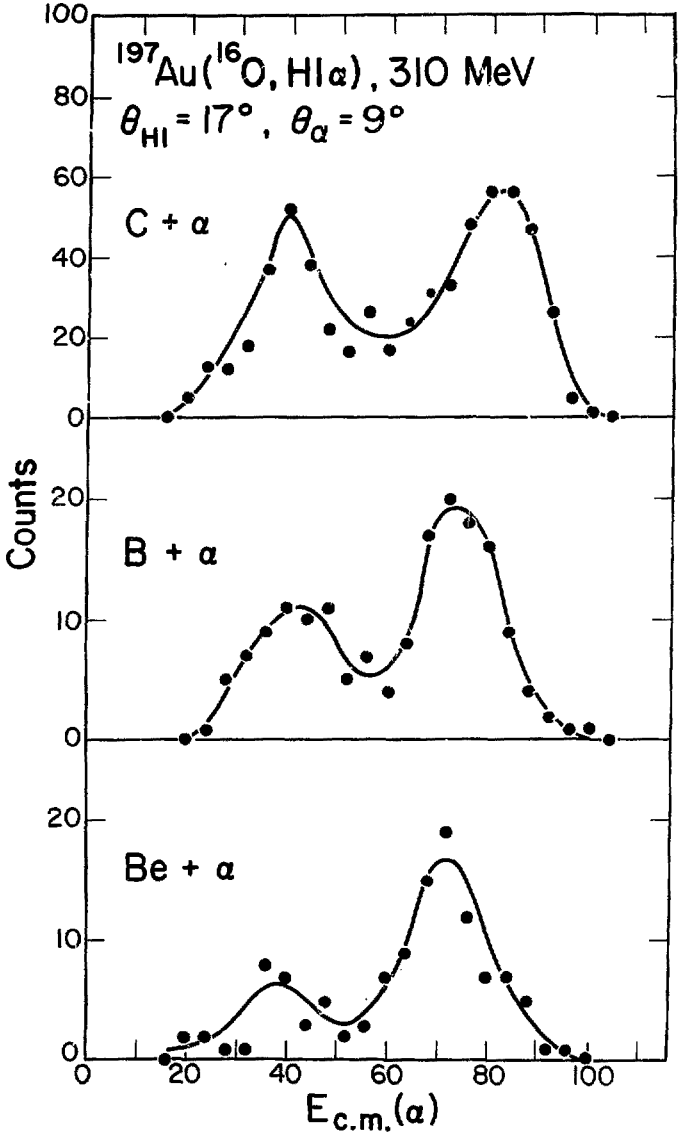

Fig. 11.32

XBL 778-1578 A

Momentum transfer to target ?

Argonne, LBL, Maryland, NSU - collaboration.

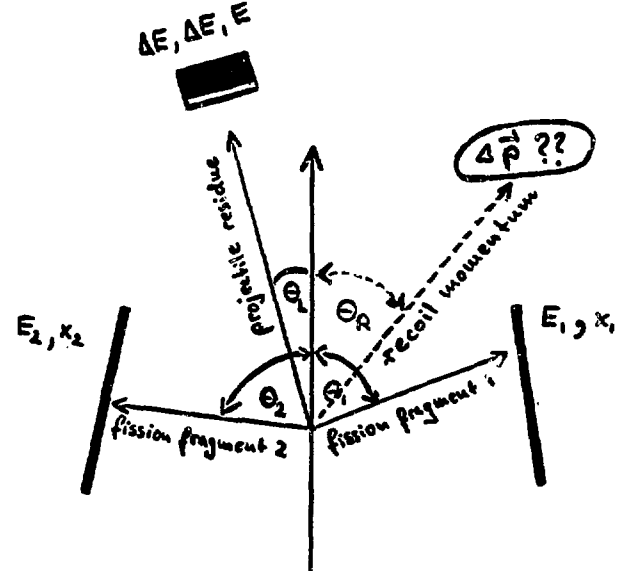

$$\frac{M_1}{M_2} = \frac{E_2 \sin^2(\theta_R + \theta_2)}{E_1 \sin^2(\theta_R - \theta_1)} \quad , \quad M_1 + M_2 = M_0$$

Test colinearity of fragments in recoiling system using assumption on $\Delta\vec{p}$.

Fig. 11.33

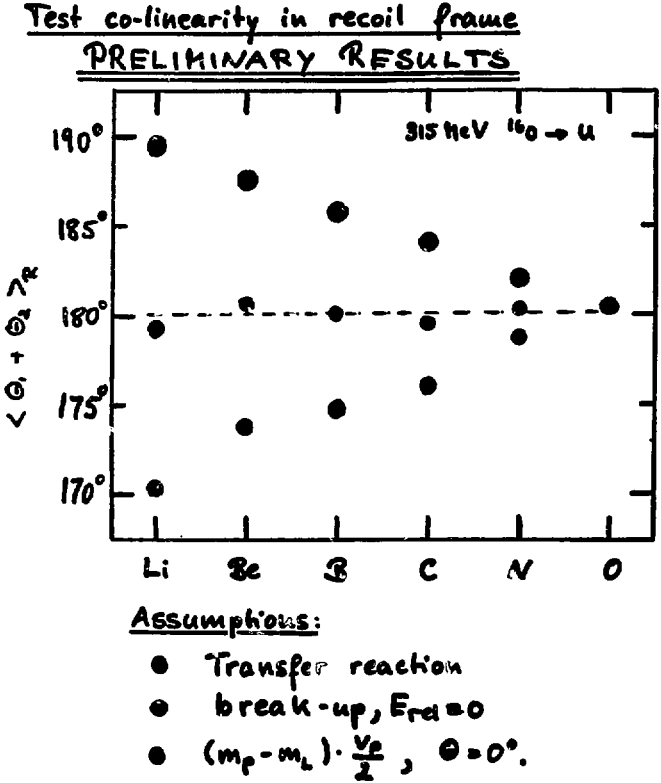
Test co-linearity in recoil frame
PRELIMINARY RESULTS
315 MeV $^{16}O \rightarrow U$
190°
185°
180°
175°
170°
$\langle \Theta_1 + \Theta_2 \rangle^{lab}$
Li
Be
B
C
N
O
Assumptions:
Transfer reaction
break-up, $E_{rel} = 0$
$(m_p - m_t) \cdot \frac{v_p}{2}$, $\Theta = 0°$.

Fig. 11.34

Central vs. peripheral collisions.

PRELIMINARY RESULTS

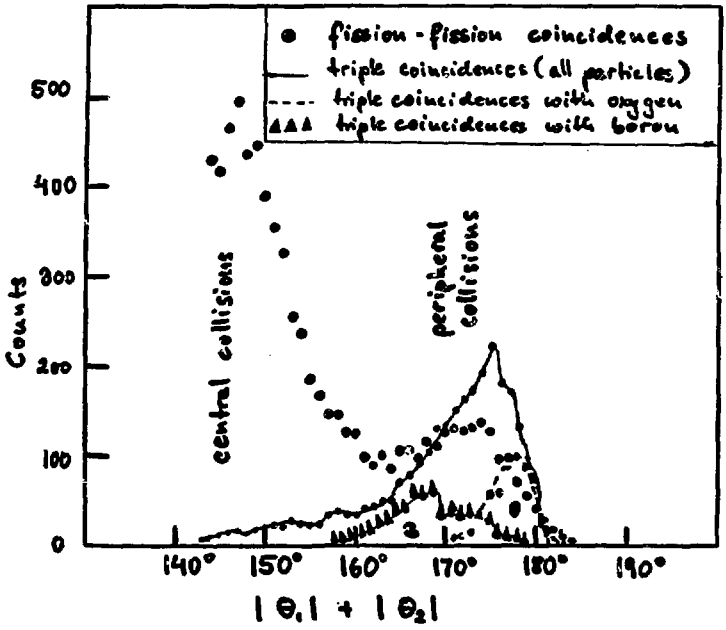

Fig. 11.35

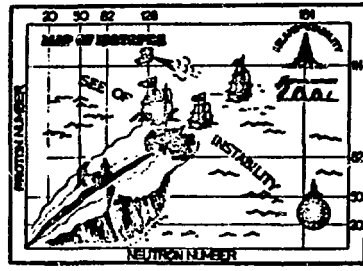

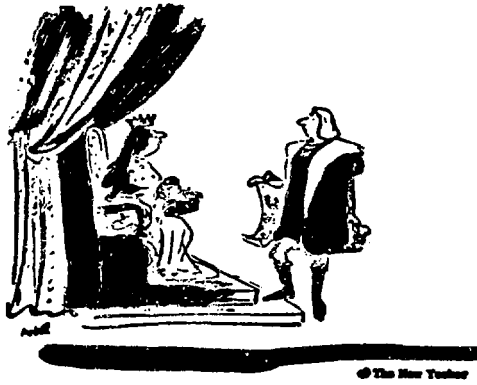

Masefield:

"....all I ask for is a tall ship
and a star to steer her by."

Fig. 11.36

WHAT LIES BEYOND INCLUSIVE MEASUREMENTS?

Steve E. Koonin

The metaphor of the "Flowers and Weeds" is something that's run continually through the series of summer workshops that we've had at Berkeley in the last couple of years. If you'll let me indulge myself for a little bit I'd like to try to summarize what might have been the mood of the conference two years ago within the framework of that metaphor. It might look something like Fig. 12.1, There were a lot of very pretty Flowers standing up very tall from some ugly brown Weeds down at the bottom. With very little effort we were going to be able to pick those Flowers. Listening to all the experimental and theoretical talks that I've heard this week, I might try to portray the present mood of the people doing relativistic heavy ion physics by an alternative picture that might look something like Fig. 12.2. It's pretty clear that the Weeds have gotten a lot bigger, but on the other hand there are a few more Flowers showing up. Also, and this is perhaps most important, we've now got much more powerful tools with which to do the harvesting, and perhaps to learn something about nuclear physics.

The title of my talk today is "What Lies Beyond Inclusive Measurements?" What I want to do first of all is to try to make a critical and cautious appraisal of relativistic heavy ion physics currently; second, to try to highlight some of the more significant experimental results that we've heard this week; and, finally, to give you a somewhat personal and biased view as to which direction this field should be heading the next couple of years.

My talk can be divided into five sections according to roughly decreasing impact parameter: 1) peripheral reactions, 2) direct dynamics, 3) collective dynamics, 4) evidence for and against equilibrium, and 5) the use of nuclear interferometry (a very hot topic now) to probe the collisions that we've been hearing about all week.

Let's start off with the peripheral reactions. The previous speaker covered them well and already said many of the things that I would like to say, so I guess they must be right! What's "old" first of all? What did we understand about peripheral reactions before we got all the new data that we have seen here? There was factorization and limiting fragmentation, concepts which by now should be familiar to most of this audience. We also understood that there was a correlation between the net parallel momentum transfer to the fragments and the change in fragment mass, and that there was a rather simple correlation between the width of the fragment momentum distribution and the mass of the fragment. What's "new" now are several things. First of all, there's been a detailed study of the spectra of fragments in the fragmentation peak by Anderson et al. This data hasn't been discussed at this conference, so let me show you an example of it (Fig. 12.3). This is the spectrum of protons in the fragmentation peak from alphas on various targets at 0°, plotted as a function of the proton momentum. You can see that there is a near independence in the shape as a function of the target. Moreover, we now have some rather detailed and accurate data concerning these high

momentum tails, which stick out well beyond any reasonable momentum you might expect to be present in the nuclear wave function. At the same time Anderson's measurements show us that this peak is anisotropic. Here's a contour plot of the peak in the plane of rapidity and transverse momentum (Fig. 12.4). The peak is very large near the beam rapidity and then falls off in some exponential way, which is anisotropic with respect to directions parallel and transverse to the beam. This is something rather new in peripheral reactions.

At the same time we also heard from Van Bibber et al. (in the last talk) about some energy dependence in the fragmentation peak (Fig. 12.5). Here are the widths of the momentum distribution for the reactions O + Au and Be in the forward direction. The widths measured are above, and the widths taken from systematics of the much higher energy 2-GeV data are below. There's a clear discrepancy and we really don't understand it. Perhaps there is a change in the reaction mechanism at this point.

What is needed is fairly clear from looking at the data and at things we have seen in previous years. First of all, there are gaps in the energy and beam dependence. We'd like to know what happens in the region around 100 MeV/nucleon. Secondly, the Anderson data are striking in their systematics and it is clear that somehow it would be nice to relate them to nuclear structure. One possible way of doing that would be to view the target as a time-dependent nuclear field, which was suggested a long time ago by Feshbach et al., and try to relate the data to the nuclear structure function (namely the response of the nucleus when you give it a kick with momentum k and energy ω). There's clearly some work here that might be done by the structure people.

In order to get a better hold on what is going on in the fragmentation process we might try to look at correlations within the fragmentation peak. In particular, try to pick up the whole fragment as it is breaking up, asking the following questions: 1) how does it break up, and 2) is it an evaporation process or does it split apart into two pieces immediately under the influence of the time-dependent nuclear field? By looking at the angular distribution of the fragments in the fragmentation peak we might be able to say something about the angular momentum transfer. It would be very nice to do that kind of experiment in coincidence with the measured shift in the momentum along the beam directions. The more the shift, the harder the collisions. It would be interesting to see how these quantities, the break-up mode and the angular momentum transfer, change with $\Delta p_{\parallel}$.

Something that seems to have escaped many people here is the relation of the beam fragmentation studies to some of the target fragmentation work that we saw by the more traditional nuclear chemists. Let me show you an example of what might be called limiting target fragmentation (Fig. 12.6). We are talking here about Ar + Cu at 2 GeV/nucleon (these are some data from Haustein). You can see that if you plot the ratio of the cross section for producing a given product from argon to that from protons there is a very nice uniformity in the ratios. This indicates that the copper falls apart more or less independently of the way it is excited.

Clearly what is needed at this point is some simple way of deciding how a nucleus disassembles, a disassembling theory, if you like. Let me show you some data from Porile et al. (Fig. 12.7). This is C + Ar at 2.1 GeV. You can see that the data can be well reproduced by a rather complicated evaporation and cascade calculation by Zeev Fraenkel et al., so what we really need is some simple way of understanding how a very excited nucleus falls apart. Does it fall apart into several large chunks or does it emit many light particles sequentially? This seems to be a very interesting theoretical problem. One possible way to approach this would be to simply count phase space in the same way that Fermi did a long time ago for pion production in proton-proton collisions, and just ask how consistent are these curves with the available phase space.

I am no expert on peripheral reactions, so let me turn to something else I do know a little more about. Next I will talk about what I would call direct dynamics and the signatures that we have seen this week. We're not dealing with a totally equilibrated process, but are instead observing something with a much more elaborate dynamical evolution (Fig. 12.8). The direct dynamics is something that you could call the first step processes, the first things that happen when two nuclei collide. As you will see in a second, they have a very good kinematic signature that can be picked out of the data very simply, and we are starting to do that. I think it is clear that for the future progress of the field, we have to learn how to remove these rather uninteresting and trivial direct dynamics from the data before we can start to talk about fireball, firestreak, and any other equilibrated models. There is already direct experimental evidence that there are direct contributions to the spectra.

Let me show you an example of this. It is something we've seen already a couple of times at this conference (Fig. 12.9). This is the ratio of in-plane to out-of-plane correlation in a two-particle coincidence experiment by Nagamiya et al. The spectrometer sits at 40° and the tag counter at 40°, and we see a very nice quasi-elastic peak for the light system at just the expected energy in the spectrometer. On the other hand, these results appear to be inconsistent with another experiment that we saw from the Poskanzer/Gutbrod group (Fig. 12.10). Here is essentially the same kind of experiment looking for protons in coincidence with other light fragments. What one would expect to see if there were a direct contribution to the reaction mechanism would be a nice peak at 180° consistent with the quasi-elastic nature of two-body scattering. We don't see the peak very clearly in any of the data here, although there are several factors in the experimental conditions which might lead one to suspect that you wouldn't see it as clearly as you did in the Nagamiya experiment. For example, there's a rather poor kinematic selection here. The telescope is sometimes as far back as 90 or 130 degrees, where you don't expect to see much quasi-elastic scattering. Secondly, there isn't a good resolution on the second detector. There are paddle detectors here, which cover a rather large solid angle, whereas Nagamiya's tag counters cover a much narrower angular region. Consequently, the random rate in these experiments is much higher. Also there is a much higher multiplicity, particularly in uranium and even in the aluminum, than we had in the carbon-carbon and, as you will see, high multiplicities mask the signatures for the direct dynamics.

Finally, there may be a real effect here because at 400 MeV/nucleon we're at too low an energy to see a significant direct component and other, more complicated things are contributing to the spectrum.

At 800 MeV/nucleon there is other indirect experimental evidence that we're seeing something that is characteristic of nucleons colliding rather than of nuclei colliding. The spectra at large transverse momenta are more or less independent of the system we are looking at. Here, for example, is more Nagamiya data (Fig. 12.11). We have the spectra going out at 90° in the center-of-mass, transverse to the beam, as a function of the proton energy. You can see that, within a fair approximation, the spectra are all more or less independent of which nuclei are colliding, whether it is carbon, sodium or argon. This seems to me to be a signature for nucleons rather than nuclei. The pions also show the same thing, perhaps to an even greater degree (Fig. 12.12). Here we see pions from carbon, from neon, and from argon, all with spectra roughly independent of the nuclei being observed.

Another striking observation is that if we take an asymmetric system, neon on lead, and look at the distribution, we notice that as we swing out to larger and larger transverse momenta the distributions tend to get more symmetric around half the beam rapidity (Fig. 12.13). It is not at all obvious from this plot whether they actually become exactly symmetric around half the beam rapidity, or about some rapidity slightly lower than half. This is clearly something we would like to know. If we are talking about nuclei on nuclei, there's no reason to expect symmetry in the nucleon-nucleon center-of-mass frame, whereas if you are talking about nucleon on nucleon, the symmetry is very natural. I would conclude from this that at large transverse momenta something fundamental having to do with nucleons is contributing to the process, and that it doesn't matter what nucleus you are looking at. The pions in this reaction show an even more striking symmetry (Fig. 12.14). Here is the π^- spectrum, again symmetric around half the beam rapidity and having nothing to do with the unequal masses. You should remember that this is at rather large transverse momenta. I'll have much more to say about the pion spectrum at low transverse momentum in a second.

We also have some rather indirect theoretical support for these direct processes (Fig. 12.15). There is a hard scattering model on the market by Bob Hatch and myself which is able, in fact, to reproduce most of the large transverse momentum region of the spectrum in terms of a single nucleon-nucleon interaction. On the other hand it is also possible to reproduce the spectra in terms of a multiple collision model. Fig. 12.16 is Kent Smith's calculation for the protons from neon on neon, and you can see that there is a pretty good reproduction of the data without any need to invoke a hard scattering model explicity. In fact, all of his high momentum tails are undoubtedly due to multiple collisions.

So there seems to be a real quantitative question here as to what fraction of the spectra we are observing is direct and what fraction represents more complicated processes due to nuclei colliding. There are several ways that one might imagine answering this experimentally. We can get a quantitative

determination of the fraction of nucleons that is direct by imagining the following situation (see Fig. 12.8, bottom). Let us take a nucleon from the target and a nucleon from the beam in momentum space (the spheres have radii on the order of the Fermi momentum). These two nucleons are going to scatter in some direction, and for each nucleon that comes out at some momentum there will be a partner roughly at the beam momentum per nucleon minus the momentum at which we observed the first nucleon. This correlation will, of course, be spread out due to the Fermi motion. We also might expect from this picture that the mechanism is going to be favored at a high transverse momentum, since this is a very efficient way of delivering a large momentum transfer to the nucleon without changing its energy very much. So we should look at large $p_\perp$ if we want to see these hard scattering nucleons, which is, in fact, where the hard scattering model does the best job in reproducing the data.

It is obvious now that what we need to do experimentally is integrate the correlation enhancement in the double differential cross section (Fig. 12.17). In other words, we need to measure the peak we saw in Nagamiya's data over a whole range of kinematics of the partner nucleon, integrate the enhancement, and extract quantitatively what knock-out fraction we have for a proton observed at some particular region of phase space. You should also notice - and this is why I wonder whether the Poskanzer experiments on the knock-out signature are really definitive - that the signal decreases as one over the multiplicity. If we have a lot of particles coming out of the reaction it will be very difficult to decide which partner comes from a given observed nucleon. Therefore we need to do rather precise experiments to defeat this one-over-multiplicity effect in the high multiplicity collisions. Nonetheless, you might imagine making a plot of the integrated knock-out fraction in the transverse momentum and rapidity of the observed nucleon. For the large transverse momentum we would like to see a very high knock-out fraction in the central rapidity regions. At low transverse momentum nucleons probably result from much more equilibrated processes, and we would like to see a very small knock-out fraction.

The interpretation of these experiments has become rather complicated as a result of several comments during the conference. One comment was that it would be nice to know if two-body kinematics, of the kind we are looking for here, survive in a multiple collision event. Knoll, in particular, has suggested that they might survive in a nucleon undergoing two or three collisions. This is clearly something that could be checked with the cascade calculation, and I urge the cascade people to do just that. Another thing you might ask is, are we scattering from clusters or from single nucleons when we observe nucleons coming out at the high transverse momenta? One thing we might decide to do, and this something that has been suggested by Woloshyn, is to look for other kinds of correlations, not just nucleon-nucleon but also nucleon-deuteron, nucleon-triton, nucleon-alpha, and ask how these correlations change as we change the kinematic region in which we observe the proton.

Finally, it is also possible that there are other kinds of correlations that would show the direct reaction mechanism equally well. Let me show you a sample calculation by Randrup in which he has considered the rapidity-rapidity

correlation between nucleons (Fig. 12.18). This is 800-MeV/nucleon neon on neon, neon on lead, and neon on lead again with a central impact parameter cut. Here is the expected correlation function is plotted for Randrup's slab-on-slab cascade model as a function of the rapidities of the two particles. You can see that there are nice clean signatures of the quasi-elastic events, namely, when the sum of the two rapidities is a constant. Also there is other structure due to multiple collision processes in the center of the plots. Perhaps such information from an experiment would be useful in untangling the direct fraction.

Let me make some remarks at this point concerning the application of scaling to relativistic heavy ion collisions. This is usually invoked in the context of the mechanism proposed by Schmidt and Blankenbecler and has been used at this conference to explain pions produced in the backward direction. Let me remind you that scaling requires that the energy of the observed particle be much greater than all of the other energy scales in the problem. This assumption is manifestly false in the heavy ion collisions that we've been looking at. Namely, we have other energy scales like the Fermi momentum, the pion mass, and the energy dependence of the nucleon-nucleon cross section in both its angular distribution and its integrated value. This says, to me at least, that scaling is a manifestly crazy thing to expect in heavy ion reactions. In fact, even if you look at something like protons on copper (Fig. 12.19), here as a function of X, you see that the data are nowhere near scale. Let me make the remark that even if scaling were true, if the energy were much greater than the other energy scales in the problem, it's true that the Schmidt and Blankenbecler formulas work only near X=1. These functions of 1-X to some power are asymptotic things valid only for X close to 1 and it is wrong to try to apply them in the region where X is 0.2. This suggests to me that the people who are trying to apply these theories should perhaps read the papers a little bit more carefully. Perhaps scaling is not crazy at much higher energies where it sets in for nucleon-nucleon collisions namely at several tens of GeV. But in the energy per nucleon range where we are at the moment, at least, and in the kinematic regions where we're measuring the fragments, I don't think that scaling has anything to teach us.

Let me turn now to something else we've heard here that is fairly new. We've seen what I would consider to be the first real signatures of collective dynamics, namely, we really have nuclei interacting and not just a trivial sum of single nucleon interactions (Fig. 12.20). The experimental evidence that we have so far is still very gross, but nonetheless I think we can clearly say that we're starting to see some structures due to the fact that we're doing relativistic heavy ion physics. One of these is change in the inclusive spectra as we gate on the different multiplicities. Let me remind you of how that looks. Here is some of the Nagamiya data (Fig. 12.21). The ratios of the high multiplicity spectra are plotted to the inclusive spectra for 800-MeV/nucleon argon on lead. You can see that there are rather dramatic changes in the forward direction and in the two backward directions as we select on the higher multiplicity events. A simple direct reaction mechanism would predict that the spectrum would be roughly independent of the multiplicity. Already we can see that there's some sign of nuclei here.

Another signature of some collective nuclear behavior that's been seen here is the high-Z-light fragment correlations from the Poskanzer/Gutbrod group (Fig. 12.22). This is neon on gold, and what you're looking at is the azimuthal correlation function for a heavy fragment of some specified Z observed in the telescope at 90° in coincidence with light fragments as a function of the azimuthal angle. You can see that there are very clear and consistent structures here. Hans interprets this in terms of a side-kick delivered to the high-Z fragment — the beam comes in, kicks the heavy fragment off to the side and then a shower of light fragments goes out oppositely.

Another indication of interesting structure in the data we've seen are the low transverse-momentum pion spectra that Kevin Wolf showed us, as well as that shown by John Rasmussen earlier this year (see Fig. 12.23). Here we're looking at neon on uranium, and you can see that there's some interesting structure in the data if we increase the beam energy to 400 MeV/nucleon (Fig. 12.24). One starts to see mountains developing and if we go up to 1 GeV/nucleon and change the beam to argon (Fig. 12.25), there's also some rather interesting structure there. These things obviously can't arise as a trivial superposition of nucleon-nucleon interactions. Perhaps it's an indication, as Kevin suggested, that there's some kind of shadowing going on, that the pions can't get out very well through the heavy nucleus. I'll have more to say about that in a second. On the other hand, we've also heard the rather depressing news from Jim Carroll that at least some of the spectra we see are roughly independent of the multiplicity. That suggests that certain parts of phase space are populated by these direct reaction mechanisms only.

Given that the collective dynamics exist, what possible experiments could we imagine doing that would probe the reaction mechanism a little bit more closely (Fig. 12.20, bottom)? One of the things we might imagine is making an associated multiplicity plot. This seems to be trivial with the experimental techniques we have at hand and might be rather illuminating as to where the nucleons or fragments come from. All we need to do is plot the multiplicity observed in coincidence with a fragment at some transverse momentum and some rapidity. What we might expect to see is that the very low multiplicity events populate the high transverse momentum regions and the more central events populate the low transverse momentum regions.

We also might ask if we can observe this geometrical shadowing directly in some sort of multiparticle correlation. We've seen that as far as the average multiplicities go, geometry in terms of participants and spectators and clean cuts is rather a good description. Can we get a better handle on this geometry directly? We might try to use the multiparticle correlations to do this. In particular, let's see if we can use the side-kick that Gutbrod is talking about to define the reaction plane, and then see if we have more high energy fragments or pions produced in the direct reaction mechanism and whether we see a larger knock-out fraction by looking transverse to the reaction plane than by looking in the reaction plane. I remind you of Shoji's picture — hard and easy directions to get out of the interaction region. Let me also remark that running cascade collisions and asking questions about these multiparticle correlations before we decide to do the experiments or

in conjunction with them would be a tremendous intuitive help. I think that the people doing cascades have tended to concentrate too much on fitting the inclusive data to a few percent and are somehow ignoring the great power that these calculations have in giving us a very good intuitive feel for what's going on. The experimentalists might be able to help them there a little bit.

Another thing that we might do in the search for collective dynamics is rapidity correlations, asking if we can see the emission of chunks of nuclear matter. (Fig. 12.26). This is an idea that we can borrow from the multi-peripheral models in high energy reactions. We might imagine a collision, and this starts to look very much like Bill Myers' firestreak geometry, in which a whole chain of matter is strung out between the target fragment and the projectile fragment, which then breaks up into chunks. It's clear that if we look at nucleons near $y_1 = y_2$ we would expect to see a large correlation between them just because they come from the same chunk, which has roughly the average $[(y_1+y_2/2)]$ rapidity. Let me contrast this kind of rapidity plot with the correlation function for the direct reaction mechanism, which had the contour lines going at 90° to the ones shown in Fig. 12.26. So, by measuring (y_1,y_2) correlations maybe we can look for the emergence of these chunks. Other intermediate range phase-space correlations might also be useful, like correlations in transverse momentum to determine whether we knock out a whole chunk of matter at some average transverse momentum. We might look to see if a large number of nucleons emerge with about the same transverse momentum from that chunk.

Finally, one other thing (which is more of an inclusive experiment) that we might do is to look into what is the stopping power of nuclear matter, in the following sense. If we integrate the differential cross section over $p_\perp$ and just plot $d\sigma/dy$, then we would expect (and we haven't yet seen this from the counter experiments) that the cross section would look something like Fig. 12.26, bottom, for an inclusive selection of events. We see large peaks at the target and projectile rapidities and then some broad central region due to nucleons, which undergo a more violent interaction. If we were to start to do cuts on low multiplicity and high multiplicity, we might expect to see the low multiplicity events showing a strong fragmentation peak and little population of the central region. In higher multiplicity events these peaks would start to move in and perhaps the central region would start to fill up. The rates at which curves change as a function of the beam energy, as a function of the thickness of the target nucleus, and as a function of the multiplicity, tells us something about how efficiently the projectile is stopped in the target. It would be very interesting, therefore, to investigate how these patterns change with those parameters. There's also a suggestion by Hans Pierce, although there are not calculations to back it up yet, that if one saw some anomalous behavior in the data from this type of experiment it might be a signal for the critical opalescence associated with pion condensation.

Let me turn now to the matter of equilibrium and seriously call into question the evidence we have for equilibration. Well, I'm not so sure that there is very much conclusive evidence. What we've seen so far is that the

thermal models, whether it's the fireball or the firestreak or something even more elaborate, are usually capable of fitting the inclusive data, although some discrepancies appear. But I raise the question, and this is something that Reinhard Stock brought up first, of whether or not we are being fooled by some sort of implicit ergodic hypothesis. Namely, are we implicitly assuming that all particles in one event behave like an average particle in an average event? In other words, the inclusive measurements that we're performing do a gross averaging for us. Not only do they average over all the events we observe, but they also average over all the particles in a given event. I wonder if the dynamics in these collisions are being washed out by our inclusive averaging, and if all that we're really counting in the inclusive measurements is phase space. That is, in fact, a very nice explanation for why we can generate so many different models with so many different dynamic assumptions and still manage to fit the inclusive data. I think that there's a real need to prove the equilibrium event by event. That means rather complicated multiparticle coincidence measurements.

There are two necessary conditions that we have to establish to prove that there is equilibrium. First, all of the participant fragments (those in the central rapidity region) must be independent of one another. In other words, there should be no kinematic correlations at all except those imposed by overall energy and momentum conservation. That means that the direct peaks we saw in Nagamiya's data for carbon on carbon and for neon on sodium fluoride should be absent if we're going to claim that there is equilibrium. Second, the composite particle production is something that several people have talked about in terms of an equilibrium model - the law of mass action as applied to nucleons. There are several tests of this that one might imagine doing as well. The equilibrium models predict that most of the alpha particles produced in these collisions come from the breakup of a mass-5 system. That's because mass-5 has a ground state spin of 3/2 and so carries a large statistical weight compared to the alpha particle which has a spin-zero ground state. So we might hope to look for p-α correlations to get a handle on precisely what the mass-5 fraction is in the equilibrated system, if it exists. This has to be in agreement with all the other proton-deuteron-triton ratios that we're observing. We might also look for the π-p correlation and see the resonance enhancement at the Δ. If we can do that, we can probe the π-N-Δ equilibrium that might be there and ask if it is consistent with the equilibrium that we're seeing in the ratios of the nuclear particles.

Let me also talk a little bit about the relevance of bulk nuclear properties to all the experiments we've seen so far. The first new and interesting result that I've heard in the last few months is that the hydrodynamic calculations done by Nix et al. are relatively insensitive to the equation of state that's used. Ray takes his equation of state and changes the compressibility by a factor of two one way or the other and sees essentially no change in the inclusive spectrum. That is perhaps a warning that we may not be able to learn very much about the equation of state by doing these inclusive measurements. Also, there's the question of what exotic phenomena associated with bulk nuclear properties we might expect to observe in these reactions. After sitting through the discussion on Wednesday, I got the vague impression that

pion condensation, the sigma model, quarks and bags are somehow relevant to relativistic heavy ion physics, but it wasn't quite clear how. It is clear that we need rather specific models for how these phenomena appear in reactions. In particular, after carousing a bit at the winery last night, I did manage to come up with a rather concrete model for the sausage mechanics that Kerman and Lee discussed. After playing around with this model for quite a while and devouring several of its predecessors, I finally came to the conclusion in Fig. 12.27. Seriously though, I think that the people who have been doing studies of exotic matter under thermal conditions should be compelled to come up with some concrete, testable suggestions for experiments we might do to look for these things. The experimentalists, I think, have been rather negligent in not pursuing their theoretical colleagues a little bit harder for this kind of information.

Let me now turn to something that is dear to my heart, something that shows the first exciting results at this conference: the use of nuclear interferometry to probe these reactions (Fig. 12.28). Let me remind you a little bit about what we mean by nuclear interferometry and how we might apply it in practice. The idea here is to exploit various quantal properties of the final state to say something about the dynamics of the system. Now offhand you might expect that quantum mechanics doesn't have much to do with relativistic heavy ions at the energies where we are - the deBroglie wavelengths are short, and so on. On the other hand, in the final state, when you produce particles with small relative energies and momenta, quantal effects can start to be important. Those are the things that we're going to try to exploit. We've already seen the first data on $\pi^-\pi^-$ correlations from the Riverside group. They did a streamer chamber experiment and directly observed the Hanbury-Brown-Twiss effect. Let me remind you what their curve looks like and then we'll explain it again in a little bit more detail. Fig. 13.29 is a sketch of the data. It is the ratio of two-pion inclusive cross sections to single-pion inclusive cross section squared as a function of the relative momentum between the two pions. As you see, for large relative momentum on the order of 200 or 300 MeV/c, the pions are basically uncorrelated; the ratio of the double to single cross sections is one. For small momenta, however, the correlation suddenly takes a big jump upward. This is being interpreted as a signature for the Hanbury-Brown-Twiss effect in nuclear collisions and is due to the boson symmetry of the pion. From the width of that correlation enhancement you can deduce that for argon on barium iodide the size of the radiating system is something like 5.5 fermis with a lifetime of about 1.6×10^{-24} seconds, although this last number has a large uncertainty.

I want to go into this a little further because later I want to talk about quite a few more experiments that we could do to exploit this kind of phenomenon. The basic idea for this (Fig. 12.28) is that the collision volume is a large source of particles, which are emitted more or less independently. In a heavy ion reaction a lot of particles are made at once and there are essentially no kinematic constraints on the particles at all; there's always a much bigger system to absorb energy and momentum so that the particles are uncorrelated in an overall kinematic sense. That's quite different from three-body reactions where you look at the correlation between two particles that come out very constrained by the overall energy and momentum conservation

in the system. From the heavy ion reaction, two particles come out with momenta $\vec{p}_1$ and $\vec{p}_2$. They are generated by a source function D, which is a function of both space and time and that is big inside the system and small outside. The correlation function, R, which is a function of the momenta of the two pions, $\vec{p}_1$, and $\vec{p}_2$ is of interest to the experimentalists and is plotted in the data in Fig. 12.29. As you can see, it is the appropriately normalized ratio of the double-differential cross section to the single-differential cross section minus one. If we assume that the particles are produced completely chaotically; namely, from a source with no dynamic correlations at all, then we can write down a very simple expression for this correlation function in terms of the source function D. It is an integral over all the space and time where the two particles are produced at D and a wave function to the two particles. In the pion-pion case we have to symmetrize the wave function between particle one and particle two. We square it and then subtract one to get R. For the pions, it is simplest to assume that the pions produced in the interaction region get out with no further interactions, so that we take plane waves. When we square the wave function, the interference term is going to essentially take a Fourrier transform of the source function. What we're going to be looking for then are features of this source function as revealed by the Fourrier transform, or, equivalently, the R function.

I need to make several comments now about this effect. First of all, the same effect exists in proton-proton pairs. Igo et al. are now looking for this and expect to have data in January. One advantage of working with protons is that you get a lot more of them in a heavy ion collision. On the other hand, you have to worry about the influence of the Coulomb and nuclear forces between the protons, which are not so important for pions, and at the same time there's fermion statistics, rather than boson statistics. Nonetheless you can try to make reasonable estimates of what the correlation function might look like (Fig. 12.30), as a function of the relative momentum of the two protons, in MeV/C. The correlation function in the cases that are calculated above is a function only of $\Delta p = |\vec{p}_1 - \vec{p}_2|$, since the lifetime τ, is set to zero. You can see that there is sizable structure in the correlation function on an experimentally accessible scale. Namely, for very small sources (r_o is the size of the emitting region) the correlation function shows a minimum at zero relative momentum due to the Coulomb interaction between the two protons. There is a large maximum due to the strongly attractive nucleon-nucleon force at low relative momenta, which falls off. As we increase the size of the system, or make r_o bigger, the particles tend to be emitted farther and farther apart in space, consequently the height of the nuclear correlation peak decreases. Notice that you are rather sensitive to r_o, so this might be a way of getting a good handle on the size of the system. You can, of course, also turn on the time. In Fig. 12.30 (bottom) are curves associated with various lifetimes of the system at fixed size, and you can see that they are also sensitive to the time. By measuring these correlation functions, therefore, we can get both the size and the time.

It is clear that there is quite a bit of future work to be done, having seen that the effect exists for pions. First of all, we need more exclusive kinematic selection on the pions that we are willing to consider. This is something that Fleur Yano has been thinking a lot about in the last year.

If we imagine a given pion pair, there is a total momentum $\vec{p}$, which is the sum of the momenta and a relative momentum, $\vec{k}$, which is the difference of the momenta. So far, in the streamer chamber data, we have taken all possible values for the total momentum of the pion pair, mainly because we need a lot of good statistics to build up that correlation curve. But in general we know that R is a function of $\vec{p}$ and $\vec{k}$. And so you can ask, given that we might be able to measure both those dependences, what can we get out? Well, a way of quantifying this can be seen in Fig. 12.31. Here we have some direction, $\vec{p}$, which is fixed - that is the total momentum of the pion pair - and some direction, $\vec{k}$, which is the relative momentum of the pion pair. The relevant variables at fixed $\vec{p}$ (at a fixed place in phase space) are the angle between $\vec{p}$ and $\vec{k}$, θ, and the length of $\vec{k}$. The angle controls whether we're measuring particles in the same direction (when θ is zero) with different energies, where the momenta are parallel but have different lengths, or whether we're measuring particles at different directions with the same energy. Clearly, two different kinds of measurements are possible. What we can then do is define the mean square k of the enhancement. Namely, we can take the correlation function R and integrate it over k, weighted with k^2. (Remember that the peak we saw in the correlation function dropped off very quickly). This is a measure of the overall width of that peak. At the same time we might also consider calculating the "quadrupole" moment, which is a measure of the asymmetry in the correlation when $\vec{k}$ is along $\vec{p}$ or $\vec{k}$ is transverse to $\vec{p}$. These are two gross quantities that you can imagine extracting from the data at fixed $\vec{p}$. Then you ask how these quantities are sensitive to both the space and the time correlation of the source. Let's have a look at that in Fig. 12.32. Here is a plot of the mean k^2 of the enhancement as a function of the size of the system. This assumes a Gaussian source and these are curves plotted for different values of the lifetime of the source. You can see that for reasonable nuclear sizes, 2-4 fermis, there's not much sensitivity to time. You're mainly measuring the size, r_o. Now let's take a look and ask what happens when we measure the quadrupole moment, or the asymmetry, in the correlation (see Fig. 12.33). You can now see that this quadrupole moment is quite sensitive to τ for various different values of r_o. So by measuring both the quadrupole moment and the mean square size of the enhancement, we can probably pin down both the size and the lifetime. That's a tough measurement but it would be even tougher to do what we would like the experimentalists to do, namely, to make rough cuts on the total momentum, $\vec{p}$. For example, take all pions which are emitted forward in the center-of-mass, or all pions which are emitted transverse in the center-of-mass, and then evaluate r_o and τ separately for those pions. Even better would be to make a whole plot in rapidity space, p_l and y, and have r_o and τ as contour plots in that plane. With data like that we could start to get some idea of what the evolution of the system is.

So much for the experimental subjects. What kind of physics can we extract from the data should shown in Fig. 12.31, bottom? Well, first of all you can ask, are the fast particles direct? Are they coming from the first collision? The answer is that they would be associated with a relatively small geometric size determined by the overlap of the target and projectile and with a very short time because they are emitted first in the direct reaction. You can also ask are the slow particles decayed? Are things undergoing several collisions produced over a much longer time and perhaps

over a much larger region of space? You can also ask how do r_o and τ correlate with multiplicity? Can you, in fact, get a direct geometrical handle on the impact parameter by seeing that low multiplicity events have a small r_o because they have a small overlap region and high multiplicity events have a big r_o because they blow up the whole nucleus. Given that we can also do the experiments with nucleons (which has yet to be demonstrated), we can ask how the nucleon parameters agree with the pion parameters. Is the space-time evolution of the pion source the same as the nucleon source, or is it different? By asking these things we can start to get an idea of the evolution and the shape of the system. Finally, Gyulassy has made the interesting suggestion that we can get some handle on the coherence of the pion field. All of the the discussion so far assumes a totally chaotic pion source. On the other hand, if there is some particular mode in the pion field which is excited more than others, these correlation curves change, and they can change in such a way that you could measure that coherence, perhaps as a signature of pion condensation. However, this might be clouded a bit by the Coulomb interaction of the pions. Finally, what's also needed is a rigorous theory for all of this, particularly for the nucleons. Most of the discussions so far are couched in rather crude semi-classical terms, and it would be nice to know what things we really are measuring. The collision should be describable by a T-matrix, and we want to know what properties of the T-matrix we are probing in these experiments. Also important are possible distortions in the final state, namely replacing those plane waves by something more complicated.

At this point it is probably worthwhile to return to the Grim Reaper and ask exactly where we are (Fig. 12.2). (I should have put a star up there for Gelbke - I forgot!) It's become clear to me at this meeting that we are learning at a tremendous rate: both how to do experiments in a technical sense and also how to look at the data that come out to perceive the underlying physics. That is not necessarily a bad thing, as we really need to sharpen our scythes a little bit on reactions at 2 GeV/nucleon before we can start to talk about reactions at 20 GeV/nucleon, if and when we get that capability. It is also clear to me is that even though the Weeds have grown up tremendously, and perhaps some of the original Flowers have wilted a little bit, there are a lot of new Flowers in the garden, and people are pursuing the reaping with a tremendous vigor. Maybe that's what all the fun of physics is about anyway!

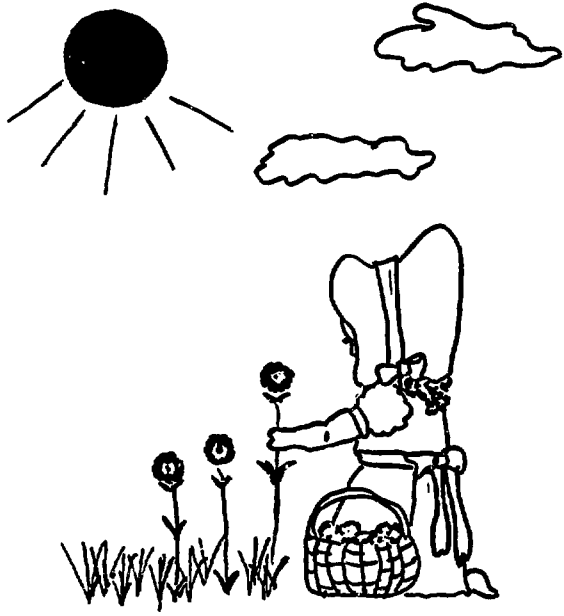

Fig. 12.1

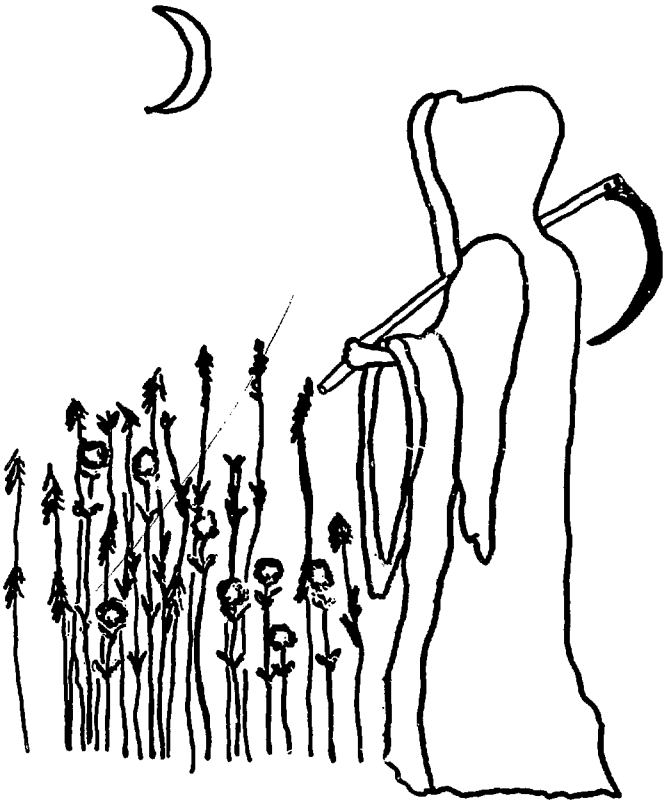

Fig. 12.2

Andersen

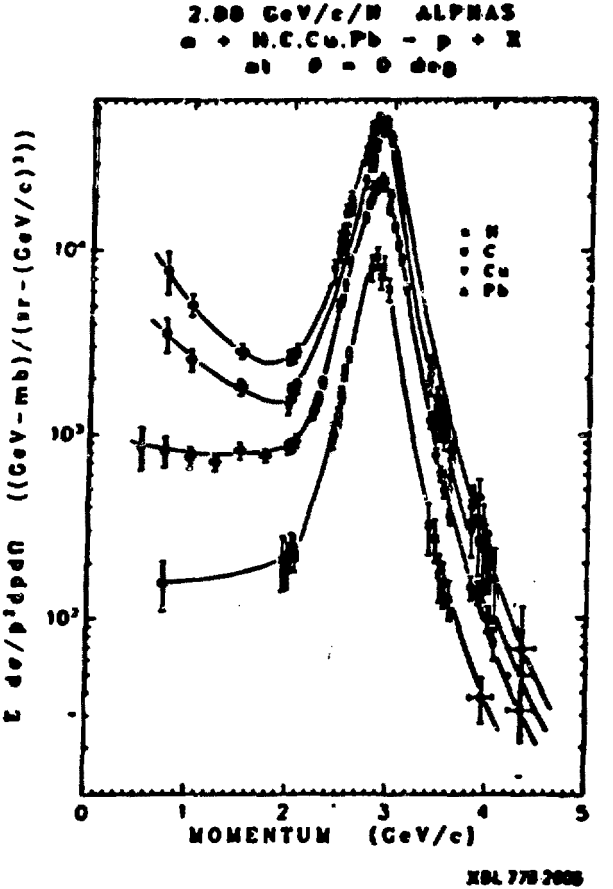

Fig. 12.3

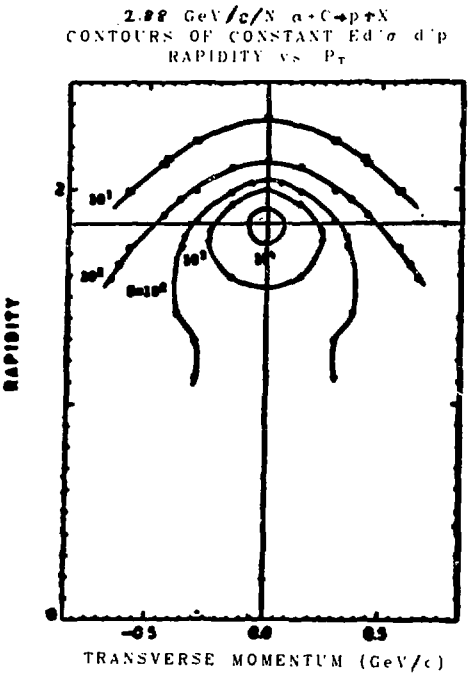

XBL 779-2457

Fig. 12.4

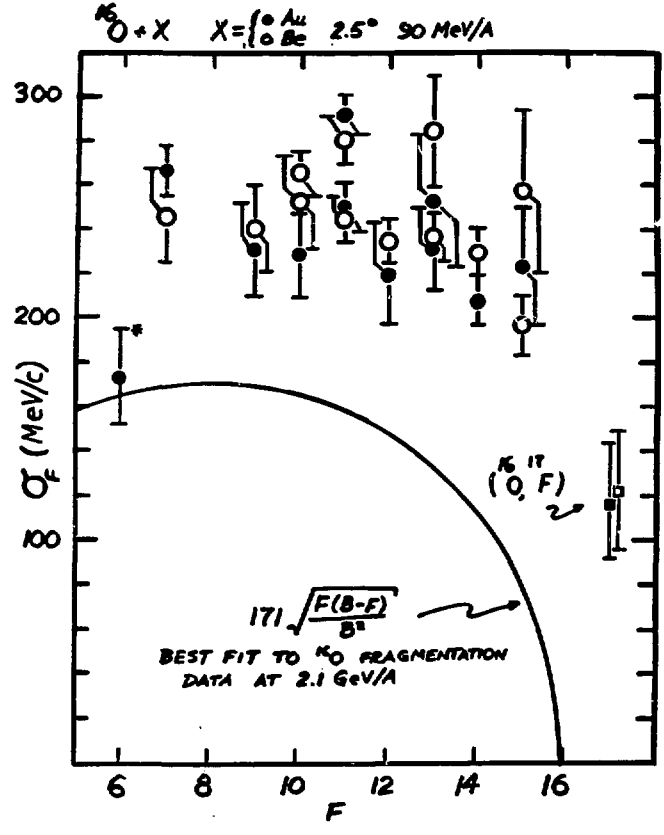
$^{16}O + X$ $X = \begin{cases} \bullet\ Au \\ \circ\ Be \end{cases}$ 2.5° 90 MeV/A
300
200
100
σ_F (MeV/c)
$(^{16}O, ^{17}F)$
$171\sqrt{\frac{F(8-F)}{8^2}}$
BEST FIT TO ^{16}O FRAGMENTATION DATA AT 2.1 GeV/A
6
8
10
12
14
16
F

Fig. 12.5

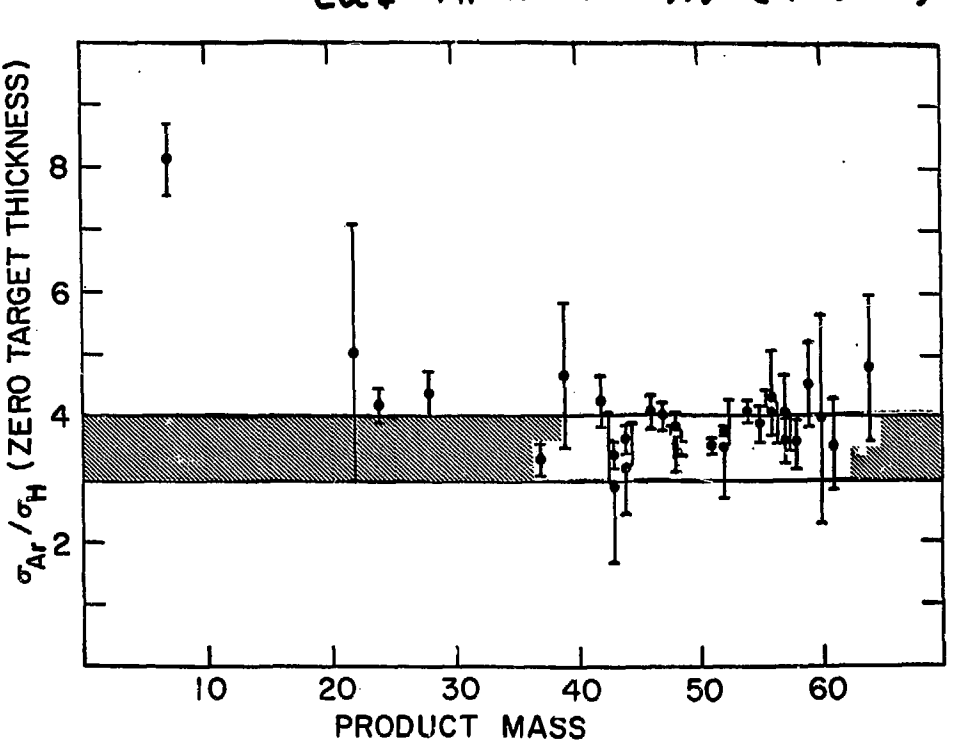
Cu + 40Ar at 2 GeV/N (Haustein)
σAr/σH (ZERO TARGET THICKNESS)
8
6
4
2
10
20
30
40
50
60
PRODUCT MASS

Fig. 12.6

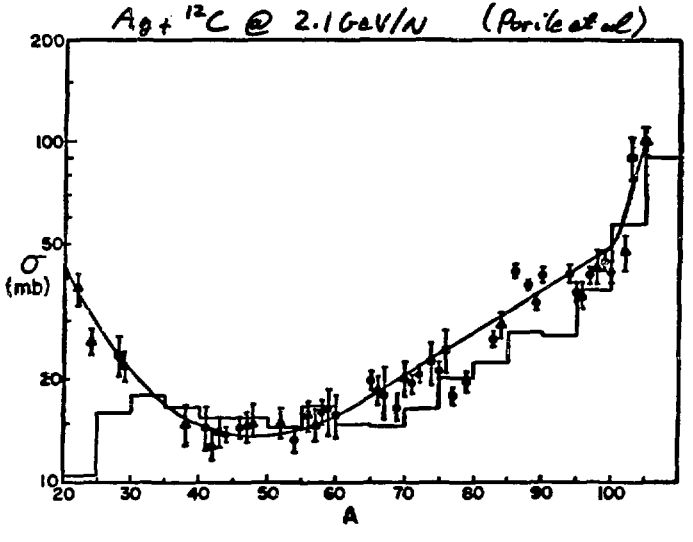
Ag + 12C @ 2.1 GeV/N (Porile et al)
200
100
50
20
10
σ
(mb)
20
30
40
50
60
70
80
90
100
A

Fig. 12.7

11

Direct Dynamics: i) "first step" processes
ii) clear kinematic signal
iii) Must remove this

Direct Expt. Evidence: In-plane correlation (C+C, Ne+Na
but contradicted by Poskanzer-Gutbrod
(poor kinematic selection, high $\langle A \rangle$, too low E/A?)

Indirect Expt. Evidence: i) Large P_T independent of A
for both p and π^-
ii) Symmetry at large p_T about $y_B/2$ in Ne + Pb
(need to measure larger p_T spectrum)

Theoretical Support: Hard-scattering model for
inclusive spectra [R. Hatch & SEK]; $f(p) = \gamma p / \sinh \gamma_p$
$\gamma^{-1} \approx 90$ MeV/c

but cascade models without fermi tails also
reproduce results

Quantitative Determination: i) For each nucleons at
$\vec{p}$, a partner at $-\vec{p}_0 - \vec{A}$.

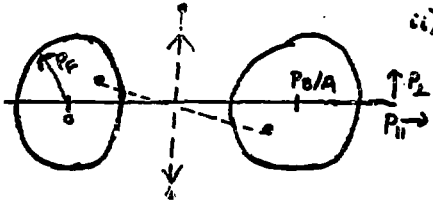

ii) spread by Fermi
motion

iii) Mechanism fa
at high p_T

Fig. 12.8

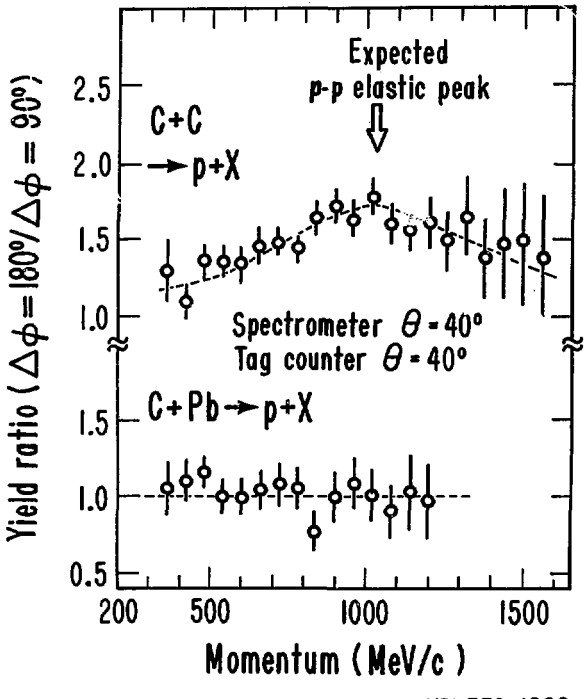

XBL779-1882

Fig. 12.9

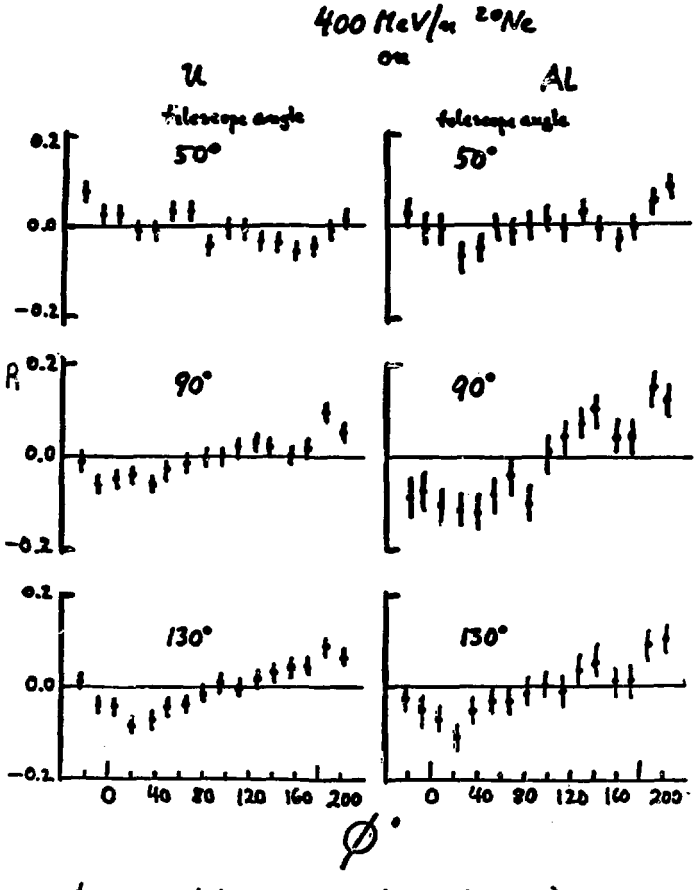

trigger particle proton ($35 \leq E_p \leq 200$)

Fig. 12.10

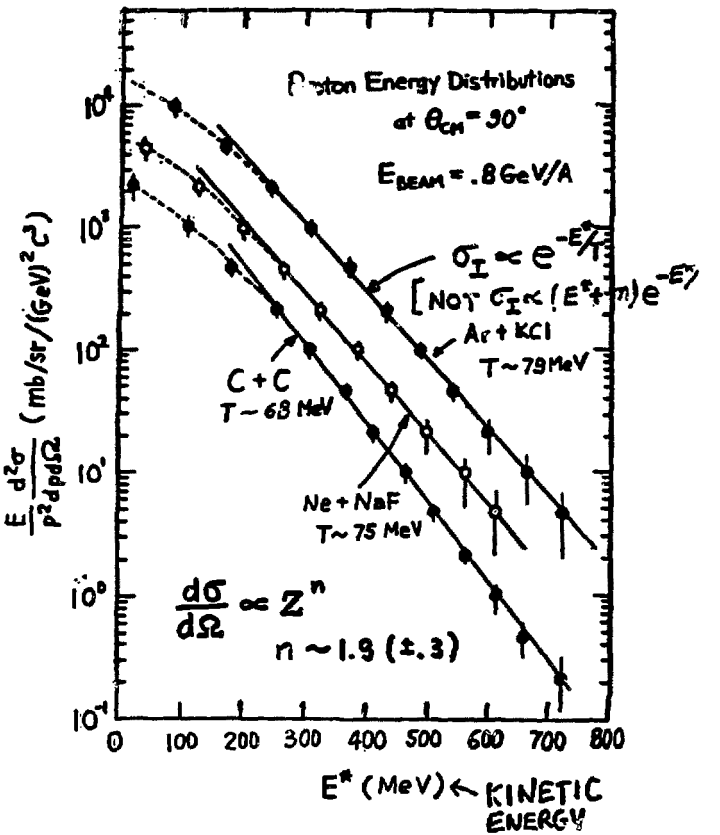
Proton Energy Distributions
at θ_{CM} = 90°
E_{BEAM} = .8 GeV/A
$\sigma_I \propto e^{-E^*/T}$
[Not $\sigma_I \propto (E^*+m)e^{-E^*/T}$]
Ar + KCl
T ~ 79 MeV
C + C
T ~ 68 MeV
Ne + NaF
T ~ 75 MeV
$\frac{d\sigma}{d\Omega} \propto Z^n$
$n \sim 1.9\ (\pm .3)$
$\frac{E\,d^2\sigma}{p^2 dp d\Omega}$ (mb/sr/(GeV)^{2}c^3)
10^4
10^3
10^2
10^1
10^0
10^{-1}
0
100
200
300
400
500
600
700
800
E* (MeV) ← KINETIC ENERGY

Fig. 12.11

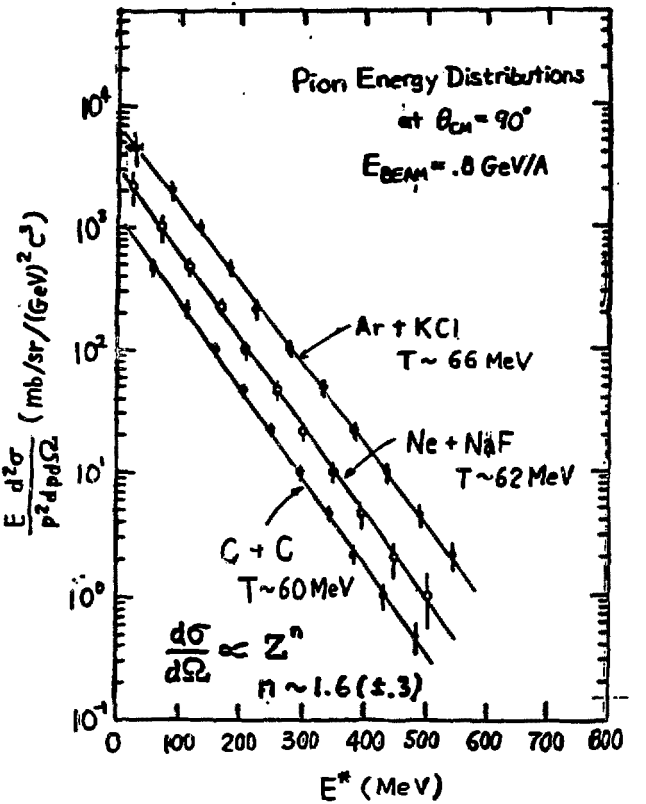
Pion Energy Distributions
at $\theta_{CM} = 90°$
$E_{BEAM} = .8$ GeV/A
Ar + KCl
T ~ 66 MeV
Ne + NaF
T ~ 62 MeV
C + C
T ~ 60 MeV
$\frac{d\sigma}{d\Omega} \propto Z^n$
$n \sim 1.6 (\pm .3)$
$\frac{E\, d^2\sigma}{p^2 dp d\Omega}$ (mb/sr/(GeV)^{2}c^3)
10^4
10^3
10^2
10^1
10^0
10^{-1}
0
100
200
300
400
500
600
700
800
E* (MeV)

Fig. 12.12

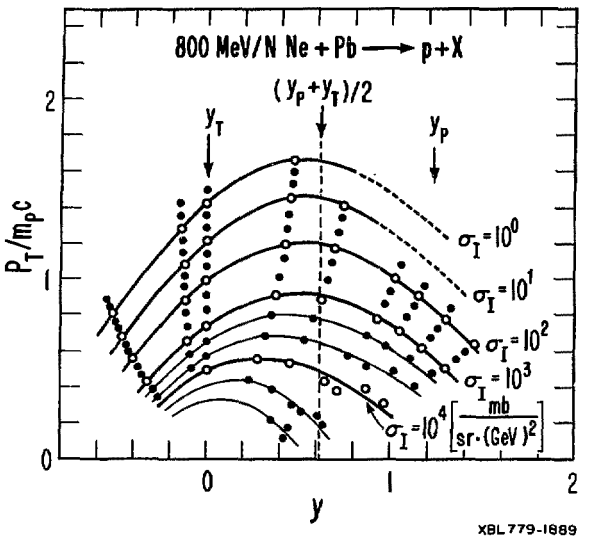
800 MeV/N Ne + Pb ⟶ p+X
$(y_p+y_T)/2$
y_T
y_P
$\sigma_I = 10^0$
$\sigma_I = 10^1$
$\sigma_I = 10^2$
$\sigma_I = 10^3$
$\sigma_I = 10^4 \left[\frac{mb}{sr\cdot(GeV)^2}\right]$
P_T/m_pc
y
0
1
2
XBL779-1889

Fig. 12.13

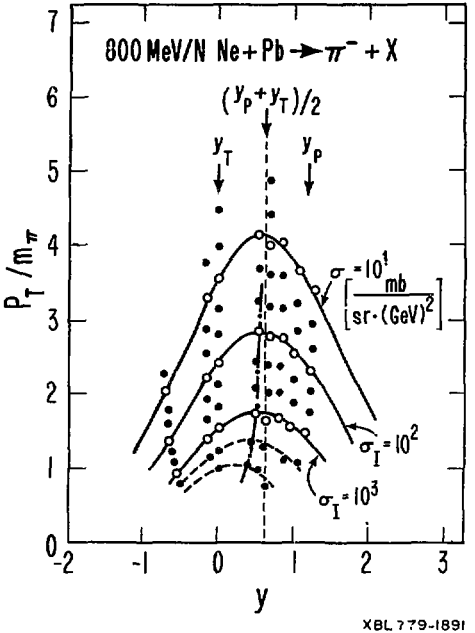
800 MeV/N Ne+Pb → π⁻ + X
(y_P + y_T)/2
y_T
y_P
σ = 10¹ mb / [sr·(GeV)²]
σ_I = 10²
σ_I = 10³
P_T /m_π
y
0
1
2
3
4
5
6
7
-2
-1
0
1
2
3
XBL 779-1891

Fig. 12.14

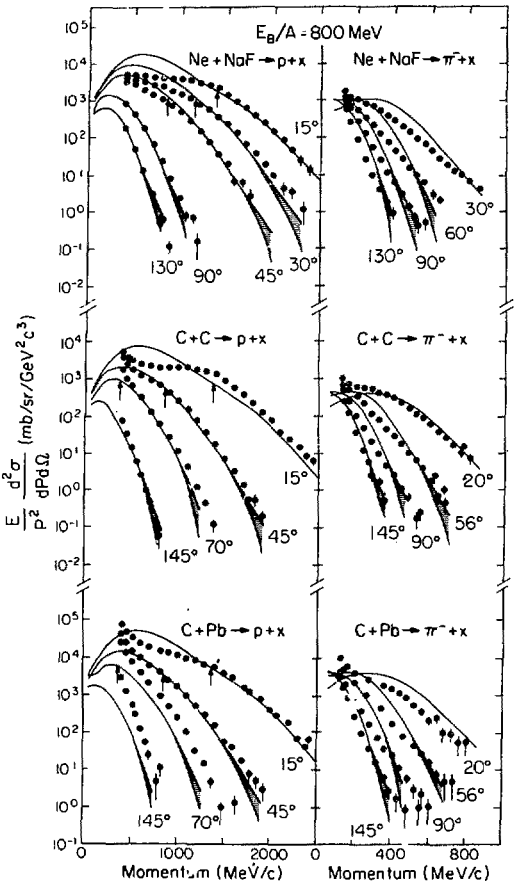

XBL 787-9821

Fig. 12.15

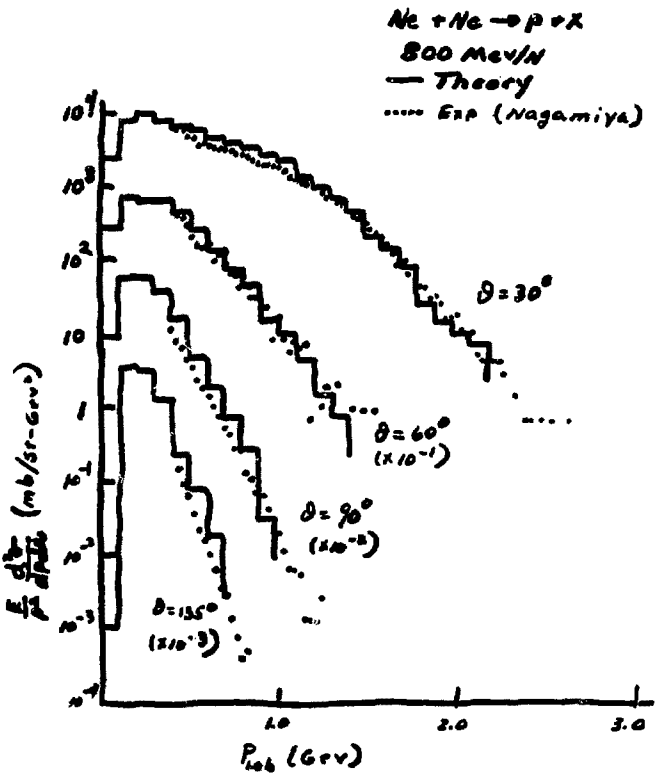
Ne + Ne → p + X
800 Mev/N
— Theory
····· Exp (Nagamiya)
θ = 30°
θ = 60°
(x 10⁻¹)
θ = 90°
(x 10⁻²)
θ = 135°
(x 10⁻³)
E d³σ/dp³ (mb/sr-Gev²)
P_lab (Gev)
1.0
2.0
3.0

Fig. 12.16

Experimentally integrate correlation enhancement in $d^2\sigma/dp_1 dp_2$ to find K-O fraction f [Note signal decreases $\sim 1/\langle n \rangle$]

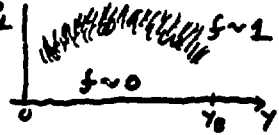

Such plots for various M cuts also useful

Does 2-body kinematics survive in multiple collisions? Check with cascade calculations [Knoll]

Cluster scattering from p-d, p-t, p-α correlations [Wolosh-]

Other correlations [e.g. y_1-y_2] also show direct [Randrup]

Scaling: Schnidet Blankenbecler
Requires $E \gg$ all other scales in the problem
Manifestly false in HI collisions [k_F, m_π, σ_{NN}...] (Landau)
Even if this were true, SB formulas work at $x \sim 1$

They are usually applied at much smaller x
Maybe this concept works at much higher $E/A \sim$ 10's GeV

Fig. 12.17

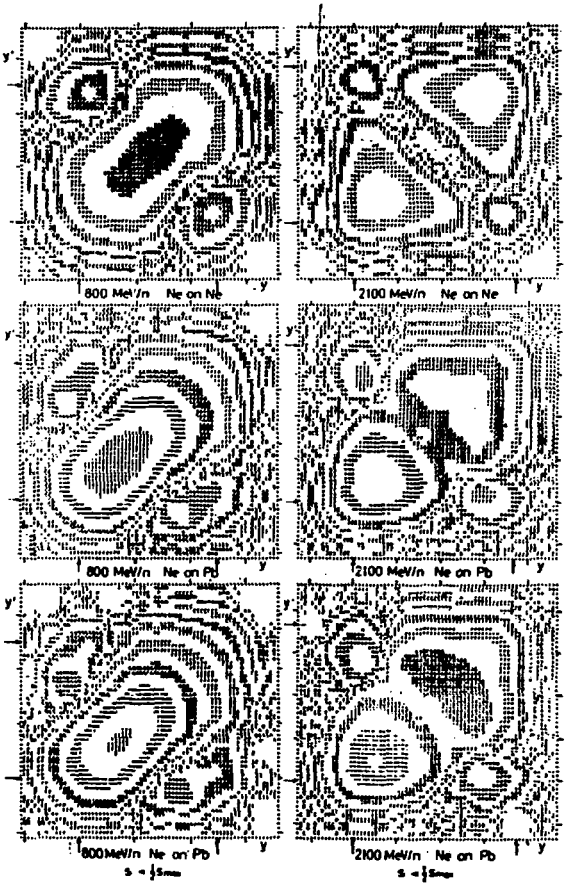
800 MeV/n Ne on Ne
2100 MeV/n Ne on Ne
800 MeV/n Ne on Pb
2100 MeV/n Ne on Pb
800 MeV/n Ne on Pb
s < ½s_max
2100 MeV/n Ne on Pb
s < ½s_max

Fig. 12.18

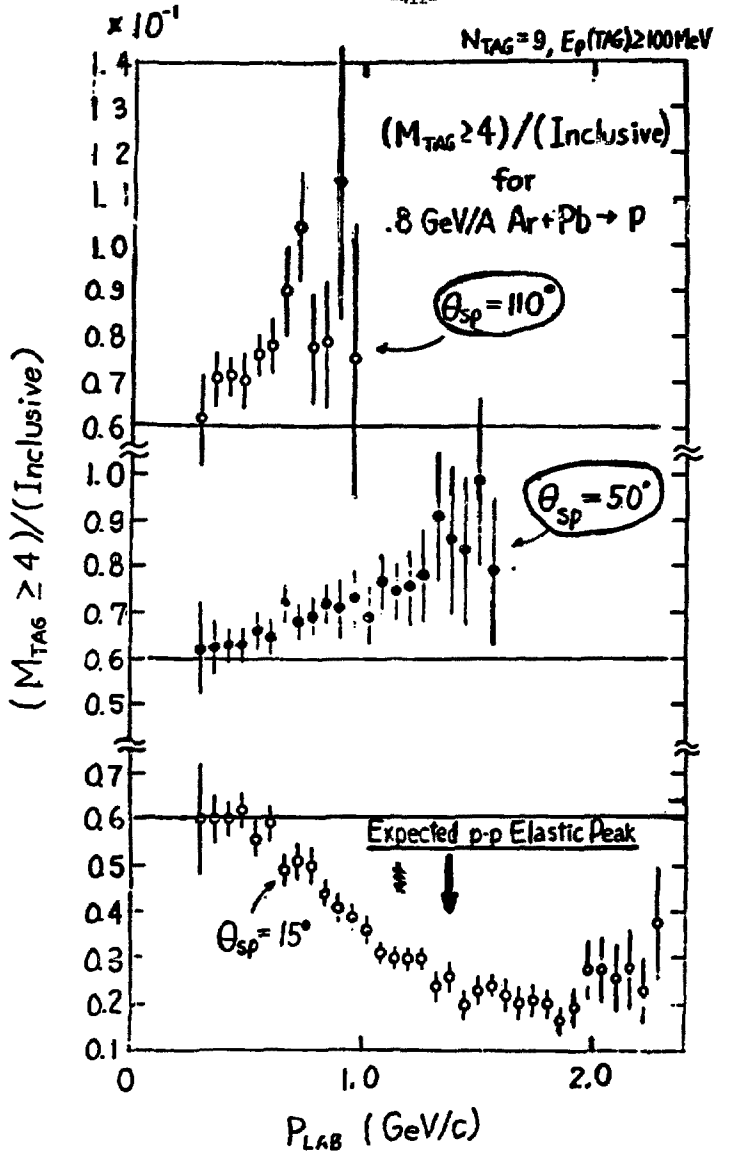
x 10⁻¹
N_TAG = 9, E_p(TAG) ≥ 100 MeV
(M_TAG ≥ 4)/(Inclusive)
for
.8 GeV/A Ar+Pb → p
θ_sp = 110°
θ_sp = 50°
θ_sp = 15°
Expected p-p Elastic Peak
(M_TAG ≥ 4)/(Inclusive)
P_LAB (GeV/c)

Fig. 12.21

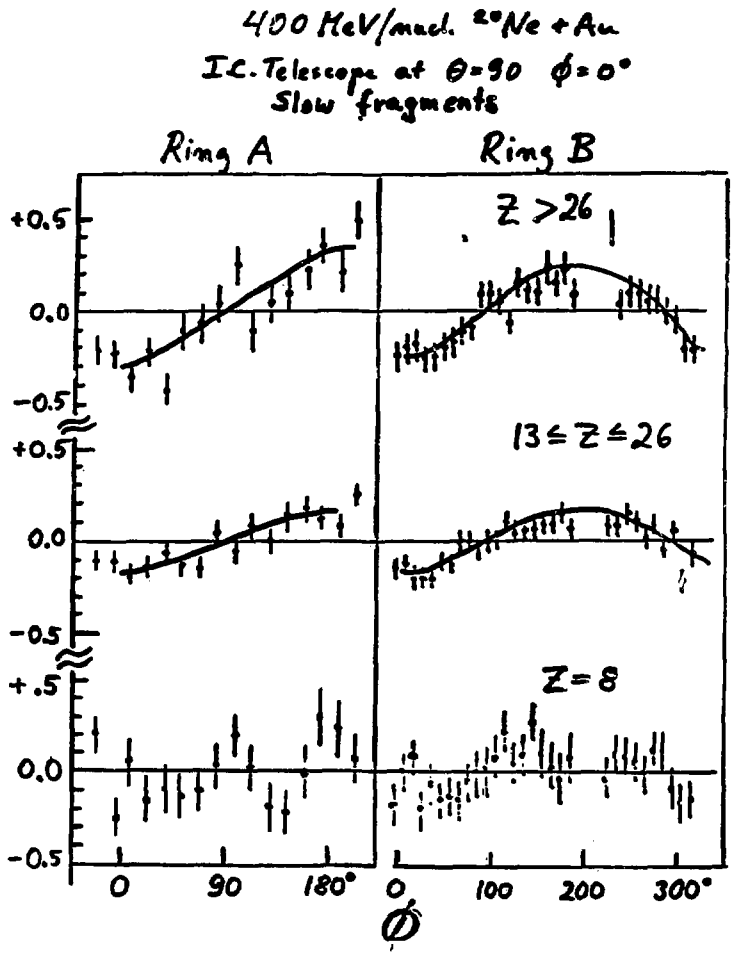
400 MeV/nucl. 20Ne + Au
I.C. Telescope at θ=90 φ=0°
Slow fragments
Ring A
Ring B
Z >26
13≤Z≤26
Z=8
+0.5
0.0
-0.5
+.5
0
90
180°
100
200
300°
Ø

Fig. 12.22

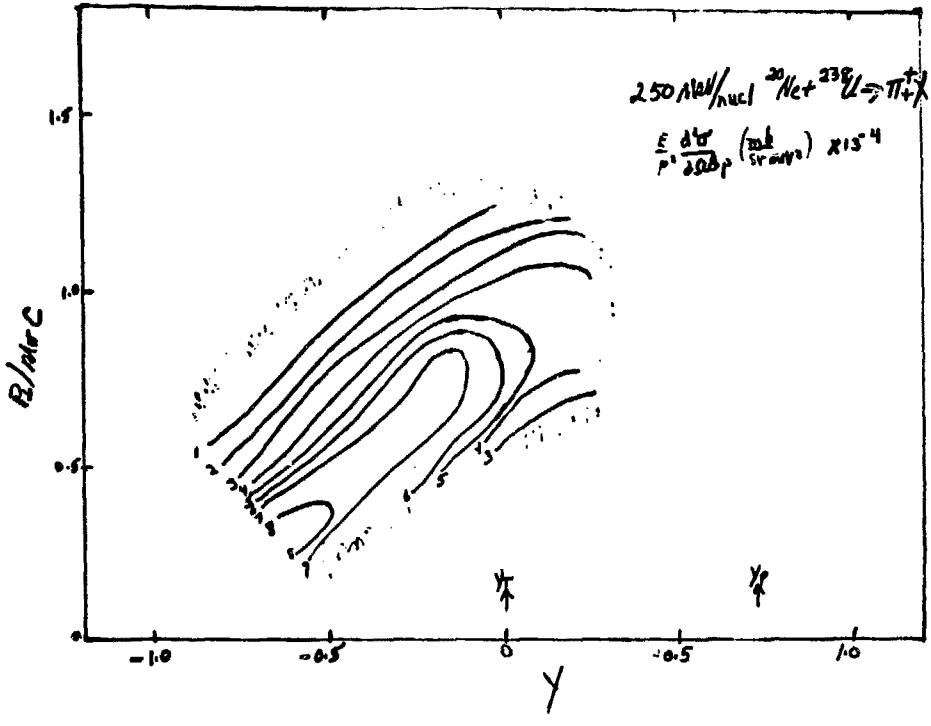
250 MeV/nucl $^{20}Ne + ^{238}U \Rightarrow \pi^+ X$
$\frac{E}{p^2}\frac{d^3\sigma}{d\Omega dp}\left(\frac{mb}{sr\,MeV^2}\right) \times 10^{-4}$
R/Rorc
1.5
1.0
0.5
0
-1.0
-0.5
0
0.5
1.0
Y
Y_T
Y_P
1
2
3
4
5
6
7

Fig. 12.23

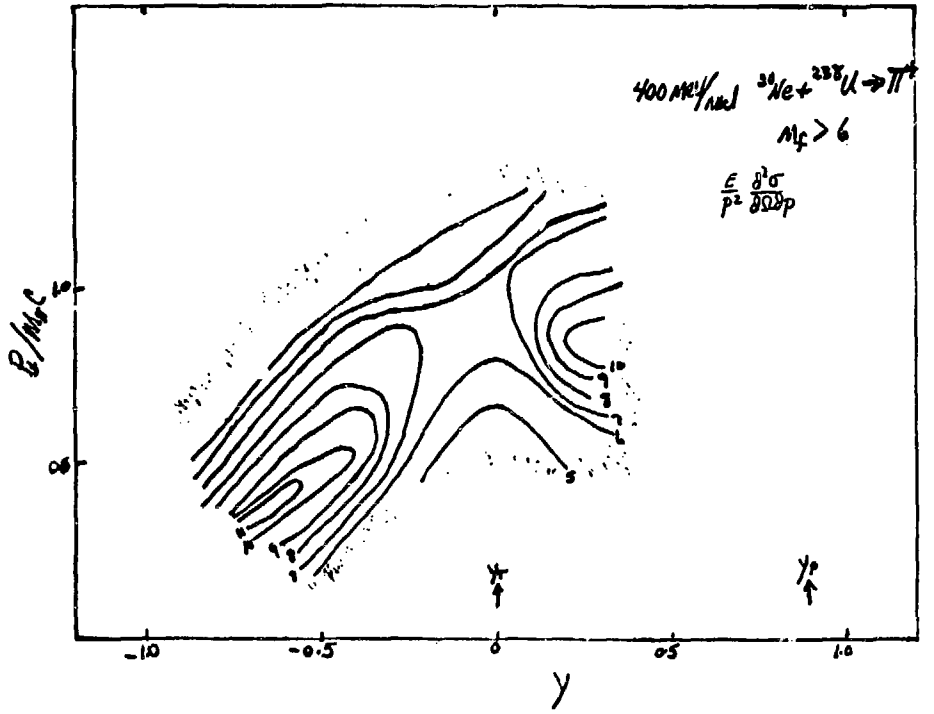
400 MeV/nucl $^{36}Ne + ^{238}U \rightarrow \pi^+$
$M_f > 6$
$\frac{E}{p^2}\frac{d^3\sigma}{d\Omega dp}$
p/M_0c
2.0
0.5
-1.0
-0.5
0
0.5
1.0
y
y_t
y_p

Fig. 12.24

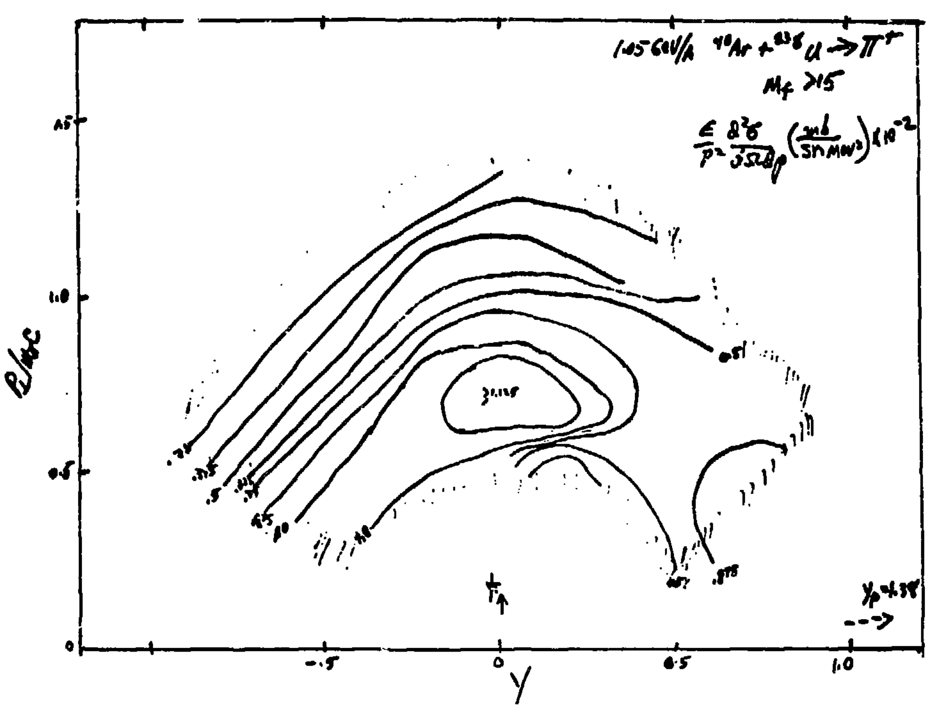

Fig. 12.25

iii) Rapidity correlations for emission of chunks

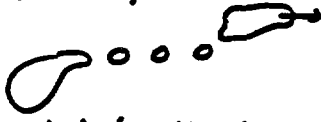

Other intermediate-range phase-space correlations also

iv) Stopping power of nuclear matter

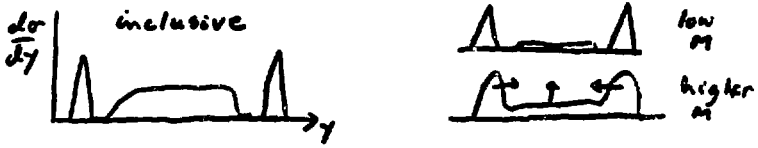

investigated vs E/A, target size

Anomalous behavior = π-condensation?

[Pirner]

Fig. 12.26

Sausage Mechanics:

The wurst possible situation:

Frankly, no link with experiment!

Fig. 12.27

Nuclear Interferometry: exploit quantal final state properties to probe the collision

First data $\pi^- - \pi^-$ correlations ⇒ Brown-Twiss effect [Riverside]

For $^{40}Ar + BaI_2$; $R \sim 5.5$ fm, $\tau \sim 1.6 \times 10^{-24}$ sec

Basic Idea Collision volume a source of particles

$= D(x)$ $(x = \vec{r}, t)$

$$R(p_1, p_2) = \frac{\left(\frac{1}{\sigma} d\sigma / dp_1 dp_2\right)}{\left(\frac{1}{\sigma} \frac{d\sigma}{dp_1}\right)\left(\frac{1}{\sigma} \frac{d\sigma}{dp_2}\right)} - 1$$

For a chaotic source:

$$R = \int dx_1 \int dx_2 \, D(x_1) D(x_2) \left[\left| \phi(x_1, x_2) \pm \phi(x_2, x_1) \right|^2 \right] - 1$$

(± Bosons)

$$\phi \sim e^{i p_1 x_1 + i p_2 x_2}$$

Interference term ⇔ Fourier transform of D

Same effect exists for p-p pairs [Sekj, Igo et al] Coulomb + nuclear forces, fermion statistics

Future Work

i) Fourier kinematic selection [F. Yano]

$\vec{P} = p_1 + p_2$; $\vec{\Delta} = p_1 - p_2$: So far, take all P for statistics

but $R = R(\vec{P}, \vec{\Delta})$

Fig. 12.28

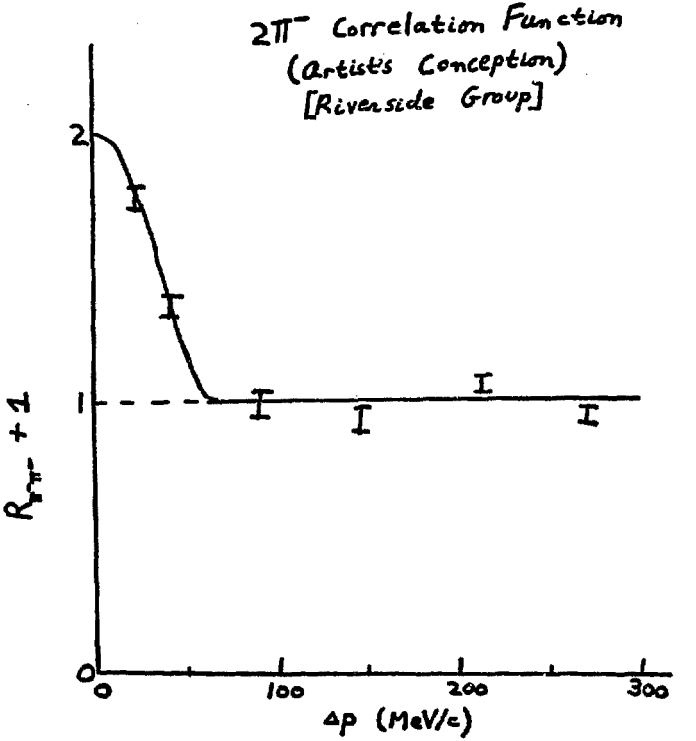
2π⁻ Correlation Function
(Artist's Conception)
[Riverside Group]
2
1
0
$R_{\pi^-} + 1$
0
100
200
300
Δp (MeV/c)

Fig. 12.29

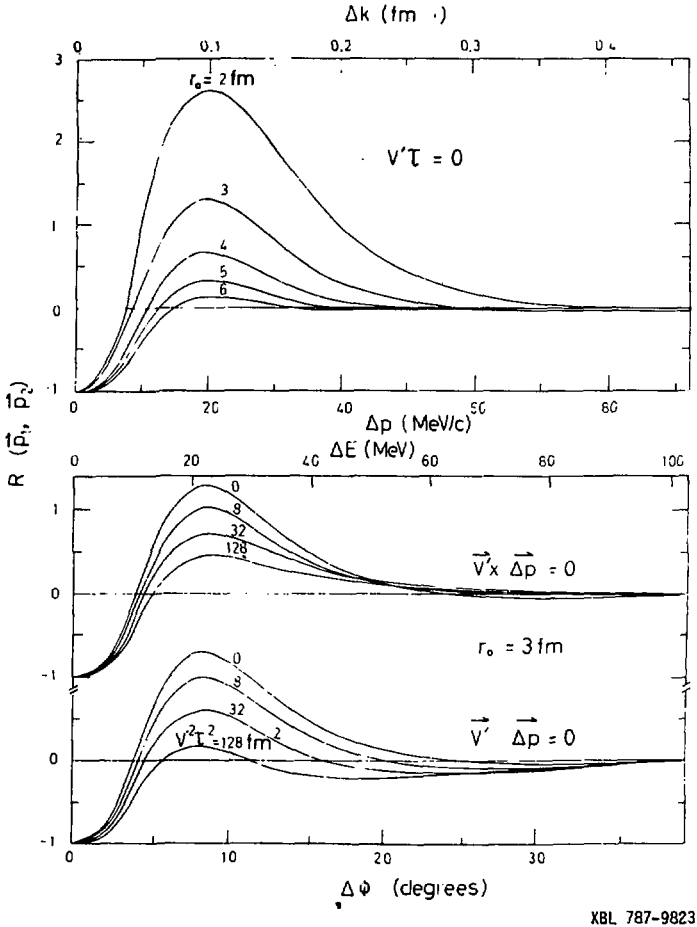

XBL 787-9823

Fig. 12.30

At fixed P:

$\theta_{Pk} = 0$: same direction, $\sigma \neq 0$

$\theta_{Pk} = \pi/2$: different direction, $\sigma = 0$

Define $\langle k^2 \rangle_p = \int R(p,k)\, k^2 d^3k$

$Q = \langle k^2 P_2(\cos\theta) \rangle_p = \frac{1}{\langle k^2 \rangle_p} \int R(P,k)\, k^2 P_2(\cos\theta_k) d^3k$

These separately sensitive to R, τ

Make rough cuts on P or plot to map out source shape

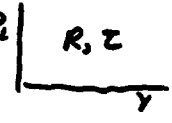

ii) Extract the physics!

Are fast particles direct (small R, τ)
Are slow particles delayed (large R, τ)
Correlate with M to measure impact parameter
Do nucleon parameters agree with π parameters
Evolution of the shape of the system

Coherence in the π field [Cygulassy]

iii) A rigorous theory (for nucleons especially)
What part of T-matrix is determined?
Distortions in the final state

Fig. 12.31

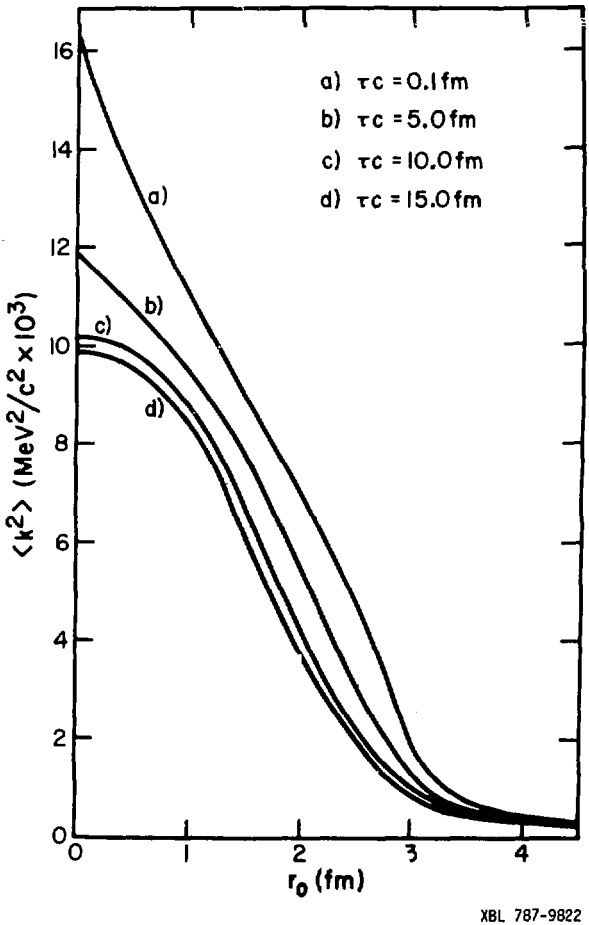

XBL 787-9822

Fig. 12.32

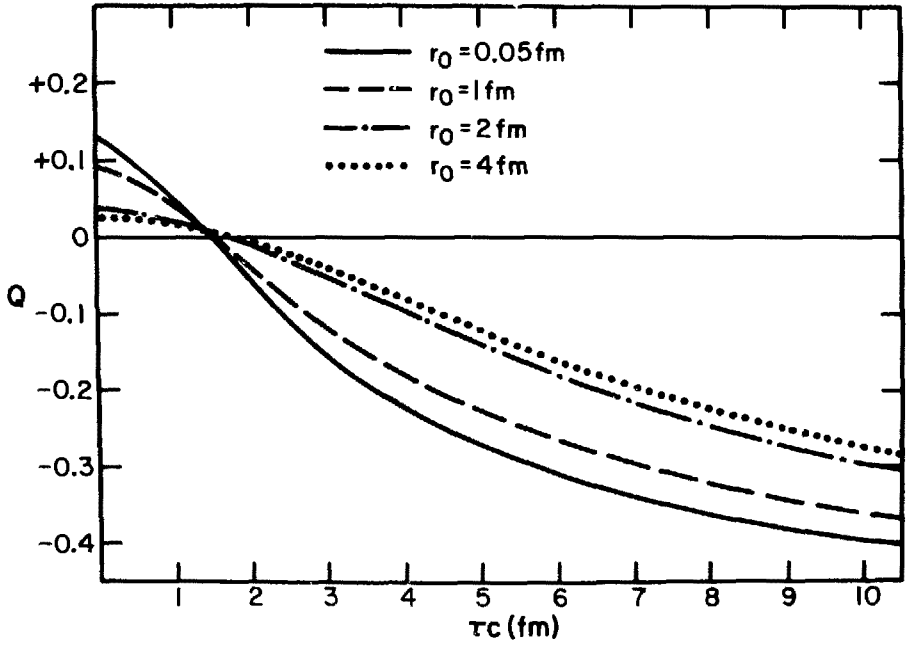

XBL 787-9820

Fig. 12.33

FOURTH SUMMER STUDY LIST OF PARTICIPANTS

Alexander, Yehuda	TRIUMF, Canada
Alhassid, Yoram	Hebrew University of Jerusalem
Allen, K. W.	Oxford University
Axelrod, Alan	Lawrence Berkeley Laboratory
Babinet, Regis	CEN de Saclay
Berman, B. L.	Lawrence Livermore Laboratory
Bishop, Raymond	Lawrence Berkeley Laboratory
Bodmer, Arnold	Argonne National Laboratory
Bonche, Paul	Saclay
Bondorf, Jakob	Niels Bohr Institute
Bonnifield, Michael	
Brochard, Francois	Lawrence Berkeley Laboratory
Budiansky, Michael	Lawrence Berkeley Laboratory
Busza, Wit	Massachusetts Institute of Technology
Carroll, Jim	Lawrence Berkeley Laboratory
Cassagnou, Yves	CEN de Saclay
Castillejo, Leonardo	State University of New York, Stony Brook
Cerny, Joseph	Lawrence Berkeley Laboratory
Chapline, George	Lawrence Livermore Laboratory
Chessin, Steve	Lawrence Berkeley Laboratory
Chiba, Junsei	University of Tokyo
Chin, Siu Ah	University of Illinois
Chu, Shu-Yuan	University of California, Riverside
Cork, Bruce	Lawrence Berkeley Laboratory
Crawford, Hank	Lawrence Berkeley Laboratory
Crowe, Ken	Lawrence Berkeley Laboratory
Curtis, Stanley B.	Lawrence Berkeley Laboratory
Dar, Arnon	Technion-Israel Institute of Technology
Das Gupta, S.	Lawrence Berkeley Laboratory
De Jarnette, W. T.	Johns Hopkins University
De Vries, Ralph	LASL, Los Alamos
Doll, Paul	Lawrence Berkeley Laboratory
Faraggi, H.	Saclay & Lawrence Berkeley Laboratory
Ford, James	Oak Ridge National Laboratory
Fraenkel, Zeev	Weizmann Institute
Frankel, Ken	University of California, Berkeley
Freier, Phyllis	
Friedlander, Erwin	Lawrence Berkeley Laboratory
Friedman, William A.	University of Wisconsin
Fung, Sun-Yiu	University of California, Riverside
Ganssauge, Eberhard	Institute für Theoretische Physik, Marburg
Garpman, Sten	Lawrence Berkeley Laboratory
Geaga, Jorge V.	Lawrence Berkeley Laboratory
Gelbke, Claus-Konrad	Michigan State University
Gemeinhardt, Wieland	University Marburg
Glendenning, Norman K.	Lawrence Berkeley Laboratory
Gorodetzky, Philippe	Laboratoire Spectrometric Nucleaire, Strasbourg
Gosset, Jean	CEN de Saclay
Greiner, Douglas E.	Lawrence Berkeley Laboratory
Grossiord, Jean-Yves	Lawrence Berkeley Laboratory

Grunder, Hermann	Lawrence Berkeley Laboratory
Gutbrod, Hans	Gesellschaft fUr Schwerionforschung and LBL
Gylassy, Miklos	Lawrence Berkeley Laboratory
Halbert, Edith	Oak Ridge National Laboratory
Harris, John	State University of New York, Stony Brook
Hatch, Robert L.	California Institute of Technology
Haustein, Peter E.	Brookhaven National Laboratory
Heckman, Harry	Lawrence Berkeley Laboratory
Hendrie, David L.	Lawrence Berkeley Laboratory
Holmgren, Harry D.	University of Maryland
Hufner, Jorg	University of Heidelberg
Huie, Arthur	University of California, Riverside
Hyde, Earl K.	Lawrence Berkeley Laboratory
Jain, P. L.	University of New York, Buffalo
Kapusta, Joe	Lawrence Berkeley Laboratory
Karant, Yasha	Lawrence Berkeley Laboratory
Kast, John	Lawrence Berkeley Laboratory
Kerman, Arthur K.	Massachusetts Institute of Technology
Kiernan, Gerald P.	University of California, Riverside
King, Charles	Lawrence Berkeley Laboratory
King, George	Lawrence Berkeley Laboratory
Klapisch, Robert	Laboratoire Rene Bernas, Orsay
Knoll, Jorn	University of Tokyo
Koike, Masahiro	Lawrence Berkeley Laboratory
Koonin, Steven E.	California Institute of Technology
Korner, Hans J.	Tu München Physik Department
Kurashov, A.	USSR
Landau, Rubin H.	Lawrence Berkeley Laboratory
Lande, Alex	Groningen University
Larsh, A. E.	Lawrence Berkeley Laboratory
Laskowich, Gloria	Lawrence Berkeley Laboratory
Lee, T. D.	Columbia University
Levin, R. D.	Hebrew University, Jerusalem
Lewis, David	Iowa State University
Lindstrom, Peter	Lawrence Berkeley Laboratory
Loveland, Walter	Oregon State University
Lu, Jia-Jih	University of California, Riverside
Mahoney, Jeannette	Lawrence Berkeley Laboratory
Maier, Michael R.	Lawrence Berkeley Laboratory
Malfliet, Rudi	University of Groningen
Mallet-Lemaire, M. C.	Lawrence Berkeley Laboratory
Mantzouranis, G.	Lawrence Berkeley Laboratory
Marquez, Luis	Centre d'Etudes Nucleaires, Gradignan
Masuda, Naohiko	Yamagata University
Mathews, Grant	Lawrence Berkeley Laboratory
McClelland, John	UCLA and Lawrence Berkeley Laboratory
McCusker, Brian	University of Sydney
McGrath, Robert	State University of New York, Stony Brook
McManus, H.	Michigan State University
McVoy, Kirk W.	University of Wisconsin-Madison
Mekjiam, Aram	Rutgers University
Meng, Ta-chung	Free University of Berlin
Meyer, William G.	Lawrence Berkeley Laboratory
Minich, Roger W.	Purdue University

Morrison, Harry L.	University of California, Berkeley
Morrissey, David J.	Lawrence Berkeley Laboratory
Moszkowski, Steven A.	University of California, Los Angeles
Mueller, Mark	4909 Beeher Circle, Madison, Wisconsin
Mukherjee, Shankar	Banaras Hindu University, Varanasi, India
Myers, William D.	Lawrence Berkeley Laboratory
Nagamiya, Shoji	Lawrence Berkeley Laboratory
Nagatani, K.	Texas A & M University
Negele, John	Massachusetts Institute of Technology
Nguyen, Van Sen	Lawrence Berkeley Laboratory
Noack, Cornelius C.	Universitaet Bremen
Ogloblin, A.	USSR
Orland, H.	Saclay
Otterlund, Ingvar	University of Lund
Perez-Mendez, Victor	Lawrence Berkeley Laboratory
Pirner, Hans J.	CEN de Saclay
Pitthan, Rainer	NP,S Monterey
Poe, Robert T.	University of California, Riverside
Porile, Norbert T.	Purdue University
Poskanzer, Arthur	Lawrence Berkeley Laboratory
Price, P. B.	University of California, Berkeley
Pugh, Howel	National Science Foundation
Radi, Hafez	Kuwait University
Radvanyi, Pierre	Institut de Physique Nucleaire, Orsay
Randrup, Jorgen	Nordisk Institut for Teoretisk Atomfysik
Rasmussen, John	Lawrence Berkeley Laboratory
Redlich, Martin G.	Lawrence Berkeley Laboratory
Rho, Mannque	CEN de Saclay
Riess, Fritz	Institute fur Kernphysik, Darmstadt
Robel, Michael	Lawrence Berkeley Laboratory
Ruck, Herbert M.	Duke University
Sagle, Allan	Lawrence Berkeley Laboratory
Sandel, Margaret	Iowa State University
Schimmerling, W.	Lawrence Berkeley Laboratory
Schnetzer, Steve	Lawrence Berkeley Laboratory
Scott, David K.	Lawrence Berkeley Laboratory
Schroeder, Lee	Lawrence Berkeley Laboratory
Seaborg, Glenn T.	Lawrence Berkeley Laboratory
Sedlak, Joseph	University of Wisconsin
Seglie, Ernest	Yale University
Smith, Roger Alan	State University of New York, Stony Brook
Smith, R. Kent	Duke University
Steadman, Stephen	Massachusetts Institute of Technology
Steiner, Herbert	Lawrence Berkeley Laboratory
Stevenson, John	Lawrence Berkeley Laboratory
Stock, Reinhard	Gesellschaft für Schwerionenforschung
Strayer, Michael	Texas A & M University
Sugimoto, Kinzo	Osaka University
Sullivan, John	Lawrence Berkeley Laboratory
Symons, T. J. M.	Lawrence Berkeley Laboratory
Treuhaft, Robert	Lawrence Berkeley Laboratory
Van Bibber, Karl	Lawrence Berkeley Laboratory
Vary, James P.	Iowa State University
Vautherin, Dominique	Insititut de Physique Nucleaire, Orsay
Viyogi, Y. P.	Lawrence Berkeley Laboratory

Ward, Thomas E.	Indiana University
Weber, Christine	Lawrence Berkeley Laboratory
Weiss, Morton	Lawrence Livermore Laboratory
Westfall, Gary D.	Lawrence Berkeley Laboratory
Wiedenbeck, Mark	Lawrence Berkeley Laboratory
Wilets, Lawrence	University of Washington
Wohn, Fred K.	Iowa State University
Wolf, Kevin	Lawrence Berkeley Laboratory
Woloshyn, Richard M.	University of British Columbia
Wolschin, Georg	Institut für Theoretical Physik, Heidelberg
Wong, Cheuk-Yin	Oak Ridge National Laboratory
Wozniak, Gordon	Lawrence Berkeley Laboratory
Yano, Fleur	California Institute of Technology
Yariv, Y.	Weizmann Institute of Science
Yoccoz, Jean	Institut National de Physique Nucleaire, Paris
Zabek, Mark	Brookhaven National Laboratory
Zarbakhsh, Farshid	Lawrence Berkeley Laboratory
Zielinski, Iwo P.	Institute of Nuclear Research
Zingher, Arthur R.	Lawrence Berkeley Laboratory
Zisman, M. S.	Lawrence Berkeley Laboratory


THEORIES! THEORIES! READ ALL ABOUT 'EM! GET 'CHER RED-HOT THEORIES!
EINSTEIN'S THEORY BREAKS

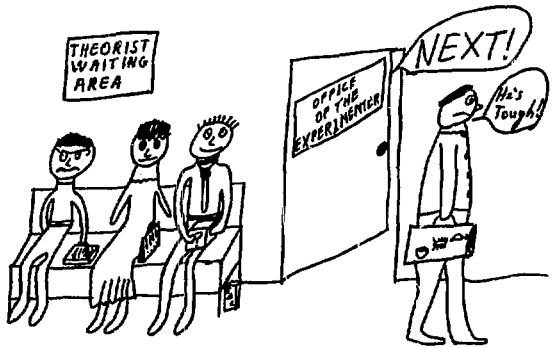
THEORIST WAITING AREA
OFFICE OF THE EXPERIMENTER
NEXT!
He's Tough!

HAND-OUTS

At the conclusion of the 4th Summer Study, two sets of material were passed out to the participants. These included:

1) Three new homework problems, which were developed during some of the Summer Study lectures, and

2) "A Predictor's Partial Shopping List" - a guide to acquaint our theoretical colleagues with some of the data that will be available over the next year. The guide includes information on the experiments and the parameters that will be measured, as well as the names of the experimenters who can be contacted for further questions.

Lee Schroeder

4th Summer Study
Home Work Problems

1) Coalescence model vs. chemical equilibrium in composite particle production.

Study the relation: $\frac{d\sigma}{dk_d^3}(Proj.+A \to d+x) = C\left[\frac{d\sigma}{dk_p^3}(Proj.+A \to p+x)\right]^2$

a) How well is the square law fulfilled? (expt. & theor.)

b) How does the constant C depend on proj.-tgt combination and energy?

2) Calculate mean and variance of the multiplicity distribution as a function of impact parameter for 250 MeV/n $^{20}Ne + ^{238}U$ and 1.05 GeV/n $^{40}Ar + ^{40}Ca$.

3) What is the contribution of multiple scattering to backward particle (π and p) production? What is its dependence (contribution) on bombarding energy?

(Data exists for both proton and heavy-ion beams – See "A Predictor's Partial Shopping List").

"A PREDICTOR'S PARTIAL SHOPPING LIST"

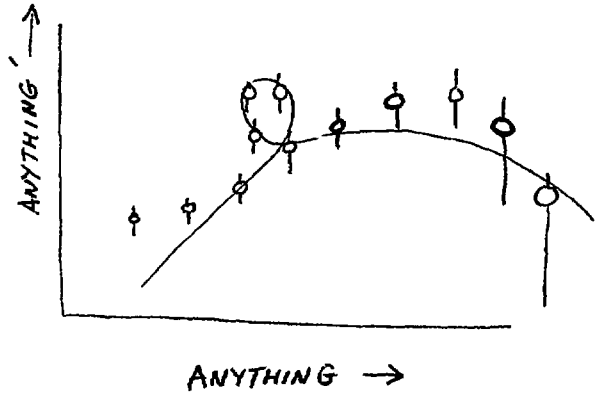

SAT URNE → Heavy ion programme (1)

- Multiple n and p correlations with a 4π TPC system (Saclay NE-BE-NE, J. Gomez (Saclay NE-NE) Strasbourg, Clermont FN)
- Nucleus-nucleus and p-nucleus correlations with SPES IV (Lyon, Orsay IPN, Saclay NE) T. Radvanyi (Saturne)
- Low energy fusion J. Harris (Saclay BE) (Saclay BE-SE)
- Cluster production by quasi-elastic and other reactions on H target with SPES IV (CNRS, Clermont F3, Caen) L. Goldzahl (SE-SI, Saturne)
- π production below 500 MeV/Amu with SPES III (Strasbourg, Orsay IPN) B. Asllanaj (Strasbourg)
- $^{12}C + ^{12}C$ fusion (Orsay CSNSM) F. Yon (Orsay, CSNSM)
- Fragment production for astrophysics (cosmic rays) (Orsay CSNSM, CNRS) F. Yon
- Dosimetry and Radiobiology (Fontenay, Villejuif) M. Parmentier (Fontenay)

(2) E299H

O. Chamberlain, M.C. Mallet-Lemaire, S. Nagamiya, S. Schneider, G. Shapiro, H. Steiner, I. Tanihata + Previous Member (L. Anderson, W. Brückner)

RUN UP TO SUMMER 1978 ⟵ ⟵ Data Analysis Finished ⟶ ⟶ In Analysis

Beam	Target	Detected Fragments	θ_{LAB}	Fragment E_{LAB}	2-Particle Correlation: θ_{LAB}	2-Particle Correlation: Features	High Multiplicity Events: # of tags	High Multiplicity Events: Features
.8GeV/N C	C, Pb	π^-, p, d, t, ^{3}He, α	15°–145°		40°, 22.5°	• 3 sets of tag counters at fixed θ • 3 are at φ = 90, 180, 270° (Spectrometer at φ = 0°) • Tag can separate: { 100 MeV < E_p < 200 MeV E_p > 200 MeV	5 at 90° (22.5°)	• φ distribution of tags:
.8GeV/N Ne	NaF, Cu, Pb	"	15°–130°	$E_\pi \geq$ 60 MeV	90°, 60°		9 at 45° (▶ 60°) 8 at 90°	
.4 GeV/N Ne	C, NaF, Cu, Pb	"	20°–140°	$E_p \geq$ 50 MeV	40°		8 at 90°	
2.1 GeV/N Ne	NaF, Cu, Pb	"	15°–140°	$E_d \geq$ 40 MeV	"		9 "	
.8GeV/N Ar	C, KCl, Pb	"	10°–145°	etc.	"		9 "	
.8GeV P	C, NaF, KCl, Cu, Pb	"	15°–110°		"		9 "	
2.1 GeV P			10°–110°		"		9 "	
Nov. '78 1.8 GeV/N Ar	C, KCl, Pb	π^+, π^-, K^+, p, d, t, ^{3}He, α ... Note!!					14 tag counters available in Fall, 1978. Tag can separate: • E_p < 100 MeV • 100 MeV < E_p < 200 MeV • E_p > 200 MeV	
1979 ?								

Possibility
- 2.8GeV/N
- .8GeV/N to study 2-particle corr.
- Continuous Energy Change.

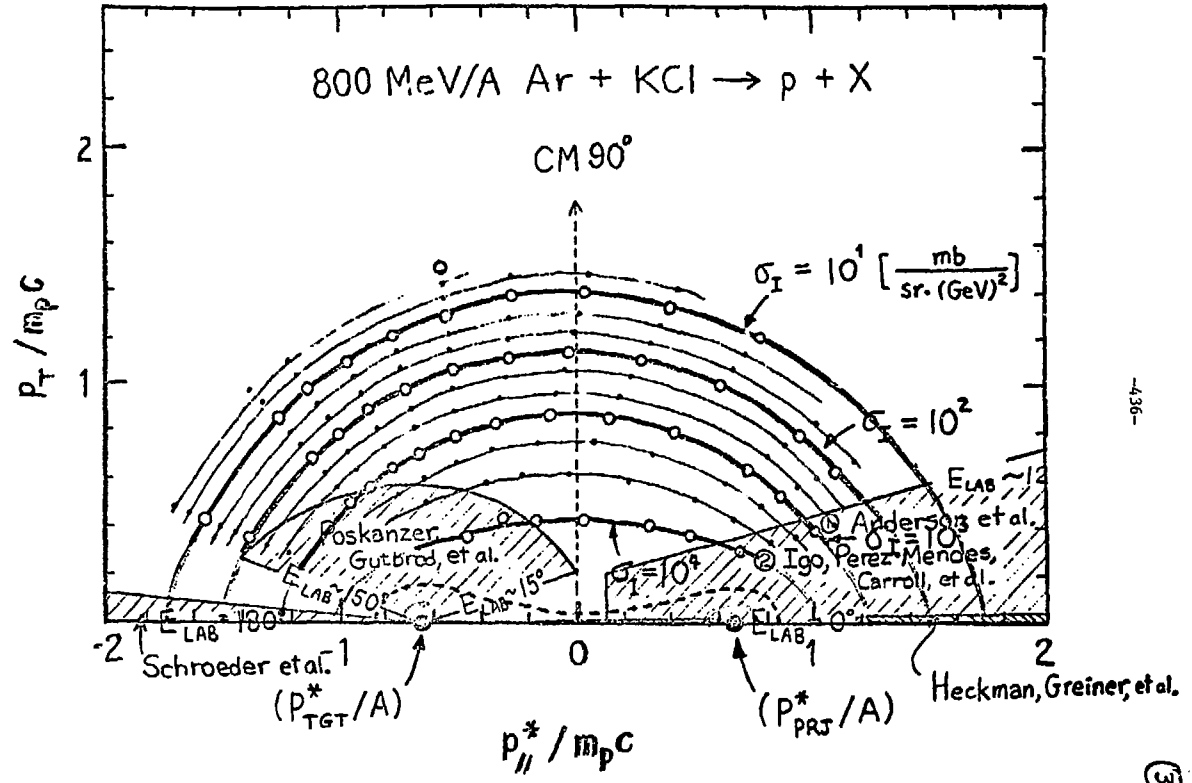
800 MeV/A Ar + KCl → p + X
CM 90°
$\sigma_I = 10^1 \left[\frac{mb}{sr.(GeV)^2}\right]$
$\sigma_I = 10^2$
$\sigma_I = 10^3$
$\sigma_I = 10^4$
$E_{LAB} \sim 12$
Poskanzer, Gutbrod, et al.
Anderson, et al.
Igo, Perez-Mendes, Carroll, et al.
$E_{LAB} \sim 50°$
$E_{LAB} \sim 15°$
$E_{LAB} \sim 0°$
$E_{LAB} = 180°$
Schroeder et al.
(P^*_{TGT}/A)
(P^*_{PRJ}/A)
Heckman, Greiner, et al.
$p_T / m_p c$
$p^*_{//} / m_p c$
2
1
0
-2
-1
1
2

④

K. Frankel T. Stevenson R.B. Price U.C. Berkeley

^{40}Ar @ 105 MeV/nucleon + U → Fragment + X

Target Thicknesses: 1, 2, 5 mil
Total Beam Fluence: 10^{12} ions

Data taken with Lexan and CR-39 plastic detectors at the following angles:
10°, 14°, 24°, 35°, 55°, 80°, 100°, 125°, 145°, 155°, 162°, 170°

We are currently obtaining data only from the Lexan. We will be able to obtain angle and energy distributions for $Z \geq 3$. We can measure fragment energies from ≈ 10 MeV/nucleon to 100 MeV/nucleon (Boron) or 140 MeV/nucleon (Oxygen).

By December 1 we plan to have data for:

Boron and Carbon: 10° to 125°
≥ Oxygen: 10°, 16°

We are open to suggestions for interesting aspects of this experiment from which we can obtain data.

(5)

Title: Coulomb Dissociation Effects in Heavy-Ion Target Fragmentation

Experimenters: J.C. Hill*, D.A. Lewis, F.K. Wohn* *Spokesman
Iowa State Univ. and DOE-Ames Laboratory

Beams and Targets:

2.1 GeV/A { ^{1}H, ^{4}He, ^{12}C, ^{20}Ne } each on { ^{12}C, ^{45}Sc, ^{89}Y, ^{197}Au, ^{238}U }
1.8 GeV/A ^{40}Ar

target foils (~1 g/cm²) irradiated for 2-3 h each in each beam. (12 h total beam time for each beam.)

Measurements: Production cross sections for radioactive products will be determined by γ-ray spectroscopy with GeLi(i) detectors initially at LBL (short $T_{1/2}$) and finally at Iowa State (long $T_{1/2}$). Absolute cross sections will be determined. Separation chemistry will be used for the heavier targets.

Goals: (1) Establish the relative roles of nuclear versus coulomb dissociation for one-nucleon removal, two-nucleon removal, spallation and fission; (2) Compare coulomb dissociation effects in target and projectile fragmentation; (3) Study the relationship between coulomb dissociation effects in heavy-ion reactions and photo-nuclear processes.

(6)

HADRON-NUCLEUS AND HEAVY ION REACTION STUDIES

UN.V. OF LUND. SÖLVEG. 14 S-22362 LUND SWEDEN
S. HERTZMAN, B. JAKOBSSON, R. KULLBERG, B. LINDKVIST, I. OTTERLUND, A. OSKARSSON AND E. STENLUND

HADRON-NUCLEUS REACTIONS

p + Em 200, 360 and 400 GeV. ~4000 interactions, emission angles Θ and charged particle multiplicities.

p + W 400 GeV (wire loaded emulsions) ~500 reactions, multiplicities of charged particles. (almost finished)

π + Em 300 GeV measurements of Θ and charged particle multiplicities have just started.

HEAVY-ION REACTIONS

^{4}O + Em 50-100 A MeV ~300 interactions are measure Θ, projectile cross sections, charged part. multiplicities.

^{16}O + Em 100-200 A MeV ~700 interactions Θ, fragmentation cross sections, multiplicities.

^{16}O + Em } 2.1 A GeV ~700 interactions Θ and $\pi^{\pm}$ -
^{12}C + Em } multiplicities. (finished)

^{20}Ne + W 340 A MeV (wire loaded emulsions) ~100 interactions Θ and charged particle multiplicities. (finished)

^{40}Ar + Em 1.2 A GeV ~700 interactions, Θ and charged particle multiplicities, samples of central and peripheral with energy distributions for p and He

^{40}Ar + Em 6 or 8 GeV, will start fall '84. fragmentation cross sections, Θ and charged part multiplicities, energy distr. for p and He

(7)

352 H: K. VAN BIBBER (LBL)

"Projectile Fragmentation of ^{16}O, ^{12}C at 100 MeV/Nuc"

Singles: Beams of ^{16}O, ^{12}C
Targets: Be, Al, Cu, (Ag), Au, (Th)
Angles: 2.5° – 8° (Lab)
Measured: Identification A, Z (A≥6, Z≥3)
Energy Spectra (Beam Rapidity)
Angular Distributions
Energy: ^{12}C = 90 MeV/nuc ^{16}O = 50, 90, 120

Coincidence: $^{16}O + X$, 100 MeV/Nuc.
i) Heavy fragment – Light Particle (p → Li)
both of beam rapidity

ii) Heavy fragment (beam rapidity) –
Light Particle (target rapidity)

(8)

1) NAME : L. SCHROEDER (LBL) 351 H

2) EXPT :

$$A_1 + A_2 \rightarrow \begin{pmatrix} \pi^{\pm} \\ p \\ d \\ t \end{pmatrix} \Big|_{180^\circ} + X$$

A_1 = proj, A_2 = tgt

$\pi^{\pm}$, p data available ≈ Sept/Oct '78

proj = A_1 =
- p at 0.8, 1.05, 2.1, 3.5, 4.8 GeV
- α at 1.05, 2.1 GeV/n
- ^{12}C at 0.4, 1.05, 2.1 "
- ^{40}Ar at 1.05, 1.8 "

tgt = A_2 = C, Al, Cu, Sn, Pb for most of the meas, also some data with H_2, D_2, Ag targets

0.8, 4.8 GeV protons only

3) RANGE OF OBSERVABLES (Typical values) :

$\theta_{LAB} = 180 \pm 1^\circ$

$100 \lesssim P_\pi \lesssim 700$ MeV/c

$300 \lesssim P_p \lesssim 1100$ "

$600 \lesssim P_d \lesssim 1500$ "

$600 \lesssim P_t \lesssim 1200$ "

R.T. POE
S.Y. FUNG (9)

UC RIVERSIDE — STREAMER CHAMBER

current and proposed data:

^{40}Ar at 0.25, 0.4, 0.6, 0.9, 1.2, 1.5, 1.8 GeV/N
incident on Pb_3O_4, BaI_2, NaF, LiH targets

^{12}C at 0.4, 2.1 GeV/N on same targets

Data Analyses — Exclusive data for charged particles
1. Total charged particle and Negative Pion MULTIPLICITIES
2. Momentum & Angular Data of all particles
— can be plotted w/ all variety of p_T, multiplicity cuts
3. 2 Pion Correlations using Handbury-Brown—Twiss effect

(10)

Also su pg. 11.

Sandoval, Stock (LBL-GSI-Marburg)
Gyaga, Schroeder

Streamer Chamber

400 H Done: Ar + KCl 1.8 GeV/A
inelastic trigger 4000 events
central " 15000 "
→ Search for π^- – pair correlation
Enough statistics for size determination
of source in longitudinal + transverse direction.
→ Investigate proton / pion emission in events with
extreme π^- multiplicity
Data to be available by mid November 78
Planned: Ar + KCl at 1 GeV/A
+ perhaps Fe or Cu "

400 H To be done in late fall: proton – nucleus interaction
studied in streamer chamber, 400 MeV, 1, 2 GeV
proton on several targets
First scanning results available in Spring 79

(11)

STREAMER CHAMBER

Also see pg. 10

1) NAME : SCHROEDER (LBL)/STOCK (GSI/MARBURG)

2) EXPT : A) 400 H $p + A \rightarrow$ backward trigger particle, SC triggered, one backward particle (mostly π or p), backward $\Rightarrow$ $180° \geq \theta_{LAB} \geq 150°$ Will be able to see all (light) charged particles in final state with energies $\gtrsim$ 5-10 MeV. Will be able to look for "leading particles, jets, ---" Initial run with proton beam in 1-2 GeV range. Expect to take data Nov '78.

B) 401H - High statistics experiment, 1.56 GeV/n ^{40}Ar + KCl, looking for $\pi^- \pi^-$ correlations. Using central collision trigger, only indications from our observed π^- multiplicity distribution indicates that we are getting $b \simeq 0-2$ fermis.

Scanning under way, measurements just begun.

(12)

Phyllis S Freier & C.J. Waddington
School of Physics & Astronomy, U. of Minnesota.

Projectile: cosmic rays: $Z = 8\text{-}26$, $E \geq 7.5 \frac{GeV}{nucleon}$, $\bar{E} = 20 \frac{GeV}{n}$

TARGET: Emulsion.

350 of 500 interactions analysed now.
Ionization angles, of all charged particles over 4π measured.
Particles are projetile fragments, target fragments, π's.
Preliminary data shows evidence of some PION "PAIRING"
and some interactions show π emission in "jets".

(13)

Institution School of Physics.
University of Sydney, N.S.W.
AUSTRALIA 2006

Name Brian McCusker

Expt 1.9 GeV/nucleon Fe on nuclear emulsion

Observation Number of a) Heavy tracks, N_h
b) grey - N_g
c) α particles
d) pions (minimum tracks outside 7°)
e) protons (in cone 7°)
g) heavy fragments from projectile & their Z.

Angles of all tracks.

So far (July 1978) 123 interactions

(14)

LBL (Schimmerling, Kost) – KSU (Maday, Anderson, Baldwin, Cecil)

Inclusive Neutron Spectra from Heavy Ion Collisions
(Exp 339 H)

Detectors: Large volume plastic scintillator
Measured: Time of flight, Energy in detector, θ_{Lab}

I. Analysis in Progress
(Some preliminary data reported at Summer Study)

Ne 250 MeV/A + {U, C, Al} → n + X

Ne 400 MeV/A + {C, Al, Cu, Pb, U} → n + X

θ_{Lab} = 15°, 30°, 45°, 60°, 90°, 120°, 150°
E_{Lab} = ~ 20 to ~ 300 - 600 MeV

II Experiments planned ~ Oct 78

{Ne, α} {250 MeV/A, 400 MeV/A} + {C, Al, NaF, Cu, Pb, U} → n + X

θ_{Lab} = 0°, 15°, 30°, 120°, 150°
E_{Lab} = ~ 10 - 20 to 300 - 600 MeV

(15)

The following data will be available from The Heckman/Greiner Group 0° Spectrometer in Dec next year:

Reaction: $B(\text{beam}) + T(\text{target}) \rightarrow F(\text{fragment}) + X(\text{anything})$

Beams: ^{14}N at 2.1 Gev/nuc, ^{15}N at 1.9 Gev/nuc. ^{40}Ar at 1.8 Gev/nuc } measured $\left.\frac{d\sigma}{dp_{\parallel}}\right|_F$

Targets: CH_2, Be, C, Al, Cu, Ag, Pb

Fragments: all particle-stable nuclei with $A_F \leq A_B$

Range of fragment momentum covered:

$-400 \text{ Mev/c} \leq p_{\parallel,F} \leq 400 \text{ Mev/c}$ in projectile rest frame

The experimental method and similar data are presented in Greiner et al, PRL 35#3 p.152, 1975

(16)

The following data will be available from the Heckman / Shreiner group in the next year concerning "internal target" telescope results.

Reaction : $B + T \rightarrow F + X$

Beams : ^{56}Fe at 1.88 GeV/nucl.

^{40}Ar at 1.8 GeV/nucl.

$Z/A = 1/2$; $^{10}B \rightarrow {}^{36}Cl$, 1.8 GeV/nucl

Targets : H, Li, Be, C, S, Cu, Ag, Ta, Pb, U

Measurements :

1) elemental production cross sections

$\sigma(Z)$, $Z = (Z_p - 1)$ to $Z_p/2$
Z_p = projectile atomic number

2) charge changing cross sections

$\sigma_{\Delta Z \geq 1}$

3) mass changing cross sections

$\sigma_{\Delta A \geq 1}$

(17)

JOHNS HOPKINS UNIVERSITY

LEON MADANSKY, W. DEJARNETTE, T. HALLMAN, E. MCINTYRE, R. SEMPER

HAVE DATA ON: π^0 PRODUCTION IN C + Pb @ 1.05 GeV/n CENTRAL COLLISIONS

$\pi^\pm$ PRODUCTION IN C+ Pb @ 1.05 GeV/n CENTRAL COLLISIONS (still being analysized.)

C+ OTHER TARGETS @ 1.05 GeV/n

WITHIN ONE YEAR: $\pi^0, \pi^\pm$ PRODUCTION Ar+Pb @ 1.05 GeV/n CENTRAL COLLISIONS

POSSIBLY EXCITATION FUNCTION MEASUREMENT OF HIGH P_T $\pi^\pm, \pi^0$ PRODUCTION IN CENTRAL COLLISIONS WITH C+Pb @ .8 - 2.1 GeV/n.

(18)

PEREZ-MENDEZ / IGO / CARROLL / EAGLE et AL

1.85 GeV/A $^{40}A_r$ + Cu, Be, Pb at all θ → p, d, T, ^3He, ^4He + X

2.1 GeV/A ^{12}C + Cu, Be, Pb as above

4° ≤ θ_L ≤ 14.7° 1.7 ≤ P ≤ 6.5 GeV/c

The associated multiplicity of Fast Fragments

4° < θ_m < 12° and 5° < θ_m < 16° $\Phi \sim 2\pi$

IN LBL 7276

RECENT DATA HAVE extended SINGLE PARTICLE inclusive for

1.8 GeV/A $^{40}A_R$ + Cu, Be, Pb → π, p, d, T, ^3He, ^4He + X

down to P = 1.0 GeV/c at midway rapidity range for protons

we have also studied the associated multiplicity as a function of the angle of the array and have data for

5° < θ_m < 12° 9° < θ_m < 27° 12° < θ_m < 35° 18° < θ_m < 46° *

* with spectrometer trigger at θ_L = 10° P = 1.5 GeV/c

In the near future we will take data for

1.5 MeV/A ^{40}Ar + Ca → p + p + X, p + d + X FOR 5 $\frac{MeV}{c}$ < P_{REL} < 250 $\frac{MeV}{c}$

at θ_L = 6° ... θ_L = 14.3° ...

P = 1 GeV/c, 1.65 GeV/c and 2.4 GeV/c

with various triggers 1. 2 part. in Spec.
2. " " " and high multiplicity and Barrels
3. " " " " " "

(19)

LBL - GSI - Marburg Collab (Poskanzer/Butler/Stock)

284H π^+ 15 - 100 MeV
p 7 - 200 MeV
d 10 - 250 MeV
t 10 - 300 MeV

from p on U at 1.05 GeV
^{4}He on U at 0.4 and 1.05 GeV/n
^{20}Ne on U at .25, .4, 1.05 and 2.1 GeV/n
^{40}Ar on Ca and U at .4 and 1.05 GeV/n
^{20}Ne on Al, Ag, Au at 400 MeV/n

377H light fragments $4 \le Z \le 13$
heavy fragments $\sum_{Z=13}^{26} \frac{d^2\sigma_Z}{d\Omega dE}$
heavy fragments $\sum_{Z>26} \frac{d^2\sigma_Z}{d\Omega dE}$
} from ^{4}He on Au, U at 1.05, 2.1 GeV/n and 400 MeV/n ^{20}Ne on Au, U

Associated with the fragments listed above (284H + 377H) we measured associated charged particle multiplicities (if $E_{charged\ particle} \geq 25$ MeV/nucleon) and θ and ϕ correlations of these associated charged particles with respect to the trigger particle

(20)

Search for Previously Undiscovered Isotopes

M. Budiansky J. Stevenson P.B. Price

(July, 1978 Bevalac Experiment)

BEAM: ^{40}Ar at 200 MeV/nucleon
TARGET: 212 mg/cm^2 Al
DETECTORS: Stacks of sheets of Lexan plastic.

Measurement of projectile fragment rigidity, using the Zero Degree Spectrometer, and measurement of projectile fragment range and dE/dx, using the Lexan stacks, allow identification of isotopes.

The fragment rigidities examined include both neutron-rich and neutron-deficient isotopes.

A similar experiment, using a ^{48}Ca beam, is planned for around December, 1978.

(21)

Rasmussen / Nakai Group

0.4 GeV/N Ne + C
0.8 GeV/N Ne + NaF
Cu
Pb

π^+
θ_{Lab} : 30° ~ 150°
T_{Lab} : 20 ~ 100 MeV